UNIVERSITY OF KWAZULU-NATAL

INYUVESI YAKWAZULU-NATALI

Microchemostat technologies for characterization of efflux pumps associated with multidrug resistance in *Mycobacterium tuberculosis*

By

JARED MACKENZIE

Submitted in fulfilment of the requirements for the degree of Doctor of Philosophy in the Discipline of Medical Microbiology, School of Laboratory Medicine and Medical Sciences, College of Health Sciences

University of KwaZulu-Natal

South Africa

November 2016

AHRI AFRICA HEALTH RESEARCH INSTITUTE

DECLARATION

I, Mr JARED MACKENZIE, declare as follows:

1. That the work described in this thesis has not been submitted to UKZN or any other tertiary institution for purposes of obtaining an academic qualification, whether by myself or any other party.
2. That my contribution to the project was as follows:

    - I fabricated all microchemostat chips used throughout the project.
    - I constructed the "microfluidic board" that facilitated the actuation of the microfluidic device and automation of the microchemostat system.
    - I performed all conventional cell culture (liquid cultures in tissue culture flasks and solid phase cultures on agar plates) and microchemostat cell culture experiments.
    - The development of the qualitative and quantitative models was performed with the assistance of Dr. Frederick Balagaddé.
    - I performed the image processing and analysis of all data with the assistance of Dr. Frederick Balagaddé.

3. That the contributions of others to the project were as follows:
    - The recombinant *E.coli* strains were constructed by Dr. Alissa Myrick from the Eric Ruben lab at Harvard University, who is now located at H3D at the University of Cape Town.

JARED MACKENZIE (Candidate)
Dated this, 9th day of March 2017

As the candidate's Supervisor, I agree to the submission of this thesis

DR FREDERICK BALAGADDÉ (Supervisor)
Dated this, 9th day of March 2017

CONFERENCE CONTRIBUTIONS

1. **Mackenzie JS**, Myrick A, Rubin EJ, Balagaddé FK (25/04/2015 - 01/05/2015). **The use of a microfluidic chemostat for the study of drug resistance mechanisms in *Mycobacterium tuberculosis*.** Gordon research seminar and conference for Multi-Drug Efflux systems, Luca (Barga), Italy. Oral and poster presentations.

2. **Mackenzie JS**, Myrick A, Rubin EJ, Balagaddé FK (16/09/2015 – 19/09/2015). **A microchemostat for the study of *M. tuberculosis* efflux pumps.** Microsystems technology 3rd International Workshop on Microsystems Technologies for African Health, Microsystems for African Health, Protea Hotel, Stellenbosch, South Africa. Oral and Poster Presentations.

3. **Mackenzie JS**, Myrick A, Rubin E, Balagaddé FK (16/11/2015 – 20/11/2015). **Antibiotic resistance and its cost in *E.coli* cells expressing Tap—a multidrug efflux pump of *Mycobacterium tuberculosis*.** Biophysics in the Understanding, Diagnosis and Treatment of Infectious Diseases, Spier Hotel, Stellenbosch, South Africa. Poster presentation.

4. **Mackenzie JS**, Myrick A, Rubin EJ, Balagaddé FK (22/11/2015 – 24/11/2015). **Antibiotic resistance and its cost in *E.coli* cells expressing Tap—a multidrug efflux pump of *Mycobacterium tuberculosis*.** K-Rith and UCT retreat. Zimbali hotel, KwaZulu Natal, South Africa. Oral presentation.

5. **Mackenzie JS**, Myrick A, Rubin EJ, Balagaddé FK (10/09/2015 and 08/08/2016). **Microchemostat studies of *M.tb* efflux pumps.** UKZN College of health science Research day. Oral presentations

ACKNOWLEDGEMENTS

This PhD thesis would not have been possible without the experience, expert advice, inspiration, and guidance of others. In particular, I would like to thank my research advisor, Dr. Frederick Balagaddé, who has instilled a sense of excitement about microfluidics and the future. His guidance and support throughout the duration of this project proved invaluable. In particular, he has provided me with a new way of thinking that has had a significant impact on my project and life as a whole. For this, I am eternally grateful.

I am indebted to the members of the Bioengineering lab at AHRI for providing support and a stimulating environment for research. Our discussions and social activities have made this time in the lab thoroughly enjoyable, and were crucial for the success of this project. I would also like to thank my collaborators, Dr. Alissa Myrick and Dr. Erick Rubin for generously supplying us with the *E.coli* constructs and introducing me to the world of synthetic biology. In addition to this, I would like to acknowledge Dr. Al Leslie and Dr. Alex Sigal for providing thoughtful discussions and feedback that contributed to the evolution of this project.

Finally, I thank my family who have stood by me throughout. My sister Natalie has always been a great source of encouragement. Her dedication and attention to detail in her own work has been an inspiration to me, helping me to stay focused and perform every task to the best of my abilities. My uncle, Garry, has been a crucial support line throughout my life and academic studies. His guidance has proved invaluable and has contributed significantly to the man I am today. My wife, Katy, has brought a lot of joy to my life. She has helped me through many challenging times and has been an unwavering source of encouragement. Her support throughout my studies has played a significant role in getting me to this point. Without her, none of this would have been possible. Finally, I would like to thank my parents, William Mackenzie and Teresa Mackenzie, who have stood by me with unwavering love and support through my many years of studies. I am forever grateful for the sacrifices they have made and dedicate this thesis to them.

"Challenges are what make life interesting and overcoming them is what makes life meaningful."

–Joshua J. Marine

TABLE OF CONTENTS

Contents Page

ABBREVIATIONS

˚C	Degrees Celsius
ABC	ATP-binding cassette family
AHRI	Africa Health Research Institute
AIDS	Acquired immunodeficiency syndrome
ART	Antiretroviral treatment
BPER	Bacterial protein extraction reagent
CCCP	Carbonyl cyanide *m*-chlorophenyl hydrazone
CCD	Cooled charge coupled device camera
CSTR	Continuous stirred tank reactor
CURE	Current Research Seminar Series
DARPA	Defence Advanced Research Projects Agency
DST	Drug susceptibility testing
E.coli	*Escherichia coli*
EMB	Ethambutol
EtBr	Ethidium bromide
GFP	Green fluorescent protein
HAART	Highly active antiretroviral therapy
HIV	Human immunodeficiency virus
INH	Isoniazid
KatG	Catalase-peroxidase
LPA	Line probe assay
M. tuberculosis	*Mycobacterium tuberculosis*
mAGP	Mycolyl arabinogalactanpeptidoglycan complex

MATE	Multidrug and toxic compound efflux family
MDR	Multidrug resistant
MET	Multidrug endosomal transporter family
MFS	Major Facilitator family
MGIT	Mycobacteria growth indicator tubes
MIC	Minimum inhibitory concentration
MLSI	Microfluidic large scale integration
PAβN	Phenylalanine-arginine beta-naphthylamide
PDMS	Polydimethylsiloxane
PFS	Perfect focus system
pL	Picolitre
POA	Pyrazinoic acid
PZA	Pyrazinamide
PZase	Pyrazinamidase
QAC	Quaternary ammonium compounds
RIF	Rifampicin
RNA	Ribonucleic acid
RND	Resistance-nodulation cell division family
rpoB	β-subunit of ribonucleic acid polymerase
rpsA	Ribosomal protein S1
SMP	Small multidrug pumps
SMR	Small multidrug resistance family
SUG	Suppressor of *groEL* mutation proteins
TB	Tuberculosis
TDR	Totally drug resistant
UKZN	University of KwaZulu-Natal

WHO	World Health Organization
XDR	Extensively drug resistant
µm	Micrometre

LIST OF TABLES

Table Page

LIST OF FIGURES

Figure Page

PATENT

A provisional patent application has been filed at the South African Patent office based on some of the work presented in this thesis. The details of the patent are as follows:

Title of Invention:	Screening Method and Apparatus for Drug Efflux Displacement.
Official application number:	2016/07824
Full names of Inventors:	Jared Stuart Mackenzie
	Alissa Barbara Myrick
	Frederick Kiguli Balagaddé

Summary of the invention:

The invention provides a screening method to detect substrate displacement molecules. Instead of using efflux inhibitors to block the function of efflux pumps, the method and apparatus of the invention is configured to find non-toxic molecules that share substrate specificity with the efflux pumps. These molecules are selected for extrusion in preference to the drug molecules either because they have a higher affinity for the pump or they are present at much higher concentrations within the biological cell. In this way, there is no selection pressure for mutation as antibiotics are allowed to accumulate within the cells to active levels, thereby increasing treatment efficacy.

The process is preferably implemented on a microfluidic device (microchemostat) that is configured to be automated, allowing the process to run for extended periods of time, typically hundreds of hours. In such an implementation, individual efflux pumps can be studied in isolation, thereby ensuring pump results are isolated and not confounded. Individual pumps are studied using a bioengineering approach. Uncharacterised efflux pumps are isolated from a host biological cell and inserted into *E. coli* cells to "program" cellular behaviour for efflux.

ABSTRACT

Background: The *Mycobacterium tuberculosis* (*M. tuberculosis*) efflux system, estimated to comprise over 80 putative efflux pumps, represents a new frontier in the efforts to impede the ever-worsening spread of drug-resistant forms of Tuberculosis. By extruding specific drug molecules from within microbial cells, efflux pumps not only create low levels of resistance but can also facilitate progressive acquisition of chromosomal mutations that may confer higher levels of resistance. However, the field must confront the challenge of functional redundancy, which obscures the possible contributions of efflux pumps to drug resistance development.

Materials and Methods: To overcome the challenges of functional redundancy, we present a new bioengineering approach that involves expression of *M. tuberculosis* efflux pumps in transporter-deficient *E. coli* cells combined with high-resolution measurements of cellular changes using a microchemostat device.

Results and Discussion: Cells expressing the *M. tuberculosis* tap-like efflux pump Rv1258 had increased tolerance to growth-inhibiting compounds including streptomycin, gentamicin and ethidium bromide. Rv1258 expression engendered two alternating phenotypes in *E. coli* with distinct implications for drug tolerance. The first comprised of normal-sized, actively dividing cells with vibrant efflux activity, which can contribute to antibiotic resistance by extruding drug compounds. The second was characterized by arrested cell division and a filamentous cell phenotype, which are both phenotypes associated with the development of drug resistance in pathogenic bacteria. We present a new approach to characterizing efflux pumps, which can overcome the challenge of functional redundancy and will be generally applicable for understanding the interrelatedness among the transporters comprising the *M. tuberculosis* efflux system and elucidating its putative role in the evolution of drug resistance. Although the approach of engineering the expression of a single pump in *E. coli* does not require a microchemostat, characterization using the microchemostat was essential to revealing the alternating states of growth and dormancy.

DISSERTATION STRUCTURE

This dissertation is presented in the following order:

Chapter 1: Introduction

This chapter provides a brief overview of the HIV/TB epidemic and discusses TB disease. The various treatment regimens are also introduced, as well as the problem of drug resistance and the mechanisms associated with it.

Chapter 2: Current Developments for TB Diagnostics

Chapter 2 outlines the challenges associated with TB diagnosis, and outlines the phenotypic and genotypic methods currently in use.

Chapter 3: Microfluidics

This chapter is a detailed description of the field of microfluidics and its application in diagnostics. It discusses the various types of microfluidic approaches and provides a number of examples that have been used previously for the study of cellular biology.

Chapter 4: The Microchemostat

This chapter follows on from chapter 3 and introduces the microchemostat and the chemostat approach to continuous cell cultures. It provides a detailed description of the theory behind the chemostat, including benefits and drawbacks to its use. In addition to this, this chapter introduces the microchemostat as a solution to some of the drawbacks of conventional chemostats and the technology through which this study was made possible.

Chapter 5: A Microchemostat for the Study of *M. tuberculosis* Multidrug Efflux Pumps

Chapter 5 provides the rationale behind the project and outlines the research aims and objectives for the study.

Chapter 6: Microchemostat Characterization of Tap, a Putative Multidrug Efflux Pump Present in *Mycobacterium tuberculosis*.

This chapter consists of a manuscript submitted to the journal PLoS ONE that is currently under peer review. All information presented in this chapter (and manuscript) is presented in further detail throughout the remainder of this thesis.

Chapter 7: Materials and Methods

All activities undertaken throughout the study are discussed in this chapter. A description of all equipment, reagents and software is given, including the fabrication protocols for all microfluidic chips.

Chapter 8: Results

This chapter describes in detail how the microchemostat and *E.coli* expression systems were used to detect two distinct phenotypes associated with drug tolerance during expression of a multi-drug *M.tuberculosis* efflux pump that were not detectable using conventional methods.

Chapter 9: Discussion

This final chapter discusses the results obtained and the role of the microchemostat in obtaining these results. In particular, I explore the implications of the two phenotypes associated with drug tolerance within a TB disease context and current treatment options.

CHAPTER 1

1. Introduction

1.1 The HIV/AIDS Pandemic

In a few years, HIV/AIDS will eclipse the influenza pandemic of 1918 (also known as the Spanish Flu), to become "the deadliest emerging disease in recorded history"[1]. Since its discovery in 1983, HIV has been responsible for 35 million deaths worldwide, a number four times the number of deaths caused by World-War 1 [2,3]. This has created profound social and economic disruption in the disease-ravaged countries of sub-Saharan Africa.

The human immunodeficiency virus (HIV), the etiological agent of HIV/AIDS disease, is a retrovirus that can cripple the immune system through the destruction and gradual depletion of immune cells such as $CD4^+$ T cells and macrophages[4]. Treatment of HIV with highly active antiretroviral therapy (HAART) has led to the conversion of the disease from the virtual death sentence it was at the beginning of the outbreak to a manageable chronic illness, leading to a 36% decrease in HIV related deaths since 2010[2]. HAART involves the use of multiple antiretroviral drugs that target various steps of the HIV viral replication cycle to help suppress viral replication and accordingly, decrease the depletion of immune cells which in turn helps decrease the disease burden[5]. However, if left untreated, the HIV infection can progress to acquired immunodeficiency syndrome (AIDS), a condition associated with the progressive failure of the immune system that leaves the patient vulnerable to opportunistic infections and illness.

Opportunistic infections are responsible for the majority of AIDS-related deaths and are caused by organisms that would normally present with mild or no disease implications in healthy, immunocompetent individuals[6]. The most common of these infections include herpes simplex virus, *Pneumocystis carinii pneumonia* (pneumonia), *Toxoplasma gondii* (Toxoplasmosis), and *Mycobacterium tuberculosis. Mycobacterium tuberculosis (M. tuberculosis)*, the etiological agent of tuberculosis disease (TB), which was first described by Robert Koch in 1882[7], is regarded as the most important of these opportunistic infections and remains one of the deadliest curable infections the world has ever encountered[8]. This thesis will primarily focus on TB.

1.2 The HIV-Associated Tuberculosis Epidemic

HIV and *M. tuberculosis* infections are very closely related (Figure 1). Studies have shown that the risk of contracting active TB disease is 28 times greater when patients are infected with HIV[9]. African countries in particular have been hard hit by the HIV-TB epidemic (Figure 2). It is estimated that of the people living in Southern Africa with TB, 60-80% of these are coinfected with HIV[10]. The statistics below show the stark reality of the problem faced by developing countries around the world.

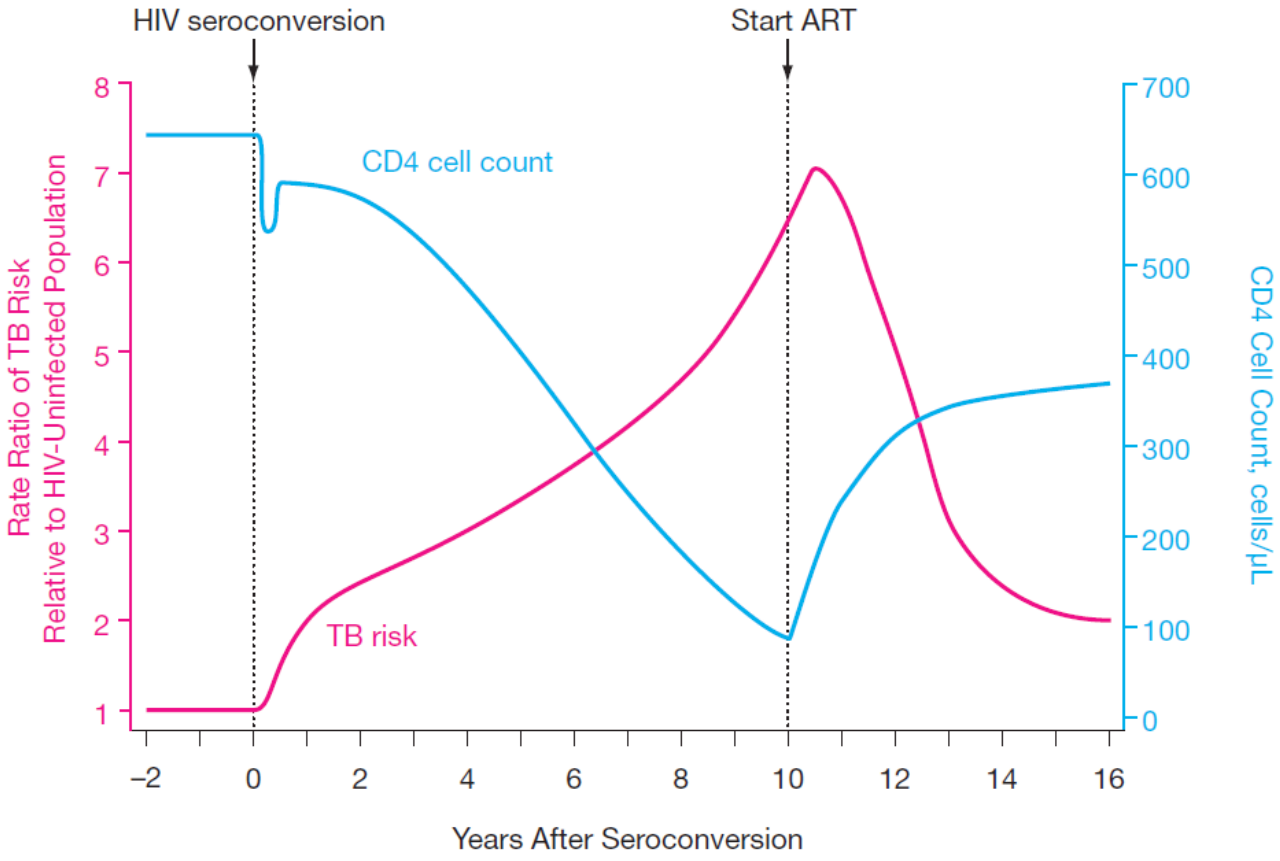

Figure 1| A schematic depicting the relationship between TB risk and CD4 cell count decline due to HIV infection. As the CD4 cell count decreases, the patient's immune system becomes compromised and is susceptible to opportunistic infections such as tuberculosis. This risk is reduced when the CD4 count increases following antiretroviral treatment (ART). Adapted from reference [11].

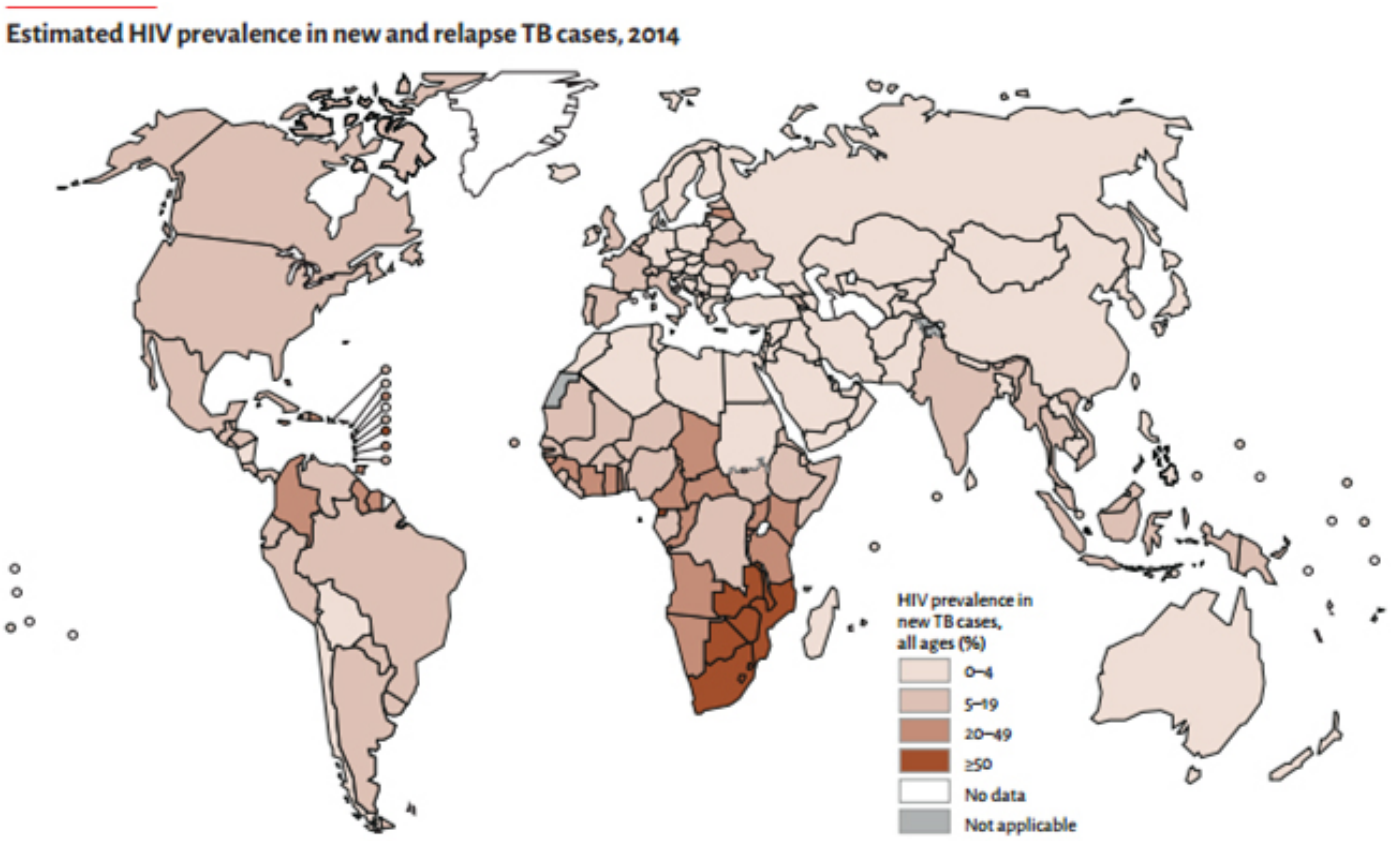

Figure 2| The estimated HIV prevalence in new and relapse TB cases around the world. The Southern African region has the highest prevalence, reaching levels greater than 50% in some cases. Adapted from reference [12].

1.3 Mycobacterium Tuberculosis, a Brief Introduction

"If anything kills 10 million people in the coming decades, it probably won't be a missile – it will be a microbe." – Quoting billionaire philanthropist and founder of Microsoft corporation, Bill Gates, as he summarized the potential devastating effects posed by infectious diseases.

Tuberculosis has been described by thought leaders in the field as the world's oldest and deadliest disease that has plagued mankind for most of human history[13]. Some have hypothesized that the genus *Mycobacterium* has been around for approximately 150 million years[14]. A study conducted by Gutierrez and colleagues at the Institut Pasteur located in Paris, France, found that an ancestor of *Mycobacterium tuberculosis* was present as early as 3 million years ago[15].

Tuberculosis spread rapidly during the industrial revolution in Europe, fuelled by the change in environmental conditions[16]. With no treatment options available, it spread uncontrolled across Europe for the next 400 years, eventually reaching sub-Saharan Africa [16].

In the early and mid 19th centuary, mortality rates due to TB began to decline slowly and continued to decline due to a number of factors including access to antibiotics and improved living conditions[13]. However, with the advent of the HIV/AIDS epidemic in the 1980s, TB had returned with full force by the early 1990s, leading to the World Health Organization (WHO) declaring it a global emergency in 1993 in an attempt to increase public and political awareness[17,18].

1.4 The Impact of Tuberculosis in South Africa

In 2013, the World Health Organization classified South Africa as having the third highest TB incidence globally, with an incidence rate that had increased by 400% since 2000[20]. It is the leading cause of death in South Africa with 13 of every 100 deaths attributed to the disease[19]. TB infection is widespread throughout South Africa. Most cases of active TB are located in the province of KwaZulu-Natal (31%). This is followed by the Eastern Cape (14%), Western Cape (14%) and Gauteng (13%)[21].

South Africa is faced with an HIV-TB syndemic, where the high rate of HIV infection is fuelling the TB epidemic. In 2007 an eye opening statistic was released showing that South Africa had 17% of the global HIV burden, with only 0.7% of the world's population[22]. The World Health Organization estimates that of the people living in South Africa with TB, 60% of these are coinfected with HIV.

The TB burden is also partly attributed to conditions of poverty that favour transmission of the disease. Many of the poorer communities within South Africa reside in informal settlements and make use of public transportation in the form of taxis and buses[23]. These are often poorly ventilated and encourage TB transmission as passengers are forced to sit in close proximity to each other with sub-optimal airflow, particularly in the winter months[23].

Often, the long distances required to travel to health care facilities also pose a major barrier to receiving diagnosis and treatment of the disease[23]. Many of these health care facilities are in the form of small crowded clinics where uninfected patients often wait in close proximity to TB patients in unventilated waiting rooms. This can increase the risk of transmission, as well as the risk of conversion to drug resistant TB.

1.5 Tuberculosis, The Disease

Tuberculosis disease can be divided into latent and active disease states. Patients who are latently infected present with no symptoms and more importantly, they are not infectious and are therefore unable to spread the disease and are thus considered to be disease free for all practical purposes[24]. In this case, the tubercular mycobacteria remain dormant, benign and controlled within the body. This type of TB infection can only be detected through performing a tuberculin skin test or a blood test. The tuberculin skin test consists of an intradermal injection that contains a small concentration of *M. tuberculosis* antigen. If the patient has previously been exposed to the bacteria, they will develop an induration at the site of injection within 48 to 72 hours.

One third of the world's population is said to be infected with TB. However, although the vast majority (~75%) of these infections are latent, with no symptoms, they remain a concern due to their potential to reactivate and form active tuberculosis[20].

Patients' presenting with latent TB infection can progress to active TB disease due to a number of reasons. The most common of these include a weakened immune system that is often observed in HIV patients or the elderly. Studies have shown that only 5 to 10% of infected patients will advance to active TB disease in their lifetime[24,25]. Patients with active tuberculosis present with a number of symptoms that include weight loss, fever, loss of appetite, fatigue and a persistent cough[24]. These patients are considered infectious and may be able to spread the disease to others. Currently, there are two threats to the management of TB — the HIV epidemic (as discussed previously), and the development of drug resistance[26].

1.6 The Treatment of Drug-Susceptible and Drug-Resistant Tuberculosis

Prior to the availability of anti- TB drugs, several treatment options were tried and tested with varying success. These included simple measures such as exposure to fresh air and sunlight, to more extreme measures such as the removal of ribs to collapse the chest wall[27-29]. However, many of these were abandoned after the introduction of antibiotics.

Drug resistant strains of *M. tuberculosis* were first recognized soon after introduction of the first anti-TB drug in the 1940s. Streptomycin was discovered by the laboratory of Selman Waksman, who accepted the Nobel Prize in 1952 and boldly claimed that it would lead to the elimination of "The great white plague" (Tuberculosis) [30]. However, within months, streptomycin resistant strains of *M. tuberculosis* were discovered[30]. This prompted the development of drug combination regimens in an effort to overcome drug resistance. Currently, the World Health Organization recommends the use of

the directly observed treatment short course strategy, or DOTS. This involves the use of a combination of drugs that are taken under the supervision of a health practitioner in order to help improve adherence and decrease the spread of TB[31].

Drug combinations offer a promising strategy for improving treatment efficacy and controlling resistance. Generally, when multiple antibiotics are combined into a single regimen, the effects may be synergistic or antagonistic. Synergistic combinations of drugs have been shown to reduce side effects, increase drug potency and help minimize the rate of evolution of multidrug resistant bacteria[32-34].

Today there are five groups of drugs that can be used for the treatment of TB, with the first new drug in 40 years, Bedaquiline, approved in 2012 (Table 1) [35,36]. Rifapentine was approved in 1998; however Bedaquiline is the first new drug with a novel mechanism of action to be approved in over four decades[37].

Table 1| Drugs with known action against *M.tuberculosis* and their respective groups[38].

Group	Drugs
Group 1: First-line , oral anti-TB agents	Isoniazid, Rifampicin, Ethambutol, Pyrazinamide
Group 2: Injectable anti-TB agents	Streptomycin, Kanamycin, Amikacin, Capreomycin
Group 3: Fluoroquinolones	Ciprofloxacin, Ofloxacin, Levofloxacin, Moxifloxacin, Gatifloxacin
Group 4: Oral second-line anti TB agents	Ethionomide, Prothionamide, Cycloserine, Terizidone, Para-aminosalicylic acid, Thioacetazone
Group 5: Agents with unclear role in treatment of drug resistant TB	Clofazimine, lenezolid, amoxicillin/clavulanate, Thioacetazone, impenem/cilastatin, high dose Isoniazid, Clarithromycin

1.7 The Management of Drug-Susceptible Tuberculosis

The activity of anti TB drugs is believed to occur in two phases—an early bactericidal phase and a later sterilizing phase[39]. During the bactericidal phase, drugs predominately kill actively growing *M. tuberculosis*. The sterilizing phase also begins early in the treatment regimen; however it continues for much longer than the first phase and is necessary to kill semi-dormant organisms[39]. A high level of early bactericidal activity seems to be associated with the ability to prevent the emergence of drug resistance, while a high level of sterilizing activity is necessary to shorten the duration of treatment[39].

Standard tuberculosis treatment normally takes 6 to 9 months to achieve complete killing and to ensure that there is no reoccurrence of infection[40]. The reason for this long treatment time is not completely understood. However, studies have shown that antibiotics can effectively kill the majority of bacilli during the first 14 days of treatment[41,42]. This lengthy treatment regimen is likely due to the presence of persister cells that form a subpopulation of phenotypically drug tolerant cells. Persisters are non-growing, dormant cells that do not grow in the presence of antibiotics but are able to regrow and form a population of cells that have the same susceptibility as the original population when the drug is withdrawn[8]. They are not affected by the majority of antibiotics as the pathways targeted by these drugs are inactive in dormant cells[8]. This long treatment duration associated with TB can lead to poor patient adherence and reduced patient follow-up, which in turn can increase the risk of developing multidrug-resistant and extensively drug–resistant strains[43].

High cure rates for drug susceptible *M. tuberculosis* can be achieved with treatment regimens consisting of the first line drugs isoniazid (INH), rifampicin (RIF), pyrazinamide (PZA), and ethambutol (EMB) (Figure 3). The standard regimen for susceptible *M. tuberculosis* includes a two-month "intensive" phase, where INH, RIF, PZA, and EMB are administered, followed by a four month "continuation" phase with only INH and RIF administered. Below I provide a brief discussion of each drug and its mechanism of action.

1.7.1 Isoniazid (INH)

Isoniazid (isonicotic acid hydrazide), one of the most effective and commonly used anti-TB drugs, has a high level of early bactericidal activity but only limited sterilizing activity[39]. As a result, there is limited activity against non-replicating bacteria or bacteria that grow under anaerobic conditions[43].

For many years, the mode of action for INH was unknown. Studies have since revealed that it is able to inhibit cell wall synthesis. INH is a prodrug that enters the bacteria through passive diffusion and is subsequently activated by catalase-peroxidase (KatG)[44]. Activation of INH leads to the production of

a range of free radicals that are toxic to the mycobacteria by damaging a variety of cellular components. Once activated, its primary target is InhA, a protein involved in the synthesis of mycolic acids that are essential for cell wall formation[44].

Resistance to INH normally occurs through mutations in the *katG* or *inhA* protein coding regions, with mutations in *katG* being the primary mechanism of resistance[44,45]. Although resistance may also arise due to mutations in several other genes such as *ndh, kasA* and the *oxyR-ahpC* intergenic region[44], studies have shown that 75% of the cases are due to mutations in *katG* and *inhA*[46]. For this reason, the majority of genetic drug susceptibility tests focus on detecting mutations in the *katG* gene, suggesting that as high as 25% of INH resistant cases may be missed by these tests[44].

1.7.2 Rifampicin (RIF)

Although rifamycin was first discovered in 1957, problems with absorption delayed the practical usefulness of the drug in clinical practice. In 1965, a hydrazone of a rifamycin B derivate, rifampicin, was discovered and found to be highly bactericidal and easily absorbed. The FDA eventually approved the drug for TB treatment in 1971[47].

The primary mechanism of action for RIF is through the binding of the β-subunit of ribonucleic acid polymerase (RpoB). This leads to the inhibition of transcription (RNA synthesis) and the subsequent death of the organism[48]. Significantly, RIF is able to target actively growing, as well as slowly metabolizing (non-growing) bacilli, which make it vital for shortening treatment duration[49]. Therefore, together with INH, rifampicin is one of the most potent drugs used in the treatment of TB.

Drug resistance to RIF normally occurs through mutations in the rpoB region, leading to decreased drug affinity and subsequent resistance[44]. Studies have shown that almost all RIF-resistant strains also present with resistance to other drugs, in particular, INH, thereby making it a good molecular marker for the detection of multi-drug resistance[44,50].

1.7.3 Pyrazinamide (PZA)

Pyrazinamide has been shown to have considerable sterilizing activity and is vital for shortening the TB treatment duration to 6 months[39,51]. This is due to its ability to target a persistent population of bacilli that are normally found within an acidic compartment in macrophages[39].

Despite its vital role in the current treatment regimen and its discovery over 50 years ago, its method of action is still poorly understood[52]. PZA is an analog of nicotinamide, and is a prodrug that becomes activated by pyrazinamidase (PZase) once it enters the cell through passive diffusion[53]. This leads to the formation of pyrazinoic acid (POA). POA is pumped to the outside of the cell through the action of a weak efflux pump, where it becomes protonated[54]. Under acidic conditions, these protonated POA molecules are able to diffuse through the membrane back into the cell where they accumulate, thereby affecting the proton gradient, reducing membrane potential, and causing cellular damage[54]. The target of POA in *M. tuberculosis* remains unknown; however it has been shown to bind to ribosomal protein S1 (RspA), leading to the inhibition of *trans*-translation[51].

Pyrazinamide resistance mainly occurs through loss of PZase activity due to mutations in the *pncA* gene that encodes this enzyme[52]. However, mutations in the *rspA* gene that encodes for RspA, can also confer PZA resistance. Resistant strains have been found that contain no mutations in *pncA* or its promoter, suggesting alternate mechanisms of resistance such as enhanced efflux.

1.7.4 Ethambutol (EMB)

Ethambutol was first used as a TB drug in 1966 and has been shown to be effective against actively growing bacilli[53]. It mainly acts through interfering with cell wall biosynthesis, in particular the synthesis of arabinogalactan[55]. EMB targets Arabinosyltransferase, the enzyme involved in arabinogalactan synthesis.

EMB resistance in *M. tuberculosis* has been shown to be associated with mutations in the *emb*CAB 10kbp operon. A study conducted by Telenti *et al.* showed that 50% of EMB resistant clinical isolates presented with mutations in codon 306 of *emb*B[56]. However, this mutation has also been observed in EMB susceptible isolates. The observation that there are many EMB resistant clinical isolates that do not possess mutations in *emb*B suggests that, like PZA, there must be alternate mechanisms of resistance[53].

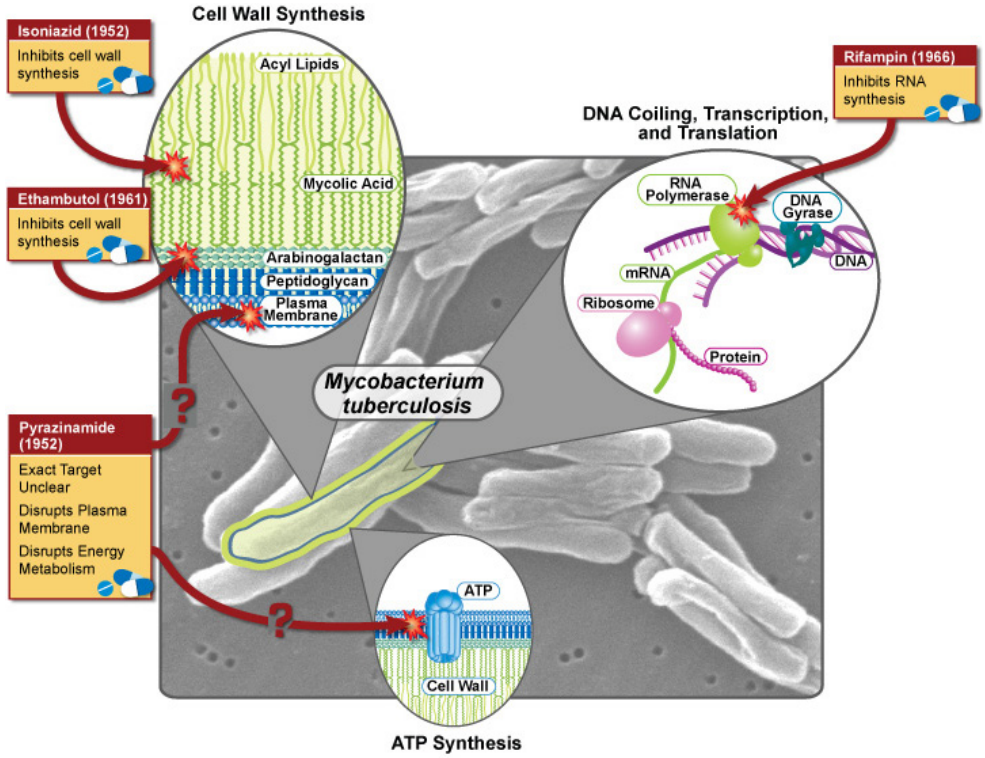

Figure 3| The various mechanisms of action for the most potent TB drugs used as the first line of treatment for patients. Adapted from reference [57].

1.8 Combating Drug-Resistant Tuberculosis

The first anti-TB drug, streptomycin, was introduced into clinical practice in the 1940s. Although it was the miracle drug of the time, resistance was observed within months of its inception by Marjorie Pyle in 1947[58]. Since this discovery, countless clinical *M. tuberculosis* isolates have been found to have resistance to many of the drugs used in TB treatment. As previously discussed, this resulted in a transition from monotherapy to the use of drug combination regimens in an effort to eliminate resistance.

A number of other solutions have been proposed to resolve the problem of monotherapy resistance. One of the most popular for HIV infected individuals include pre-exposure prophylaxis through the use of INH[59]. A previous study showed that a 6-12 month course of INH can provide up to 90% protection from *M. tuberculosis* infection[60]. This study made the World Health Organization take notice of the potential benefits of pre-exposure prophylaxis and in 1998 caused them to recommend the use of INH as a form of preventative therapy[59]. However, continued exposure to INH could in fact exacerbate the problem, leading to the development of drug resistant mutations.

Drug resistance represents a significant global health problem that threatens the progress made over the last 50 years in TB care worldwide. A patient can either present with primary resistance (infection with an already resistant strain), or develop acquired resistance (resistance due to poor adherence)[61]. This resistance may be to a number of different drugs and can lead to the disease being classified as either multidrug resistant tuberculosis (MDR- TB) or extensively drug resistant tuberculosis (XDR-TB).

1.8.1 Multidrug Resistant Tuberculosis (MDR-TB)

Multidrug resistant TB is caused by *M. tuberculosis* isolates resistant to RIF and INH, the two most potent anti-TB drugs. In 2014, an estimated 5% of the people who contracted TB presented with MDR-TB, with an estimated 190 000 deaths worldwide caused by the disease [62,63].

The cure rate for this disease is incredibly poor, with statistics showing that half of MDR patients will die due to the illness[62]. This form of TB is notoriously difficult to treat and normally takes 2 years or longer to achieve a cure. The treatment regimen relies on the use of second-line drugs (such as fluoroquinolones and injectable aminoglycosides) that are less effective, more toxic, and far more costly[64]. The standard MDR-TB regimen consists of 8 months of pyrazinamide, kanamycin, ofloxacin, prothiomide and cycloserine followed by 12 months of ofloxacin, prothiomide and cycloserine[65]. Recently, Bedaquiline has also been approved as part of combination therapy in adults for the treatment of MDR-TB[37].

1.8.2 Extensively Drug-Resistant Tuberculosis (XDR-TB)

The acquisition of resistance to second-line drugs often used in the treatment of MDR-TB defines extensively drug-resistant (XDR) TB[66]. More specifically, XDR-TB is defined as resistance to INH and RIF, as well as any fluoroquinolone and at least one of the injectable drugs (kanamycin, amikacin, capreomycin, streptomycin etc.)[62]. This form of resistance has emerged due to poor management of MDR-TB and cases have now been reported in more than 50% of countries worldwide[62]. It is estimated that 9.7% of people presenting with MDR-TB in fact have XDR-TB[62]

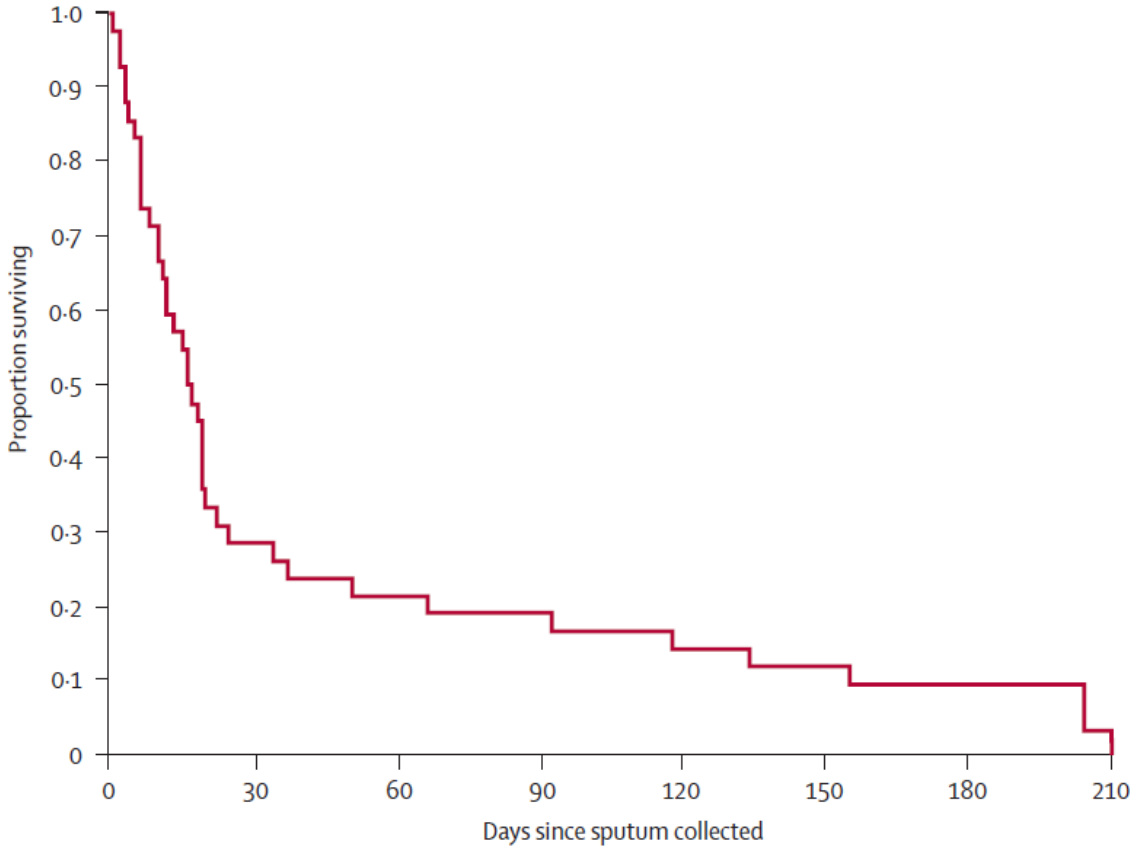

Figure 4| Survival rate of HIV infected XDR-TB patients after sputum collection at a clinic in Tugela Ferry, KwaZulu Natal, South Africa. Adapted from reference[68].

Substantial morbidity and mortality has been associated with co-infection of XDR-TB with HIV. The seriousness of this association became clear in 2006 during the Tugela Ferry outbreak in KwaZulu Natal, South Africa, where 52 of the 53 patients presenting with XDR-TB and HIV succumbed to their illness (Figure 4)[67]. Shockingly, the median time of death from sputum collection was shown to be only 16 days[30,67].

As with MDR-TB, treatment of XDR-TB is extremely expensive, toxic and less effective compared to treatment of susceptible TB. Despite these high costs, clinical outcomes remain poor, particularly in South Africa where the treatment success rate for XDR patients is less than 20%[69]. Treatment regimens are normally different for each patient based on results from drug susceptibility testing (DST) and may incorporate group 5 drugs in cases where resistance is found to all four second line drugs. Unfortunately, in many resource-limited countries, drug susceptibility testing is faced with many difficulties which can lead to the development of further acquired resistance[30].

1.8.3 Totally Drug-Resistant Tuberculosis (TDR-TB)

XDR-TB is not where the problem ends. Ten years ago, the first cases of totally drug resistant (TDR) TB were reported in Italy where two patients were shown to be resistant to all drugs tested[70]. Totally drug resistant TB is defined as resistance to all first and second line drugs, making it almost impossible to treat[71]. This form of TB has now been found around the world, and its rising prevalence threatens to push us back into a pre-antibiotic era.

The emergence of TDR-TB illustrates the rapid rate at which mycobacteria can develop resistance to drugs available in clinical practice. It is clear that the rate of development of new drugs is not keeping up with the development of resistance. In fact, resistance has already been found to Bedaquiline, the first new TB drug in over 40 years [72]. As a result, the various mechanisms of resistance have now become an important research topic and need to be understood in order to restore drug efficacy.

1.9 Mechanisms of Resistance

Drug resistance in *M. tuberculosis* can occur through multiple mechanisms and is often due to multiple mechanisms acting simultaneously[73]. These mechanisms of resistance can be divided into acquired (or genetic) resistance and intrinsic (or epigenetic) resistance.

1.9.1 Acquired Resistance

Acquired resistance is the main form through which resistance develops and normally occurs through spontaneous mutations that can interfere with drug target binding, compromise prodrug activation, or cause overexpression of the target. The two most powerful anti-TB drugs, RIF and INH, have been rendered useless in countless TB isolates through a number of these mechanisms.

The most common form of resistance to RIF normally occurs through mutations in the rpoB protein-coding region of the genome, thereby interfering with drug target binding[48]. INH is a prodrug that enters the bacteria through passive diffusion and is subsequently activated by catalase-peroxidase (KatG). Following activation, its main target is inhA, a protein involved in the synthesis of mycolic acids[44]. Although mutations in KatG are the primary mechanisms of INH resistance, mutations can also develop in the promoter region of inhA, resulting in overexpression of inhA and subsequent resistance[44,45].

These spontaneous mutations can occur as a result of low adherence to treatment, inadequacy of the drug regimen, and patient-dependent pharmacodynamic and pharmacokinetic properties of the drugs

administered[64]. Low adherence is particularly common in resource-limited settings where patients often have to travel great distances in order to obtain medication.

Acquired resistance is normally detected through the use of genetic tools such as the line probe assay (LPA), GeneExpert and DNA sequencing. I elaborate further on these tools in chapter 2.

Although the presence of mutations accounts for the vast majority of resistant isolates, studies have shown that there is a high prevalence of drug-resistant clinical isolates that do not harbour mutations in known resistance genes—reaching 30% in some contexts[66]. For example, 75% of INH resistant cases have been found to be due to mutations in KatG and inhA, suggesting that 25% of these cases present with alternate mechanisms of resistance[44]. Similar findings have been seen for PZA, where resistant strains present with no mutations in the *pncA* gene or its promoter[52]. This is strong motivation for new areas of research into epigenetic determinants of drug resistance (intrinsic resistance).

1.9.2 Intrinsic Resistance

Intrinsic resistance is another form of resistance that is not acquired through spontaneous mutations, and instead makes use of physiological attributes that the bacteria naturally possess.

A distinctive attribute of pathogenic mycobacteria is their slow growth rate. They have a relatively long doubling time of 18 to 24 hours depending on the growth conditions, a doubling time ~100 times slower than the fastest growing bacteria ever found, *Clostridium perfringens* that divides every 12 minutes[74-76]. It has been speculated that this slow growth rate is associated with the pathogenesis of the mycobacteria, as non-pathogenic species generally grow at a much faster rate. Antimycobacterial drugs generally act by targeting cell division and as a result, a slow microbial growth rate may decrease their potency. The mechanisms behind this slow growth rate are currently unknown. However, studies suggest that mycobacteria present with limited RNA synthesis which may be able to explain their slow growth[77,78].

M. tuberculosis is naturally resistant to many antimicrobials due to its unique, highly impermeable cell wall (Figure 5)[79]. This cell wall is rich in mycolic acids that are linked to arabinogalactan (arabinan and galactan), ultimately forming the mycolyl arabinogalactanpeptidoglycan complex (mAGP)[79,80]. The outer part of the cell wall is fairly complex and is composed of free lipids, glycolipids and glycoproteins[80]. These glycoproteins are rich in fatty acids that, along with mycolic acids, provide the mycobacteria with a growth and survival advantage. They allow for an

impermeable outer membrane, extreme hydrophobicity and acid-fastness. They also provide protection against harsh, stressful environments as well as a great variety of antimicrobial agents[81]. However, if antibiotics are able to overcome the obstacles posed by the cell wall, their potency can be reduced through a number of intracellular processes.

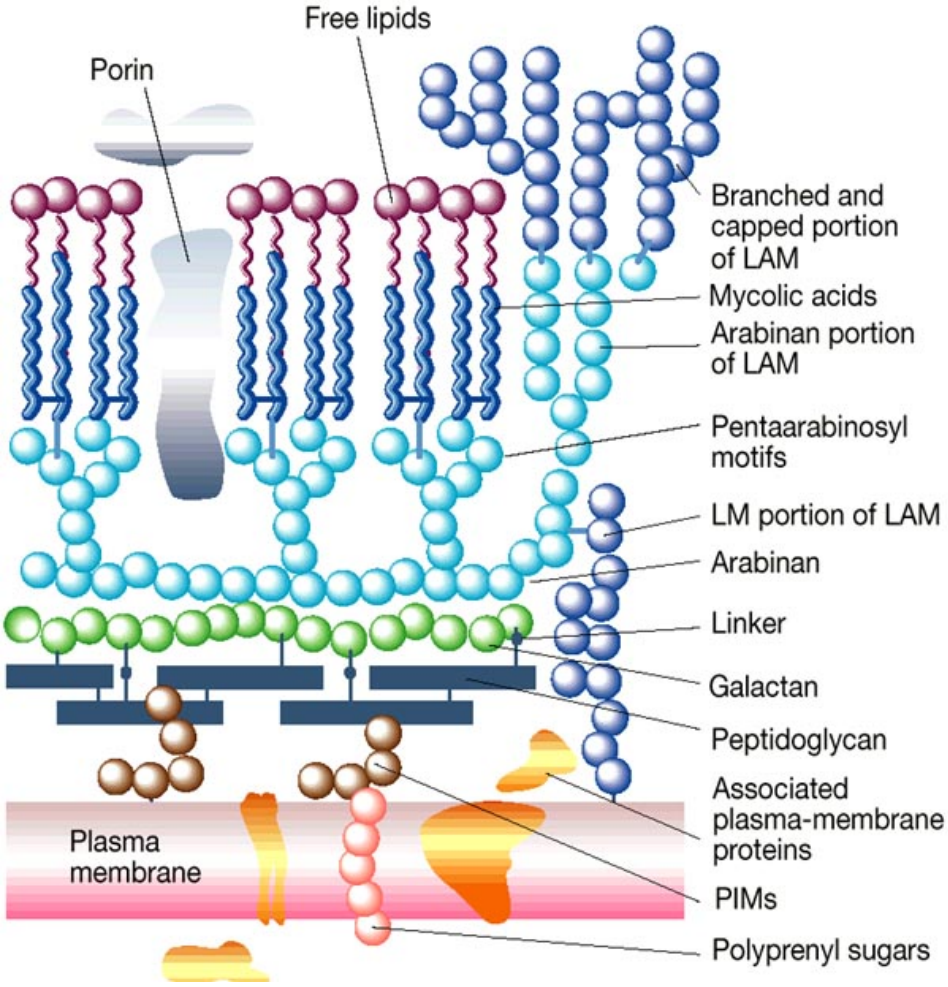

Figure 5| Schematic of the highly impermeable mycobacterial cell wall. Adapted from reference [82].

Drug extrusion through the action of efflux pumps is another mechanism employed by bacteria to develop resistance or tolerance to many antimicrobials, even acting as a precursor to the development of spontaneous mutations[79]. As a result, efflux pumps have now come into focus as a key factor influencing the rate of the evolution of resistance to antibiotics. This thesis explores mycobacterial efflux pumps, which I introduce in more detail in the next section.

1.10 Efflux Pumps as Drug Resistance Mechanisms

Efflux pumps are transport proteins that are known to be present in all organisms and are responsible for moving substances out of a cell[83]. In bacteria, the genes that encode these transport proteins can be found on the chromosome or on plasmids[84]. These pumps have a number of physiological functions that include extruding natural substrates such as spermidine in *Bacillus subtilis* and bile salts in *Escherichia coli (E.coli)*[85,86]. In this way, efflux pumps help to maintain homeostasis within the intracellular environment and enable microorganisms to adapt to biochemically hostile conditions[87]. Individual efflux pumps differ in terms of substrate specificity and energy coupling mechanisms, thereby making their characterization incredibly difficult[88]. Although information regarding their natural substrates is poor, studies have shown that efflux pumps are able to extrude antibiotics and other chemotherapeutic agents, thereby contributing to the problem of drug resistance[89].

Efflux mediated antimicrobial resistance was first described in *E.coli* in 1980 by the labs of Ian Chopra and Stuart Levy from the University of Bristol and the Tufts University School of Medicine respectively. These studies showed that an active efflux system was able to induce resistance to tetracycline[90,91]. Multi-drug efflux pumps are naturally found in wild-type bacterial cells but can be induced or upregulated through mutations or through the addition of antibiotics[64]. Active efflux has been shown to infer an important survival advantage by reducing intracellular levels of antibiotics. This in turn can lead to bacterial survival under sub-lethal concentrations of antibiotics for a long period of time, providing favourable conditions for the development and accumulation of drug resistance mutations[8,89]. This process may also be exacerbated by the presence of pumps with overlapping substrate specificities, allowing the drug to be extruded by multiple different pumps.

Multidrug efflux systems have been classified into five superfamilies based on a number of factors that include the energy source used, the number of components of the pump and the substrate specificity (Figure 6). These families include the ATP-binding cassette family (ABC), major facilitator family (MFS), resistance-nodulation cell division family (RND), the small multidrug resistance family (SMR) and the multidrug and toxic compound efflux family (MATE)[84,88]. All of these superfamilies can be found in prokaryotic microorganisms, whilst other families, such as the multidrug endosomal transporter family (MET), have only been found in eukaryotes[75]. Below I provide a brief description of each of these families.

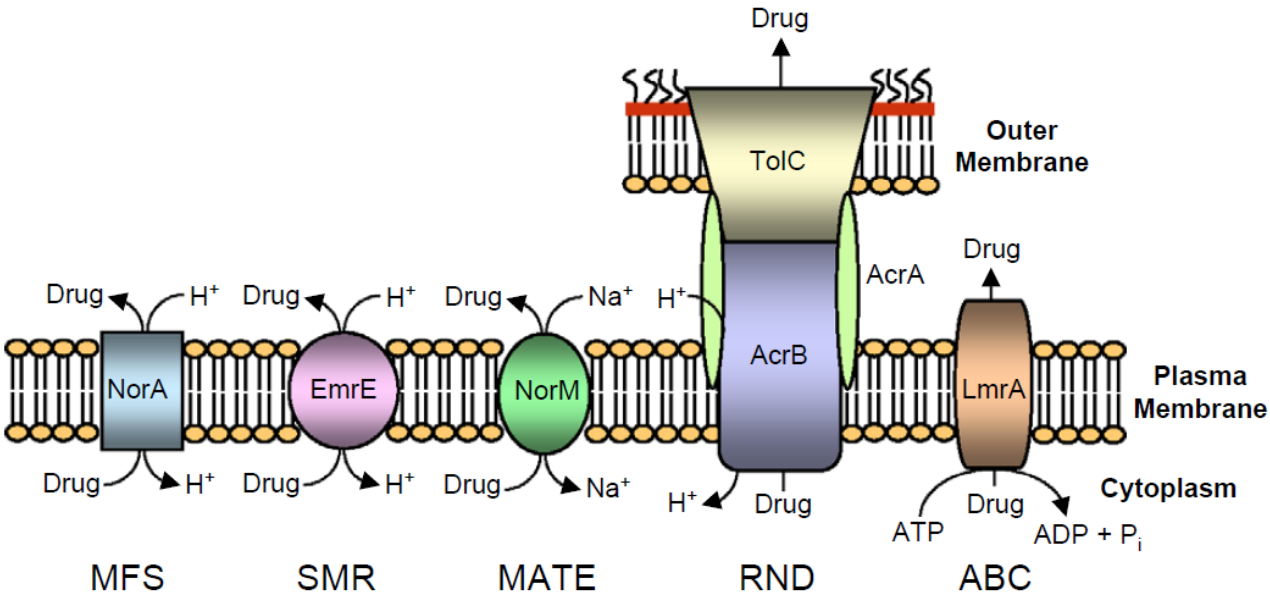

Figure 6| A schematic illustrating the five major efflux families found in microorganisms, including example transporters and their method of action. These transporters include *Staphylococcus aureus* NorA, *Escherichia coli* EmrE, *Vibrio parahaemolyticus* NorM, *Escherichia coli* AcrAB–TolC, and *Lactococcus lactis* LmrA. Adapted from reference [92].

1.10.1 ATP-Binding Cassette Superfamily (ABC)

The ABC superfamily of transporters are classified as primary transporters and are one of the largest and oldest families, consisting of 52 subfamilies that are divided into influx and efflux systems[93]. They are active transporters, capable of transporting both small molecules and macromolecules[94]. These include the transport of a wide range of substrates such as drugs, sugars, amino acids and peptides[93]. As their name suggests, this group primarily utilizes energy obtained through the hydrolysis of ATP for the efflux process, thereby explaining their classification as primary transporters[95]. ABC transporters are essential in humans for many physiological processes within the cell[96]. Mutations in the ABC genes have been shown to contribute to the development of a number of human genetic diseases that include cystic fibrosis, retinal degeneration, and cholesterol and bile transport defects[96].

1.10.2 Major Facilitator Superfamily (MFS)

Unlike the ABC superfamily, the MFS family are classified as secondary transporters as they make use of a proton gradient antiporter mechanism to extrude substrates instead of ATP[87,93]. This group of

transporters is typically made up of 400 amino acids that are arranged to allow either 12 or 14 membrane spanning helices[94,95]. This group of secondary transporters are only able to transport small solutes such as simple sugars, amino acids and some drugs through the use of chemiosmotic ion gradients[94].

1.10.3 Resistance-Nodulation Cell Division Family (RND)

The MFS and RND families are similar in that they both make use of proton motive force for the efflux process and are secondary transporters[93]. However, RND transporters are normally much larger, consisting of approximately 1000 amino acid residues, and they possess large periplasmic domains[95]. This group of efflux pumps consist of a transporter protein located in the cytoplasm, an accessory protein located in the periplasmic space, and an outer membrane channel to allow transport across the inner and outer membranes of gram negative bacteria[84,97,98]. One of the most well known RND transporter systems is the *E. coli* AcrABTolC system that has been extensively studied for its role in exporting xenobiotics through this hierarchical export system[99].

1.10.4 Small Multidrug Resistance Family (SMR)

The SMR family, a group of secondary transporters, is the smallest family, normally comprising of 100 to 140 amino acids and four alpha-helices[95,100]. Functionally, they are very similar to the MFS and RND families, relying on proton motive force for the efflux process[95]. This family has only been shown to transport lipophilic compounds. These primarily include quaternary ammonium compounds (QAC) and a number of antibiotics[100]. However, not all SMR proteins are involved in drug efflux. For this reason, they have been divided into two classes based on their phenotype, namely small multidrug pumps (SMP) and suppressor of *groEL* mutation proteins (SUG)[100].

1.10.5 Multidrug and Toxic Compound Efflux Family (MATE)

The MATE family are similar to MFS transporters in that they are composed of 450 amino acids and are secondary transporters[95]. They are also arranged into 12 helices, but do not appear to have any sequence similarity to MFS transporters. The first MATE transporter categorized in 1998 was NorM, a transporter capable of inducing resistance to norfloxacin, ethidium bromide (EtBr) and certain aminoglycosides[101]. This family utilizes the Na^+ gradient as an energy source for efflux (Figure 6)[92]. However, MATE transporters are mostly found in *E.coli* and have not yet been reported in mycobacteria[93].

1.11. The Tuberculosis Efflux System

The *M. tuberculosis* efflux system is estimated to comprise over 80 putative primary and secondary transport proteins that must be explored for their respective substrate spectra, potential contribution to multidrug resistance and role in the basic biology of the bacterium[102]. While many of these transport systems have functional homology to proteins in other bacteria, their function and role in *M. tuberculosis* has not been elucidated[103,104]. As a result, mycobacterial transport proteins (or efflux pumps) have now come into focus as a key factor influencing the rate of the evolution of resistance to antibiotics[105,106].

The first mycobacterial efflux pump to be characterized was LfrA, a pump found in *Mycobacterium smegmatis*[109]. It was found that activation of this pump confers low level resistance to fluoroquinolones, ethidium bromide (EtBr) and acridine[93,109]. This identification triggered substantial interest towards the contribution of efflux pumps in TB drug resistance.

Many studies have focused on the effect of efflux pumps on the first-line TB drugs in particular. Efflux action has been proposed to be responsible for tolerance to INH, one of the most potent anti-TB drugs currently used[89]. This tolerance is said to be mediated by IniA, the isoniazid-induced protein[110]. The mmpl7 gene was also found to upregulate an RND transporter that can confer resistance to INH[93].

Studies have shown that efflux can induce cross resistance in TB, whereby treatment with one drug may induce resistance to another through upregulation of an efflux protein[89,111]. For example, a study conducted by Louw and colleagues showed that RIF treatment of an already RIF-resistant strain of *M. tuberculosis* can lead to resistance to ofloxacin[106]. This appeared to be induced through an efflux related mechanism as the effects could be reversed through the addition of an efflux pump inhibitor[106].

Some other important efflux pumps that have demonstrated a role in TB drug resistance include the P55 transporter shown to induce resistance to streptomycin and tetracycline, and the mmr protein of the SMR transporter family, shown to cause resistance to acriflavine, ethidium bromide and erythromycin[93].

TetV and Rv1258—an *in vitro* essential tap-like efflux pump—were both found to confer resistance to tetracycline, while the latter also conferred resistance to aminoglycosides[112,113]. Expression of Rv1258 was also found to be induced through the administration of rifampicin and ofloxacin[87,93]. The expression of Rv1258 has been shown to occur through the activation of the transcriptional regulator

WhiB7 in response to sub-inhibitory concentrations of antibiotics[114-116]. Similar results were obtained in a study conducted by Jiang and colleagues at the Shanghai University of Traditional Chinese Medicine in 2008, who found that in an MDR TB isolate, Rv1258 expression was significantly increased in the presence of RIF or INH[117].

Rv1258 is a secondary transporter that belongs to the MFS family of efflux pumps. Apart from addition of rifampicin, ofloxacin or isoniazid, this efflux pump was also found to be induced following engulfment by macrophages[118]. Within the macrophage, Rv1258 acts as a virulence factor and has been shown to confer tolerance to RIF[119,120]. In the absence of antibiotics, it has been shown to play a role in the promotion of intracellular growth of *M. tuberculosis*[119]. As a result, Rv1258 represents a particularly important multidrug efflux pump that not only contributes to drug resistance, but also promotes growth of the mycobacterium. These characteristics have brought about much interest surrounding this transporter. Therefore, the main focus of this thesis will be on the characterization of the Rv1258 efflux pump.

Conventionally *M. tuberculosis* efflux pumps are studied through the use of efflux protein knockouts. However, the few experimental demonstrations published to date have underscored the daunting inadequacies of this approach, primarily due to the coexistence of multiple efflux pumps with overlapping substrate specificity and functional redundancy. Inactivation of a specific efflux pump may not yield the expected changes in resistance to an antibiotic drug known to be extruded by the pump due to compensatory overexpression by other efflux pumps with overlapping functionality[107,108]. In theory, all efflux pumps that can extrude the antibiotic would have to be inactivated simultaneously to obtain the desired effect.

Intrinsic resistance is detected through phenotypic assays, whereby mycobacteria are grown in the presence of a drug. Culture based methods are the gold standard in today's clinics and are vital for the early detection of disease. Reliable drug susceptibility tests are required to help prevent further spread of drug resistant strains within communities, and can prevent further acquisition of resistance through inappropriate treatment strategies.

CHAPTER 2

2. Current Developments for Tuberculosis Diagnostics

Early diagnosis and detection of drug-resistant cases through drug susceptibility testing is essential for the management and global control of TB disease. Conversely, the absence of proper diagnostic systems can lead to low case detection rates, increased risk of transmission and the spread of drug-resistant strains.

There are several challenges to the timely diagnosis of TB, with studies showing that current case detection rates are very low. In 2005, a global target was set by the World Health Organization to identify 70% of new smear-positive TB cases[121]. However, 9 years later, this goal had not been met, when in 2014 it was reported that only 63% of new TB cases were diagnosed[62]. This suggests that there are close to 3.6 million people with undiagnosed and accordingly, untreated TB. Even more worrying is the fact that a percentage of these may present with MDR or even XDR-TB. However, this is not where the problem ends. Even when all cases are diagnosed, drug resistant tests are not routinely carried out in most cases and it is only after treatment failure that drug resistant tests are performed. This fuels the spread of drug resistance and reinforces the need for rapid and reliable drug susceptibility tests.

There are currently a number of methods used for the diagnosis of drug susceptible and drug resistant TB. These are generally categorized into phenotypic and genotypic testing methods or assays. Phenotypic assays are considered the gold standard, and normally involve growing the mycobacteria in liquid or solid media containing anti-mycobacterial drugs to determine their drug susceptibility[122]. However, as this method relies on mycobacterial growth, and given the long doubling time of *M. tuberculosis* of about 18 hours, the turnaround time of phenotypic tests can require as long as two months. Genotypic methods involve the detection of known drug resistance associated mutations in the *M. tuberculosis* genome. These methods are often rapid and sufficiently accurate. However, they can be extremely expensive, and can only be used to detect resistance, but not susceptibility[123]. This is one major short-fall of these methods as often *M. tuberculosis* strains present with resistance whilst presenting with no mutations in the mycobacterial genome. For the purpose of providing a contextual background for this thesis, I shall briefly discuss a number of the most popular phenotypic and genotypic methods below.

2.1 Phenotypic Methods for the Diagnosis of Tuberculosis

2.1.1 Sputum Smear Microscopy

Sputum smear microscopy is by far the most commonly used method in resource-limited settings. It relies on the detection of bacilli using simple lab equipment and can be performed quickly and at minimal cost to the patient[124]. This makes it highly attractive to developing countries where the TB burden is often the highest[124]. In order to detect mycobacteria from sputum, the most common methods include the use of the carbo fuchsin Zeihl-Neelsen stain or the auramine stain.

In the 19th century, Robert Koch developed a number of ground-breaking techniques to diagnose bacterial infections. Several other researchers subsequently improved on his methods. These include Paul Ehrlich, who developed the haematoxylin stain in 1886, which was modified by a bacteriologist known as Franz Ziehl. Subsequently, a pathologist named Friedrich Neelsen changed the primary stain to fuchsin. By the 1980s, this method had become known as the Ziehl–Neelsen method[125].

Carbol fuchsin Zeihl-Neelsen staining is often used for identification of acid-fast bacilli[124]. This process involves the incubation of a sputum-smeared slide in the stain for 3 minutes, following which, the stain is rinsed and decolourized and a methylene blue solution is added. The mycobacteria are able to withstand the decolourization process and absorb the carbol fuchsin dye. This makes them appear red to purple when observed using a conventional light microscope (Figure 7)[124].

Mycobacteria can also be detected by fluorescence. Auramine, a fluorochrome dye, is added to the sputum sample, where it binds to the mycolic acid cell wall of the mycobacteria and is subsequently detected through the use of a fluorescent microscope (Figure 8)[124]. Auramine has a number of benefits over Ziehl-Nelsen staining, such as increased sensitivity. However, it is more expensive and less specific[124].

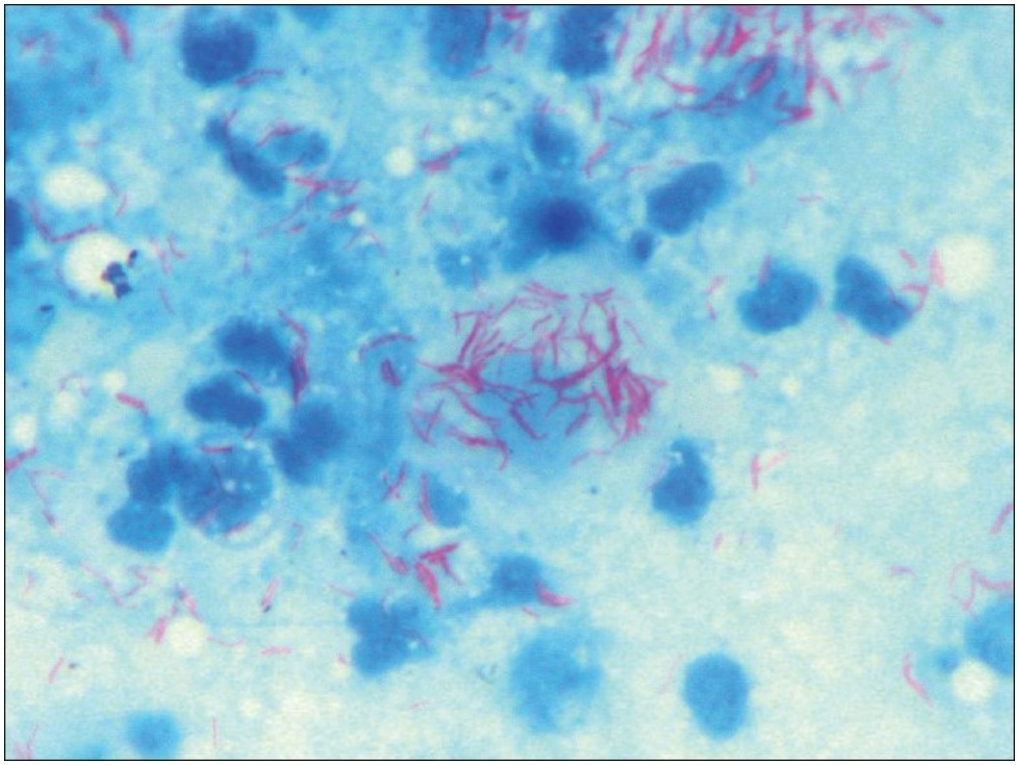

Figure 7| *M. tuberculosis* stained red/purple with the Zeihl-Neelsen stain and viewed under a conventional light microscope. Adapted from reference [126].

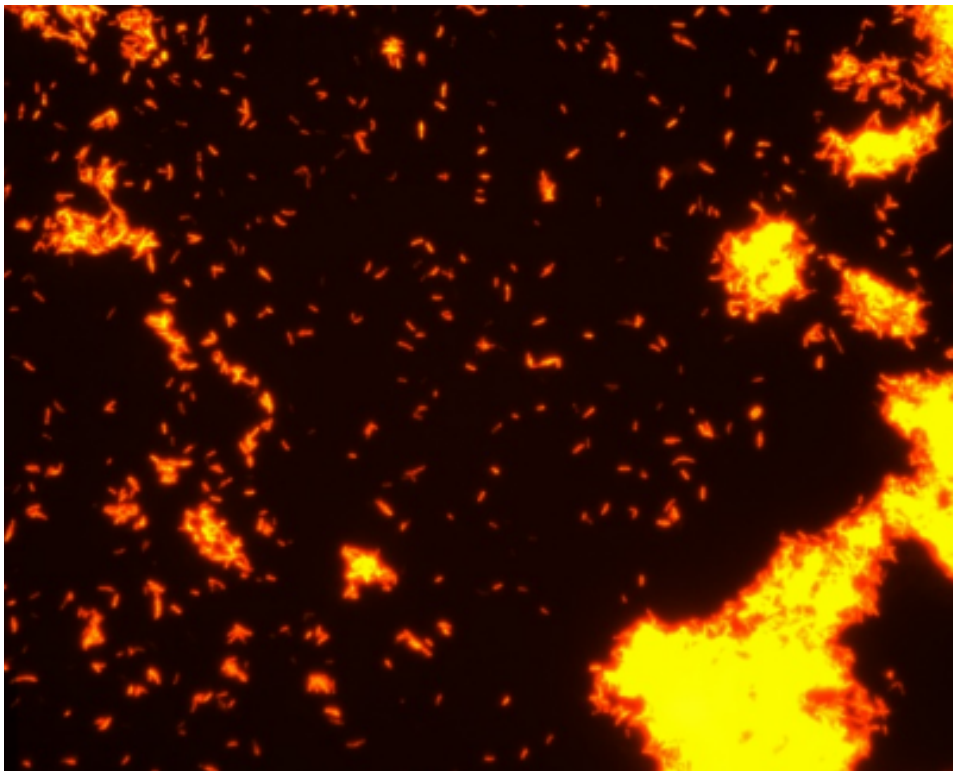

Figure 8| *M. tuberculosis* stained with fluorescent auramine stain and viewed under a fluorescent microscope. Adapted from reference [127].

The detection of *M.tuberculosis* through the use of sputum offers a number of challenges. The low sensitivity (60%) of this test suggests that a number of patients are going undiagnosed. This sensitivity is further decreased (43-51%) in HIV infected patients and paediatric TB patients, where obtaining adequate sputum samples is often challenging[128]. As a result, sputum smear microscopy is often paired with a chest X-ray when patients are presenting with TB like symptoms but sputum smear results are negative.

2.1.2 The Culture Based Method

Culture based methods are conventionally used following an initial diagnosis in order to determine drug susceptibility of the *M. tuberculosis* strain. This is one advantage over sputum smear microscopy which is unable to detect susceptibility. Conventionally, this method is divided into three different variations that all involve the culture of *M tuberculosis* in the presence of a drug at a certain concentration. The three variations include the proportion method, the absolute concentration method and the resistance ratio method. These were all first described in 1963 by a French microbiologist, Georges Canetti, who was also the first to report *Mycobacterium canetti*[129].

The proportion method is regarded as the most widely used culture based method and involves several dilutions of the culture which are inoculated onto drug free and drug containing media[130]. Growth of mycobacteria in the various dilutions is then compared. If a proportion greater than 1% of the TB population is able to grow in the presence of a drug, the strain is deemed resistant[131].

The absolute concentration method is similar to the proportion method in that mycobacteria are inoculated on agar plates both with and without drugs. However, a number of different drug concentrations are used in order to determine the concentration at which growth is inhibited. This concentration is compared to the minimum inhibitory concentration (MIC), and if greater, the strain is classified as resistant[131].

The resistance ratio method is distinguished from the previous two methods as it compares the resistance of a clinical strain to a laboratory strain such as H37Rv[132]. Each strain is grown in the presence of a drug and the MIC determined. The resistance ratio is then calculated by dividing the MIC of the clinical strain by that of the lab strain. If the ratio is 8 or more, the strain is considered resistant[132].

Culture based methods are the gold standard for drug susceptibility testing. They provide a number of advantages such as being more reliable than sputum smear microscopy, they are inexpensive, and no specialised equipment is required. However, the major drawback to this approach is the long turn-

around time. The slow growth rate of *M. tuberculosis* means that results can only be obtained in three weeks to a month. For this reason, many researchers have adopted a number of alternate approaches to detect TB and drug resistant strains.

2.1.3 The BACTEC MGIT-960 TB System

One such alternative is the BACTEC MGIT-960 TB system (Figure 9). This system is a phenotypic, culture based system that is fully automated and does not rely on the formation of colonies in order to obtain a result. Instead, it relies on fluorometric technology that is able to detect oxygen consumption by the mycobacteria growing inside the mycobacteria growth indicator tubes (MGIT)[133]. This feature allows the test to be completed within 10 to 15 days[133,134].

This test is relatively simple and involves the use of a ruthenium pentahydrate oxygen sensor at the bottom of the MGIT tube that is able to fluoresce upon a reduction in the oxygen concentration[133]. As the mycobacteria grow and divide in liquid media, they use up oxygen which leads to fluorescence that can be detected under UV light. Drug susceptibility tests can be performed through the addition of specific drugs to the media within the MGIT tubes. The presence of fluorescence indicates that the mycobacteria are metabolically active, allowing the researcher to conclude that the strain is resistant. This system is essentially able to incubate and test up to 960 culture tubes, and as mentioned previously, it is fully automated providing a great advantage over conventional culture systems[133].

However, the use of this system does present with a number of limitations. The medium used in the MGIT tubes can facilitate growth of other bacterial species that may outcompete *M.tuberculosis* and yeild false positive results. The system itself is also very expensive, making it unsuitable for use in resource limited settings. The machine required to run the tests is priced at $63,900, while a set of 100 culture tubes can cost up to $830[135].

Figure 9| The BACTEC MGIT-960 TB system used for the detection of oxygen consumption by mycobacteria.

2.2 Genotypic Methods for the Diagnosis of Tuberculosis

Genotypic methods involve the detection of known drug resistance conferring mutations within the bacterial genome. Currently, a number of mutations conferring drug resistance have been described for many first-line and second-line TB drugs. These methods are often rapid and very accurate, which makes their use more attractive compared to the phenotypic methods explained previously. However, they can be extremely expensive, and can only be used to detect resistance, but not susceptibility[123].

2.2.1 DNA Sequencing

DNA sequencing is the gold standard genotypic method for identification of *M. tuberculosis* bacilli and drug resistance. Whole genome sequencing is able to simultaneously detect mutations known to be associated with drug resistance, as well as markers that can be used to monitor transmission[136]. It can also be used to detect new mutations that could be associated with drug resistance[137].

Conventionally, DNA sequencing of a specific genomic region works using the chain termination method. A primer is bound to a single stranded DNA, following which, DNA extension occurs through the action of a DNA polymerase enzyme. This extension process is eventually terminated by a dideoxynucleotide that interrupts the formation of a phosphodiester bond. Through this process, DNA fragments are produced that can then be separated by electrophoresis and sequenced.

Sequencing often requires the culture of the sample in order to obtain adequate amounts of DNA. This can be a rate-limiting step, as cultures can take 3 weeks or longer to grow. However, studies have shown that sequencing can be performed on MGIT cultures that are no less than 3 days old[136,138]. This offers great hope for this technique.

The main challenges associated with DNA sequencing are the high costs associated with its use, as well as the need for highly trained personnel. Whole genome sequencing can become very costly, reaching as high as ~R10 000 for a single genome. Many of the results obtained require someone who has been trained extensively in order to accurately interpret them. These challenges make it impractical for use in resource-limited settings where the TB burden is the highest. Until these challenges can be overcome, other methods need to be developed and utilized.

2.2.2 The Line Probe Assay (LPA)

The line probe assay offers great potential for the rapid diagnosis of drug susceptible and drug resistant TB. In 2008, the use of this assay was endorsed by the World Health Organization for the detection of drug resistance. However, the recommendation was only for culture samples and acid fast bacilli positive samples[139].

This assay works through the use of isolated DNA or RNA obtained from culture isolates or directly from sputum samples. This is then amplified via multiplexed polymerase chain reaction and reverse hybridized onto a nitrocellulose strip that contains probes for various resistance associated mutations linked to first and second line TB drugs[139]. These nitrocellulose strips can then be interpreted using a template, with the entire process completed within a day[139]. However, according to WHO guidelines, in practice the average turnaround time for LPA results is normally between two to three days[140].

A number of different LPAs have been developed that are capable of detecting resistance to a number of drugs. The INNO-LiPA Rif TB line-probe assay (Innogenetics, Ghent, Belgium) was first developed by Rudi Rossau and colleagues and reported in 1998[141]. This assay was developed to detect RIF resistance through the presence of mutations in the *rpo*B region in the hopes of accelerating the diagnosis of MDR-TB and subsequently, the time to treatment[141,142].

The Genotype MTBDR assay (Hain Lifescience GmbH, Nehren, Germany) is an improved adaptation of the INNO-LiPA assay that also allows for the detection of INH resistance through the detection of mutations found in the KatG region[143]. This assay was further developed into the Genotype

MTBDRplus (Hain LifeScience GmbH, Germany) which also allows for the detection of mutations within the inhA region[144].

Although LPAs present with a number of advantages such as being able to perform tests directly on sputum, the ability to obtain fast results, and relatively low costs per test (~R40), they still have a few limitations. The assays are all fairly labour intensive, and they also require highly trained staff and dedicated lab space.

2.2.3 GeneXpert MTB/RIF Assay

In 2010, two years after the World Health Organization had endorsed the use of LPAs, it endorsed the use of GeneXpert for the rapid and accurate detection of pulmonary TB following extensive testing in six countries[145,146]. Following their recommendation, its use expanded significantly, with 8.5 times more cartrages being sold in 2014 compared to 2011[62].

This system is a novel, microfluidics based diagnostic device that uses heminested PCR in real-time for the detection of *M.tuberculosis* (Figure 10)[146,147]. The test also employs the use of molecular beacons for the identification of RIF resistance through the detection of mutations in the *rpo*B region of the mycobacterial genome[146]. When there is nucleotide concordance between the beacons and target of interest (*rpo*B), the beacon emits a fluorescent signal. If there is no fluorescence, this suggests that there is a mutation present within the target region[148]. The detection of RIF resistance can be used as a marker for MDR-TB, as studies have shown that almost all RIF-resistant strains also present with resistance to other drugs, in particular, INH[44,50]. The entire process can be completed in less than 2 hours, a significant improvement over the 3 days required for LPAs[146,147].

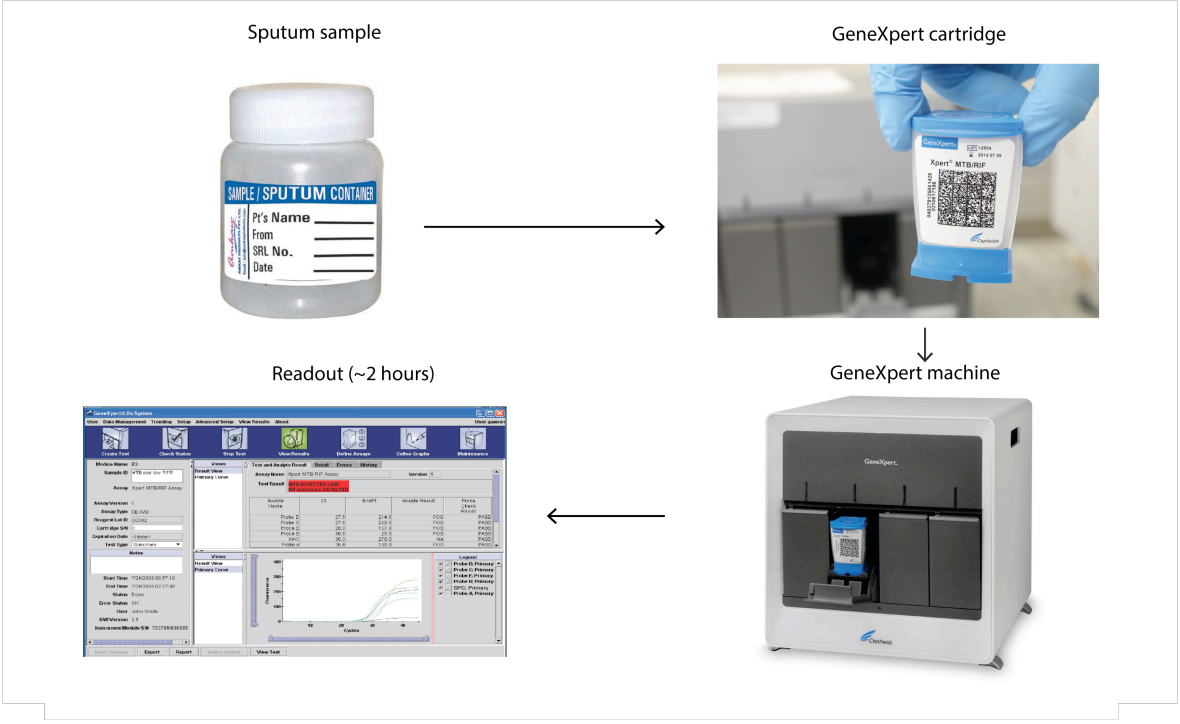

Figure 10| An example of one of the GeneXpert machines from Cepheid. A sputum sample is processed within 2 hours using PCR. Resistance to rifampicin is determined by detecting mutations in the *rpo*B region of the *M. tuberculosis* genome. Adapted from reference [149].

The introduction of GeneXpert was said to revolutionize the TB industry as it has a number of advantages over previously used diagnostics. A significant contribution to its success is its fast turnaround time as mentioned above. Another benefit is the closed cartridge system that allows the device to be operated by minimally trained staff in a number of environments, even outside a conventional laboratory setting[146]. This closed system also decreases the biohazard risk, as well as the risk of cross contamination. In addition to these advantages, the assay has been shown to have high sensitivity (90%) for culture-positive TB, and is even able to detect smear negative TB, thereby providing a significant advantage over many other diagnostics[145,146].

Despite all these benefits there are a number of limitations that create a barrier to the scaling of GeneXpert technology in many countries. Although one of the major advantages of the system is the rapid turnaround time, many people only receive their results a few days later instead of the 2 hours that has been widely publicised. This is often not due to the test itself, but instead due to issues such as limited staff, inefficient training, and poor specimen referral and transport systems[145].

The machine itself is also very costly, with a single machine costing US$17,000. The cartridges required for each test can cost US$10, a price not easily affordable for patients in many resource limited settings[145]. In many of these settings, a constant power source is not guaranteed, so the need for a sustained power supply is not a feasible one. Instead, a battery operated system would provide a better solution[145]. The normal operation of this assay also requires a number of conditions that may not be possible in many cases. These include an ambient air temperature of no higher than 30˚C, storage for cartridges under 28˚C, as well as annual calibration of the machines[145].

2.2.4 Emerging Diagnostic Technologies

In order to keep up with the rapid rate of evolution, new diagnostic technologies need to be developed. One such technology is that developed by Brilliant Luthuli and colleagues in 2015 at the Africa Health Research institute (AHRI)[150]. This study describes the use of microfluidic technology in the form of a cell culture system to detect the presence of epigenetic and genetic drug resistance. This paper illustrates the power of up and coming technologies such as microfluidics that allow you to perform multiple tests at the same time, as well as detect a single division cycle, thereby shortening the time to a result by hours. More information on this device can be found in chapter 4.

CHAPTER 3

3. Microfluidics

3.1 Introduction

Microfluidics is defined as "the science and technology of systems that process or manipulate small (10^{-9} to 10^{-18} litres) amounts of fluids, using channels with dimensions of tens to hundreds of micrometres" [151]. The field of microfluidics expanded rapidly following the end of the cold war in 1991, where it was clear that chemical and biological weapons posed a major threat to national security. As a result, the US-based Defence Advanced Research Projects Agency (DARPA) supported a number of programmes aimed at developing microfluidic systems that could be used in the field to detect for chemical and biological threats[151]. This subsequently led to the rapid growth of microfluidic technology both in industrial and academic settings.

3.2 Advantages of Microfluidics

Microfluidics offers a number of benefits that make its use highly attractive in a wide range of fields that include molecular and cellular biology, biodefence, and microelectronics. These devices are highly customizable and new designs for specific applications can be constructed within a week. This provides precise control over experimental conditions via custom chip designs, thereby making this technology very flexible, tailoring to the needs of the researcher. As custom chip designs are possible, devices can be constructed that allow for multiple experiments in parallel. This, along with the opportunity to automate the experiments through computer control, provides the opportunity to run high throughput studies[152].

In addition, there is minimal to zero need for the use of conventional lab equipment such as culture flasks that require large amounts of reagents and space. Instead, entire experiments can be conducted in chip-based microfluidic reactors at the nanoliter or microliter scale, thereby greatly reducing the amount of reagents needed, as well as the labour required[153]. The risk of contamination is also greatly reduced, as these reactors are closed environments.

As mentioned previously, microfluidic devices also offer the ability to study small numbers of cells or even single cells whilst providing high temporal and/or special resolution. This is a very important

aspect as it can allow for the detection of minority events that may be masked when using larger populations of cells.

3.3 Microfluidic Developments

There are currently a number of different types of microfluidics that are in use for a number of applications. Each type offers benefits and drawbacks that prevent usefulness in other applications. To provide context for this thesis, I shall briefly describe a few of the types that are in use below.

3.3.1 Microfluidic Large-Scale Integration (MLSI)

Microfluidic large-scale integration is the most commonly used type of microfluidics in research. Due to the many benefits this form of microfluidics offers, our lab at AHRI has embraced this technology to elucidate many unanswered biological questions. Therefore, many of the results presented in this thesis were obtained through experiments conducted with a microfluidic chip that is constructed based on the principles of MLSI.

This platform emerged in 1993 along with the process of softlithography. However, this technology was expanded in 1999 to multilayer soft lithography by the lab of Stephen Quake through the use of PDMS and microfabricated valves that have become known as "Quake valves"[154,155].

This platform offers a number of advantages. For example, it enables the development of extremely complex microfluidic chips that can perform multiple steps on a single device (Figure 11). This is possible through the use of integrated microvalves[154]. A valve is normally created through the use of a glass substrate and two layers of PDMS layered on top of each other[155]. One of the PDMS layers contains the "flow channel" that contains the fluid, whilst the other PDMS layer is known as the "Control channel." A valve is created when the control channel crosses a flow channel. Once the control channel is pressurized, it expands and pinches off the flow channel below it, thereby blocking the flow of liquid, essentially closing the valve (figure 12a,b). This system can also be used to create pumps for mixing, whereby several valves can be positioned alongside each other and then actuated in a peristaltic sequence (Figure 12d, e)[155]. As a result, multiple devices can be integrated onto a single chip, thereby significantly reducing space requirements. The valve system can also be automated which can lead to improved throughput[154]. However, the presence of valves often makes these chips very complex. For this reason, they are normally not suited for simple applications.

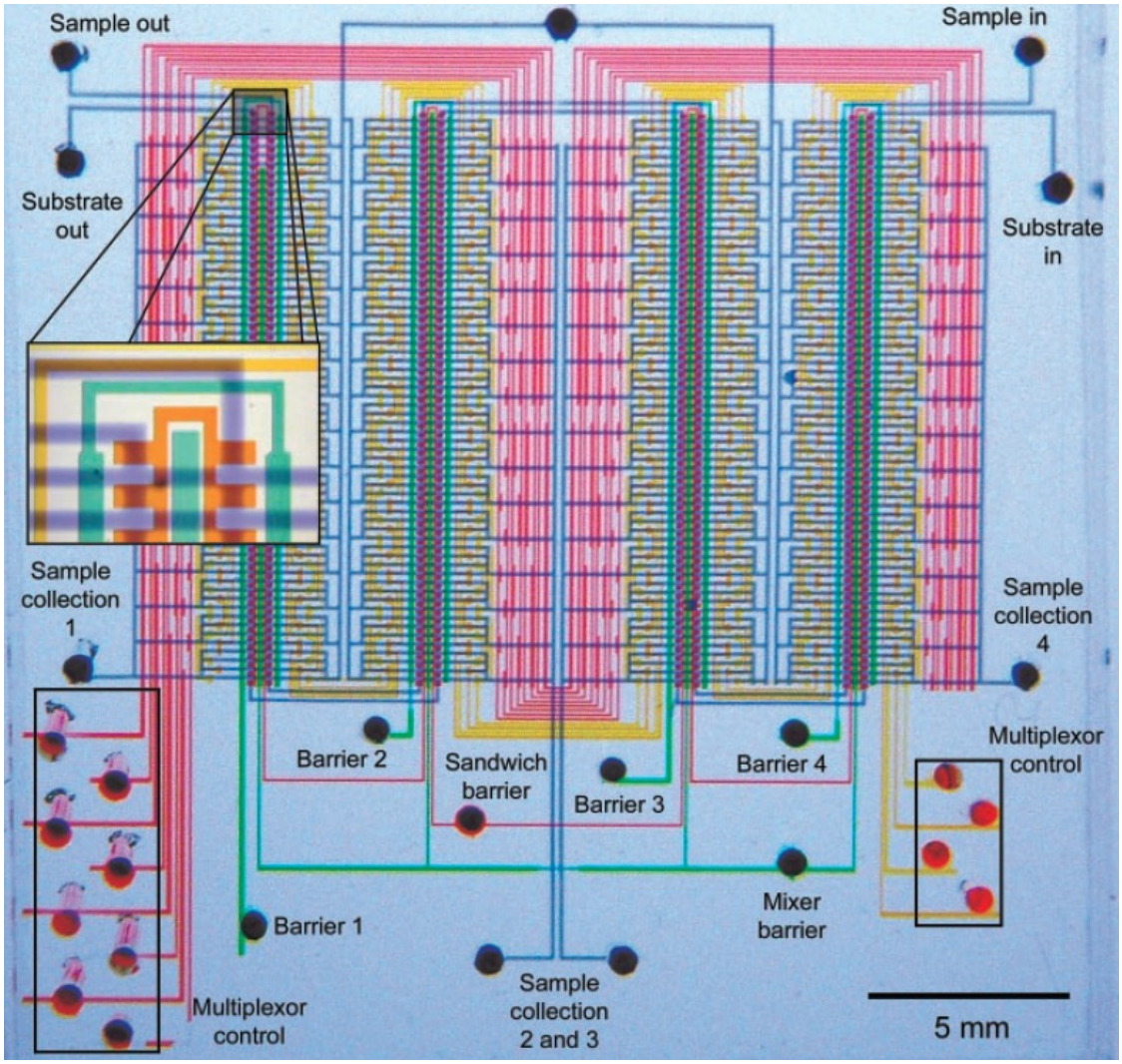

Figure 11|An example of a chip designed using the principles of microfluidic large-scale integration. This device contains 256 reaction chambers and 2056 microvalves that allow for complex fluidic manipulation. Adapted from reference [154].

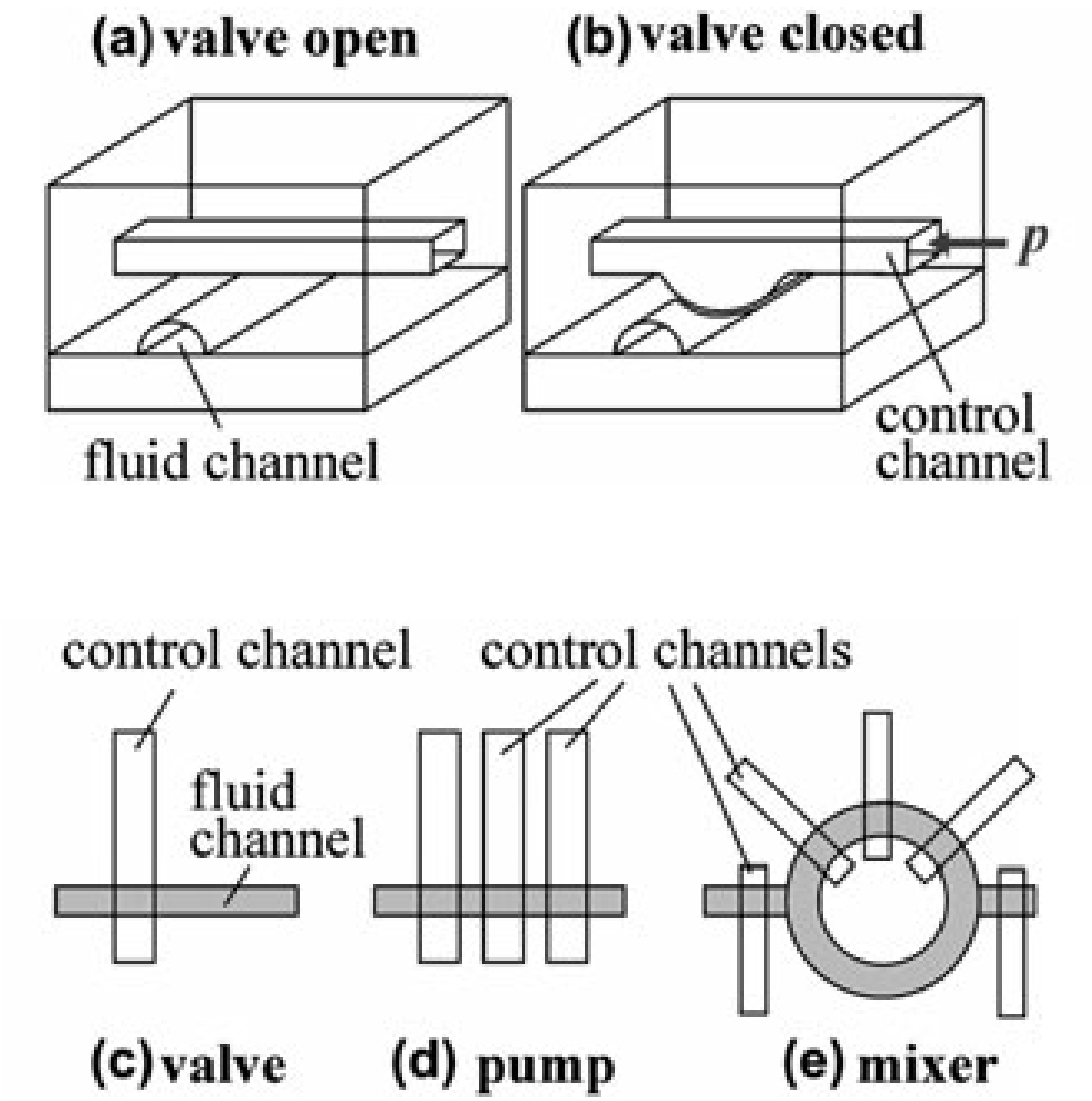

Figure 12| Valve operation in the multilayer PDMS based large-scale integration platform. The valve is open when no pressure is applied (a), and is closed when a pressure *p* is applied (b). Multiple valves (c) can be positioned to create pumps (d) and (e) through peristaltic like action. Adapted from reference [155].

One example of a device created according to these principles is a chip developed in 2002 by the lab of Stephen Quake for high throughput screening of cells with desired gene expression phenotypes (Figure 11)[156]. The unique attributes offered by microfluidics allowed this device to outperform all conventional techniques at the time. This chip is able to perform 144 parallel reactions whilst only using 10nl of reagent sample per reaction, an amount two orders of magnitude less than conventional methods[156].

3.3.2 Lateral Flow Microfluidics

Lateral flow microfluidics was one of the first successfully commercialised type of microfluidics and has evolved significantly over the last 30 years. Devices based on this type normally work through the use of capillary forces, whilst the movement of liquid is controlled by the wettability and size of the substrate[157]. Conventionally, these are simple devices that, unlike MLSI, do not contain valves. Instead, all reagents are pre-stored on the device and the readout is typically in the form of a colour change that can be detected by eye within a few minutes (Figure 13). Today, this form of microfluidics is used for a number of applications such as at home pregnancy tests, glucometers for the detection of blood glucose levels, as well as devices for the detection of infectious agents such as anthrax and salmonella[157].

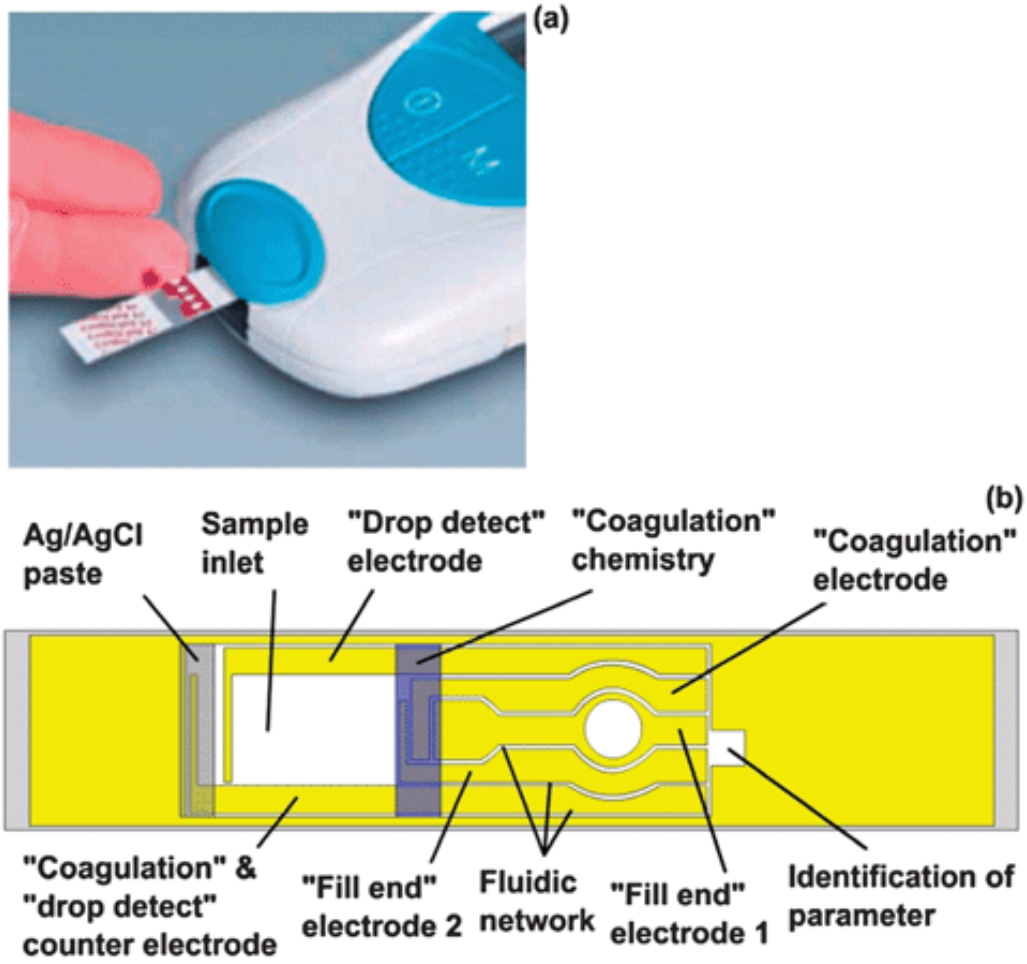

Figure 13| A lateral flow test for blood coagulation using a hand held device from Roche diagnostics (a). The blood flows into the device through capillary action where it rehydrates the coagulation chemistry. A number of different electrodes are used to detect the presence of blood, as well as used as standards for calibration and analysis. A final result is obtained through optical or electrochemical detection. Adapted from reference [157].

3.3.3 Linear Actuated Microfluidics

Linear actuated microfluidic devices are similar to lateral flow tests. However, fluid is transported through the use of mechanical displacement in the form of a plunger (e.g. syringe). The liquid normally moves in a linear fashion, with all reagents and buffers pre-stored on the device. An example of one such device is the i-STAT analyser (Figure 14), which is used to measure a number of blood parameters such as blood gas concentration and cardiac disease markers[157].

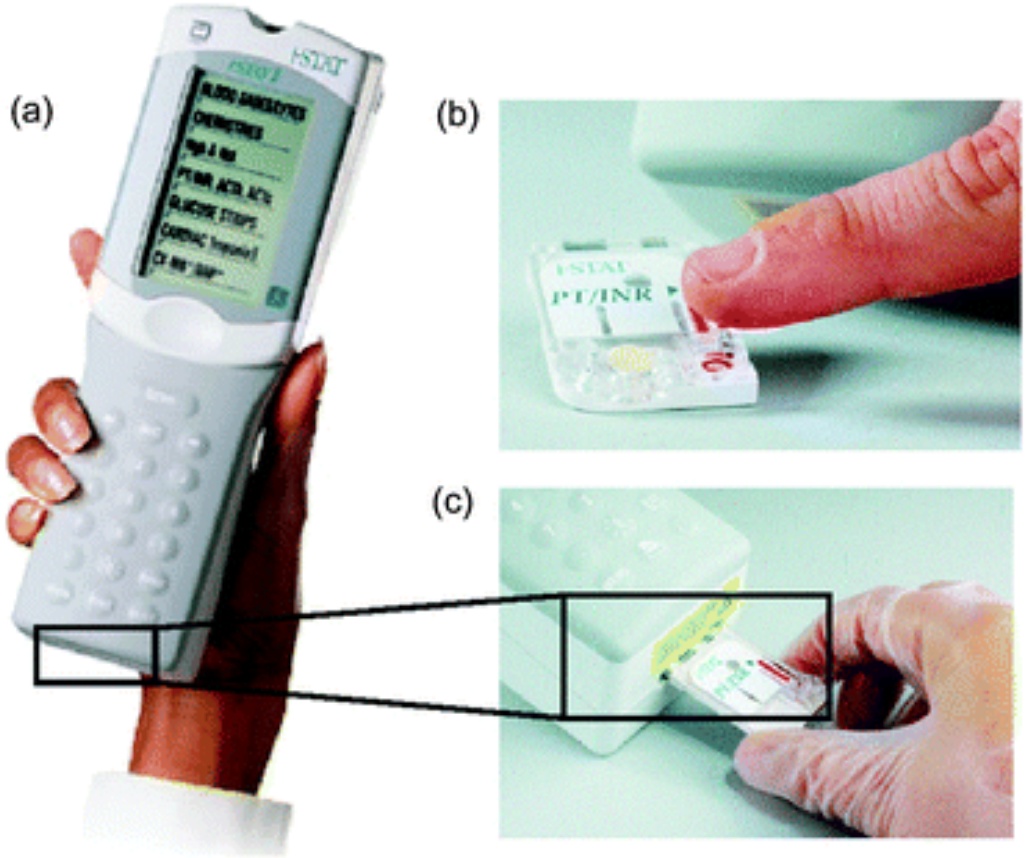

Figure 14| The i-STAT analyser used for clinical blood tests (a). Blood is loaded onto a disposable cartridge that acts as the "plunger" in this case (b). This cartridge is then inserted into the device for processing (c). Adapted from reference [157]. (Images courtesy of Abbott Point of Car Inc , NJ, USA).

3.3.4 Segmented Flow Microfluidics

Segmented flow microfluidics involves "the separation of fluids or gas through the use of plugs or droplets that are confined to microfluidic compartments or channels"[157]. This form of microfluidics can also be combined with MLSI to create more complex devices. An example of this technology is droplet based microfluidics or digital microfluidics. Individual droplets can be used as compartments in which single cells can be trapped and then studied in isolation (Figure 15). This can provide the user with single cell information which may be very useful for a number of applications as well as provide high throughput through the generation of hundreds or even thousands of cell containing droplets[157]. To date, a few droplet-based systems have been commercialised. One such system is the QX200 Droplet digital PCR system from Bio-Rad used for absolute quantification of DNA or RNA. However, one drawback associated with this form of microfluidics is that the cell capture rate can be very low.

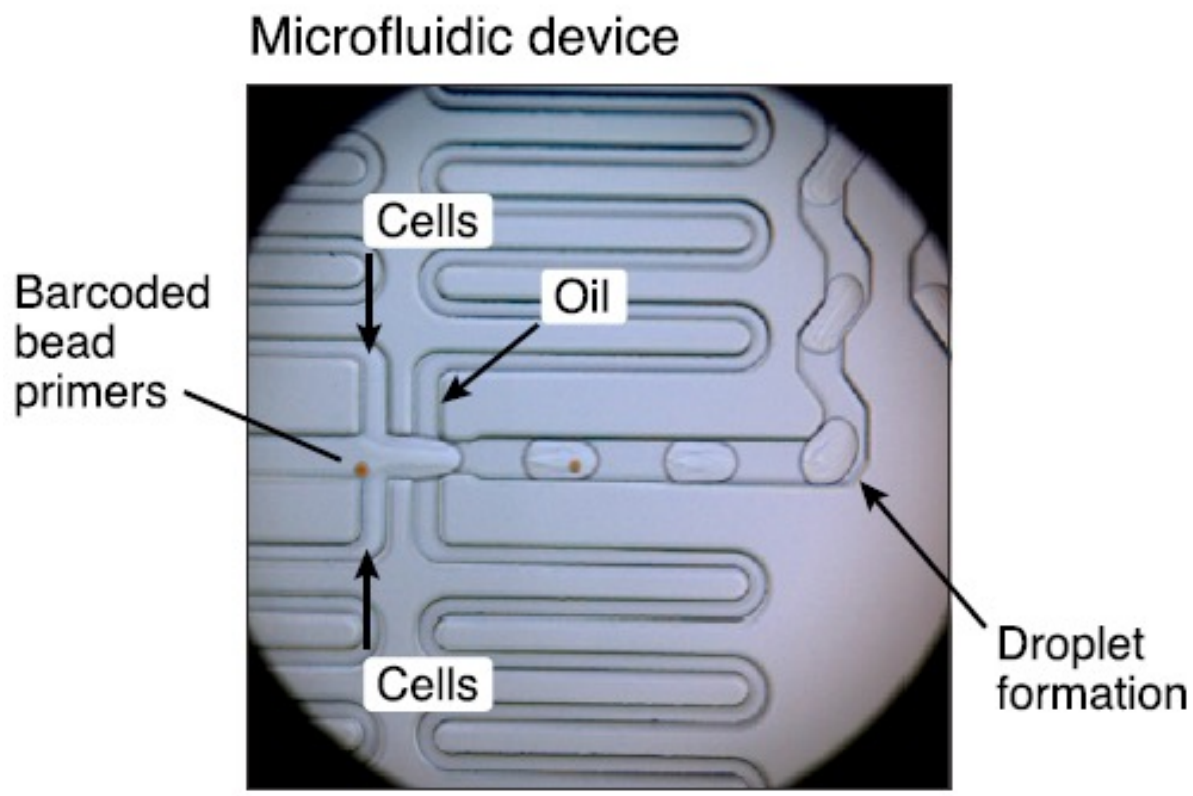

Figure 15| A droplet microfluidic device designed by the McCarroll lab at Harvard University for the study of single cell genomics. The cells, barcoded bead primers, and oil are all combined to form a droplet that acts as a miniaturized bioreactor for the study of single cells. Adapted from reference [158].

3.3.5 Centrifugal Microfluidics

Centrifugal microfluidics is one of the most rapidly expanding types of microfluidics and has even been adopted by some corporations for commercial use that include Panasonic, Roche, Samsung, Qiagen and Abaxis[159].

Normally, these devices are circular in shape, with all processes performed through the use of a rotating microstructured substrate (Figure 16). The device can be placed on a centrifuge like system and then spun at varying revolutions per minute, thereby exploiting a number of forces to facilitate liquid transport. These forces include centrifugal force, Euler force, Coriolis force and capillary force. Conventionally, the assays are performed in a sequence arranged from radially inward to radially outward positions with all reagents pre-loaded[157].

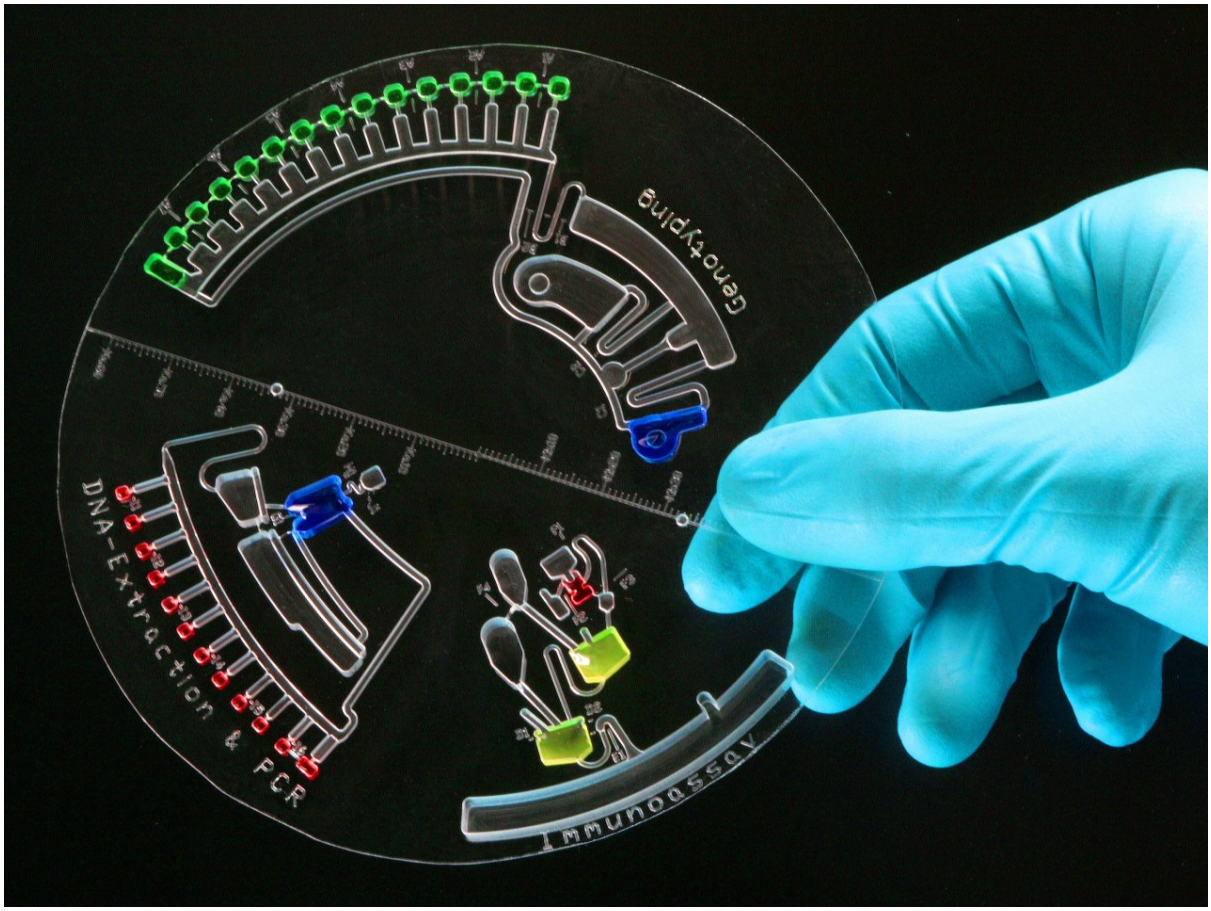

Figure 16| An example of a centrifugal microfluidic device developed by Qiagen for the processing and analysing of samples for a number of different tests. The rotation of the disk generates centrifugal forces which act to move the sample fluid though the different channels and compartments on the disk. Adapted from reference [160].

3.3.6 Paper Based Microfluidics

The invention of paper based microfluidics has been attributed to the lab of George Whiteside; however, the technology was initially described in 1949 by Ralph Muller and colleagues[155].

This form of microfluidics is based on creating a hydrophilic-hydrophobic contrast on paper in order to create capillary like channels (Figure 17). This technology is rapidly expanding as it offers a number of attractive properties for use in the diagnostics field, particularly in the developing world. Paper is an easily available and portable cheap material that is compatible with many applications and is also easily disposable[161]. It allows for the transport of fluids through the use of capillary forces, and as a result does not require any external forces, thereby reducing the need for complicated equipment. However, paper based microfluidic systems are normally limited to simple assays and therefore may face challenges when multiple steps are required before sample analysis[155].

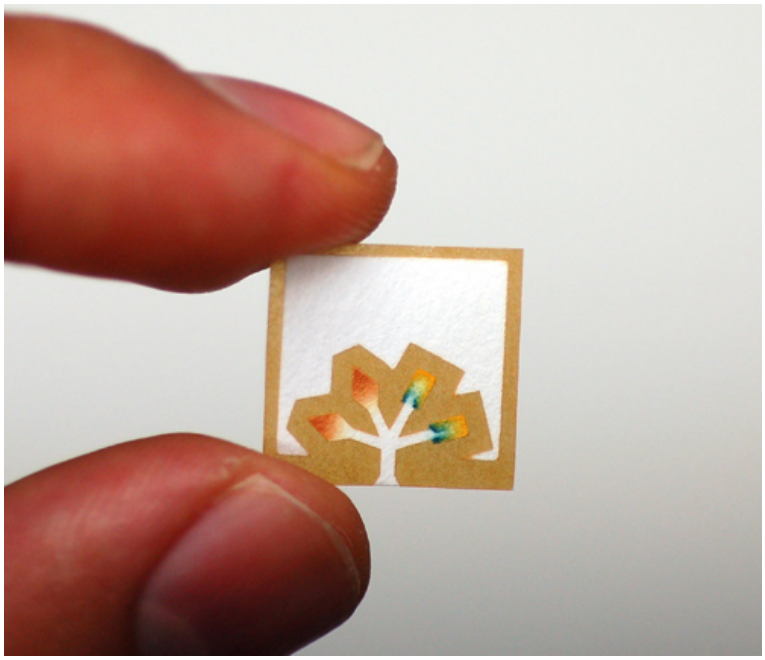

Figure 17| An example of a paper based microfluidic device created by the Wyss Institute at Harvard University for the detection of glucose (brown colour) and protein (blue colour) in 5µl of urine. Adapted from reference [162].

3.4 Fabrication of Microfluidic Chips

These devices can be created through the use of a number of different methods and materials. Conventionally, construction of a microfluidic device requires the use of a cleanroom in order to perform the processes of photolithography and soft lithography that were initially developed for

integrated circuit design[151,157]. A cleanroom is an area in which the temperature, humidity and amount of dust particles are highly regulated in order to provide optimal working conditions for the construction of devices such as microfluidic chips[163].

Over the years, a number of different substrates have been used for the development of microfluidic devices. Silicon was initially the most widely used substrate and contributed significantly to the rapid evolution of the technology[164]. However, the use of silicon requires a complicated fabrication process that can be very costly. This led to the widespread use of polymer materials such as polymethacrylate, polycarbonate and polydimethylsiloxane (PDMS)[164].

Polydimethylsiloxane or PDMS is now the most widely used substrate for the development of microfluidic chips (particularly those developed using the principles of MLSI) due to its biocompatibility, good optical transparency, permeability to air, and relatively low manufacturing costs[164]. PDMS based microfluidic chips are fabricated through photolithography and soft lithography. Initially, a silicon mould is developed through the process of photolithography that will have the pattern for the microfluidic chip etched onto the surface. This mould can then be used to develop the microfluidic chip through a number of steps involving the layering and curing of PDMS[165]. A more detailed description of this entire process can be found in appendix A.

3.5 Microfluidic Applications in Cell Culture

A major area of research that has leveraged the use of microfluidics is cell biology. Microfluidic devices have become useful tools for the study of eukaryotic cells and bacteria due to a number of reasons. They can be created to accommodate any cell type, with channels being constructed with similar dimensions to those of eukaryotic cells. This makes their visualisation easier and can offer single cell resolved measurements. Many microfluidic chips are also made from PDMS, a substrate that offers excellent optical transparency, low toxicity, and high permeability to oxygen and carbon dioxide, making them highly suited for the culture and study of a number of different cell types[151].

The ability to create custom chip designs offers enormous potential to create a microfluidic device for any assay. Since the inception of microfluidics, there have been a number of published examples of devices developed specifically for academic purposes that have provided researchers a significant advantage over traditional techniques. A few of these have been described briefly below.

3.5.1 A Microfluidic Device for Determining Drug Cytotoxicity

Sugiura and colleagues from the Research Centre of Advanced Bionics in Japan developed a "pressure driven perfusion cell culture system" with an 8 x 5 array of microchambers (Figure 18)[166]. This microfluidic chip was developed from PDMS through the process of softlithography and was used to test the cytotoxicity of seven anticancer drugs on the HeLa cell line from a human cervical carcinoma. Drug containing medium was transferred into the culture chambers through the use of a micropipette connected to an external pressure source. Cytotoxicity tests were performed over 3 days with seven different drugs tested in parallel[166]. This device illustrates the opportunity provided by microfluidics for high throughput drug screening, and may become in indispensable tool in the future. For further information on this device, please see reference [166].

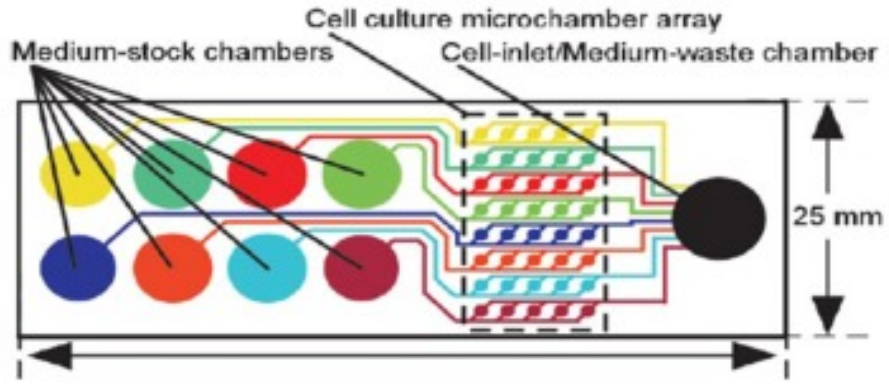

Figure 18| A schematic representation of the perfusion culture chip illustrating the microchamber array used for determining drug cytotoxicity. Adapted from reference [166].

3.5.2 The Microdialyser

The microdialyser system was developed in 2015 by Luthuli and colleagues in the Bioengineering lab at AHRI. This device contains 120 microdialyser culture chambers that are able to operate independently from each other (Figure 19). Each chamber can be monitored through the use of automated optical microscopy that is able to provide the researcher with a real time, non-invasive measurement of cell density[150]. In this study, the microdialyser was utilised for mycobacterial drug susceptibility testing.

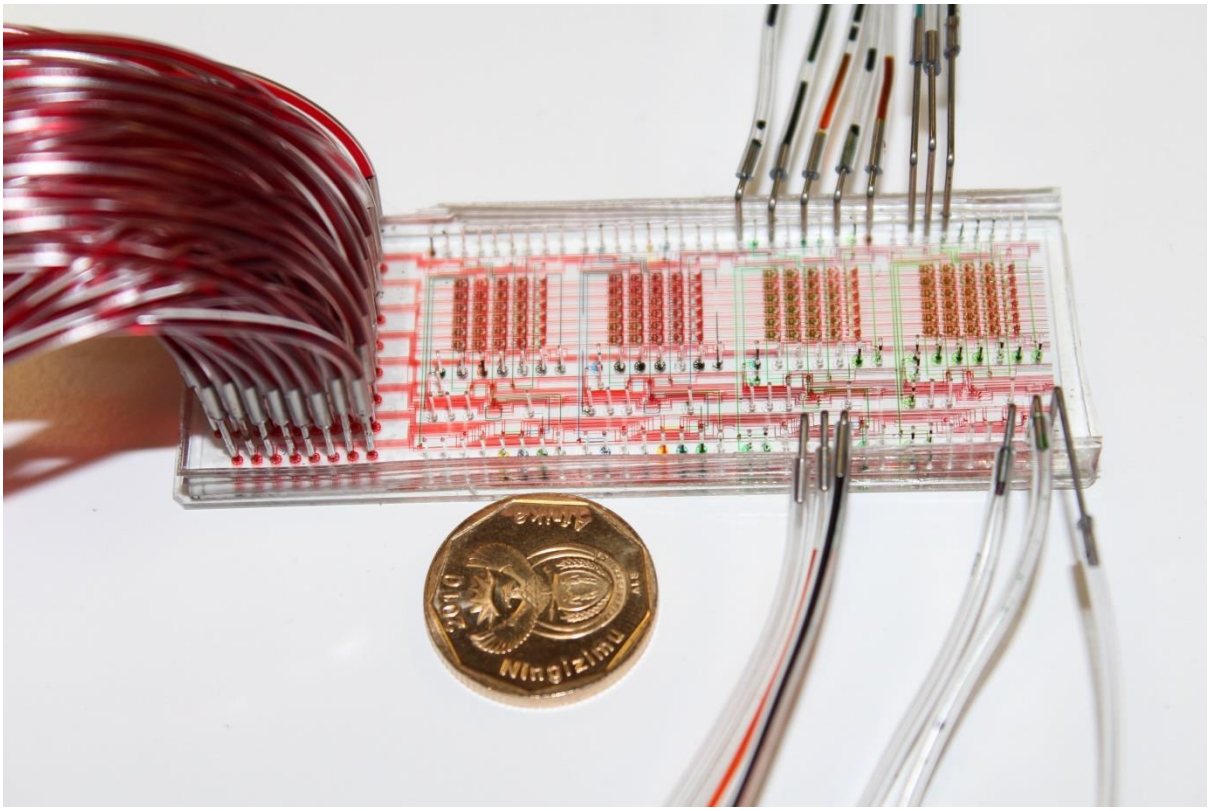

Figure 19| A Microdialyser chip with 120 microchambers that can operate independently. Food dyes have been used to visualise the individual channels and growth chambers. The coin is 10mm in diameter. (Image reproduced with permission from ref. [150]).

This microfluidic device is based on the Microfluidic Large Scale Integration platform and works using a microdialysis scheme. It contains multiple growth chambers with varying volumes, with the smallest being 200pL. Fresh nutrients are periodically introduced and waste removed through diffusion in these small chambers, thereby mimicking the exchange of factors across the macrophage membrane[150].

This device is able to provide real time, non-invasive measurements of cell density allowing for the detection of small changes in bacterial growth (Figure 20). The authors describe an epigenetic drug tolerant phenotype of *M. smegmatis* to rifampicin that was induced when cells were cultured in small reactors (~200pL). This effect was not observed in larger reactors. The study revealed that this tolerance appears to be induced through an efflux mechanism that only becomes active in space-confined bioreactors (Figure 21).

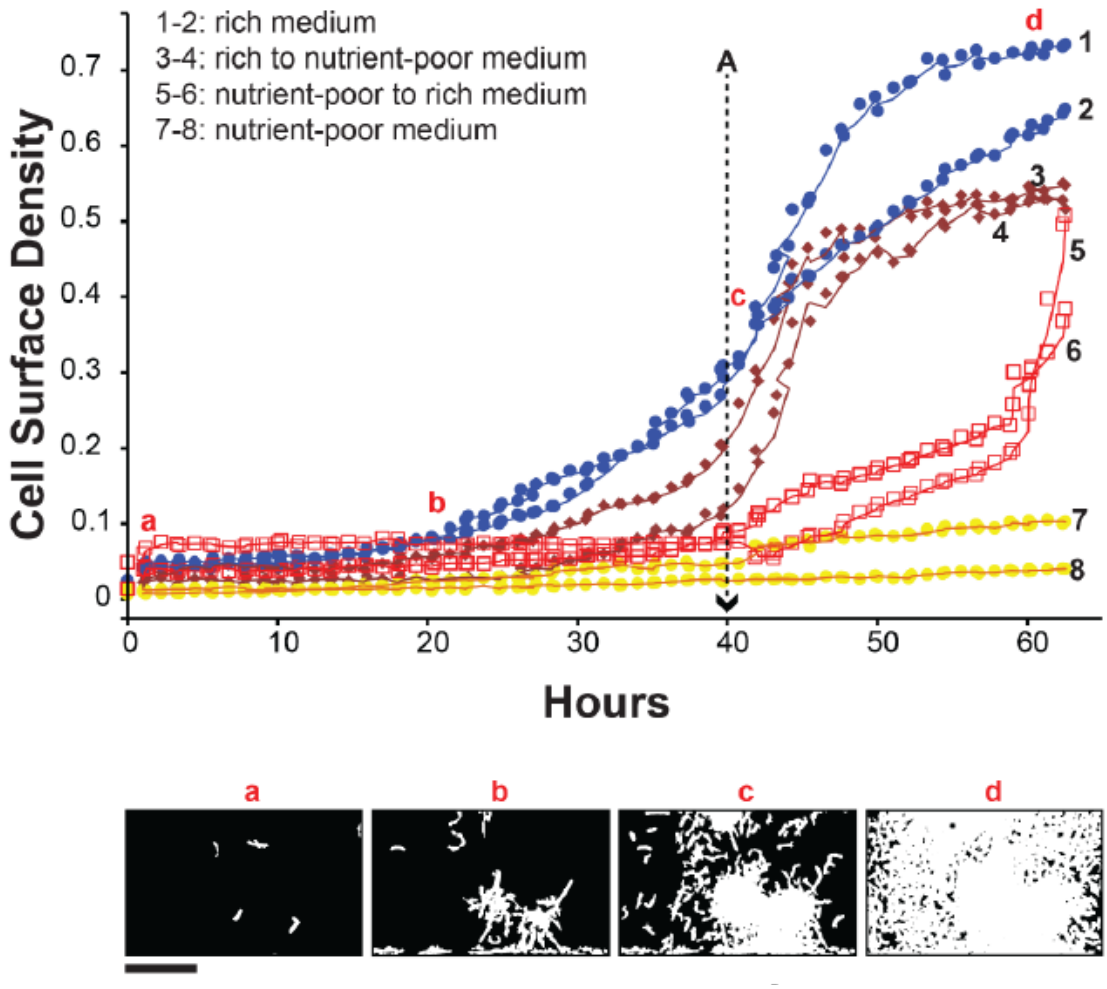

Figure 20| Typical growth curves of *M. smegmatis* Mc2155 in a 200pL growth chamber in a microdialyser. Medium is switched from nutrient rich to nutrient poor and vice versa. At 40 hours (point A), cultures 3 and 4 were switched to nutrient poor medium using microdialysis, which resulted in a decreased steady state cell density. At the same time, cultures 5 and 6 were switched to nutrient rich medium through microdialysis, resulting in faster growth. These cultures were all grown simultaneously on the same chip at 37˚C. Bottom panels (a to e) show micrographs of the cell density in growth chamber 1 at the corresponding time points. The scale bar represents 50µm. Adapted from reference [150].

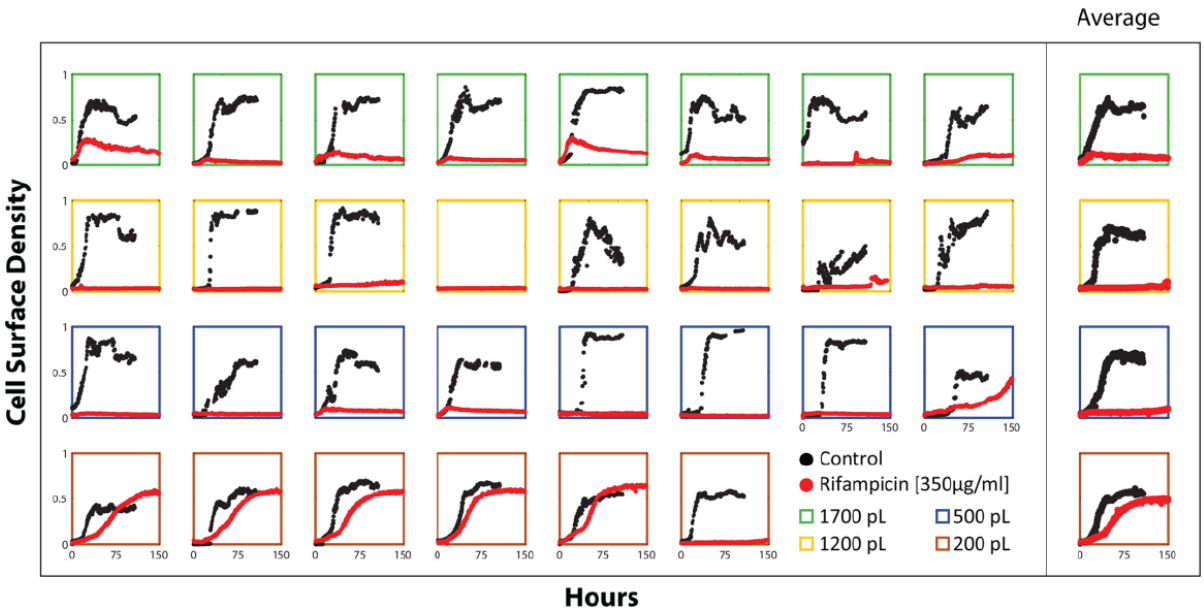

Figure 21| Growth dynamics of *M. smegmatis* cells with and without rifampicin in reactors of varying size. The growth curves in the right most column represent the average cell density of the reactors on the left. In drug free medium (black curves), the cells grow as normal. Rifampicin (red curve) was able to suppress growth in all reactors, with the exception of the 200pL reactors where 5 out of 6 cultures were able to grow in the presence of the drug. The cultures were grown simultaneously on the same chip at 37˚C. Adapted from reference [150].

This device offers great promise for rapid cell culture-based drug susceptibility tests in the future, as it allows for multiple tests in parallel and can detect single mycobacterial cell division events. This removes the need to wait for the growth of an entire colony in order to confirm resistance. Therefore, the time to a result can be significantly decreased, with an answer being obtained in less than a day compared to a month as is common with conventional culture-based tests. For further information on this device, please see reference [150].

3.5.3 The Microchemostat

The microchemostat is a novel microfluidic bioreactor developed by Balagaddé and colleagues in 2005 (Figure 22). This device functions in a similar manner to a conventional chemostat in that it allows for long-term culture and monitoring of bacteria[167]. However, it offers a number of other benefits over a conventional chemostat that make its use highly attractive in a research setting. For instance, the small reactor volume of the microchemostat suppresses the total mutation rate

proportionately. This, in turn, effectively insulates the micro-cultures from rapid evolution and allows prolonged monitoring of genetically programmed behaviour[167]. This small reactor volume and the ability to monitor bacteria through optical microscopy also allows for single cell resolution.

In this particular study, the microchemostat enabled researchers to observe the behaviour of bacterial populations over a long period of time (~100 hours). This elucidated unnatural behaviour induced by a synthetic circuit that included oscillations in cell density and changes in morphology[167]. For further information regarding this study, please see reference[167].

For this current study we have made use of the microchemostat to characterize a multidrug efflux pump in *M.tuberculosis*. For this reason, the operation of chemostats and the microchemostat will be explained in more detail in the next chapter.

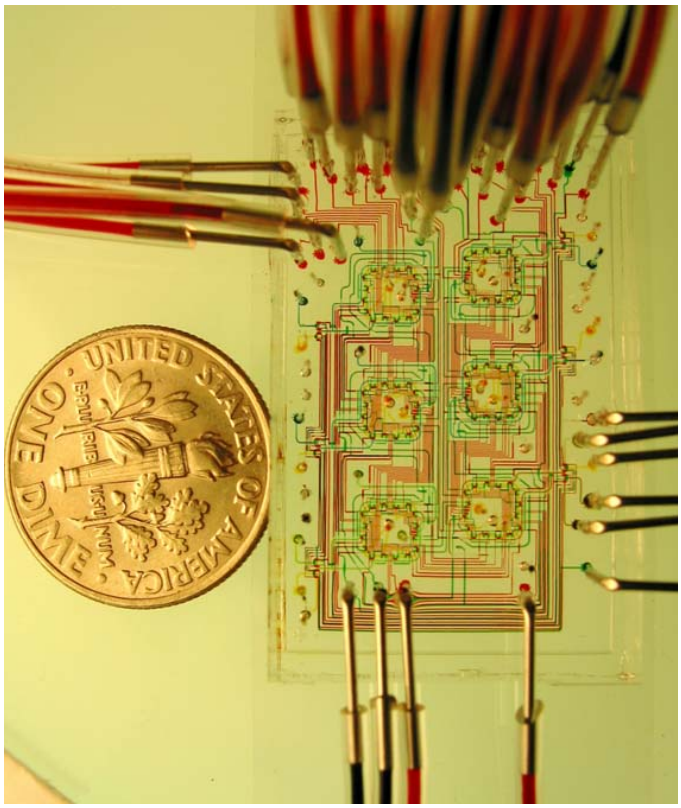

Figure 22| The original microchemostat chip. This device contains six individual microchemostat reactors that operate in parallel. Various inputs have been loaded with food dyes in order to visualise the microchannels and reactors. The coin is 17.91mm in diameter (Image reproduced with permission from ref [167]).

CHAPTER 4

4. The Microchemostat

4.1 The Conventional Chemostat

A chemostat or continuous stirred tank reactor (CSTR) is a simple piece of laboratory equipment used to continuously culture microbial populations in steady state. By eliminating stationary growth, it allows for the study of microbial populations over an indefinitely long period of time[168-171].

The invention of the chemostat is attributed to Hungarian born physicist Leo Szilard. He initially became famous for his development of the first self-sustained nuclear reactor based on uranium fission in 1940. Following his invention it was realised that nuclear chain reactions could be used in bombs. This marked the advent of nuclear warfare. However, after the end of the Second World War Szilard realised the devastating effects his invention could have on the world, and subsequently changed careers in 1947 and became a Biologist.

"*We turned the switch, saw the flashes, watched for ten minutes, then switched everything off and went home. That night I knew the world was headed for sorrow.*"

— Leo Szilard

Leveraging his experience as a physicist, he went on to develop a continuous microbial bioreactor based on binary fission in 1950 along with his colleague Aaron Novick. This invention they later called the chemostat[168].

4.1.1 Chemostat Operation

Often referred to as a continuous culture device or a continuously stirred tank reactor (CSTR), the chemostat allows for active growth of bacterial populations over indefinitely long periods of time. This is achieved by continually substituting a fraction of the culture with fresh, sterile nutrients whilst removing waste products (a dilution).

A conventional chemostat normally consists of a growth chamber where the bacteria are cultured, a reservoir that contains fresh, sterile medium, and an overflow that is used to maintain the volume in the growth chamber at a constant (Figure 23)[168]. Fresh media is added via the reservoir and results in

the displacement of a portion of the culture into the overflow. As a result, the displaced bacterial suspension leaves at the same rate at which fresh nutrients enter the growth chamber. This maintains a constant volume in the growth chamber whist replenishing nutrients and removing waste products. The growth chamber is kept well stirred and all parameters that affect growth (temperature, pH etc.) are kept constant[168].

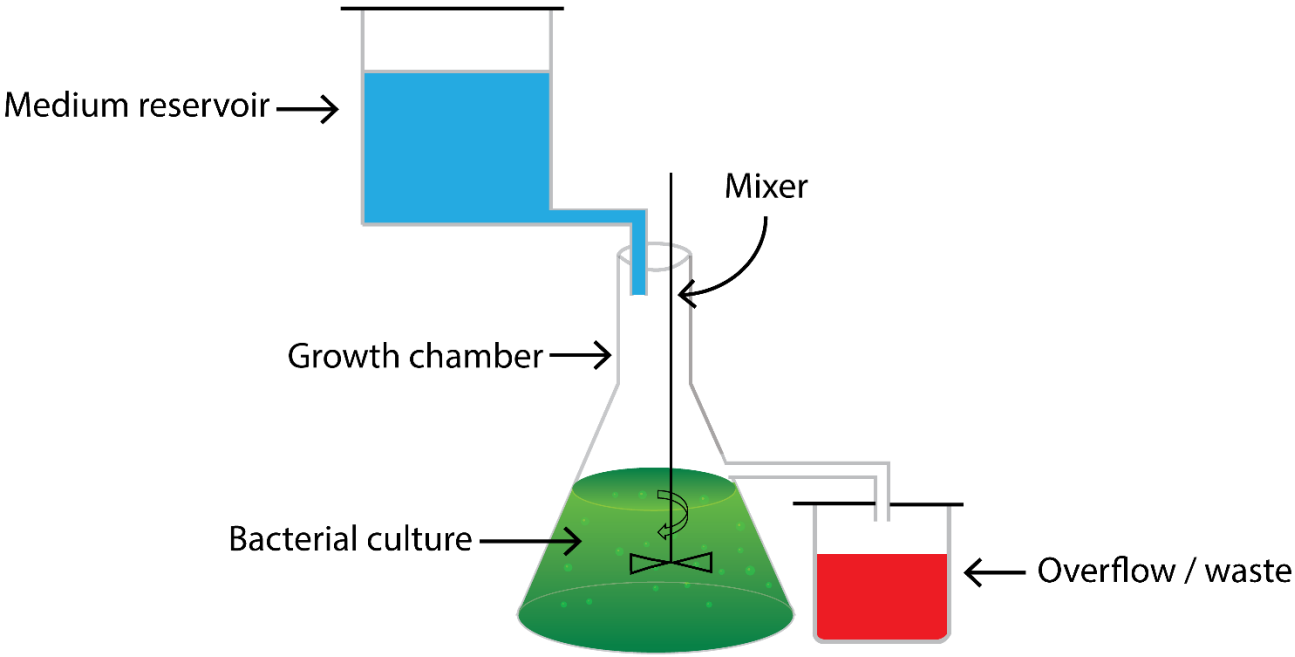

Figure 23| Schematic of a conventional chemostat showing the medium reservoir that contains fresh sterile medium, the growth chamber containing the bacterial culture, and the overflow or waste. The culture is kept continuously mixed through the use of a mechanical mixer.

Chemostats offer a significant advantage over the use of conventional batch culture systems such as culture flasks and test tubes[170]. In batch cultures, nutrients are not replenished and waste products are not removed. As a result, bacterial growth is restricted by the amount of nutrients present in the media and the amount of waste products produced. In these closed systems, the bacterial growth rate changes over time as there is a constant pressure exerted by a decreasing nutrient concentration and an increasing waste product concentration. This ultimately slows down bacterial division. However, in a chemostat there is an indefinitely long steady state period of active growth as nutrients are being replenished, and waste products removed. This allows for long-term experimentation of microbes under near constant conditions[170].

4.1.2 Chemostat Applications

Over the years, chemostats have become an indispensable tool in research settings. The ability to allow for indefinite bacterial growth provides an ideal environment for the study of microbial metabolism, programmed cell behavior and other regulatory processes. It has also emerged as an important means of studying mutation rates and evolution in bacteria. This is hugely beneficial in the drug resistance field where acquisition of genetic mutations can lead to drastic changes in the phenotype of the bacteria. A study conducted in 2007 followed the growth and mutation of *Acinetobacter baylyi* over 2 weeks and 200 generations, a feat that would not be possible with conventional batch cultures[172].

The unique ability of chemostats to culture microbes indefinitely has been exploited for a number of commercial processes. In the pharmaceutical industry, chemostats are used to analyze the response of bacteria to antibiotics, as well as for the production of insulin through the use of genetically altered microorganisms. They also play a significant role in the production of fermented food such as cheese, and the fermenting of sugar to produce alcohol[173]. Governmental institutes have utilized chemostats as a model for the wastewater treatment process. A study conducted by Qu and Bhattacharya made use of a chemostat to study the toxicity and degradability of formaldehyde found in industrial wastewaters[174].

4.1.3 Theory of the Chemostat

The normal operation of a chemostat is governed by a number of differential equations. These can be used to help explain its operation, as well as determine a number of factors related to bacterial growth that include growth rate, steady state cell density and the maximum number of cells possible within the reactor.

As mentioned previously, in a conventional closed system a number of factors come into play that eventually stop the growth of the organism once it has reached a significantly large population size. These factors include decreased nutrient and oxygen concentration, as well as increased production of toxic metabolites. Therefore, in these systems the growth rate is a function of the population size (n):

$$\frac{1}{n}\frac{dn}{dt} = f(n), \quad [1]$$

where $f(n)$ is some function of n.

However, this equation can be adjusted to incorporate the maximum number of microbes allowable based on the nutrients available, here denoted as N_{max}:

$$\frac{1}{n}\frac{dn}{dt} = \mu\left(1 - \frac{n}{N_{max}}\right), \quad [2]$$

where μ represents the specific growth rate.

In a chemostat, nutrients are replenished and waste products are removed through the dilution process. As a result, the factors that would normally suppress growth are no longer present, leading to the maintenance of the population in a state of active growth. In this situation, let V represent the volume of the culture or growth chamber with units l^3 that stand for length. The volumetric flow rate is denoted by v and contains the units l^3/t, where t is time. Therefore, the standard growth equation in a chemostat can be represented as:

$$\frac{1}{n}\frac{dn}{dt} = \mu\left(1 - \frac{n}{N_{max}}\right) - n\frac{v}{V} \quad [3]$$

This differential equation illustrates that the growth of cells in a chemostat is denoted by the growth of the organism (μ [1-n/N_{max}]) less the amount that is removed during a dilution (n[v/V]). This equation can be further simplified by replacing the dilution rate n[v/V] with D that has units t^{-1}. Therefore, the equation becomes:

$$\frac{1}{n}\frac{dn}{dt} = \mu\left(1 - \frac{n}{N_{max}}\right) - D \quad [4]$$

Within a chemostat, the bacterial population grows at a state of active growth and eventually reaches a steady state. During this state cells are replenished at the same rate at which they are lost through dilution, leading to a constant cell density. The cell density at steady state may be changed by altering the dilution rate as well as other growth factors. At steady state the chemostat equation [4] becomes:

$$\frac{1}{n}\frac{dn}{dt} = \mu\left(1 - \frac{n}{N_{max}}\right) - D = 0, \quad [5]$$

as a result of the cells being washed out (D) at the same rate that they are being replaced through bacterial growth (μ [1-n/N_{max}]).

4.1.4 Drawbacks of the Conventional Chemostat

Although chemostats offer a number of benefits for the culture of bacteria in industry and academia, their use has not been widely adopted due to a number of reasons. Conventionally chemostats take up a lot of space and are difficult to maintain, often requiring frequent services (Figure 24). Their large size also necessitates the need for large amounts of culture medium which can become extremely costly with frequent use.

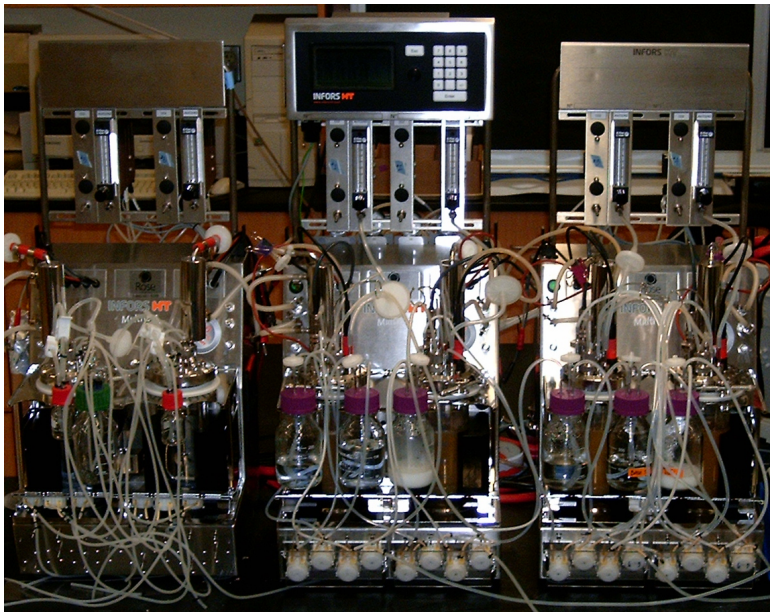

Figure 24| An example of a conventional chemostat used for the study of microbiota in the gastrointestinal tract. Adapted from reference [175].

One of the most significant challenges with chemostat operation is the development of biofilms. Biofilms were first described in the 17th century by a dry-goods merchant and scientist named Antonie van Leeuwenhoek, the "father of microbiology," who reported the presence of "animalcules" or microscopic animals in dental plaque through the use of one of his own microscopes[176,177]. However, biofilms themselves were not completely described until 1978[176]. Biofilms are present in virtually all ecosystems and are defined as "matrix enclosed bacterial populations adherent to each other and/or to surfaces or interfaces"[178].

"...I observed certain animalcules, within whole bodies I saw so quick a motion as to exceed belief; they were about the size of a large grain of sand, and their bodies being transparent, that the internal motion could plainly be seen..."

—Antonie van Leeuwenhoek

Biofilms interfere with chemostat operation by attaching to the growth chamber walls[178,179]. As a result, they are not removed through the dilution process and can therefore consume a significant proportion of the growth media. This essentially decreases the benefit associated with removing a portion of the culture, introducing characteristics similar to that seen in batch cultures. Biofilms are also phenotypically different from planktonic cells and therefore introduce heterogeneity into the population, a potentially confounding factor in many studies[178].

Furthermore, another challenge associated with chemostat operation is that of evolution. It has been shown that the variation in fitness of an organism increases with population size[180-182]. The number of mutations introduced into the bacterial genome is proportional to the number of cell division events within a unit time period[180]. This can ultimately lead to evolution of the population and possibly a change in the phenotype of the bacteria, rendering the experiment invalid. The ability of a chemostat to allow for constant active growth of large populations of cells leads to an increase in the number of cell division events and therefore makes the population susceptible to mutations and evolution.

Another challenge with the use of chemostats is the quantification of the population within the growth chamber. Conventionally, bacterial colonies are counted using plates in order to obtain an estimate of the population. However, in a chemostat this can lead to inaccurate results as cultures are able to actively grow at varying rates during the dilution period. As a result, plating may not be the best method for determining the growth rate of a bacterial population growing within a chemostat. Other methods can be used such as the use of a haemocytometer, whereby the number of cells within a certain area of the counting chamber are used to make predictions based on the entire population. However, this method is manually performed and as a result prone to human error. A few other methods have been described such as the use of a Coulter counter. However, this can be very laborious and expensive and as a result is not practical in many settings.

Due to these many considerable challenges associated with maintaining and operating continuous bioreactors, a microfluidic chemostat or microchemostat has been developed by Balagaddé and colleagues that is able to overcome many of these challenges, thereby providing an indispensable tool for the study of bacterial growth[167].

For this study, we have made use of the microchemostat to achieve high-resolution measurements of bacteria growing whilst expressing efflux pump genes.

4.2 The Microchemostat

Lab on a chip technology has being growing exponentially over the years with the process of miniaturization providing a number of benefits that have been explained previously in the microfluidics chapter. These include low reagent consumption, as well as the possibility for automation that can lead to increased speed, precision and reproducibility of experiments.

4.2.1 Description of the Microchemostat

The microchemostat is one such example that represents the epitome of lab on a chip technology. This microfluidic device has been developed based on the principles of MLSI and therefore makes use of microfabricated Quake valves in order to mimic the operation of a conventional chemostat. A more detailed description of the fabrication process can be found in appendix A. The current microchemostat chip that we are using at AHRI contains 14 independent microchemostat reactors on a single chip (Figure 25). These reactors can operate in parallel through automation, essentially allowing us to conduct 14 different experiments simultaneously.

Each microchemostat reactor on the chip consists of a growth chamber (yellow reactor Figure 25b) that is 10µm high, 100µm wide and ~13mm in circumference. This small growth chamber volume allows for the growth of small populations of bacteria (~10^4 compared to ~10^9 in batch cultures). This essentially reduces the number of cell division events per unit time leading to a decreased mutation rate and decreased microbial evolution. This chip also contains five input ports per microchemostat reactor for the introduction of media and other reagents, as well as 3 additional ports that can be used as input or waste ports (Figure 25b).

4.2.2 Microchemostat Operation

The operation of the microchemostat occurs in two different states that allow for the continuous culture of bacteria whilst minimizing biofilm formation. The first is the continuous culture state whereby the bacterial culture and media are mixed throughout the reactor through the use of a peristaltic pump (Figure 25b). During this phase, the culture is able to grow as normal whilst receiving fresh nutrients. The second state is the cleaning and dilution state. During this phase the mixing process is temporarily stopped. A portion of the reactor is then isolated through the use of valves, and a lysis buffer (Bacterial protein extraction reagent or BPER) is washed through the isolated section in order to remove cells and old media, including any cells that have become stuck to

the reactor walls. This isolated section is then washed with sterile media to flush out the lysis buffer. Once this process is complete, the reactor is reopened and the continuous culture state begins again with the new media being mixed into the culture. This process is entirely automated and repeated cyclically, with a different chamber segment cleaned each time and is analogous to the dilution step in a conventional chemostat. Through these dilutions involving the use of a lysis buffer, biofilm formation—a major obstacle faced during the operation of conventional chemostats—is prevented.

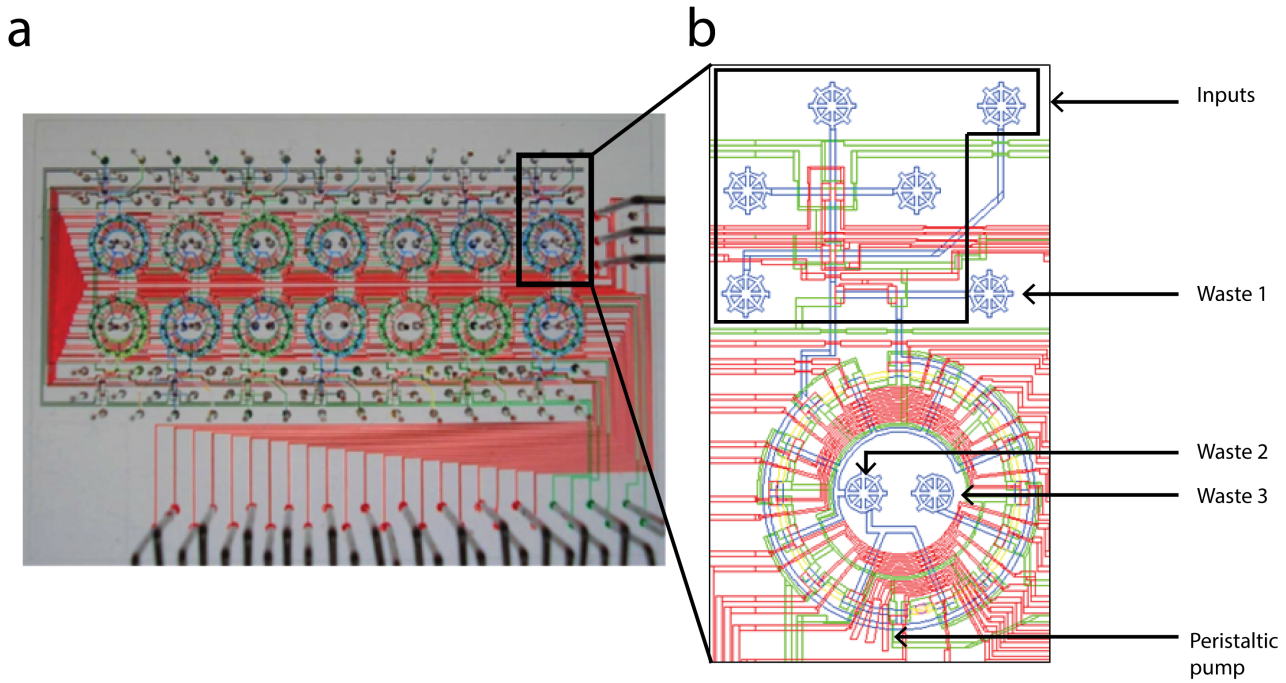

Figure 25| The microchemostat chip containing 14 individual microchemostat reactors (a). Each microchemostat reactor (b) operates in parallel allowing for high throughput experiments. Various inputs have been loaded with food dyes in order to visualise the microchannels and reactors. (Image reproduced and adapted with permission from ref [167]).

4.2.3 Quantification of Bacterial Populations in the Microchemostat

The microchemostat is fabricated from PDMS, a polymer material with excellent optical transparency. This allows for easy visualisation of bacteria within the 10µm high growth chamber through the use of a microscope. Bacterial populations can be quantified through the use of automated microscopy and image processing software such as Matlab. Images can be taken at a given location of known volume and the total number of cells within the reactor determined. As the entire process is automated, images can be taken every few minutes, allowing for high resolution measurements that can detect small changes in the bacterial growth rate. A motorized stage allows for the simultaneous documentation of cell number for all 14 microchemostat reactors. Fluorescence studies can be conducted using a ~3µm high imaging section that is incorporated along the growth loop. This smaller section was developed to enable visualisation of fluorescent cells within a single focal plane (Figure 26). Quantification of the fluorescent cell number is achieved as mentioned previously.

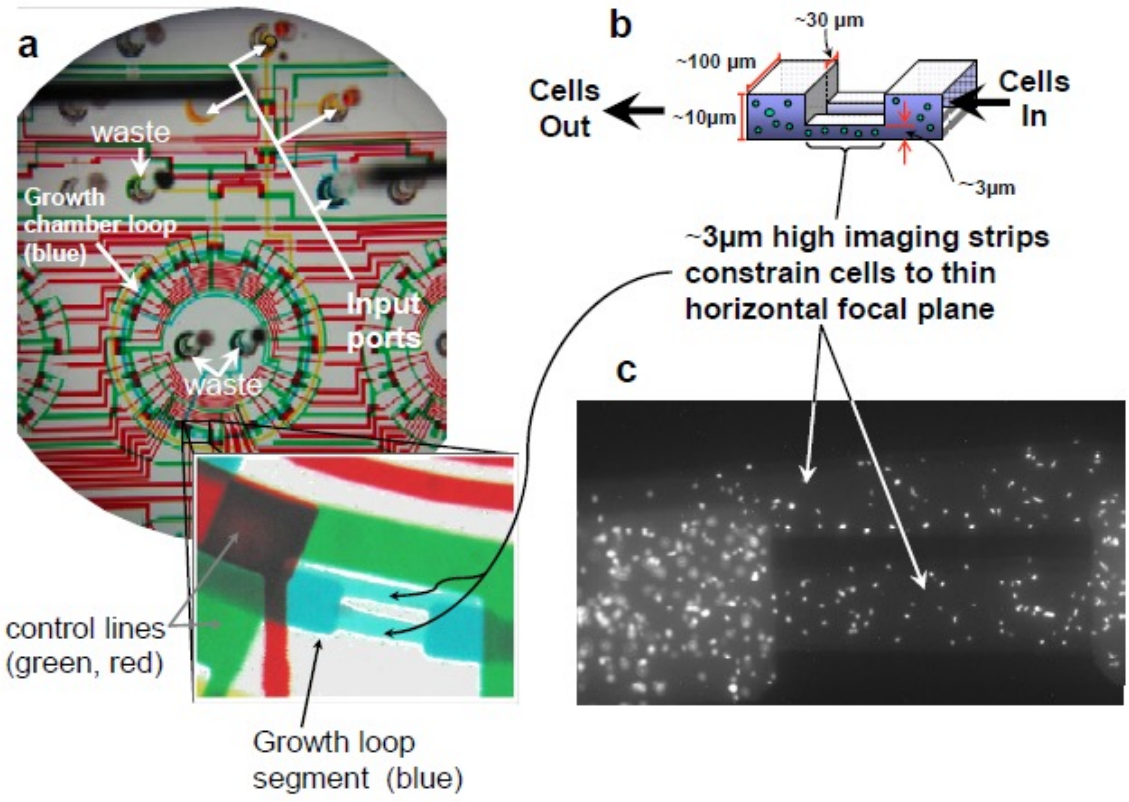

Figure 26| An enlarged view of the 3µm section (blue strips) along the growth loop used for the detection of fluorescence (a). A schematic showing a three dimensional view of the imaging section (b). A fluorescent image illustrating the improved image quality in the 3µm section compared to the 10µm section on either side (c). (Reproduced with permission from ref. [167]).

In summary, the microchemostat is an extremely powerful tool for the study of cell biology. It provides all of the benefits of a conventional chemostat whilst addressing many of the limitations. Continuous cleaning of the reactors through the use of a lysis buffer prevents biofilm growth, thereby ensuring efficient functioning of the device. The small reactor size provides a unique advantage to slow down microevolution, allowing for long-term experimentation without the risk of mutations and greatly reducing the amount of medium required for experimentation. Quantification of bacterial populations is achieved using an automated microscope and image processing software, allowing for the detection of small changes in growth rate.

CHAPTER 5

5. A Microchemostat for the Study of *M. tuberculosis* Efflux Pumps

This project was aimed at utilizing the microchemostat to develop a new way of studying *M. tuberculosis* efflux pumps over a long period of time in order to elucidate their potential role in the development of drug resistance. Individual *M. tuberculosis* efflux pumps were expressed in *E.coli* cells which have had their native transporters removed.

5.1 *E.coli* Expression System for Efflux Pump Gene Expression

Over the last 40 years, only one new TB drug has been discovered[36]. This slow rate of drug development illustrates how drug resistant *M. tuberculosis* strains are emerging at a rate that surpasses the rate of development of new antibiotics. It is therefore crucial to understand the mechanisms underlying resistance to the currently available antibiotics, with the hope of restoring efficacy to traditional antibiotics that have otherwise lost potency.

The majority of drug resistance to *M. tuberculosis* has been attributed to mutations in specific gene targets of antibiotics such as *rpoB* (rifampicin), *iniBAC* (isoniazid) and *gyrA* (fluoroquinolones)[183-185]. However, a significant portion of clinically drug-resistant isolates lack the corresponding drug resistance mutations. This discrepancy has been attributed to the presence of active efflux systems which contribute to drug resistance by extruding antibiotics[185]. Studies have shown that treatment of resistant isolates with efflux pump inhibitors can re-sensitize drug resistant mycobacteria to isoniazid[89,186]. In addition, studies on the evolution of isoniazid resistance in *Mtb* have shown that increased expression of efflux pumps is an important precursor to the development of genetic resistance to this drug[110,187]. Detailed knowledge of the molecular basis of efflux pumps is therefore required for the development of new antibiotics that are not extruded or of inhibitors that block efflux pumps and allow traditional antibiotics to remain effective.

The conventional knockout approach for studying mycobacterial efflux pumps has many limitations, primarily due to the coexistence of multiple efflux pumps with overlapping substrate specificity and functional redundancy. Inactivation of a specific efflux pump may not yield the expected changes in resistance to an antibiotic drug known to be extruded by the pump due to compensatory

overexpression by other efflux pumps with overlapping functionality [107,188]. Therefore, in order to obtain the desired effect, in theory all efflux pumps would need to be inactivated.

Within the mycobacterial host, some efflux pumps are essential for growth, and therefore inhibiting their expression may kill the organism. At the same time, excessive expression of an efflux pump—to enhance and document its function—can also be deleterious to the host because of the direct, physical disruption of membrane integrity or the undesirable export of essential metabolites[189]. Furthermore, the *M. tuberculosis* genome contains 82 proteins that are secondary transporters capable of engendering intrinsic drug resistance via efflux mechanisms[102]. The sheer number of these pumps presents a monumental research challenge, which makes it difficult for scientists to assign a function to every single pump.

In order to overcome the challenges of functional redundancy we have characterized *E.coli* strains constructed by Dr. Alissa Myrick from the Eric Ruben lab at Harvard University, who is now located at H3D at the University of Cape Town. In order to develop these strains, uncharacterized efflux pumps were isolated from *M.tuberculosis* and inserted into transporter-deficient *E. coli* cells in order to 'program' cellular behaviour[190]. This *E. coli* expression system insulates the inserted efflux pumps against interference from co-functional transporters that are normally encountered in the native host species, and allows researchers to more cleanly pinpoint antibiotic substrates extrudable by the pump than would be possible by working entirely within the native host environment. We have leveraged novel microchemostat technology to systematically monitor the dynamics of *M. tuberculosis* efflux pumps conditionally expressed in this *E.coli* system. With the use of the microchemostat we are able to resolve gene expression characteristics of individual cells, whilst monitoring the dynamics of each efflux pump in terms of substrate specificity, cognate inhibitors and efflux capacity.

5.2 Hypothesis

We hypothesize that the use of a heterologous system such as *E. coli* will provide the sorely needed breakthroughs required for systematic characterization of *M.tuberculosis* efflux pumps. By conditionally expressing an *M.tuberculosis* pump in *E.coli* strains that are deficient in transporter proteins and highly sensitive to drugs, we will characterize the pump in terms of substrate specificity, cognate inhibitors and efflux capacity. We will also leverage a novel microchemostat technology to systematically monitor the dynamics of the efflux pump conditionally expressed in transporter-deficient *E.coli*, with the ability to resolve gene expression differences between individual cells.

5.3 Objectives

1. To implement the microchemostat system at UKZN. Implementation of the system involves the construction of the chips, microscope setup and development of Matlab scripts for image processing.
2. To utilize the microchemostat to culture *E.coli* constructs whilst monitoring the effects of long-term efflux gene expression on bacterial growth in the absence of drugs.
3. To characterize a multidrug TB efflux pump in terms of substrate specificity and to determine whether efflux gene expression is able to provide a survival advantage in the presence of these drugs.
4. To investigate the main methods through which efflux gene expression can induce resistance.

CHAPTER 6

Microchemostat Characterization of Tap, a Putative Multidrug Efflux Pump Present in *Mycobacterium tuberculosis*.

Jared Mackenzie, [1] Alissa Myrick, [2]* Eric J. Rubin, [2] Frederick K. Balagaddé[1]

[1]Africa Health Research Institute, Nelson R. Mandela School of Medicine, University of KwaZulu-Natal, Durban 4001, South Africa

[2]Department of Immunology and Infectious Diseases, Harvard School of Public Health, Harvard Institutes of Medicine, Room 1007, 4 Blackfan Circle, Boston MA. 02115

*Present address: H3D Drug Discovery and Development Centre, PD Hahn Bldg., University of Cape Town, Rondebosch 7700 Cape Town, South Africa

This chapter consists of a publication submitted to the journal PLoS ONE. At this time, this paper is currently under review. All information presented in this chapter (and publication) is presented in further detail throughout the rest of this thesis. The end of the publication section of this thesis is denoted by a separator page titled “End of Publication”.

PLOS ONE

Microchemostat Characterization of Tap, a Putative Multidrug Efflux Pump Present in Mycobacterium tuberculosis.

--Manuscript Draft--

Manuscript Number:	PONE-D-16-40372
Article Type:	Research Article
Full Title:	Microchemostat Characterization of Tap, a Putative Multidrug Efflux Pump Present in Mycobacterium tuberculosis.
Short Title:	Microchemostat Characterization of a Putative Multidrug Efflux Pump of Mycobacterium tuberculosis.
Corresponding Author:	Frederick K. Balagaddé, Ph.D. KwaZulu-Natal Research Institute for Tuberculosis and HIV Durban, KwaZulu-Natal SOUTH AFRICA
Keywords:	microchemostat; microfluidic; chemostat; Tap; efflux pump; redundancy; Rv1258; ethidium bromide; EtBr; gentamicin; streptomycin; filamentation; dormancy
Abstract:	The Mycobacterium tuberculosis efflux system, estimated to comprise over 80 putative efflux pumps, represents a new frontier in the efforts to impede the ever-worsening spread of drug-resistant forms of Tuberculosis. However, the field will have to confront the challenge of functional redundancy, which obscures the possible contributions of efflux pumps to drug resistance development. We present a new bioengineering approach that involves expression of M. tuberculosis efflux pumps in transporter-deficient E. coli cells combined with high resolution measurements of cellular changes using a microchemostat device. Cells expressing the M. tuberculosis tap-like efflux pump Rv1258 had increased tolerance to growth-inhibiting compounds including streptomycin, gentamicin and ethidium bromide. Rv1258 expression engendered two alternating phenotypes in E. coli with distinct implications for drug tolerance. The first comprised of normal-sized, actively dividing cells with vibrant efflux activity, which can contribute to antibiotic resistance by extruding drug compounds. The second was characterized by arrested cell division and a filamentous cell phenotype, which is associated with the development of drug resistance in pathogenic bacteria. We present a new approach to characterizing efflux pumps, which can overcome the challenge of functional redundancy and will be generally applicable for understanding the interrelatedness among the transporters comprising the M. tuberculosis efflux system and elucidating its putative role in the evolution of drug resistance. Although the approach of engineering the expression of a single pump in E. coli does not require a microchemostat, characterization using the microchemostat was essential to revealing the alternating states of growth and dormancy.
Order of Authors:	Jared Mackenzie
	Alissa Myrick
	Eric J Rubin
	Frederick K. Balagaddé, Ph.D.

Microchemostat Characterization of Tap, a Putative Multidrug Efflux Pump Present in *Mycobacterium tuberculosis*.

Jared Mackenzie,[1†] Alissa Myrick,[2*†] Eric J. Rubin,[2] Frederick K. Balagaddé[1‡]

[1]Africa Health Research Institute, Nelson R. Mandela School of Medicine, University of KwaZulu-Natal, Durban 4001, South Africa
[2]Department of Immunology and Infectious Diseases, Harvard School of Public Health, Harvard Institutes of Medicine, Room 1007, 4 Blackfan Circle, Boston MA. 02115
*Present address: H3D Drug Discovery and Development Centre, PD Hahn Bldg., University of Cape Town, Rondebosch 7700 Cape Town, South Africa

[†]These authors contributed equally to this work.

[‡]To whom correspondence should be addressed. Dr. Frederick K. Balagaddé, Africa Health Research Institute, Nelson R. Mandela School of Medicine, University of KwaZulu-Natal, Durban 4001, South Africa.
Tel. +27 31 260 4544, Fax. +27 31 260 4203, E-mail: frederick.balagadde@k-rith.org

Abstract

The *Mycobacterium tuberculosis* efflux system, estimated to comprise over 80 putative efflux pumps, represents a new frontier in the efforts to impede the ever-worsening spread of drug-resistant forms of Tuberculosis. However, the field will have to confront the challenge of functional redundancy, which obscures the possible contributions of efflux pumps to drug resistance development. We present a new bioengineering approach that involves expression of *M. tuberculosis* efflux pumps in transporter-deficient *E. coli* cells combined with high resolution measurements of cellular changes using a microchemostat device. Cells expressing the *M. tuberculosis* tap-like efflux pump Rv1258 had increased tolerance to growth-inhibiting compounds including streptomycin, gentamicin and ethidium bromide. Rv1258 expression engendered two alternating phenotypes in *E. coli* with distinct implications for drug tolerance. The first comprised of normal-sized, actively dividing cells with vibrant efflux activity, which can contribute to antibiotic resistance by extruding drug compounds. The

second was characterized by arrested cell division and a filamentous cell phenotype, which are both phenotypes associated with the development of drug resistance in pathogenic bacteria. We present a new approach to characterizing efflux pumps, which can overcome the challenge of functional redundancy and will be generally applicable for understanding the interrelatedness among the transporters comprising the *M. tuberculosis* efflux system and elucidating its putative role in the evolution of drug resistance. Although the approach of engineering the expression of a single pump in *E. coli* does not require a microchemostat, characterization using the microchemostat was essential to revealing the alternating states of growth and dormancy.

Introduction

Over the last several years, the frequency and spectrum of multidrug-resistant infections due to *Mycobacterium tuberculosis* have increased resulting in higher rates of morbidity and mortality [191]. The increasing frequency of drug resistance has mostly been attributed to microbial mechanisms typically associated with spontaneous mutations that interfere with drug-target binding, compromise prodrug activation, or cause overexpression of the target. However, the high prevalence of drug-resistant clinical isolates that do not harbor mutations in known resistance genes—reaching 30% in some contexts—is a strong motivation for new areas of research into epigenetic determinants of drug resistance [66]. Bacterial transport systems such as the *E. coli* AcrABTolC system have been extensively studied for their role in exporting xenobiotics through a hierarchical export system [190]. *M. tuberculosis* does not have an analogous system to mediate resistance to dozens of antibiotic classes; however, the large number of primary and secondary transporters may contribute to the intrinsic resistance of mycobacteria, in addition to essential housekeeping functions. Mycobacterial transport proteins (or efflux pumps) have now come into focus as a key factor influencing the rate of the evolution of resistance to antibiotics [192,193].

Studies primarily using single efflux protein knockouts have shown that by extruding specific drug molecules from within microbial cells, efflux pumps not only create low levels of resistance but can also facilitate progressive acquisition of chromosomal mutations that may confer higher levels of resistance [44,194-196]. However, the few experimental demonstrations published to date have underscored the daunting inadequacies of this approach, primarily due to the coexistence of multiple efflux pumps in specific bacterial species with overlapping substrate specificity and functional redundancy. Inactivation of a

specific efflux pump may not yield the expected changes in resistance to an antibiotic drug known to be extruded by the pump due to compensatory overexpression by other efflux pumps with overlapping functionality [107,188]. In theory, all efflux pumps that can extrude the antibiotic would have to be inactivated simultaneously to obtain the desired effect. The functional interplay between the efflux transporters is a key but poorly understood component of microbial efflux systems.

We are developing bioengineering strategies for understanding microbial efflux systems that overcome the challenge of functional redundancy through isolating uncharacterized efflux pumps from native bacterial species and inserting them into transporter-deficient *E. coli* cells [190] in order to 'program' cellular behavior. The *E. coli* expression system insulates the inserted efflux pumps against interference from co-functional transporters that are normally encountered in the native host species, and allows researchers to more cleanly pinpoint antibiotic substrates extrudable by the pump than would be possible by working entirely within the native host environment. Attributes conferred to the *E. coli* cells by expression of the inserted efflux genes are then investigated using a microchemostat—a miniaturized 10 nanoliter bioreactor that enables automated culturing of small populations (10^2–10^4) of bacteria for hundreds of hours with single cell resolution monitoring using optical microscopy [197,198]. By reducing the reactor volume by a factor of at least 10^5 when compared with conventional cell culture vessels, the microchemostat suppresses the total mutation rate proportionately. This, in turn, effectively insulates the micro-cultures from rapid evolution and allows prolonged monitoring of genetically programmed behavior.

The *M. tuberculosis* efflux system represents an interesting challenge because *M. tuberculosis* is the causative agent of Tuberculosis—a respiratory disease which is a leading cause of death worldwide with increasing reports of multidrug-resistant isolates that present a major challenge to effective global control of the disease [199]. Its efflux system is estimated to comprise over 80 putative transport proteins that must be explored for their respective substrate spectra, potential contribution to multidrug resistance and role in the basic biology of the bacterium [102]. While many of these transport systems have functional homology to proteins in other bacteria, their function and role in *M. tuberculosis* has not been elucidated [200,201].

In the present work, we investigated Rv1258, an *in vitro* essential tap-like efflux pump found in *Mycobacterium tuberculosis* that has been associated with resistance to multiple antibiotics including rifampicin, streptomycin, tetracycline, and gentamicin [202-204]. We inserted the Rv1258 gene into transporter-deficient *E. coli* cells and used the microchemostat system to perform high-resolution measurements of the perturbations in cellular behavior due to expression of the Rv1258 genes in the presence and absence of growth-inhibiting substrates of the pump. Nonlinear regression analysis of the microchemostat data (described in the methods section) yielded transitory phenotypic properties—including the instantaneous growth rate and cell filamentation rates, which were essential for quantifying the efflux attributes but not obtainable with conventional culturing platforms.

In addition to increasing tolerance to growth-inhibiting compounds including streptomycin, gentamicin and ethidium bromide in *E. coli* cells, constitutive expression of the Rv1258 gene engendered two alternating phenotypes representing distinct implications for drug-tolerance: active and dormant efflux. During active efflux, the pump actively extruded substrates from within the cells, which were normal-sized and actively dividing. A decrease in the intracellular concentration of antibiotics is associated with antibiotic resistance development [44,194-196]. Conversely, the dormant efflux phase was characterized by suppressed efflux activity, filamentous cell morphology and cell division arrest. Filamentation is a recurring phenotype in many pathogenic bacterial species, providing several survival advantages [205] and in some cases enhancing the development of antibiotic resistance [206,207]. A non-dividing cell phenotype can also contribute to resistance to antibiotics that rely on active cell division to achieve rapid killing, which may include antibiotics that are not directly extruded by the efflux pumps [208,209]. In this study we present a new approach to characterizing efflux gene expression dynamics and evaluating the specificity of drug substrates to specific efflux pumps, which can overcome the challenge of functional redundancy encountered in the native mycobacterial environment. We believe this approach will be generally applicable for understanding the interrelatedness among the efflux transporters comprising the *M. tuberculosis* efflux system and elucidating its putative role in the evolution of drug resistance.

Materials and Methods

***E. coli* strains:** The wild type *E coli* cells—BW25113 *ΔemrE ΔmdfA*—lacked two of the transporters responsible for multidrug resistance [99]. Cloning of the Rv1258 tap-like efflux pump into arabinose inducible vector, pBAD-DEST49, was performed by standard Gateway cloning by amplifying complete genes minus the stop codon with attB and promoter regions modified within the primers (S1A Fig.). The plasmid was maintained with 100μg/ml of ampicillin. The GFP plasmid (S1B Fig.) was cloned similarly and was maintained using 100μg/ml of chloramphenicol.

Microchemostat cultures, medium and growth conditions: Luria Bertani (LB) medium (Sigma Aldrich) used in the microchemostat and off-chip cultures contained tryptone (10g/L), yeast extract (5g/L), NaCl (5g/L), inert binding agents (2.2g/L) and bovine serum albumin (10g/L) as an anti- cell adhesion adjuvant. Pre-cultures for microchemostat experiments were prepared by inoculating 10 ml of sterile medium with 100μl of glycerol stock cultures and shaking at 120 rpm for 4 hours at 37˚C in a bench top incubator (Scientific Orbital Shaking, model 260). The pre-cultures were then used to seed microchemostat reactors. The pBAD-DEST49 plasmid was maintained with 100μg/ml of ampicillin (Sigma-Aldrich). The heterologous efflux pump, under control of a synthetic promoter was inducible with arabinose (Sigma-Aldrich) at concentrations ranging from 0.0002% to 0.0008% (v/V). All the microchemostat chip experiments were performed on a heated stage to maintain the growth temperature at 37˚C.

Preparation of conditioned medium: *E. coli* cells carrying the GFP or the Rv1258 plasmid were grown in LB medium containing arabinose (3.2mg/L) for 24 hours at 37°C to a final OD_{600} of 1.65. The supernatant was collected and sterilized by filtration through a 0.2-μm-pore-size filter.

Antibiotic treatment: To determine the effect of antibiotics, cells were grown in the microchemostat in drug-free medium for 24 to 40 hours to establish a steady state cell density. Medium containing the test drugs including streptomycin (0.78μg/ml) or gentamicin (1.56 μg/ml) was then introduced to the microchemostat cultures for the remainder of the experiment.

Microchemostat chip design and fabrication: Microchemostat chips were fabricated out of silicone elastomer polydimethylsiloxane (Momentive Performance Materials, Columbus, OH, RTV 615) using multi-layer soft lithography as described previously. In this chip, the number of reactors per chip was increased to 14 as described previously [197,198].

Microscopic cell counting: The total number of cells in each reactor was determined directly through automated phase contrast microscopy by counting the number of cells present in a growth chamber section of the microchemostat of known volume. Phase-contrast images were captured using a cooled charge coupled device camera (XM10, monochrome from Olympus). A Nikon Ti Eclipse inverted microscope (Nikon UK Ltd, Surrey, UK) with a 40×/0.6NA Ph2 objective (Nikon, UK) was used for all measurements. Labview software was used to control all chip operation. Typically, a set of eight phase-contrast images was taken in each reactor, with mixing of the culture in between each snapshot. Image processing algorithms written in Matlab software were used to determine the average number of cells in each set of pictures, from which the total cell count was determined as described previously [197,198]. A motorized stage system on the Nikon Ti-E microscope enabled simultaneous documentation of multiple microchemostat experiments that operated in parallel on a single chip. Focus was maintained using the perfect focus system (PFS) feature of the Nikon microscope.

Regression analysis: Step 1. Cubic spline interpolation. We employed cubic spline interpolation using Matlab's curve fitting tool with a (fit parameter = 0.5) to fit smooth curves to cell density and cell length data obtained from the microchemostat cultures. Box 1, panel 1 shows on the primary axis, the cell density data (grey points) and the cubic spline fit (blue curve); and on the secondary axis, the cell length data (orange dots) and the cubic spline fit (red curve). Interpolation also served the purpose of denoising the data by removing point-to-point noise variations, which made it possible to obtain the instantaneous derivatives from the smoothed data in Step 4. **Step 2. Cell length transformation.** To perform the cell length transformation, the cell length value in each data point was multiplied by a constant -A and then, another constant B was added to the result. This transformation flipped the cell length graph about the horizontal axis, shrank it by a factor of A, and then shifted the entire graph upward by a value of B. Box 1, panel 2 shows the original cell length trend (**L**(t); dashed red curve) as well as the transformed trend ($-A \cdot \mathbf{L}(t) + B$; solid red curve). **Step 3. Cell density transformation.** To perform the cell density transformation, a time constant τ_D was added to

the time value of each cell density data point, which had the effect of shifting the cell density graph to the right by the value, τ_D. Box 1, panel 3 shows the entire graph of the original cell density trend (**n**(t); dashed blue curve) as well as the transformed trend (**n**(t-τ_D); solid blue curve). The values A, B and τ_D were adjusted as necessary until the best fit was obtained for the transformed length graph $[-A \cdot \boldsymbol{L}(t) + B]$ superimposed over the transformed cell density graph [**n**(t-τ_D)] in terms of periodicity and amplitude. **Step 4. Finite Element Derivatives.** At each time point, *i*, the finite element derivative, $[dy/dt]_i$ for the cell density or cell length (designated y_i) was obtained from the interpolated data generated in Step 1 using the equation:

$$\frac{dy}{dt}_i = \frac{y_{i+1} - y_i}{t_{i+1} - t_i}$$

The derivative graphs for cell density ($d\boldsymbol{n}/dt$, or cell division rate) and cell length ($d\boldsymbol{L}/dt$, or the filamentation rate) were then transformed using the approach outlined in steps 2 and 3. Box 1, panel 4 shows the first derivatives of the transformed graphs, $d\boldsymbol{n}\,(t - \tau_D)/dt$ and $-A \cdot d\boldsymbol{L}/dt$.

Results and Discussion

Effect of Rv1258 expression on *E. coli* cell morphology. The tap-like efflux pump gene designated Rv1258, which encodes a multidrug efflux pump in *M. tuberculosis* was isolated and expressed from a plasmid in transporter-deficient *E. coli* under control of an arabinose-inducible promoter (S1A. Fig.). Efflux gene expression dynamics were measured by monitoring the *E. coli* cells using a microchemostat—a miniaturized 10 nl bioreactor that enables automated culturing of small populations (10^2–10^4) of bacteria for hundreds of hours. By continually substituting a fraction of a bacterial culture with sterile nutrients, the microchemostat creates a near-constant environment that is ideal for long-term controlled studies of microbes and microbial communities. Some cell populations carrying the Rv1258 plasmid were induced with arabinose (efflux ON) and others were not induced (efflux OFF), and yet others contained no plasmid but were cultured with arabinose (Fig. 1A). Efflux OFF (reactor 5 and 6) and plasmid-free (reactors 7 and 8) cultures grew exponentially to a steady-state density of ~2.5 cells/pL. In contrast, growth in efflux ON cultures 1 and 2 exhibited damped oscillations whereby the cell density dropped dramatically after the first oscillation cycle and then sustained smaller amplitude oscillations about a reduced steady state of ~0.7 cells/pL.

Fig. 1. (**A**) **Typical microchemostat growth curves of *E. coli* cells expressing the efflux or GFP plasmids**. Graphs are shown for growth with the efflux ON (reactors 1 to 2), efflux OFF (reactors 5 to 6), GFP ON (reactor 3), GFP OFF (reactor 4), or plasmid-free (reactors 7 to 8**). (B) Graphs of the average specific cell length corresponding to each of the cell populations depicted in (A) measured at each time point.** All graphs are smoothed spline interpolations of raw data shown in S2 Fig. Bottom panels (a to e) show micrographs of the cells in reactor 1 at the corresponding points during the first oscillation (scale bar, 25 μm). Cells were grown at 37°C in LB medium at a dilution rate of 0.32 $hour^{-1}$ and induced with 3.2 mg/L arabinose.

To ascertain that the damped oscillation in the efflux ON cultures were due to expression of the Rv1258 gene, we utilized a control plasmid in which the green fluorescent protein (*GFP*) gene was substituted for the Rv1258 efflux pump gene (S1B Fig.). As shown in Fig. 1A, cells in reactor 3 carrying the GFP plasmid that were induced with arabinose (GFP ON) grew without oscillation in cell density to a steady-state of ~1 cell/pL. The uninduced *GFP* culture (GFP OFF) in reactor 4 also grew without oscillation in cell density to a steady state of ~2 cells/pL, which was double that of the GFP ON cultures. Induction with arabinose led to a ~25% reduction in the steady state cell density of GFP cells but increased the fraction of GFP fluorescent cells from ~8% in the GFP OFF population to ~67% in the GFP ON population (S3 Fig.). The reduced density of the GFP ON population relative to the GFP OFF culture demonstrates the fitness cost associated with expression of plasmid encoded genes. However, the variations in steady-state cell density of GFP ON cells were negligible compared to the overall population oscillations observed in the efflux ON cultures. Thus, the oscillations observed in the efflux ON cultures could neither be accounted for by arabinose induction nor the plasmid backbone but were attributable to Rv1258 gene expression.

A deterministic relationship between cell density and cell length during expression of Rv1258 by *E. coli* cells. By monitoring specific cell morphologies in the microchemostat cultures, we observed that expression of Rv1258 induced cell filamentation (Fig. 1B). Efflux ON cells were on average 2 to 3 times longer than the cells in the non-effluxing populations, with specific cell lengths routinely reaching 30μm, which was ~10 times greater than the typical length of the cells in the non-effluxing cultures. Remarkably, the average cell length

in the efflux ON populations exhibited oscillatory behavior that was not observed in the non-effluxing populations, but was tightly coupled to the oscillations in cell density. For example, Fig. 2A shows the cell density and average cell length of the population depicted in culture 2 of Fig. 1. The oscillations in cell density were reversed relative to the oscillations in the average cell length and phase delayed by ~12 minutes. This deterministic relationship is illustrated in Fig. 2B and specified by a phase-shifted linear equation:

$$\boldsymbol{n}(t-\tau_D) \cong -A \cdot \boldsymbol{L}(t) + B \tag{1}$$

where $\boldsymbol{n}$ is the cell density (cells/pL), $\boldsymbol{L}$ is the cell length (μm), and τ_D represents the ~12-minute time delay between the cell density and length waves. A and B are relationship constants that were measured to be 0.45 cells/pL·μm and 2.15 cells/pL respectively.

Fig. 2. (A) Growth curve (blue; primary axis) and cell length (red; secondary axis) with the Rv1258 efflux pump ON. **(B)** Growth curve (blue) shifted forward in time by a time delay (τ_D= 12 minutes) and linear transformation of cell length as per equation 1 (red). **(C)** Finite element derivatives of experimental data showing the cell division rate (blue, primary axis) and cell elongation rate (red, secondary axis). **(D)** Finite element cell division rate (blue) shifted forward in time by the time delay (τ_D = 12 minutes) and the linear transformation of the elongation rate as per equation 2 (red).

To probe the interrelation between cell density and length, and the link to Rv1258 gene expression, we looked to the first derivative association of the time-variable parameters in equation 1:

$$\frac{d\boldsymbol{n}(t-\tau_D)}{dt} \cong -A \cdot \frac{d\boldsymbol{L}(t)}{dt} \tag{2}$$

where d**n**/dt is the cell division rate (cells/pL·hour) and d**L**/dt is the filamentation rate (μm/hour). This relationship was consistent with the finite element derivatives obtained from the experimental data (Fig. 2C) whereby the oscillations in the filamentation rate were reversed relative to the oscillations in the cell division rate and phase-shifted by the time-delay of ~12 minutes, as illustrated in Fig. 2D. Except for the 12-minute lag in the elongation rate signal, the cell division rate varied directly as the elongation rate. Thus, for instance, a decrease in the growth rate coincided with a proportional increase in the elongation rate, and

vice versa, although the changes in the filamentation rate were always delayed by a ~12-minutes lag, designated τ_D.

The time-shifted but direct proportionality relationship between the cell division and filamentation rates suggest that the filamentous phenotype adopted by efflux ON cells was due to cell division arrest, whereby rod-shaped cells ceased to divide into separate daughter cells but instead continued to grow in volume and length. Cell filamentation behavior has been observed in other bacterial species in response to a variety of stressful environments, including nutrient deficiency [210], extensive DNA damage through the SOS response pathway [211], host innate immune responses [212], and antibiotic treatment [213-215]. In addition, the filamentation response was not permanent, because periodically, the filamentation rate was reversed during periods when the cells gradually reverted back towards a normal rod-shaped phenotype (Fig. 2 and S4 Fig.). The transitions between the alternating periods of increasing and decreasing filamentation rates in the efflux ON populations were notably abrupt and switch-like (Fig. 2C). Population-wide synchronized control of gene expression is necessary for such switch-like transitions; from which we can infer that the cyclic cell filamentation pattern was a response to fluctuations in a population-wide factor, such as the extracellular concentration of a stress factor. We have previously shown that the observed filamentation pattern was caused by Rv1258 gene expression, and therefore we attributed the filamentation process to the extracellular concentration of a bio-chemical signal extruded from within the cells by the Rv1258 efflux pump (referred to as the natural efflux product in the remainder of this manuscript). This inference was supported by cell culture experiments performed using conditioned medium (i.e., medium containing the suspected growth-inhibiting factors extruded by the Rv1258 efflux pump). We observed a 20% reduction in growth of GFP cells supported by medium conditioned with *E. coli* cells expressing the Rv1258 plasmid-encoded gene relative to GFP cells supported by medium conditioned with cells expressing the GFP gene (S5 Fig.).

An extension of this inference is that the natural product extruded by the Rv1258 efflux pump suppresses its own production—a necessary condition for the observed oscillatory behavior. Together, our results show that the Rv1258 efflux pump extrudes a natural product, synthesized intracellularly that is evidently non-disruptive to cell growth and morphology in the intracellular environment—a necessary requirement for the observed switch-like transitions. However, once extruded from the cell, the natural efflux product can accumulate

in the extracellular environment and at sufficiently high concentrations, effect cell-division arrest, resulting in cell filamentation, and a decreased production of the natural efflux product. Eventually, when the production rate of the natural efflux product falls below the dilution rate, the natural efflux product gets diluted out of the microchemostat culture, which reverses the filamentation process, and the population recovers and enters the next cycle.

Consistent observations were made in conventional liquid batch cultures (S6 Fig.). Following the lag and exponential growth phases, the non-effluxing cultures entered stationary phase after ~8 hours of culturing with a cell density of ~1.6 (OD_{600}). The typical non-effluxing cell length decreased from ~10μm during lag phase to ~3μm during stationary phase. By contrast, efflux ON cultures prematurely entered stationary phase after only 4 hours of culture with a lower cell density of ~0.8 (OD_{600}). The typical efflux ON cell length increased from ~10μm during lag phase to ~16μm during stationary phase. In the absence of continuous dilution, these stationary phase characteristics persisted throughout the remainder of the culturing process, in contrast to the microchemostat cultures that underwent oscillatory behavior.

Rv1258 expression increases tolerance to growth-inhibiting compounds in *E. coli* cells. We next investigated the efflux phenotype due to Rv1258 expression at various concentrations of ethidium bromide (EtBr)—a known inhibitor for *E. coli* cell growth [216,217] that has previously been documented as a substrate of the Rv1258 pump [218]. As shown in the top row of Fig. 3A, in the efflux OFF cultures, as the ethidium bromide concentration was increased from 0 to 0.25, 0.5 and 1μg/ml, the steady-state cell density decreased from ~2.6 to ~2.5, ~1.7, and <0.7 cells/pL respectively, illustrating the deleterious effect of EtBr in the absence of efflux. As described previously, in the absence of EtBr, the typical efflux ON culture displayed damped oscillations in the cell density, attaining a steady-state density of ~0.7 cells/pL that was ~3× lower than the corresponding efflux OFF culture. However, in contrast to the efflux OFF trend, the efflux ON steady state density was maintained at ~0.7 cells/pL when the EtBr concentration increased to 0.25μg/ml EtBr, and even increased slightly to ~0.85 cells/pL at a higher EtBr concentration of 0.5μg/ml. Clearly, EtBr extrusion by the Rv1258 efflux pump enabled the efflux ON cells to maintain a high cell density—comparable to the density in the EtBr-free culture—at EtBr concentrations that affected growth in the equivalent efflux OFF cultures (0.25 and 0.5μg/ml). When the EtBr concentration was increased further to 1μg/ml, the Rv1258 efflux pump became overwhelmed and the efflux ON culture registered a major decrease in growth and steady-

state density. The corresponding dynamics in cell length are shown in the bottom row of Fig. 3.

Fig. 3. (A) Top row graphs represent the effects of the ethidium bromide (EtBr) concentration on population dynamics of *E.coli* cells with efflux ON or OFF. In the efflux OFF cultures, the steady-state cell density decreased with increasing EtBr concentration. The efflux ON cultures maintained their steady state density as the concentration of EtBr was increased except for the highest EtBr concentration of 1μg/ml. Bottom row graphs represent dynamics in cell length corresponding to the growth curves in the top rows. All graphs are smoothed spline interpolations of raw data shown in S7 Fig. Cells were grown at 37°C in LB medium at a dilution rate of 0.32 $hour^{-1}$ and induced with 3.2 mg/L arabinose. **(B) Time delay (τ_D) between the growth and elongation oscillatory dynamics as a function of ethidium bromide concentration (EtBr).** As the EtBr dose was increased from 0 to 0.25, 0.5 and 1μg/ml, the time-delay τ_D increased from 12 minutes, to 40 minutes, 1 hour and 1 hour, respectively.

At higher concentrations of EtBr (12.5 and 25μg/ml), microbial biofilms, which are not subject to wash-out through continuous bioreactor operation of the microchemostat, supplied most of the bulk culture cells in both the efflux OFF and ON cultures, leading to much higher cell densities than were achievable under more ideal chemostat conditions at lower EtBr concentrations (S8 Fig.). Exactly why biofilm formation was exacerbated at high concentrations of EtBr is unclear. However, as a result of elevated biofilm formation, we observed that at 12.5 μg/ml EtBr, the efflux ON and OFF microchemostat populations attained cell densities as high as ~2.5 cells/pL, which was at least 3× higher than the densities attained at 1ug/ml EtBr, in spite of the growth inhibitory effect of EtBr. At 25μg/ml of EtBr, the efflux ON cell density (~ 4 cells/pL) exceeded that of the efflux OFF culture (~3 cells/pL), further illustrating increased biofilm formation at higher concentrations of EtBr and the EtBr extrusion advantage conferred by the Rv1258 efflux pump to the efflux ON cells.

The interference between the efflux extrusion of EtBr and the natural efflux product of the Rv1258 pump was observable in the efflux ON cultures at the various concentrations of EtBr. As the EtBr dose was increased from 0 to 0.25, 0.5 and 1μg/ml, the frequency of the oscillations in the steady-state cell density and length increased while their amplitude

decreased in tandem, and these oscillations essentially disappeared in the 0.5 and 1μg/mL EtBr concentration efflux ON graphs (Fig. 3A). Furthermore, the time-delay τ_D between the cell density and cell length oscillations increased from 12 minutes, to 40 minutes, 1 hour and 1 hour, respectively (Fig. 3B). The response dynamics slowed down as the EtBr concentrations was increased. We speculate that this behavior was due to efflux substrate displacement whereby the EtBr molecules competed with the natural efflux product molecules for extrusion through the Rv1258 pump, which delayed accumulation of the natural efflux product in the extracellular environment and the onset of cell filamentation.

We next investigated drug-tolerance under Rv1258 gene expression by introducing antibiotics including streptomycin and gentamicin to microchemostat cell populations that had reached a steady state density. In a representative set of experiments involving streptomycin (Fig. 4A), the efflux pump was turned ON in culture 1; left OFF in culture 2; and absent (no plasmid) in culture 3. In the absence of streptomycin (time 0 to 40 hours), the non-effluxing cultures grew to a steady-state density of ~2 cells/pL, while the efflux ON cell density oscillated to a lower density of ~0.5 cells/pL. When medium containing streptomycin (0.78 μg/ml) was introduced at 40 hours, the non-effluxing cultures decayed exponentially and were washed out by 90 hours. By contrast, upon introduction of streptomycin, the cell density in efflux ON culture 1 initially dropped to ~0.1 cells/pL but recovered at 60 hours to the pre-streptomycin steady state of ~0.5 cells/pL that was maintained during the remainder of the experiment, which lasted to 130 hours. Similar dynamics were apparent when gentamicin (1.56 μg/ml) was introduced to different cell populations under otherwise similar conditions (Fig. 4B). Prior to introducing gentamicin, the efflux OFF and plasmid-free populations attained steady-state cell densities of ~3 cells/pL, and the efflux ON culture ~0.5cells/pL. Upon introduction of gentamicin, the non-effluxing cells washed out of the microchemostat reactors while the efflux ON culture dropped to a cell density of ~0.1cells/pL and did not wash out of the reactor. Altogether these results illustrate that expression of the Rv1258 efflux pump increased tolerance to streptomycin and gentamicin.

Fig. 4. (A) Growth of *E. coli* cells in the presence of streptomycin (0.78μg/ml) including a log scale in the inset. Initially, the efflux pump was turned ON in culture 1 and left OFF in culture 2. Culture 3, which was plasmid-free and inoculated at time 20 hours (point A) was cultivated on a separate chip in a different experiment under the same conditions. At 40 hours (point B), medium containing streptomycin was introduced to all cultures. The cell density in

the non-effluxing cultures 2 and 3 decayed and washed out, whereas that of the effluxing culture 1 attained a non-trivial steady-state of 0.5 cells/pL. **(B) Growth of *E. coli* cells in the presence of gentamicin (1.56µg/ml) including a log scale in the inset.** Initially, the efflux pump was turned ON in culture 1, left OFF in culture 2, and absent in culture 3. At 24 hours (point B), medium containing gentamicin was introduced to all cultures. Whereas the non-effluxing cultures washed out, the efflux ON culture attained a lower steady-state density of 0.1 cells/pL. All graphs are smoothed spline interpolations of raw data shown in S10 Fig. All cells were grown at 37°C in LB medium at a dilution rate of 0.16 $hour^{-1}$ and induced with 3.2 mg/L arabinose.

Conclusions

Our data demonstrate that there is a yet unidentified natural efflux product extruded by the Rv1258 efflux pump, which suppresses its own production and causes cell-division arrest and filamentation at sufficiently high extracellular concentration. In a closed system without replenishment of nutrients or other growth factors during the period of incubation, constitutive Rv1258 expression led suppressed growth and a filamentous phenotype, conditions which persisted indefinitely. In the microchemostat where the cell culture was periodically substituted with fresh sterile medium, constitutive expression of the Rv1258 efflux gene engendered alternating phases of two distinct phenotypes, which we refer to here as active and dormant efflux. During active efflux, a natural efflux product was actively extruded from within the cells. This phase was characterized by normal-sized, actively dividing cells. A decrease in the intracellular concentration of antibiotics extruded by the pump during this phase impairs their accessibility to the drug target and can facilitate progressive acquisition of chromosomal mutations that confer higher levels of resistance to the respective antibiotics. Conversely, the dormant efflux phase was characterized by suppressed efflux product extrusion and filamentous cells with arrested cell division, which gradually reverted back towards a more normal cell shape, cell division rate and efflux product extrusion rate. Although drug molecule extrusion by the efflux pump may be suppressed during this phase, the filamentous shape represents a survival strategy known to protect bacteria from antibiotic medicines and allows bacteria to survive engulfment by phagocytic cells [206]. In addition, because most bactericidal antibiotics rely on bacteria to be actively dividing to achieve rapid killing, a filamentous phenotype engendered by efflux

activity can in theory confer broader phenotypic resistance to drugs that the efflux pumps may not directly extrude.

We have demonstrated, using Rv1258 as a test-case, that expression of *M. tuberculosis* efflux pumps in transporter-deficient *E. coli* cells combined with high resolution measurement of cellular properties using the microchemostat platform, can address the challenge of functional redundancy and enable researchers to more cleanly pinpoint compound substrates extrudable by the pump. The approach we have outlined should serve as a robust and widely applicable route to screen the performance of other discrete transporter proteins against a wider range of compounds and efflux pump inhibitors, with the ultimate goal of reconstructing the functional interplay between the various transporters comprising the *M. tuberculosis* efflux system, their potential contribution to multidrug resistance and role in the basic biology of the species.

Acknowledgements

This work was supported by funding from Howard Hughes Medical Institute and in part by South Africa's National Research Foundation. We thank Richard Losick, Alex Sigal and Alasdair Leslie for helpful discussions.

References

1. Global tuberculosis report 2015: World Health Organization.

2. Fonseca J, Knight G, McHugh T (2015) The complex evolution of antibiotic resistance in Mycobacterium tuberculosis. International Journal of Infectious Diseases 32: 94-100.

3. Tal N, Schuldiner S (2009) A coordinated network of transporters with overlapping specificities provides a robust survival strategy. Proceedings of the National Academy of Sciences 106: 9051-9056.

4. Lee RE, Hurdle JG, Liu J, Bruhn DF, Matt T, et al. (2014) Spectinamides: a new class of semisynthetic antituberculosis agents that overcome native drug efflux. Nature medicine 20: 152-158.

5. Louw GE, Warren RM, Gey van Pittius NC, Leon R, Jimenez A, et al. (2011) Rifampicin reduces susceptibility to ofloxacin in rifampicin-resistant Mycobacterium tuberculosis

through efflux. American journal of respiratory and critical care medicine 184: 269-276.

6. Schmalstieg AM, Srivastava S, Belkaya S, Deshpande D, Meek C, et al. (2012) The antibiotic resistance arrow of time: efflux pump induction is a general first step in the evolution of mycobacterial drug resistance. Antimicrob Agents Chemother 56: 4806-4815.

7. Rodrigues L, Machado D, Couto I, Amaral L, Viveiros M (2012) Contribution of efflux activity to isoniazid resistance in the Mycobacterium tuberculosis complex. Infect Genet Evol 12: 695-700.

8. Machado D, Couto I, Perdigao J, Rodrigues L, Portugal I, et al. (2012) Contribution of efflux to the emergence of isoniazid and multidrug resistance in Mycobacterium tuberculosis. PLoS One 7: e34538.

9. Poole K (2007) Efflux pumps as antimicrobial resistance mechanisms. Annals of medicine 39: 162-176.

10. Domenech P, Reed MB, Barry CE, 3rd (2005) Contribution of the Mycobacterium tuberculosis MmpL protein family to virulence and drug resistance. Infect Immun 73: 3492-3501.

11. Li X-Z, Barré N, Poole K (2000) Influence of the MexA-MexB-OprM multidrug efflux system on expression of the MexC-MexD-OprJ and MexE-MexF-OprN multidrug efflux systems in Pseudomonas aeruginosa. Journal of Antimicrobial Chemotherapy 46: 885-893.

12. Balagadde FK, Song H, Ozaki J, Collins CH, Barnet M, et al. (2008) A synthetic Escherichia coli predator-prey ecosystem. Molecular Systems Biology 4.

13. Balagadde FK, You LC, Hansen CL, Arnold FH, Quake SR (2005) Long-term monitoring of bacteria undergoing programmed population control in a microchemostat. Science 309: 137-140.

14. Jeyaseelan L, Williams D, Tibrewal S, Ali SA, Hassan M, et al. (2015) Tuberculosis of the Cuboid: A Case Report and Review of the Literature. The Journal of Foot and Ankle Surgery 54: 713-716.

15. Youm J, Saier MH, Jr. (2012) Comparative analyses of transport proteins encoded within the genomes of Mycobacterium tuberculosis and Mycobacterium leprae. Biochim Biophys Acta 1818: 776-797.

16. Sarathy JP, Dartois V, Lee EJD (2012) The role of transport mechanisms in Mycobacterium tuberculosis drug resistance and tolerance. Pharmaceuticals 5: 1210-1235.

17. De Rossi E, Ainsa JA, Riccardi G (2006) Role of mycobacterial efflux transporters in drug resistance: an unresolved question. FEMS Microbiol Rev 30: 36-52.

18. Aínsa JA, Blokpoel MC, Otal I, Young DB, De Smet KA, et al. (1998) Molecular cloning and characterization of Tap, a putative multidrug efflux pump present in Mycobacterium fortuitum and Mycobacterium tuberculosis. Journal of bacteriology 180: 5836-5843.

19. Ramón-García S, Martín C, Aínsa JA, De Rossi E (2006) Characterization of tetracycline resistance mediated by the efflux pump Tap from Mycobacterium fortuitum. Journal of Antimicrobial Chemotherapy 57: 252-259.

20. De Rossi E, Arrigo P, Bellinzoni M, Silva PAE, Martín C, et al. (2002) The multidrug transporters belonging to major facilitator superfamily in Mycobacterium tuberculosis. Molecular medicine (Cambridge, Mass) 8: 714 - 724.

21. Justice SS, Hunstad DA, Cegelski L, Hultgren SJ (2008) Morphological plasticity as a bacterial survival strategy. Nat Rev Micro 6: 162-168.

22. Bos J, Zhang Q, Vyawahare S, Rogers E, Rosenberg SM, et al. (2015) Emergence of antibiotic resistance from multinucleated bacterial filaments. Proceedings of the National Academy of Sciences 112: 178-183.

23. Zhang Q, Lambert G, Liao D, Kim H, Robin K, et al. (2011) Acceleration of Emergence of Bacterial Antibiotic Resistance in Connected Microenvironments. Science 333: 1764-1767.

24. Herbert D, Paramasivan C, Venkatesan P, Kubendiran G, Prabhakar R, et al. (1996) Bactericidal action of ofloxacin, sulbactam-ampicillin, rifampin, and isoniazid on logarithmic-and stationary-phase cultures of Mycobacterium tuberculosis. Antimicrobial agents and chemotherapy 40: 2296-2299.

25. Justice SS, Hunstad DA, Cegelski L, Hultgren SJ (2008) Morphological plasticity as a bacterial survival strategy. Nature Reviews Microbiology 6: 162-168.

26. Tal N, Schuldiner S (2009) A coordinated network of transporters with overlapping specificities provides a robust survival strategy. Proc Natl Acad Sci U S A 106: 9051-9056.

27. Pine L, Boone CJ (1967) Comparative cell wall analyses of morphological forms within the genus Actinomyces. Journal of bacteriology 94: 875-883.

28. Bos J, Yakhnina AA, Gitai Z (2012) BapE DNA endonuclease induces an apoptotic-like response to DNA damage in Caulobacter. Proceedings of the National Academy of Sciences 109: 18096-18101.

29. Justice SS, Hunstad DA, Seed PC, Hultgren SJ (2006) Filamentation by Escherichia coli subverts innate defenses during urinary tract infection. Proceedings of the National Academy of Sciences 103: 19884-19889.

30. ROLINSON GN (1980) Effect of β-lactam antibiotics on bacterial cell growth rate. Microbiology 120: 317-323.

31. Ryan D, Monsey D (1981) Bacterial filamentation and in vivo efficacy: a comparison of several cephalosporins. Journal of Antimicrobial Chemotherapy 7: 57-63.

32. Miller C, Thomsen LE, Gaggero C, Mosseri R, Ingmer H, et al. (2004) SOS response induction by ß-lactams and bacterial defense against antibiotic lethality. Science 305: 1629-1631.

33. Tomchick R, Mandel H (1964) Biochemical effects of ethidium bromide in micro-organisms. Microbiology 36: 225-236.

34. Tønnesen T, Friesen J (1973) The effects of daunomycin and ethidium bromide on Escherichia coli. Molecular and General Genetics MGG 124: 177-186.

35. Coelho T, Machado D, Couto I, Maschmann R, Ramos D, et al. (2015) Enhancement of antibiotic activity by efflux inhibitors against multidrug resistant Mycobacterium tuberculosis clinical isolates from Brazil. Frontiers in microbiology 6: 330.

Supporting Information

Legends to supplementary figures.

S1 Fig. Implementation of the Rv1258 and GFP plasmid constructs. (A) The tap-like efflux gene designated Rv1258, cloned from *M. tuberculosis*, was inserted into an arabinose inducible plasmid pBAD-DEST49 and maintained by Ampicillin. **(B)** The GFP gene cloned into the same arabinose inducible plasmid pBAD-DEST49 is maintained by chloramphenicol. AMP^R, ampicillin resistance; CM^R, chloramphenicol resistance; P_{ara}, arabinose promoter.

S2 Fig. Raw data of *E. coli* cells cultured in the microchemostat showing the cell density on the primary axis (red curve with black dots) or average specific cell length on the secondary axis (orange curve with gray dots) as a function of time for the curves depicted in Fig. 1A and B. Cells were grown at 37°C in LB medium at a dilution rate of 0.16 $hour^{-1}$ under conditions indicated on the right of each graph.

S3 Fig. Microchemostat growth curves of *E. coli* cells carrying the GFP plasmid construct schematized in S1B Fig. with an arabinose inducible promoter driving GFP gene expression. Cells were grown with arabinose (induced, Left) or without (uninduced, Right). The red growth curves represent the overall cell density and the green curves represent the density of the fluorescent cells. Cells were grown with a dilution rate of 0.32 $hour^{-1}$ at 37°C in LB medium and induced with 3.2 mg/L arabinose.

S4 Fig. Rv1258 expression engendered two alternating, distinct morphological phenotypes in *E. coli* cells. The first phenotype comprised of normal-sized, rod-shaped, actively dividing cells depicted in panel **(A)**. The second was characterized by arrested cell division and filamentous cells depicted in panel **(B)**. The cells shown here were grown in a microchemostat with a dilution rate of 0.32 $hour^{-1}$ at 37ºC in LB medium and induced with 3.2 mg/L arabinose.

S5 Fig. (A) Growth of *E. coli* cells expressing the Rv1258 and GFP plasmid-encoded genes in liquid media. For each condition, 10 ml of fresh LB medium containing arabinose was inoculated with cells containing the Rv1258 or GFP plasmid and incubated with shaking at 37ºC for 24 hours. **(B) Growth of *E. coli* cells carrying the GFP plasmid in conditioned medium. Conditioned with *E. coli* cells expressing the Rv1258 or the GFP plasmid.** 10 ml of medium conditioned with *E. coli* cells expressing the Rv1258 or GFP plasmid-encoded

genes was inoculated with cells containing the GFP plasmid and incubated with shaking at 37ºC for 24 hours. There was a 20% growth reduction in growth of GFP cells supported by the medium conditioned with cells expressing the Rv1258 gene.

S6 Fig. (A) Growth of *E. coli* cells in conventional liquid tissue culture flask batch cultures with the efflux pump ON (black circles), OFF (blue squares) or absent (red diamonds). Following lag and exponential growth phases, the non-effluxing cultures entered stationary phase after ~8 hours of culturing with a cell density of ~1.6 (OD600). By contrast, efflux ON cultures prematurely entered stationary phase after only 4 hours of culture with a lower cell density of ~0.8 (OD600). **(B)** Micrographs of the cells in corresponding to the graphs in A at different time points. The typical non-effluxing cell length decreased from ~10μm during lag phase to ~3μm during stationary phase. The typical efflux ON cell length increased from ~10μm during lag phase to ~16μm during stationary phase. (Scale bar, 25 μm). Cells were inoculated into 10ml of LB broth and cultivated at 37°C tissue culture flasks with shaking at 280 rpm, and induced with 3.2 mg/L arabinose.

S7 Fig. Raw data of *E. coli* cells cultured in the microchemostat showing the cell density on the primary axis (red curve and black dots) or average specific cell length on the secondary axis (orange curve and gray dots) as a function of time for the curves depicted in Fig. 3A. Cells were grown at 37°C in LB medium at a dilution rate of 0.16 $hour^{-1}$ under conditions indicated on the right of each graph.

S8 Fig. Top and bottom row graphs represent the effects of high concentrations of ethidium bromide (EtBr) on population dynamics of *E.coli* cells with efflux ON or OFF. All graphs are smoothed spline interpolations of raw data shown in S9 Fig. Cells were grown at 37°C in LB medium at a dilution rate of 0.32 $hour^{-1}$ and induced with 3.2 mg/L arabinose.

S9 Fig. Raw data of *E. coli* cells cultured in the microchemostat showing the cell density on the primary axis (red curve and black dots) or average specific cell length on the secondary axis (orange curve and gray dots) as a function of time for the curves depicted in S8 Fig. Cells were grown at 37°C in LB medium at a dilution rate of 0.16 $hour^{-1}$ under conditions indicated on the right of each graph.

S10 Fig. Raw data of *E. coli* cells cultured in the microchemostat showing the cell density on the primary axis (red curve and black dots) or average specific cell length on the secondary axis (orange curve and gray dots) as a function of time for the curves depicted in Fig. 4A and B. Cells were grown at 37°C in LB medium at a dilution rate of 0.16 $hour^{-1}$ under conditions indicated on the right of each graph.

Click here to download Figure Box 1.eps

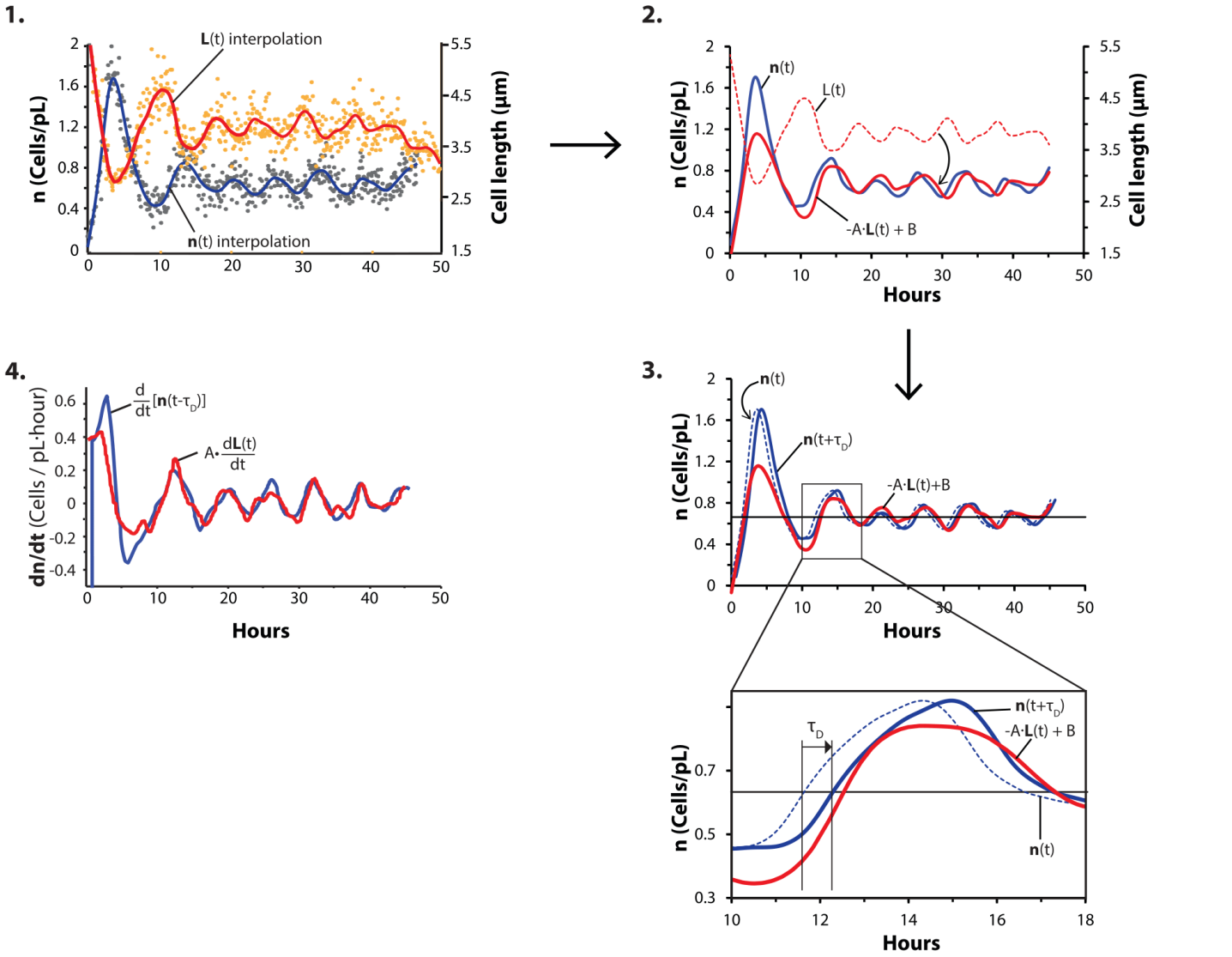

Fig 1

Click here to download Figure Fig. 1.eps

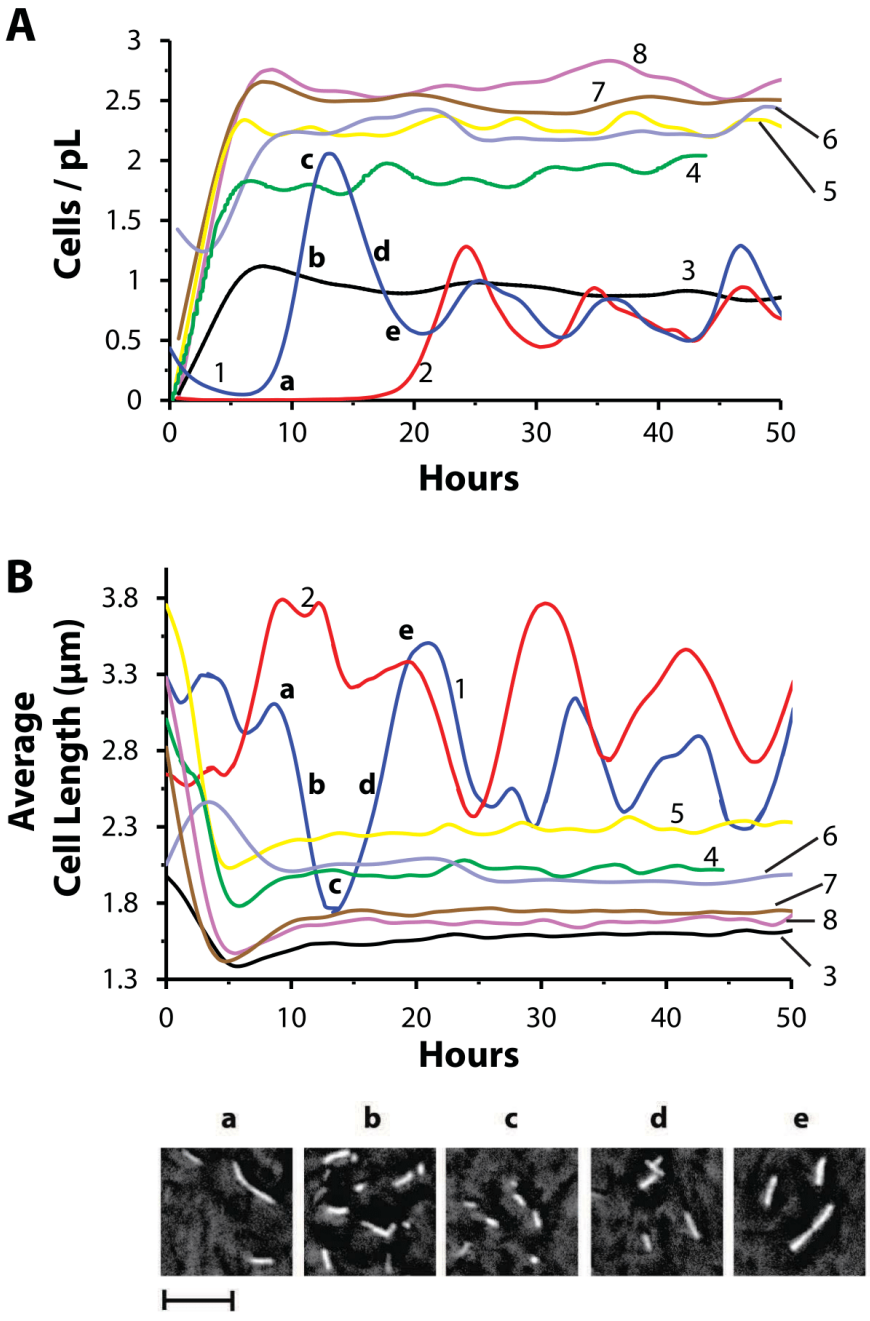

1-2 Efflux ON
3 GFP ON
4 GFP OFF
5-6 Efflux OFF
7-8 Plasmid-free

Fig 2

Click here to download Figure Fig. 2.eps

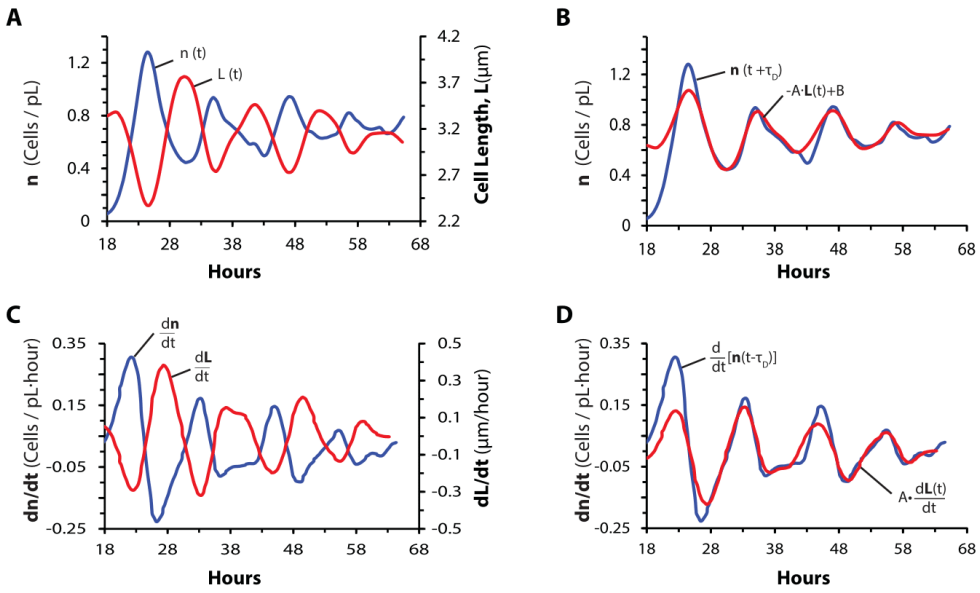

Fig 3

Click here to download Figure Fig. 3.eps

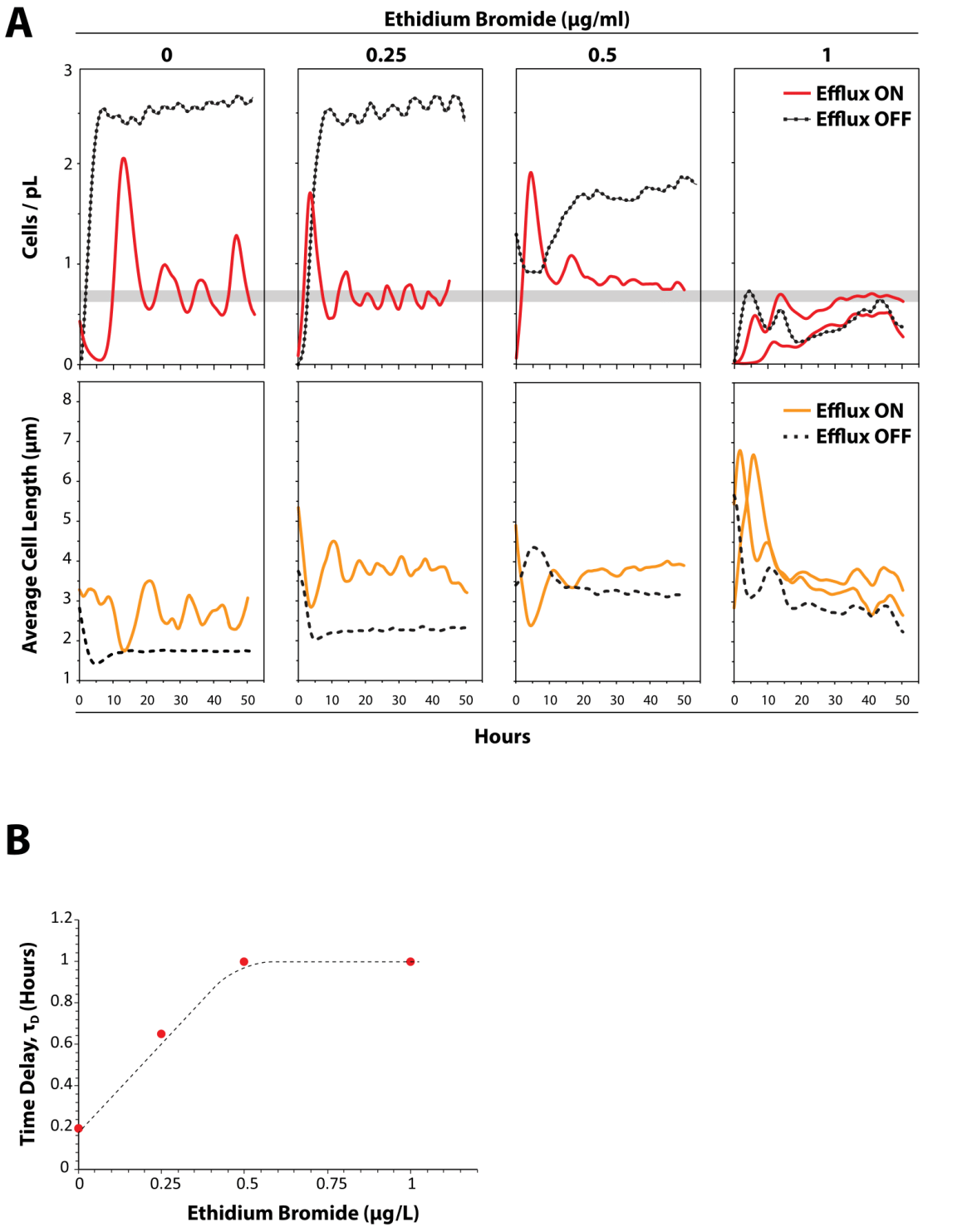

Fig 4

Click here to download Figure Fig. 4.eps

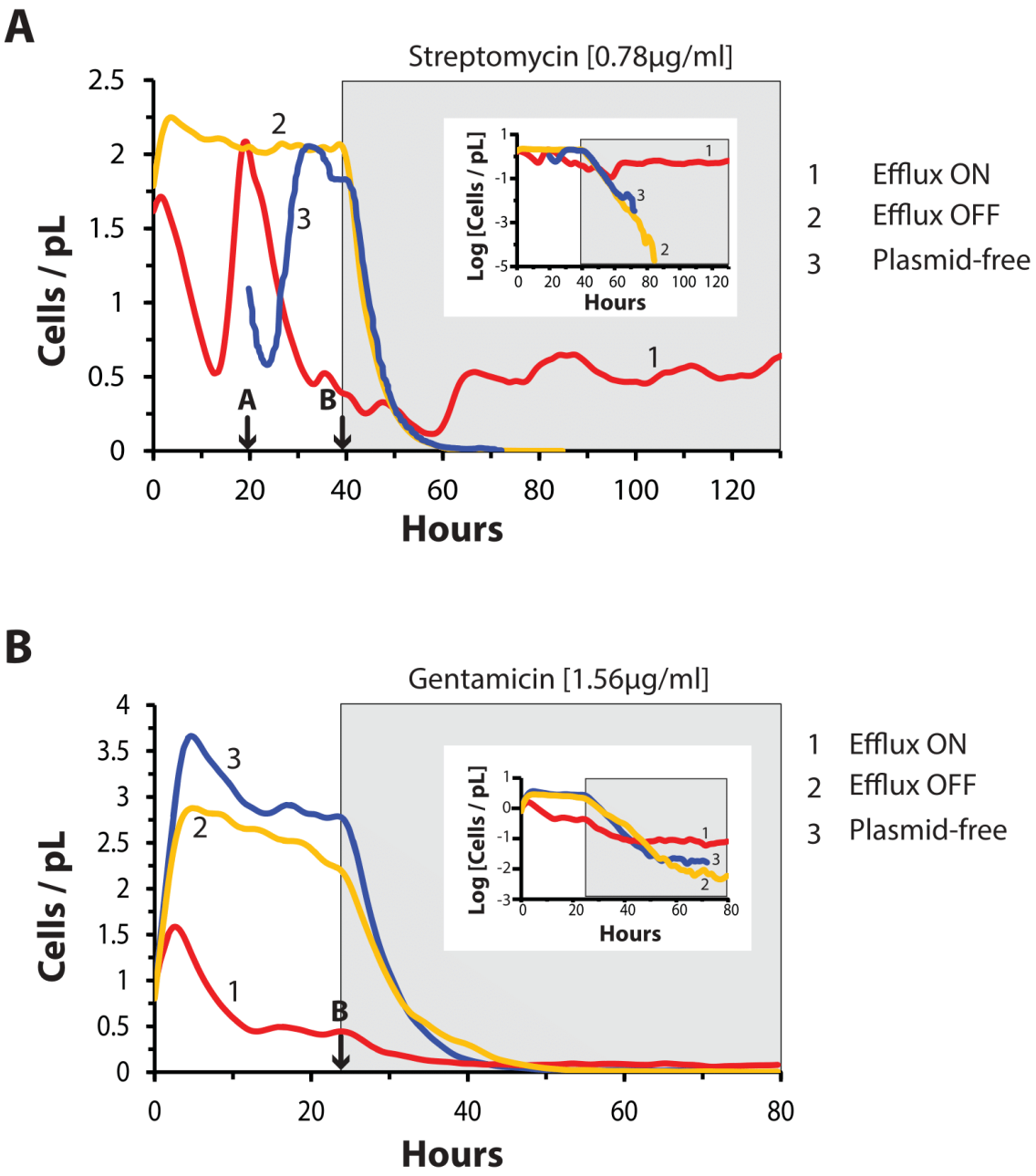

S1 Fig

Click here to download Figure S1 Fig.eps

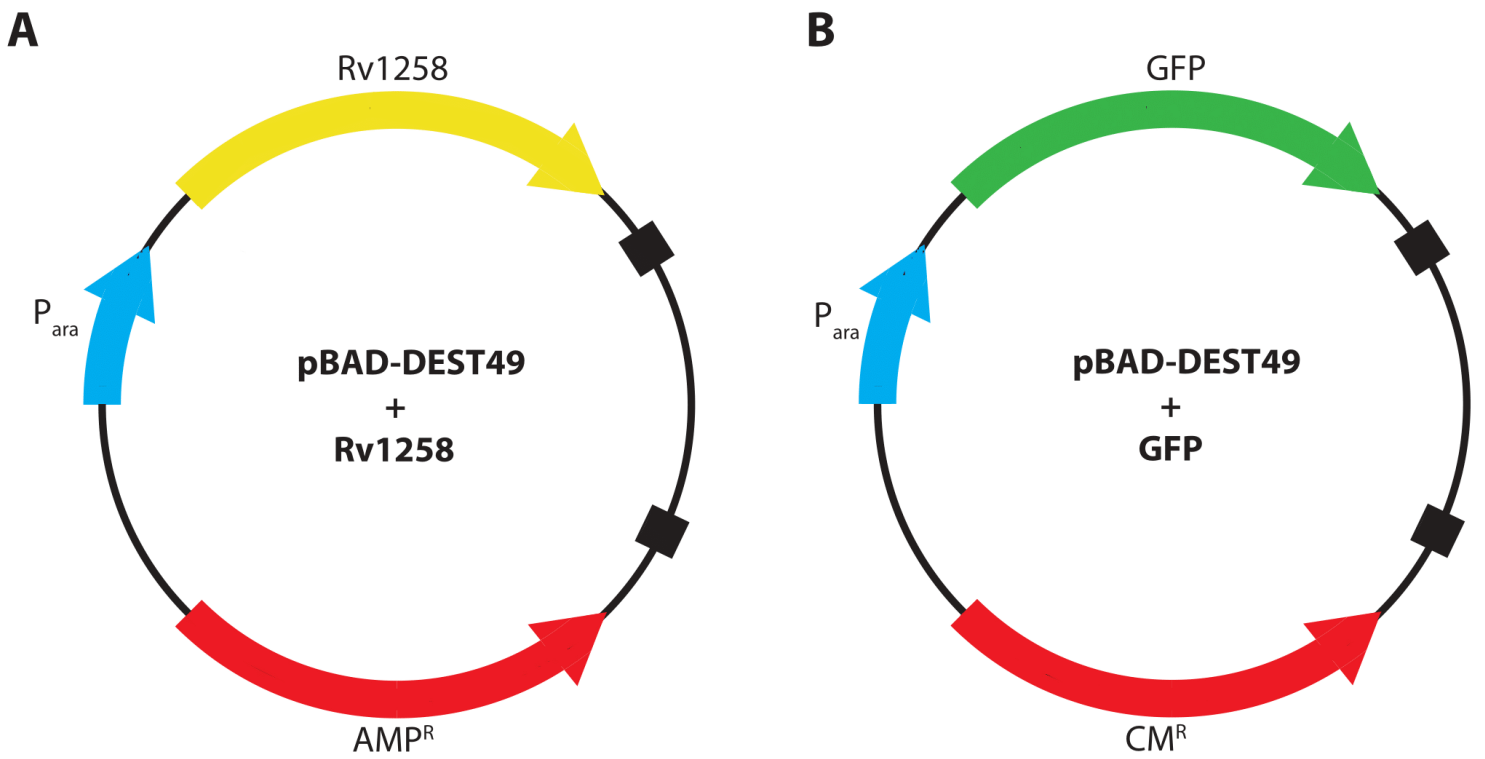

S2 Fig

Click here to download Figure S2 Fig.eps

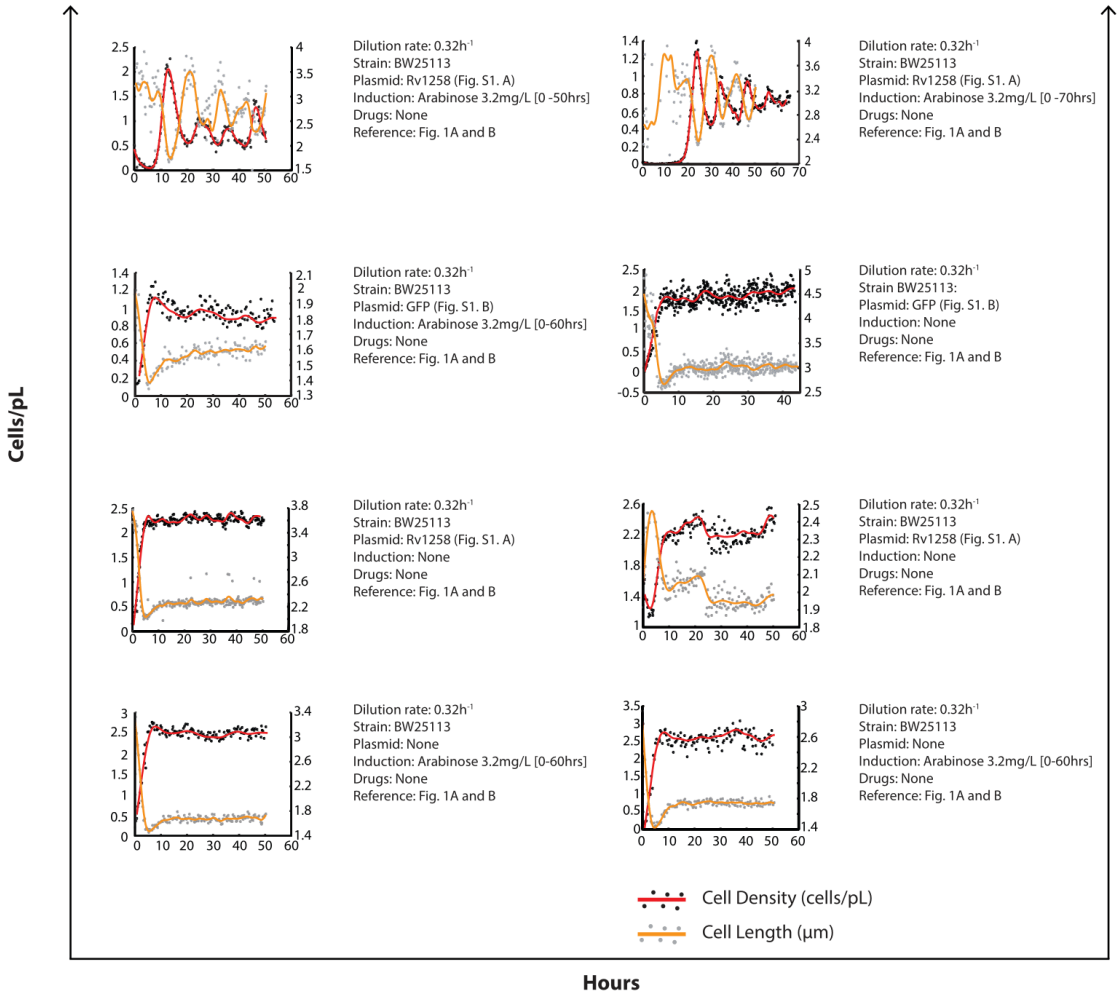

S3 Fig

Click here to download Figure S3 Fig.eps

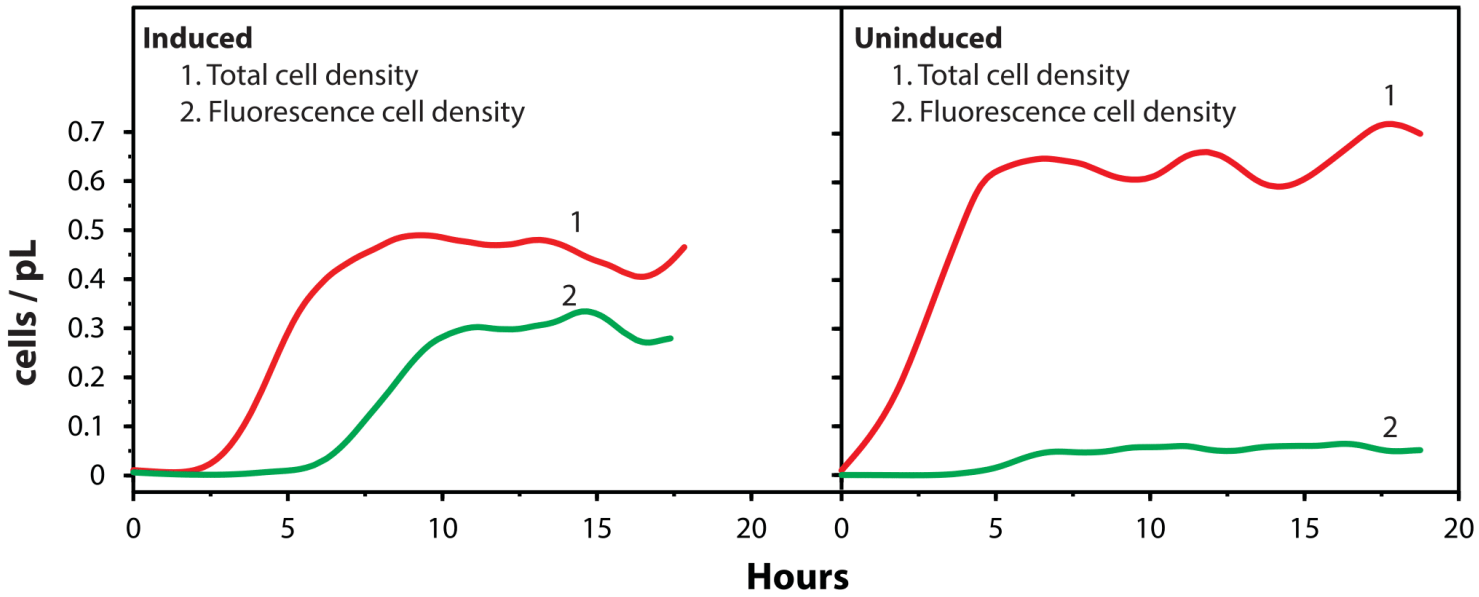

S4 Fig

Click here to download Figure S4 Fig.eps

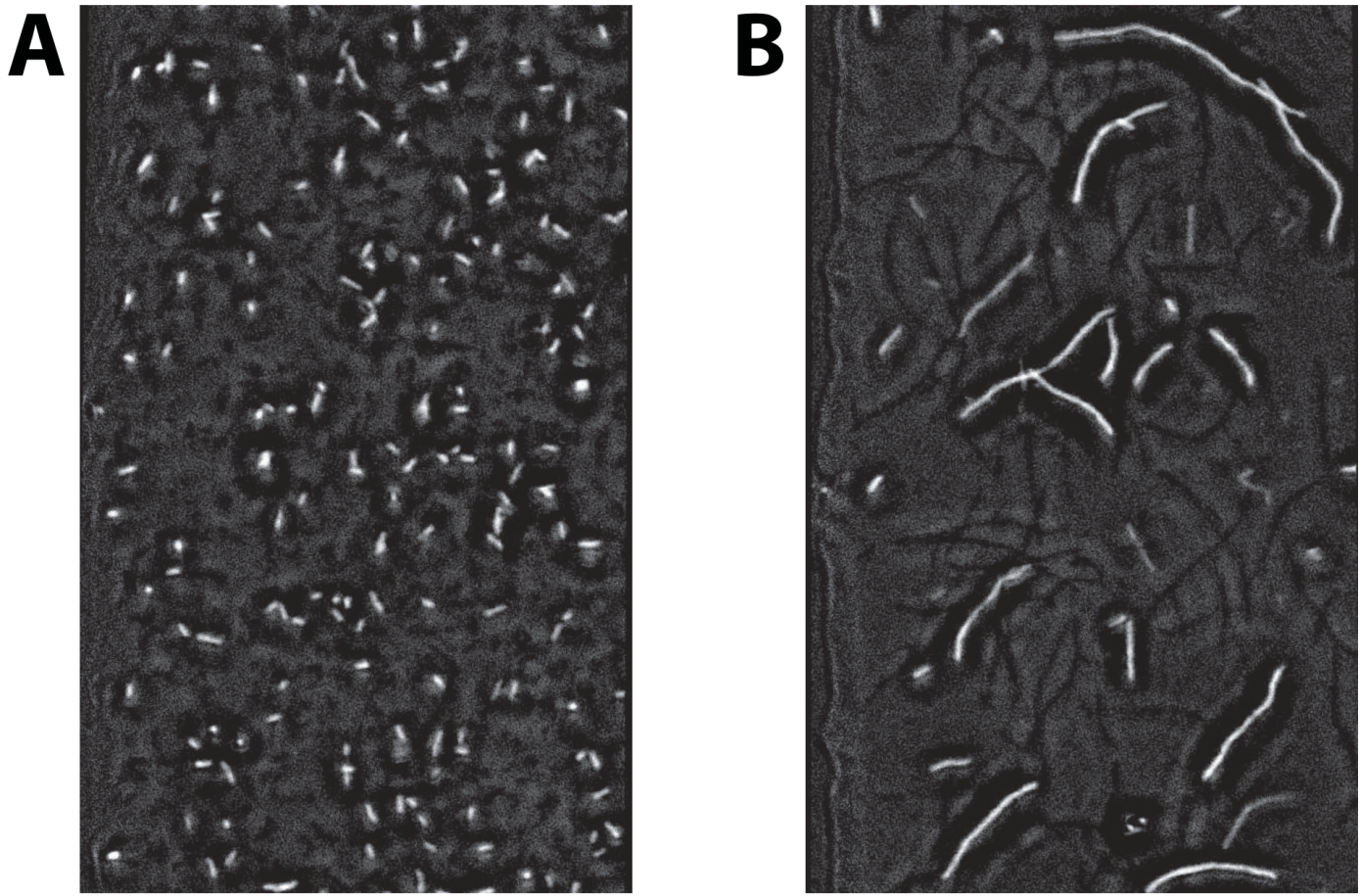

S5 Fig

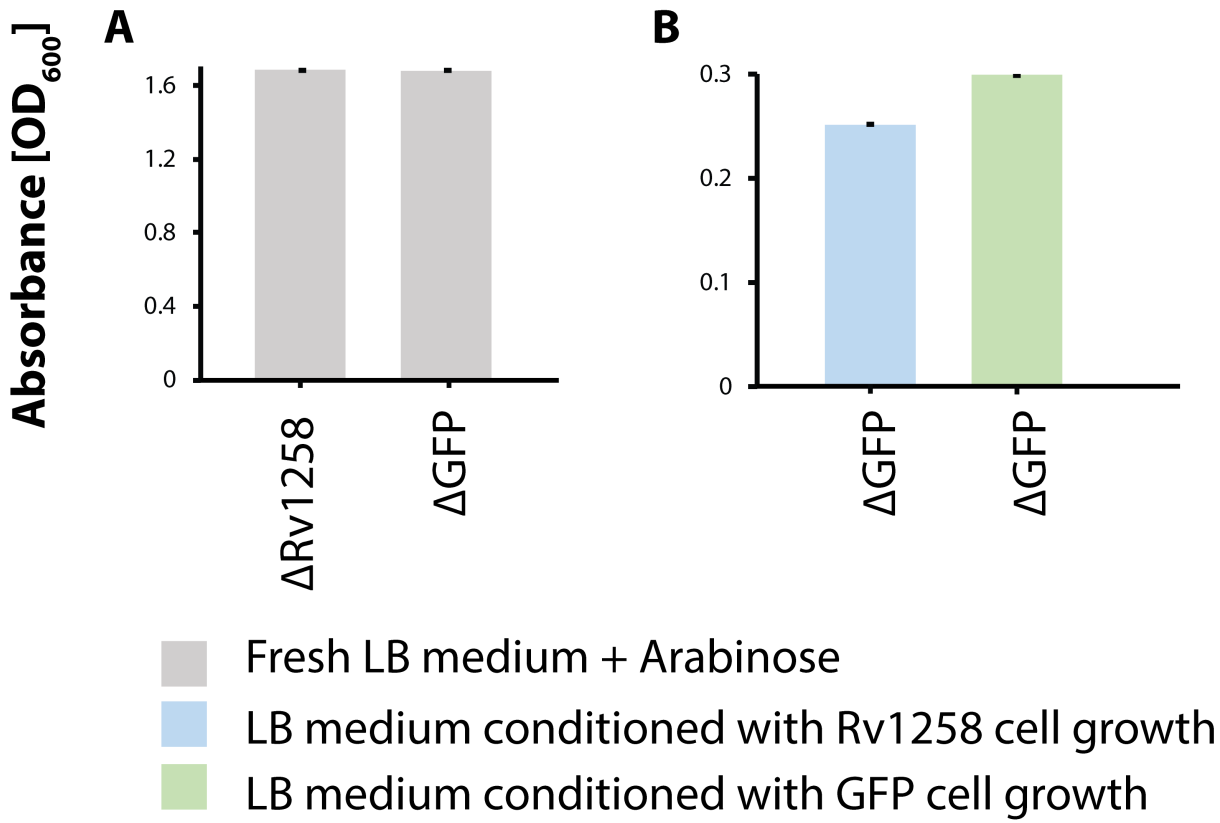
A
B
Absorbance [OD600]
1.6
1.2
0.8
0.4
0
0.3
0.2
0.1
0
ΔRv1258
ΔGFP
ΔGFP
ΔGFP
Fresh LB medium + Arabinose
LB medium conditioned with Rv1258 cell growth
LB medium conditioned with GFP cell growth

S6 Fig

Click here to download Figure S6 Fig.eps

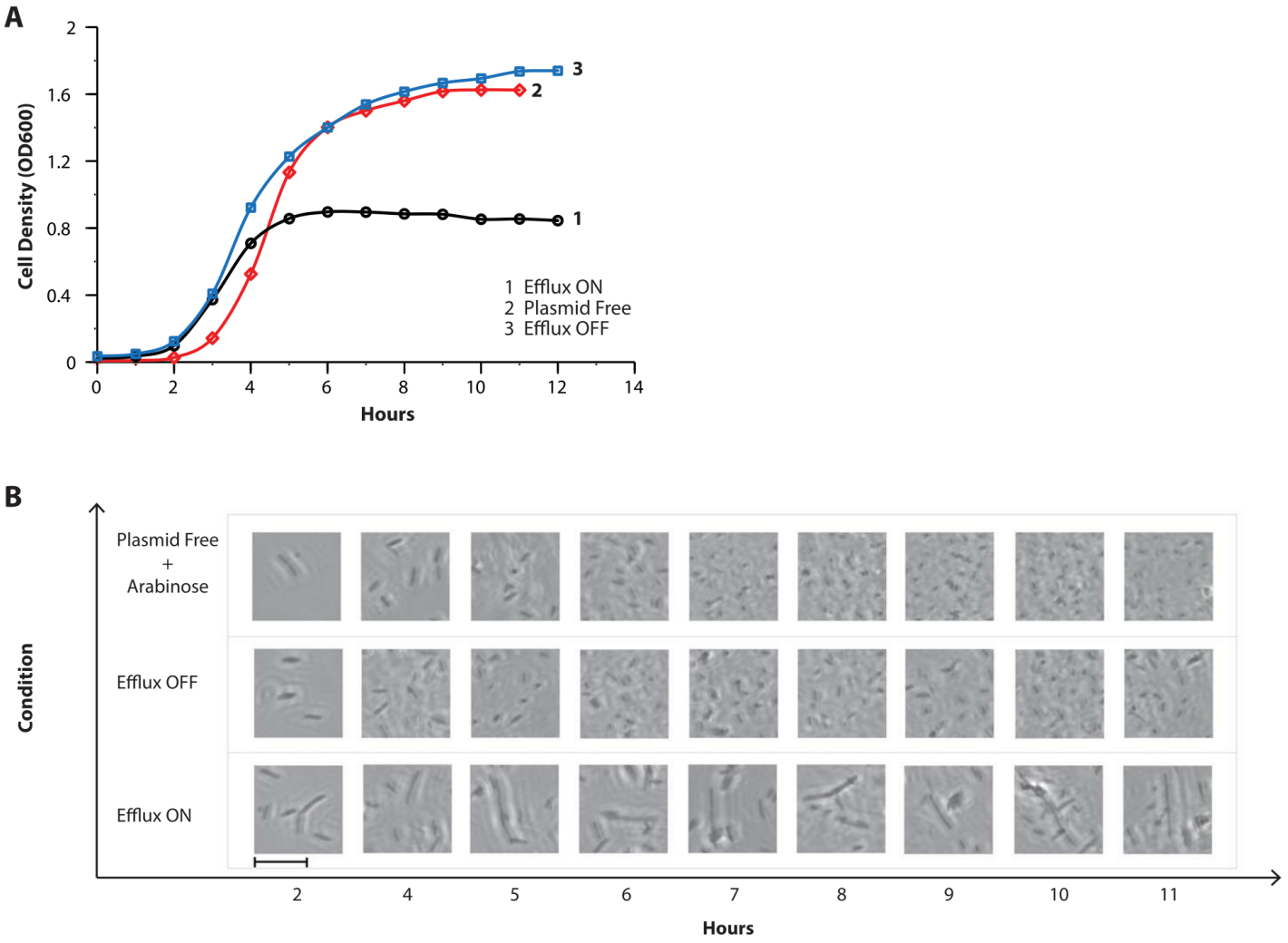

S7 Fig

Click here to download Figure S7 Fig.eps

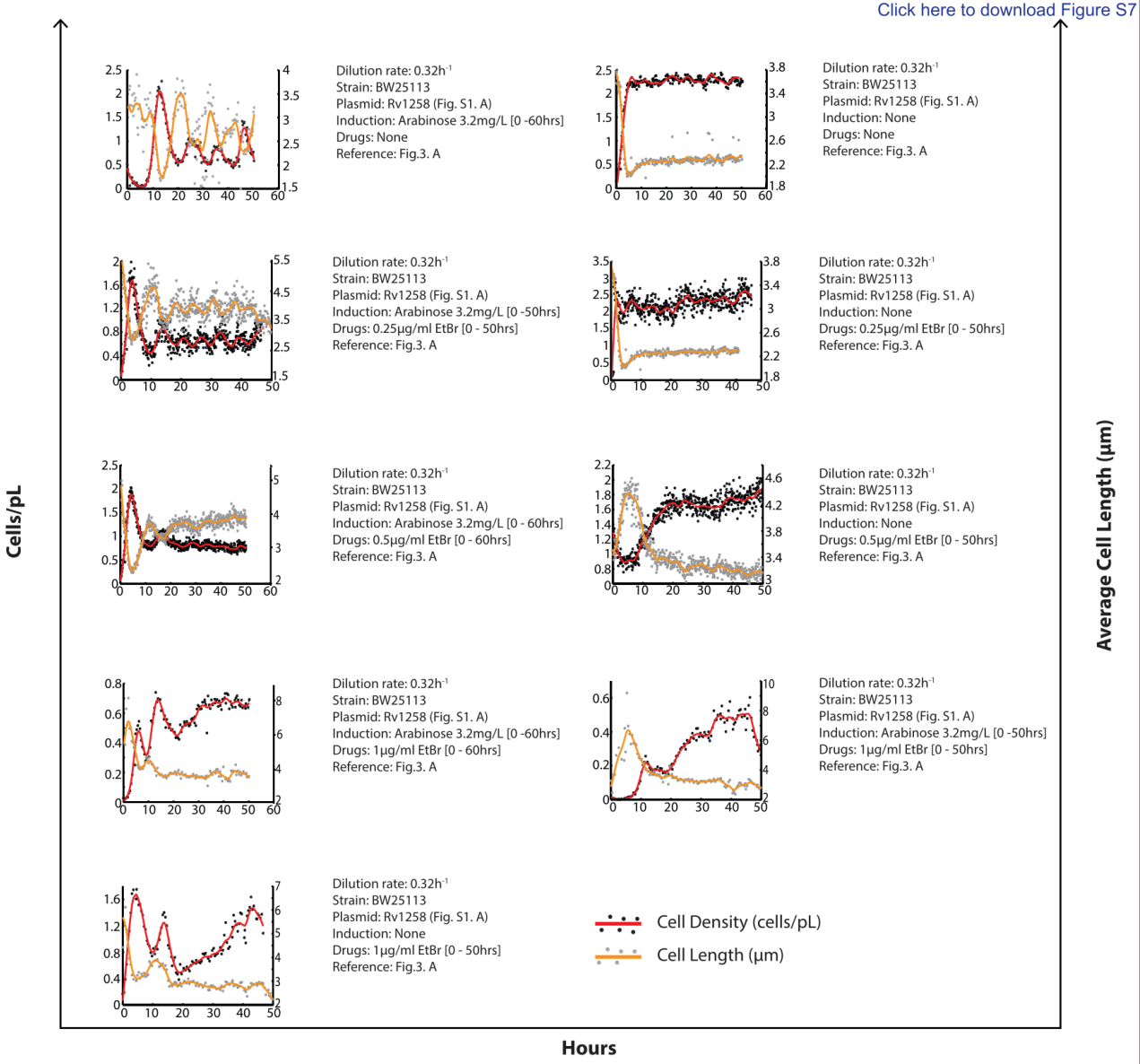

S8 Fig

Click here to download Figure S8 Fig.eps

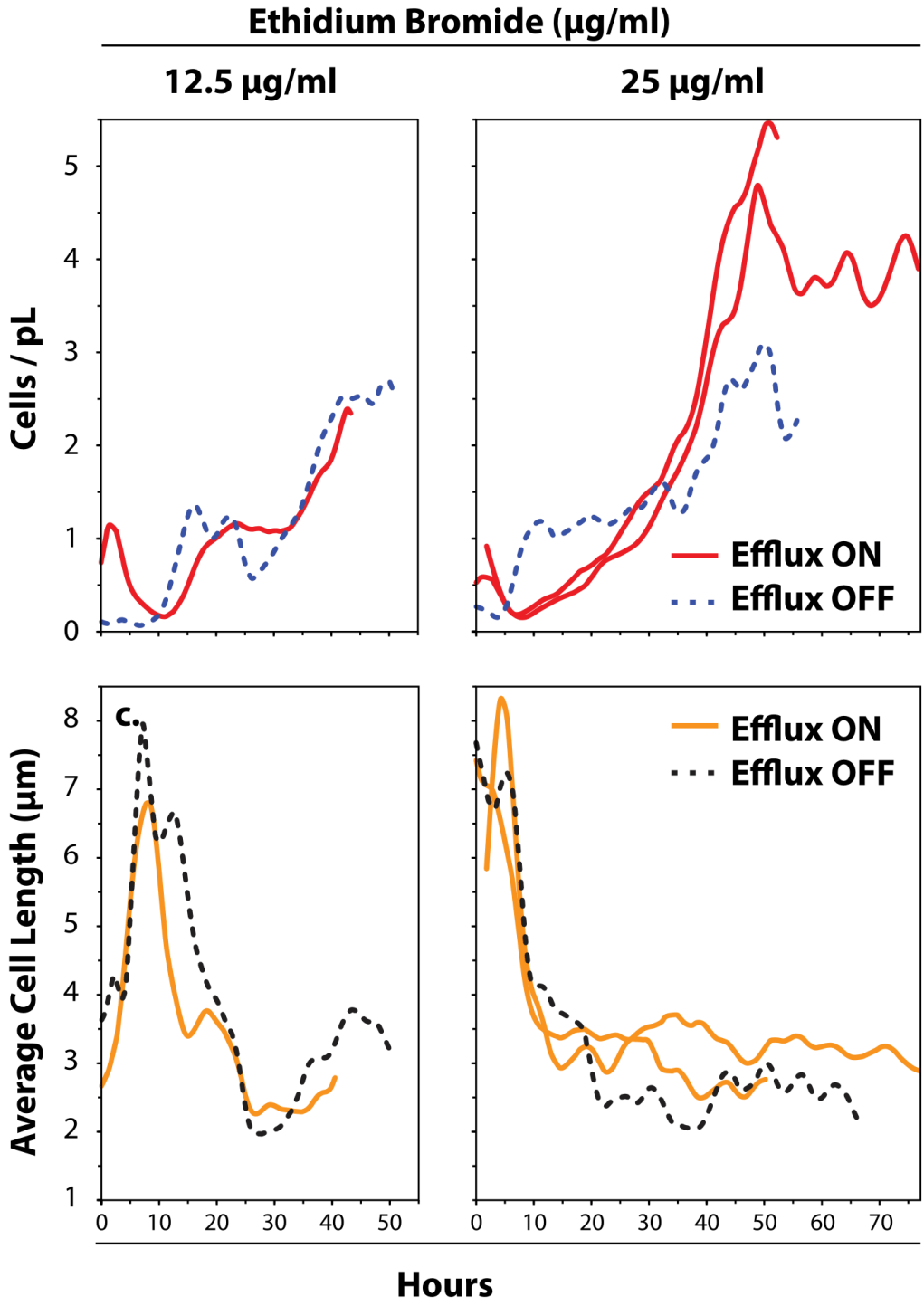

Click here to download Figure S9 Fig.eps

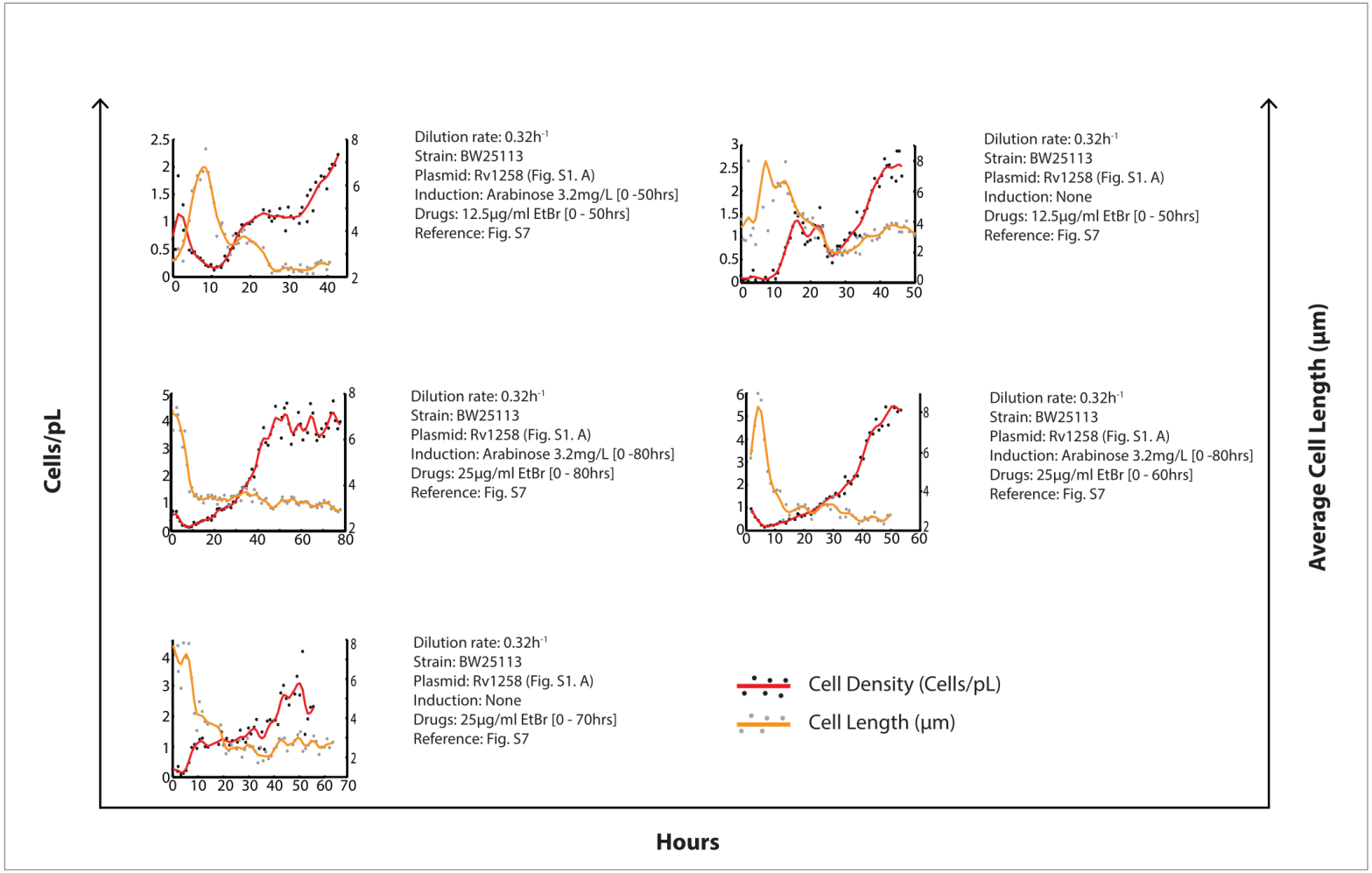

S10 Fig

Click here to download Figure S10 Fig.eps

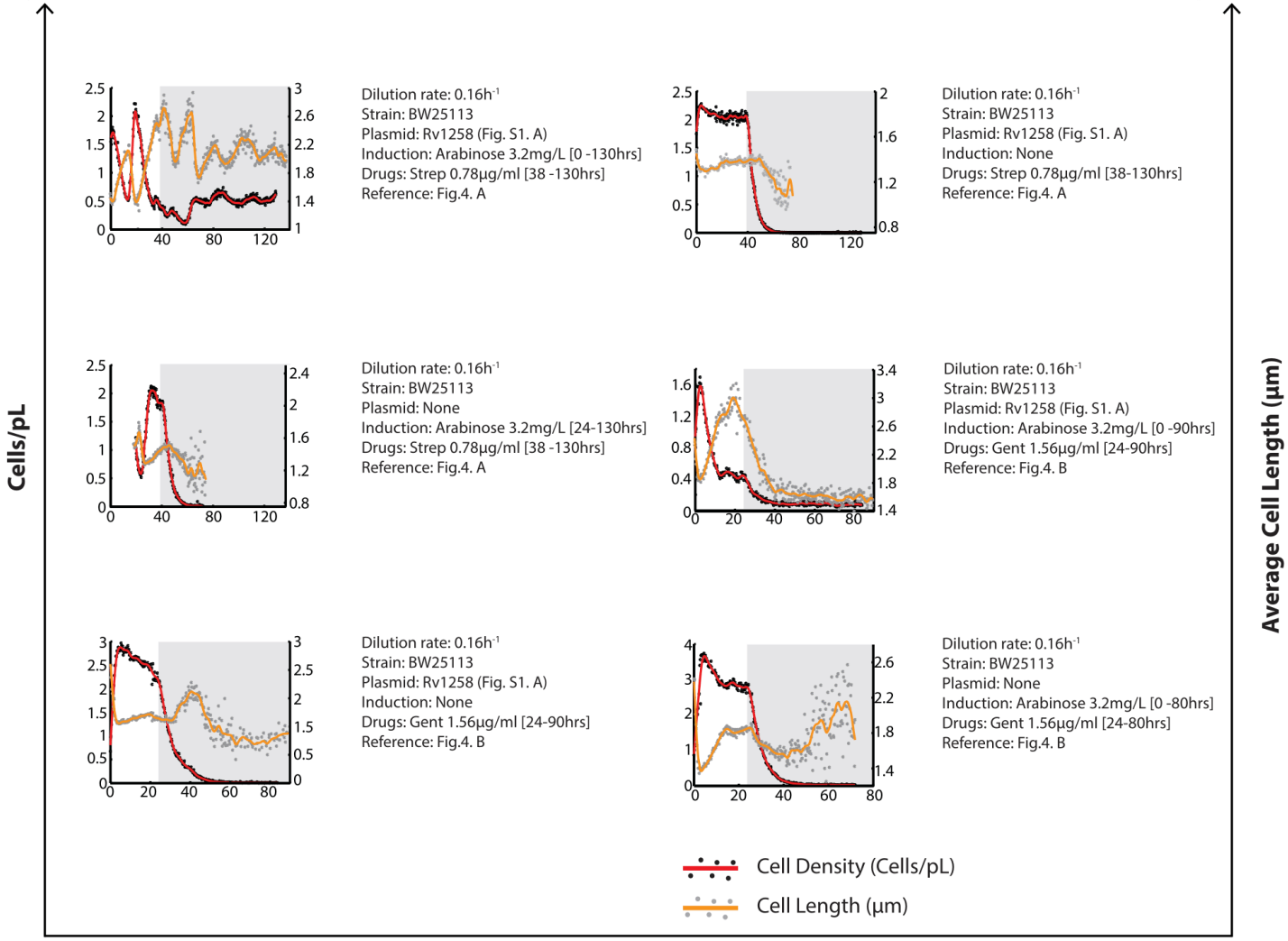

END OF PUBLICATION

CHAPTER 7

7. Materials and Methods

7.1 *E. coli* Strains.

We have made use of *E.coli* strains generously provided by Dr. Alissa Myrick from the Eric Ruben lab at Harvard University, who is now located at H3D at the University of Cape Town. The wild type *E coli* cells—BW25113 *ΔemrE ΔmdfA*—lacked two of the transporters responsible for multidrug resistance[99]. The use of these strains ensured no outside interference from native transporters. Cloning of the Rv1258 tap-like efflux pump into an arabinose inducible vector, pBAD-DEST49 (Invitrogen Corporation, Carlsbad, CA), was performed by standard Gateway cloning by amplifying complete genes minus the stop codon with attB and promoter regions modified within the primers (Figure 27A). The plasmid was maintained with 100µg/ml of ampicillin (Sigma Aldrich, South Africa). The GFP plasmid (Figure 27B) was cloned similarly and was maintained using 100µg/ml of chloramphenicol (Merck chemicals, South Africa). Wild type d2 cells lack two of the transporters for multidrug resistance (*ΔemrE ΔmdfA*) but underwent no cloning and therefore contained no efflux pump. Wild type cells were maintained with Kanamycin 50µg/ml.

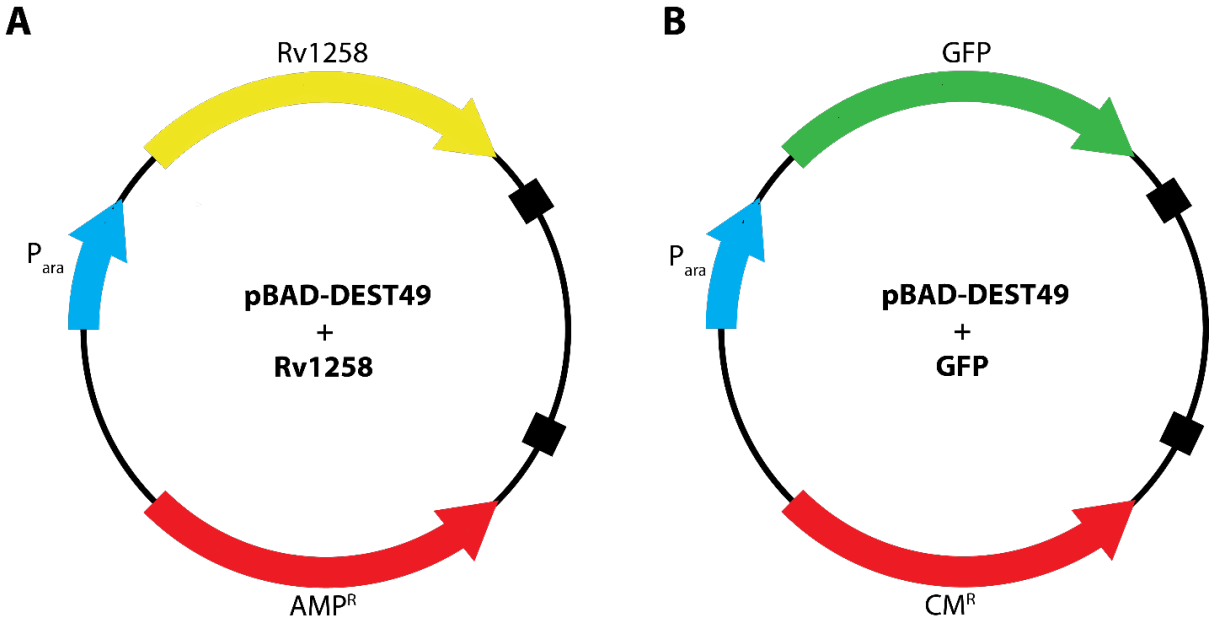

Figure 27| Implementation of the Rv1258 and GFP plasmid constructs. (A) The tap-like efflux gene designated Rv1258, cloned from *M. tuberculosis*, was inserted into an arabinose inducible plasmid pBAD-DEST49 and maintained with Ampicillin. (B) The GFP gene cloned into the same arabinose inducible plasmid pBAD-DEST49 is maintained with chloramphenicol. AMP^R, ampicillin resistance; CM^R, chloramphenicol resistance; P_{ara}, arabinose promoter. Origin of replication pUC.

7.2 Microchemostat Chip Design and Fabrication.

The microchemostat design was developed using AutoCAD software (Autodesk, South Africa). Microchemostat chips were fabricated in a cleanroom facility to prevent contamination with dust particles. All chips were fabricated out of silicone elastomer polydimethylsiloxane (PDMS) (Momentive Performance Materials, Columbus, OH, RTV 615) using the process of multi-layer soft lithography as described previously[154]. In this chip, the number of reactors per chip was increased to 14 as described previously[197,198]. A more detailed description of the chip fabrication process can be found in appendix A.

7.3 Calorimetric Assays

The food dye used in the calorimetric microchemostat characterization assays was obtained from McCormick & Co., Hunt Valley, Maryland, USA. The dye concentration in the microchemostat was determined by averaging the pixel values of optical micrographs of a region within the growth

chamber. In order to optimize mixing times and to determine the time it takes to completely replace the liquid (green dye) within the reactor with deionized water, the dye concentration within the reactor was measured throughout a series of dilutions until the reactor became completely filled with water. A standard curve was then generated. This information was used to determine how long it takes to completely replace fresh media in the reactor with drug containing media. We also made use of the standard curve to determine the drug concentration within the reactor at any given time. The dilution process is entirely automated using Labview software (National Instruments, South Africa) that was developed in house.

7.4 Microchemostat Cultures, Medium and Growth Conditions.

Luria Bertani (LB) medium (Sigma Aldrich, South Africa) used in the microchemostat cultures contained tryptone (10g/L), yeast extract (5g/L), NaCl (5g/L), inert binding agents (2.2g/L) and bovine serum albumin (10g/L) as an anti- cell adhesion adjuvant. Pre-cultures for microchemostat experiments were prepared by inoculating 10 ml of sterile medium with 100µl of glycerol (Merck Chemicals, South Africa) stock cultures (50% glycerol:50% culture) and shaking at 120 rpm for ~4 hours (or until an optical density (OD_{600}) of 0.8) at 37˚C in a bench top incubator (Scientific Orbital Shaking, model 260) (Trilab, South Africa).

The pre-cultures were then used to seed microchemostat reactors (~20 cells/nl per reactor). This was performed through the use of a 1ml syringe (Lasec, South Africa) connected to a 10cm piece of tygon tubing (Cole-Parmer, South Africa) and a steel pin (New England Small Tube Corporation, New Hampshire, United States) that was then connected to an input port of the microchemostat reactor. The pBAD-DEST49 plasmid was maintained with 100µg/ml of ampicillin (Sigma-Aldrich, South Africa). The heterologous efflux pump, under control of a synthetic promoter, was inducible with arabinose (Sigma-Aldrich, South Africa) at concentrations ranging from 0.0002% to 0.0008% (v/V). Biofilm formation within the reactors was prevented through sequential dilutions with fresh LB media and Bacterial protein extraction reagent (B-PER) obtained from ThermoFischer Scientific, South Africa. All microchemostat experiments were performed on a heated stage (IMP, South Africa) to maintain the growth temperature at 37˚C.

7.5 Antibiotic Treatment.

To determine the effect of antibiotics, cells were grown in the microchemostat in drug-free medium for 24 to 40 hours to establish a steady state cell density. Efflux ON cultures were grown in the presence of arabinose in order to upregulate the efflux pump. However, efflux OFF cultures were not

grown with arabinose. Medium containing the test drugs including streptomycin (0.78µg/ml) (Sigma Aldrich, South Africa), gentamicin (1.56 µg/ml) (Sigma Aldrich, South Africa) or ethidium bromide (0.25 - 25 µg/ml) was then introduced to the microchemostat cultures for the remainder of the experiment. Medium was introduced through the use of tygon tubing connected to a pressurized source at one side and an input on the microchemostat chip at the other side (Figure 28).

7.6 Microscopic Cell Counting.

The total number of cells in each reactor was determined directly through automated phase contrast microscopy by counting the number of cells present in a growth chamber section of the microchemostat of known volume. Phase-contrast images were captured using a cooled charge coupled device camera (CCD) (XM10, monochrome from Olympus) (Wirsam Scientific, South Africa). Fluorescent images were captured with an Andor Luca – R 604 camera (IMP, South Africa). A Nikon Ti Eclipse inverted microscope (Nikon UK Ltd, Surrey) with a 40×/0.6NA Ph2 objective (Nikon UK Ltd, Surrey) was used for all measurements. Labview software (National Instruments, South Africa) was used to control all chip operations allowing complete automation of experiments. The setup of the microfluidic system can be seen in Figure 28.

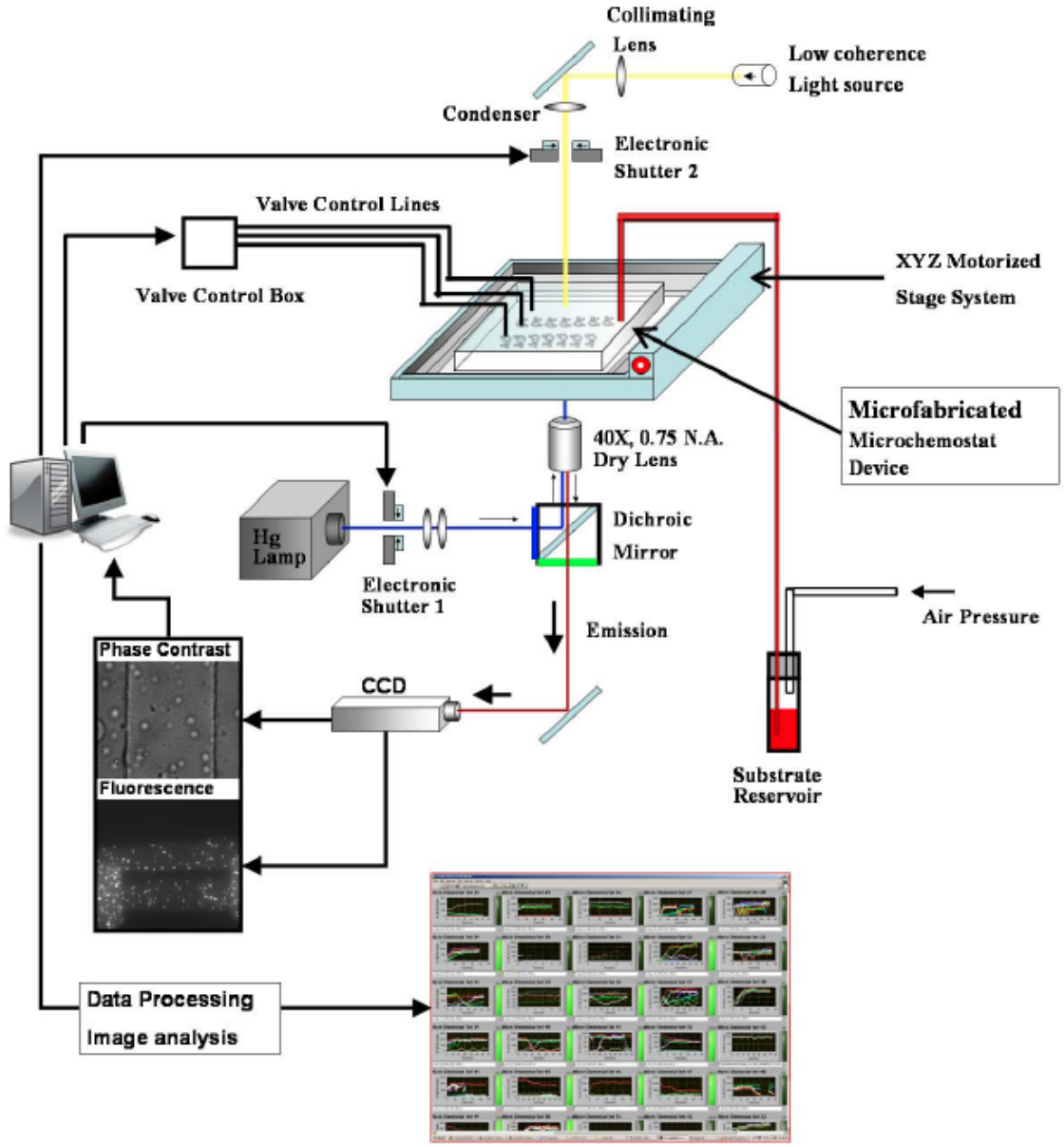

Figure 28| The setup of the microfluidic system used to achieve microchemostat results. The entire process is completely automated through computer control. Actuation of the valves, shutter control for fluorescent experiments, and acquisition of phase contrast and fluorescent images all occur through the use of Labview software. Results are also obtained in real-time through the use of Matlab software. (Used with permission from ref. [167]).

Typically, a set of eight phase-contrast images was taken in each reactor, with mixing of the culture in between each snapshot. Image processing algorithms (Appendix B) written in Matlab software were used to determine the average number of cells in each set of pictures, from which the total cell count was determined as described previously [197,198]. Briefly, the average number of cells per picoliter (pL) was calculated by determining the number of cells in a region of the microchemostat reactor of known volume. This was then be used as an estimate for the total number of cells in the reactor. An example of the calculations performed for phase contrast images can be found below.

Step 1: ***The volume (in pL) of the imaging section is first calculated:***

$$Width\ (w)\ of\ reactor\ in\ imaging\ section = 100\mu m$$
$$Length\ (l)\ of\ reactor\ in\ imaging\ section = 154\mu m$$
$$Height\ (h)\ of\ reactor\ in\ imaging\ section = 10\mu m$$

Therefore, the volume (V) of this section is equal to:

$$V = w.l.h$$
$$V = 100\mu m.154\mu m.10\mu m$$
$$V = 154000\mu m^3$$

This volume can now be converted to pL:

$$V = 154000\mu m^3 \div 1000$$
$$V = 154pL$$

Step 2: ***Using this volume we can now calculate the number of cells per pL:***

$$Number\ of\ cells\ counted\ in\ the\ imaging\ section = 200$$

Therefore,

$$\frac{Cells}{pL} = \frac{200\ cells}{154pL} = \frac{1.3\ cells}{pL}$$

Image processing algorithms written in Matlab software were also used to determine morphological changes over time induced by pump activation or drug addition. A motorized stage system (Nikon Ti-SH-W) (IMP, South Africa) on the Nikon Ti-E microscope enabled simultaneous documentation of

multiple microchemostat experiments that operated in parallel on a single chip. Focus was maintained using the perfect focus system (PFS) feature of the Nikon microscope.

7.7 Regression Analysis.

Step 1. Cubic spline interpolation.

We employed cubic spline interpolation using Matlab's curve fitting tool with a fit parameter = 0.5 to fit smoothed curves to cell density and cell length data obtained from the microchemostat cultures. Figure 29, panel 1 shows on the primary axis the cell density data (grey points) and the cubic spline fit (blue curve); and on the secondary axis, the cell length data (orange dots) and the cubic spline fit (red curve). Interpolation also served the purpose of denoising the data by removing point-to-point noise variations, which made it possible to obtain the instantaneous derivatives from the smoothed data in Step 4.

Step 2. Cell length transformation.

To perform the cell length transformation, Microsoft excel (Microsoft Corporation, Redmond, Washington, USA) was used. The cell length value in each data point was multiplied by a constant -A and then, another constant B was added to the result. This transformation flipped the cell length graph about the horizontal axis, shrank it by a factor of A, and then shifted the entire graph upward by a value of B. Figure 29, panel 2 shows the original cell length trend ($\mathbf{L}(t)$; dashed red curve) as well as the transformed trend ($-A \cdot \mathbf{L}(t) + B$; solid red curve)

Step 3. Cell density transformation.

To perform the cell density transformation, a time constant τ_D was added to the time value of each cell density data point, which had the effect of shifting the cell density graph to the right by the value, τ_D. Figure 29, panel 3 shows the entire graph of the original cell density trend ($\mathbf{n}(t)$; dashed blue curve) as well as the transformed trend ($\mathbf{n}(t-\tau_D)$; solid blue curve). The values A, B and τ_D were adjusted as necessary until the best fit was obtained for the transformed length graph $[-A \cdot \boldsymbol{L}(t) + B]$ superimposed over the transformed cell density graph $[\mathbf{n}(t-\tau_D)]$ in terms of periodicity and amplitude.

Step 4. Finite Element Derivatives.

At each time point, i, the finite element derivative, $[dy/dt]_i$ for the cell density or cell length (designated y_i) was obtained from the interpolated data generated in Step 1 using the equation:

$$\frac{dy}{dt}_i = \frac{y_{i+1} - y_i}{t_{i+1} - t_i} \tag{6}$$

The derivative graphs for cell density ($d\boldsymbol{n}/dt$, or cell division rate) and cell length ($d\boldsymbol{L}/dt$, or the filamentation rate) were then transformed using the approach outlined in steps 2 and 3 Figure 29, panel 4 shows the first derivatives of the transformed graphs, $d\boldsymbol{n}\,(t-\tau_D)/dt$ and $-A \cdot d\boldsymbol{L}/dt$.

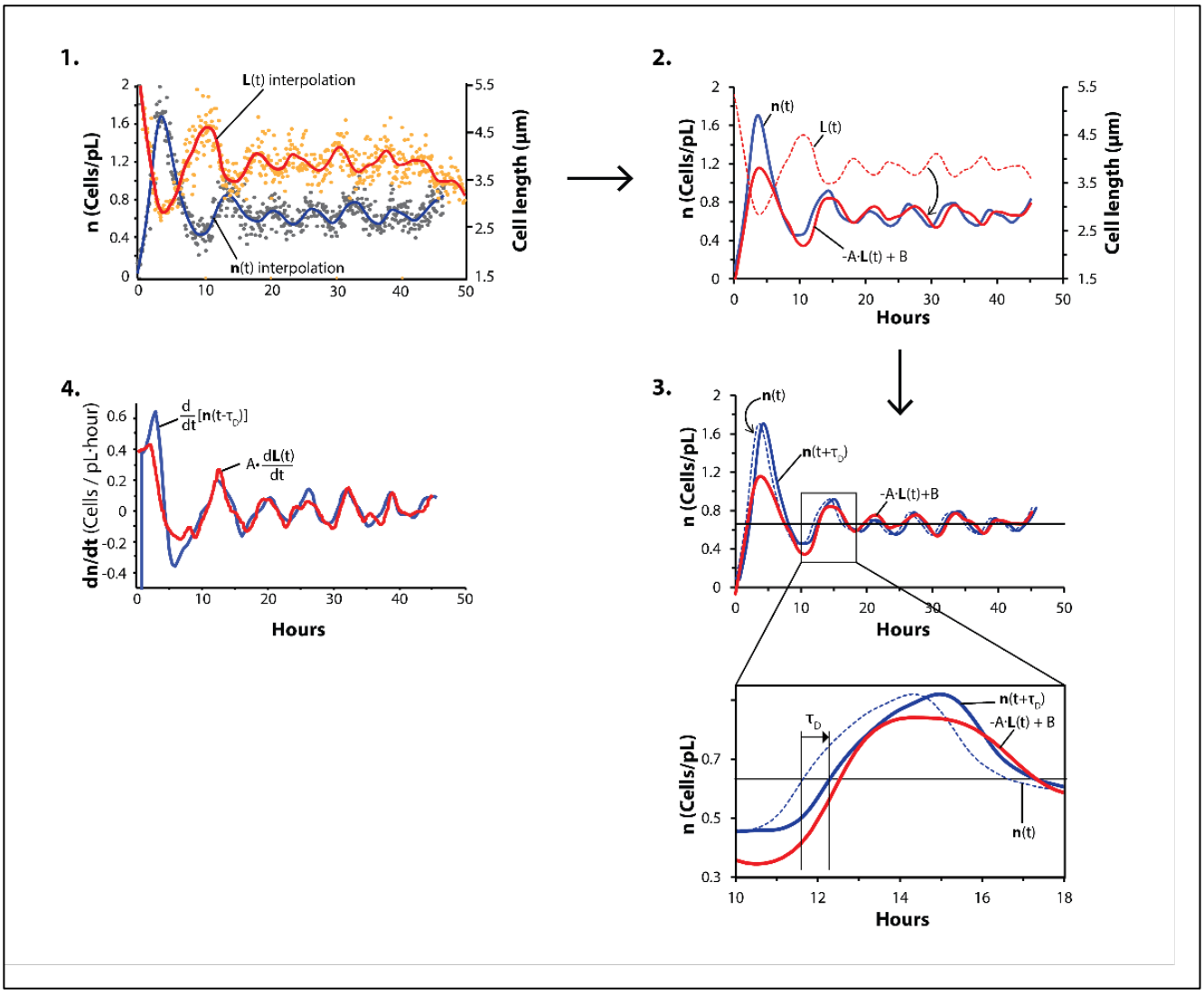

Figure 29| The cell length transformation used to help describe the relationship between cell density and cell length.

7.8 Conventional Culture Experiments

Luria Bertani (LB) medium (Sigma Aldrich, South Africa) used in the off-chip cultures contained Tryptone (10g/L), yeast extract (5g/L), NaCl (5g/L), inert binding agents (2.2g/L) and bovine serum albumin (10g/L) as an anti-cell adhesion adjuvant. Cultures for off-chip experiments were prepared by inoculating 10 ml of sterile medium with 100µl of glycerol (Merck Chemicals, South Africa) stock cultures and shaking at 120 rpm at 37˚C in a bench top incubator (Scientific Orbital Shaking, model 260) (Trilab, South Africa).

Conventional culture experiments performed in tissue culture flasks involved recording an OD reading at a wavelength of 600nm using 2ml micro cuvettes (Lasec, South Africa) and a Beckman Coulter DU730 UV spectrophotometer (California, USA) every hour until the cultures reached stationary phase (~10 – 12 hours). Off-chip experiments were conducted as controls for comparison to microchemostat experiments.

Conventional culture experiments were also conducted using conditioned medium in order to provide support for the hypothesis of a growth inhibiting efflux product. For each condition, 10 ml of fresh LB medium containing arabinose was inoculated with cells containing the Rv1258 or GFP plasmid and incubated with shaking at 37ºC for 24 hours using a bench top incubator (Scientific Orbital Shaking, model 260) (Trilab, South Africa). The growth media from these cultures (Rv1258 and GFP) was then filtered using a 0.20µm syringe filter from Lasec South Africa in order to remove all bacteria. This conditioned media was then used to culture cells expressing the GFP plasmid in order to confirm the presence of suspected growth-inhibiting factors extruded by the Rv1258 efflux pump. Bacteria were cultured for ~12 hours, with OD_{600} readings taken every hour through the use of 2ml micro cuvettes (Lasec, South Africa) and a Beckman Coulter DU730 UV spectrophotometer (California, USA).

CHAPTER 8

8. Results

8.1 Culture Conversion Rate Within the Microchemostat

We have taken a synthetic approach for the study of mycobacterial efflux pumps. As mentioned previously, we have made use of *E.coli* constructs that have the Rv1258 efflux pump cloned into an arabinose inducible promoter. Thus, we could control efflux pump gene expression by adding or removing arabinose (inducer). We required a way to determine the time it takes to completely incorporate the arabinose into the growth media within the microchemostat reactor through the continuous dilution process described in chapter 4.

Calorimetric assays were performed to determine the rate of conversion of the media within the growth chamber. Green food dye was used to determine the number of dilutions required to completely replace the liquid within the growth chamber. The rate at which the liquid is replaced depends on the dilution rate that is controlled using labview software. A description of the entire process can be found in chapter 7. In the example experiment below (Figure 30), a dilution rate of 200 seconds resulted in the liquid being completely replaced within ~5 hours.

Once an appropriate pump speed and duration was selected, the experiment was left to run to completion, resulting in the complete dilution of the green dye (Figure 30C).

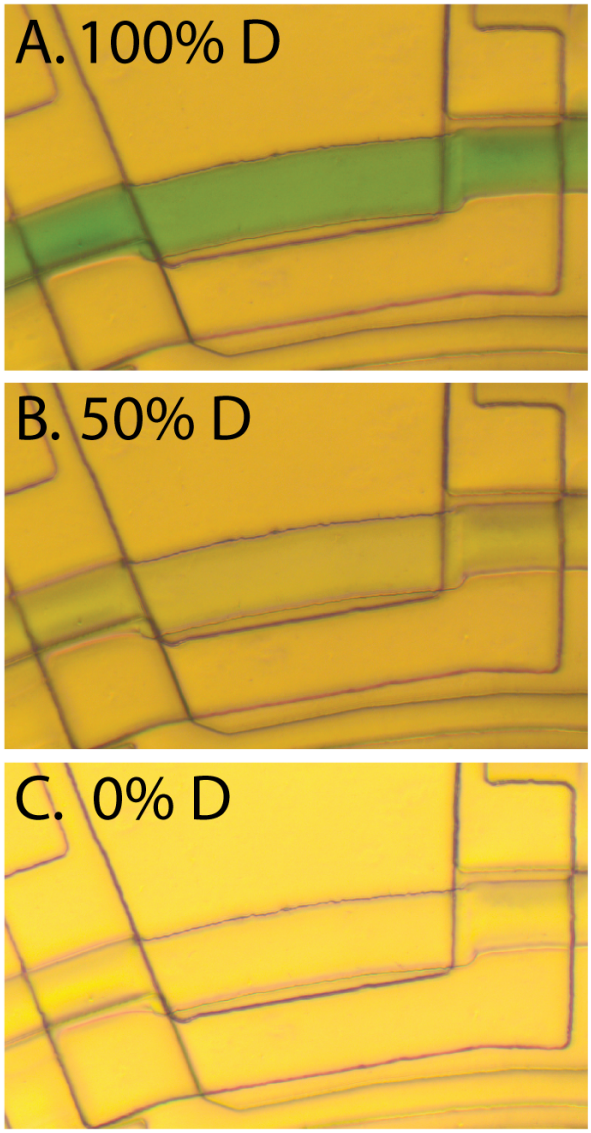

Figure 30| Screen shots from a microchemostat dye experiment showing the dye concentration (here denoted as "D") within the reactor. At the start of the experiment, the concentration in the reactor was at 100% (A). In this particular experiment, after ~2.5 hours, the concentration in the reactor had reached 50% (B). However, after ~5 hours, water had completely replaced the green dye in the reactor (C).

Throughout the experiment, screen shots were taken following every dilution (Figure 30) and the dye concentration determined. A standard curve (Figure 31) was generated to allow us to determine the time taken (or the number of dilutions) to completely replace media in the reactor with another type of

media (e.g. drug or inducer containing media). In this particular experiment, in order to convert 50%, 75% and 99% of the media within the growth chamber, 9, 16 and 60 dilutions were required respectively (Figure 31). This standard curve can also be used to determine the drug concentration within the reactor at any given time, making it a useful tool for determining the minimum inhibitory concentration of drugs.

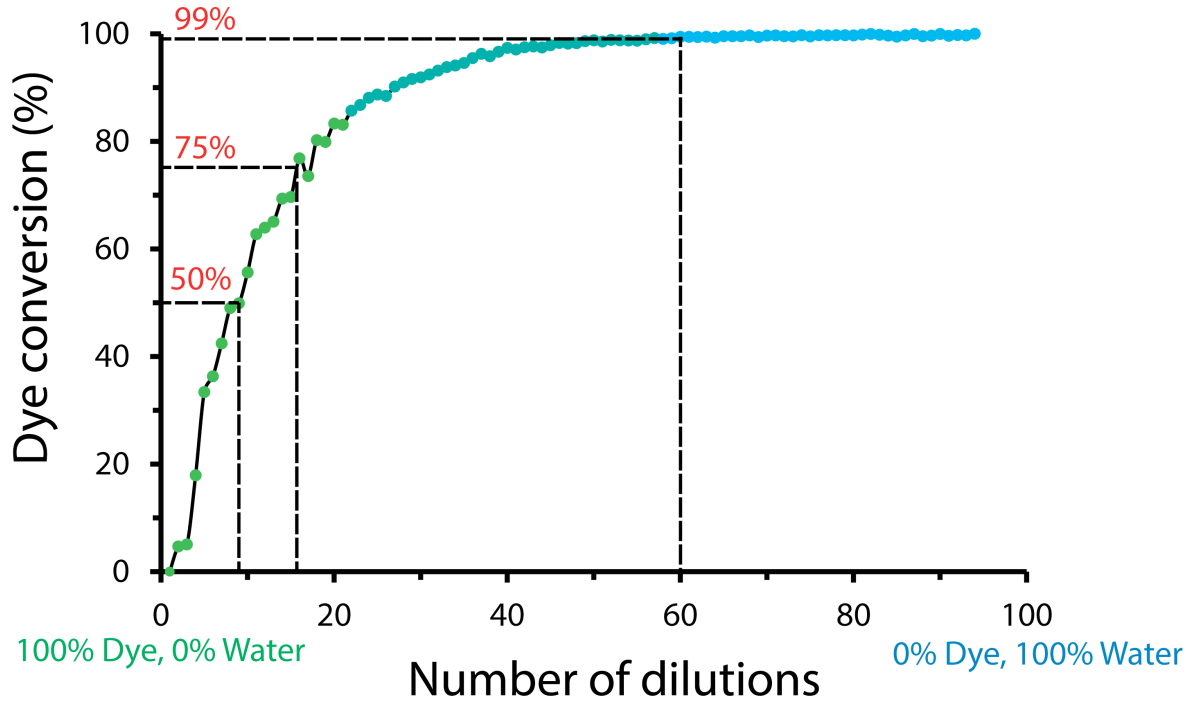

Figure 31| A standard curve generated to show the number of dilutions required at a given dilution rate to completely replace the fluid within the reactor. This standard curve can be used to determine the concentration of drugs within the reactor at any given time.

8.2 Bacterial Growth in the Microchemostat

The tap-like efflux pump gene designated Rv1258, which encodes a multidrug efflux pump in *M. tuberculosis* was isolated and expressed from a plasmid in transporter-deficient *E. coli* under control of an arabinose-inducible promoter (Figure 27A). By continually substituting a fraction of the bacterial culture with sterile nutrients, the microchemostat creates a near-constant environment that is ideal for long-term controlled studies of these microbes and efflux gene expression.

Uninduced (efflux OFF) (cultures 1 and 2) and plasmid free (cultures 3 and 4) cell populations cultured within the microchemostat grew in the characteristic fashion, containing a lag, exponential and stationary phase (Figure 32). These populations grew exponentially to a steady-state density of

~2.5 cells/pL. Corresponding cell lengths are represented in Figure 32B. Efflux OFF populations grew to an average cell length of ~2 µm compared to plasmid free populations that reached ~1.5 µm.

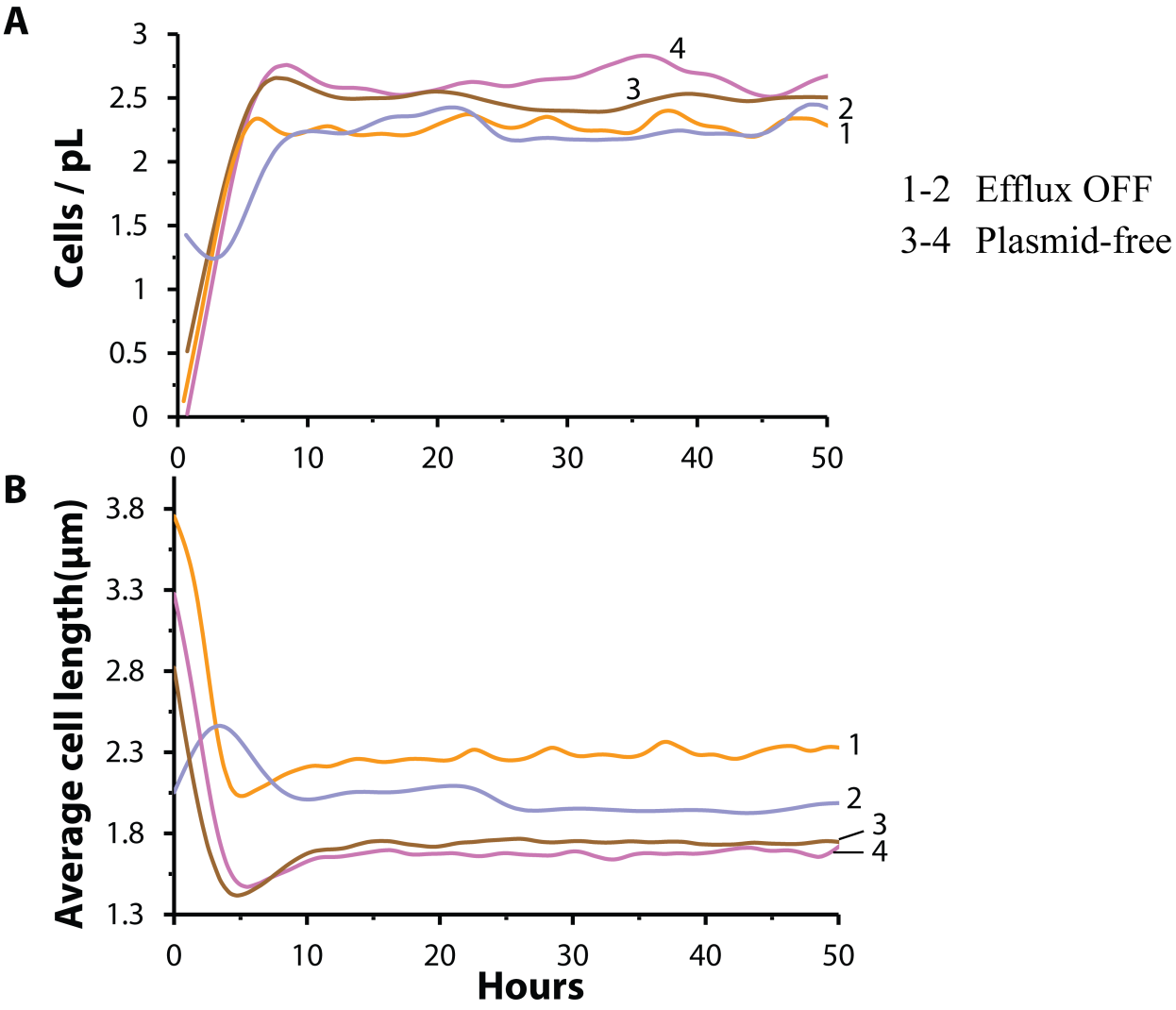

Figure 32| (A) Typical microchemostat growth curves of *E. coli* cells with efflux OFF (reactors 1 and 2), or plasmid-free (reactors 3 and 4). (B) Graphs of the average specific cell lengths corresponding to each of the cell populations depicted in (A) measured at each time point. All graphs are smoothed spline interpolations of raw data shown in appendix C. Cells were grown at 37°C in LB medium at a dilution rate of 0.32 $hour^{-1}$ and induced with 3.2 mg/L arabinose. All experiments were repeated eleven times.

8.2.1 Oscillations Due to Efflux Gene Expression

Cell populations carrying the Rv1258 plasmid were induced with arabinose (efflux ON) (Figure 33). This lead to the transcription of the Rv1258 gene and subsequent expression of the efflux pump. Growth in efflux ON cultures 1 and 2 exhibited damped oscillations whereby the cell density dropped dramatically after the first oscillation cycle and then sustained smaller amplitude oscillations about a reduced steady state of ~0.7 cells/pL. This reduced steady state illustrates the fitness cost conferred by pump activation. Corresponding cell lengths are represented in Figure 33B. Cell lengths for both efflux ON populations oscillated around ~2.9 μm.

These oscillatory dynamics appeared to be a unique characteristic of Rv1258. Two additional multidrug efflux pumps (Rv2477 and Rv2846) found in *M. tuberculosis* were induced with arabinose and cultured in the microchemostat to determine whether or not these growth characteristics are unique to Rv1258. These efflux pumps reached a similar steady state cell density (~1 cell/pL) to that seen for Rv1258; however, no oscillations were observed in the cell density and cell length (Figure 34).

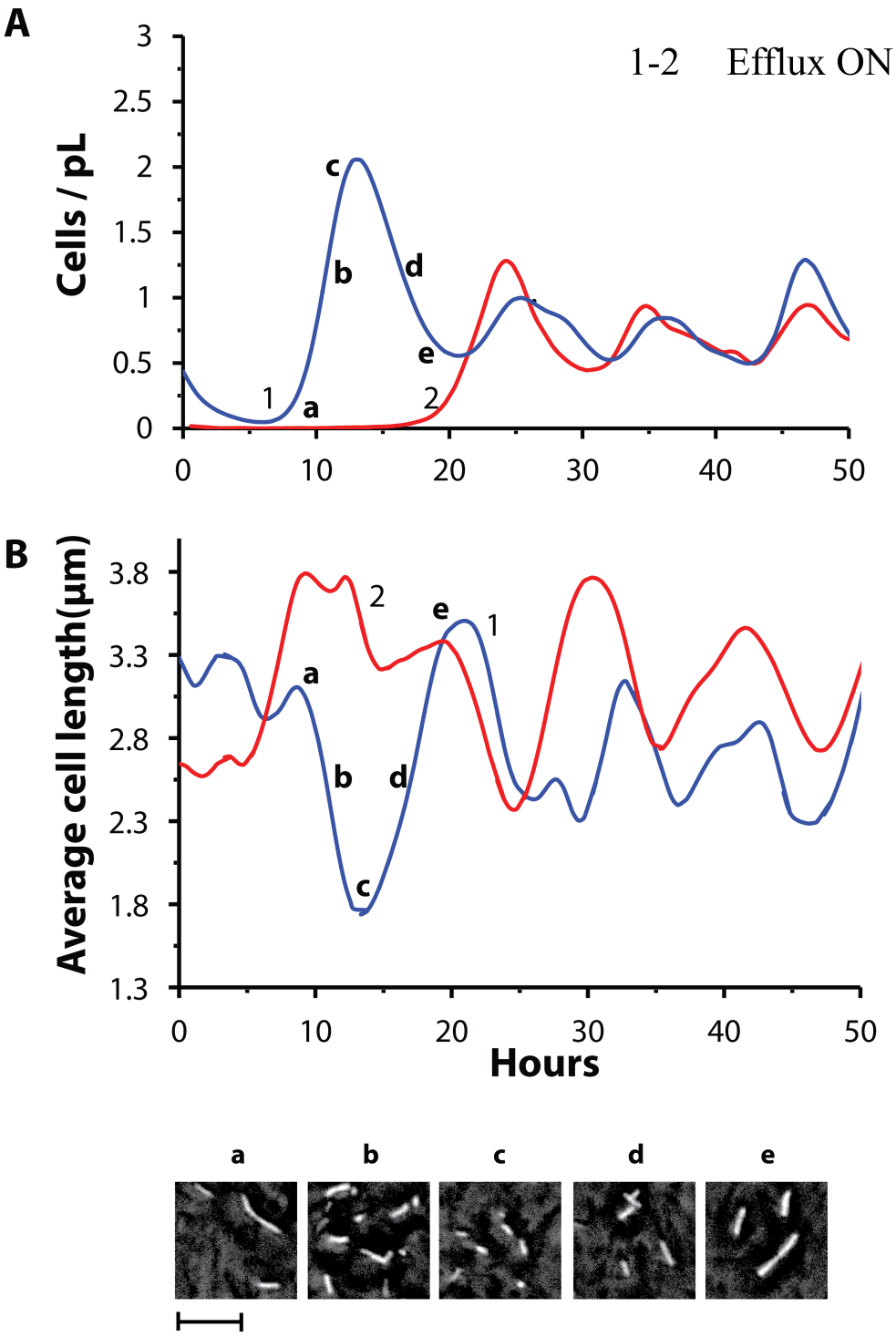

Figure 33| (A) Typical microchemostat growth curves of E. coli cells with efflux ON (reactors 1 and 2). (B) Graphs of the average specific cell length corresponding to each of the cell populations depicted in (A) measured at each time point. All graphs are smoothed spline interpolations of raw data shown in appendix C. Bottom panels (a to e) show micrographs of the cells in reactor 1 at the corresponding points during the first oscillation (scale bar, 25 µm). Cells were grown at 37°C in LB medium at a dilution rate of 0.32 hour^{-1} and induced with 3.2 mg/L arabinose. Experiments were repeated 14 times.

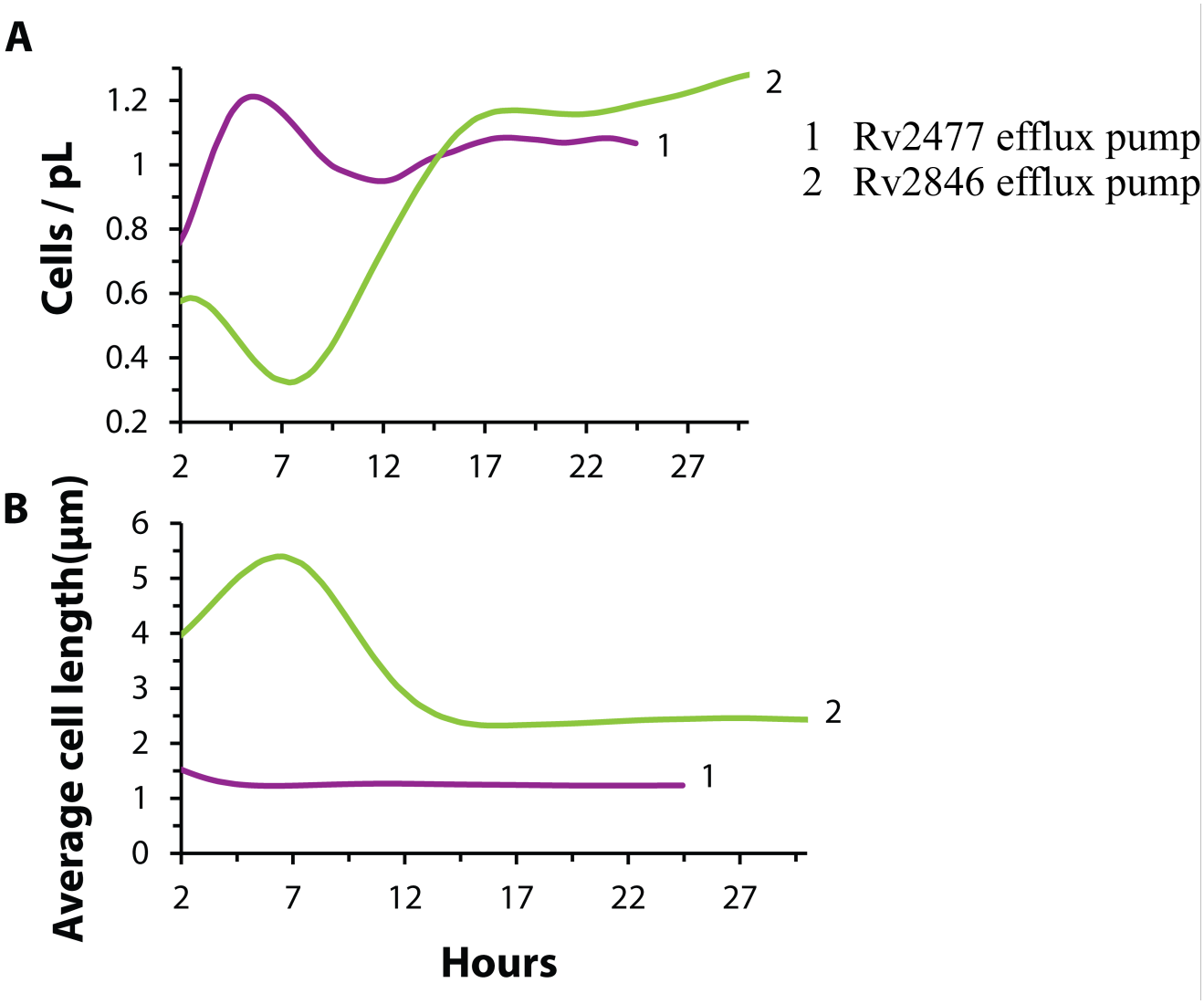

Figure 34| Cell density and length dynamics of the Rv2477 and Rv2846 efflux pumps. (A) Typical microchemostat growth curves of *E. coli* cells with efflux ON (reactors 1 and 2). (B) Graphs of the average specific cell length corresponding to each of the cell populations depicted in (A) measured at each time point. Cells were grown at 37°C in LB medium at a dilution rate of 0.16 hour^{-1} (Rv2477) and 0.32 hour^{-1} (Rv2846) and induced with 3.2 mg/L arabinose. All experiments were repeated twice.

8.2.2 A Deterministic Relationship between Cell Density and Cell Length

By monitoring specific cell morphologies in the microchemostat cultures, we observed that expression of Rv1258 induced cell filamentation (Figure 33B). Efflux ON cells were on average 2 to 3 times longer than the cells in the non-effluxing populations (Figure 32B), with specific cell lengths routinely reaching 30µm, which was ~10 times greater than the typical length of the cells in the non-effluxing cultures. Remarkably, the average cell length in the efflux ON populations exhibited oscillatory

behaviour that was not observed in the non-effluxing populations, but was tightly coupled to the oscillations in cell density (Figure 33).

For example, Figure 35A shows the cell density and average cell length of the population depicted in culture 2 of Figure 33. The oscillations in cell density were reversed relative to the oscillations in the average cell length and phase delayed by ~12 minutes. This deterministic relationship is illustrated in Figure 35B and specified by a phase-shifted linear equation:

$$\boldsymbol{n}(t-\tau_D) \cong -A \cdot \boldsymbol{L}(t) + B, \tag{7}$$

where $\boldsymbol{n}$ is the cell density (cells/pL), $\boldsymbol{L}$ is the cell length (µm), and τ_D represents the ~12-minute time delay between the cell density and length waves. A and B are relationship constants that were measured to be 0.45 cells/pL·µm and 2.15 cells/pL respectively.

To probe the interrelation between cell density and length, and the link to Rv1258 gene expression, we looked to the first derivative association of the time-variable parameters in equation 7:

$$\frac{d\boldsymbol{n}(t-\tau_D)}{dt} \cong -A \cdot \frac{d\boldsymbol{L}(t)}{dt}, \tag{8}$$

where d**n**/dt is the cell division rate (cells/pL·hour^{-1}) and d**L**/dt is the filamentation rate (µm.hour^{-1}). This relationship was consistent with the finite element derivatives obtained from the experimental data (Figure 35C) whereby the oscillations in the filamentation rate were reversed relative to the oscillations in the cell division rate and phase-shifted by the time-delay of ~12 minutes, as illustrated in Figure 35D. Except for the 12-minute lag in the elongation rate signal, the cell division rate varied directly as the elongation rate. Thus, for instance, a decrease in the growth rate coincided with a proportional increase in the elongation rate, and vice versa, although the changes in the filamentation rate were always delayed by a ~12-minute lag, designated τ_D.

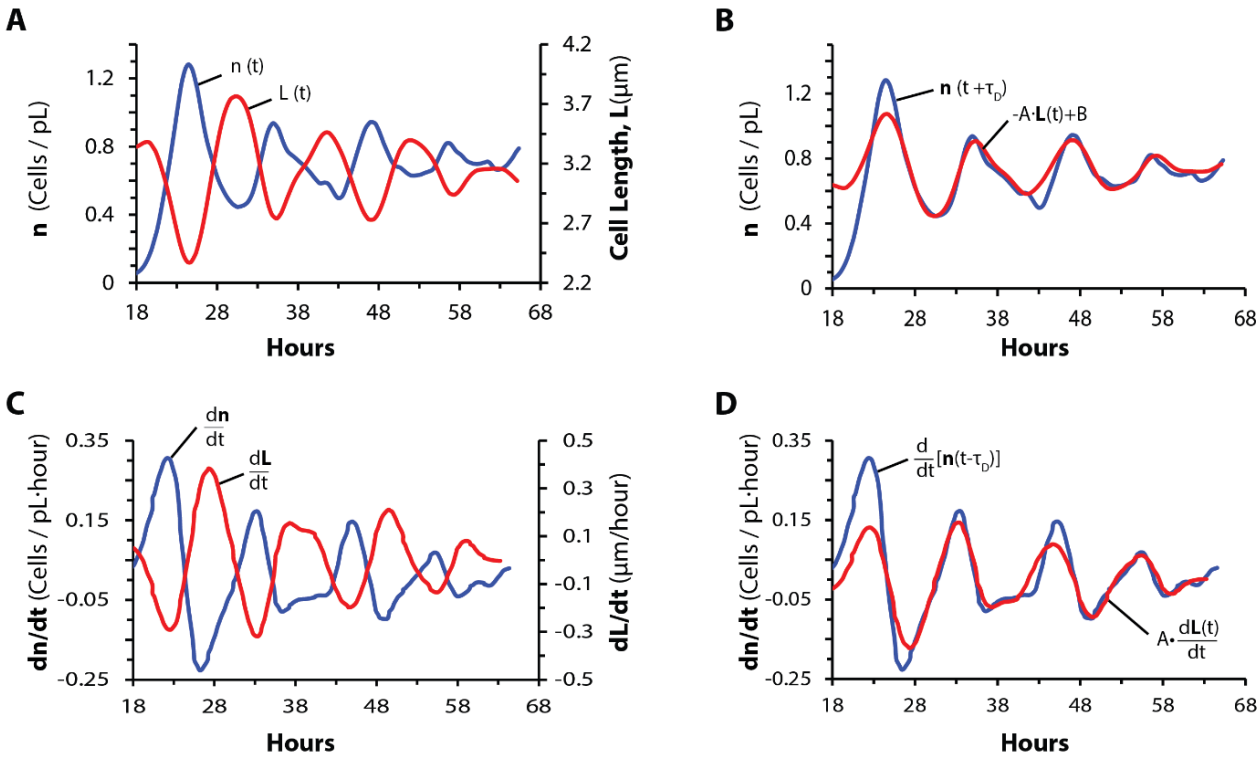

Figure 35| A deterministic relationship between cell density and cell length. (A) Growth curve (blue; primary axis) and cell length (red; secondary axis) with the Rv1258 efflux pump ON. (B) Growth curve (blue) shifted forward in time by a time delay (τ_D= 12 minutes) and linear transformation of cell length as per equation 1 (red). (C) Finite element derivatives of experimental data showing the cell division rate (blue, primary axis) and cell elongation rate (red, secondary axis). (D) Finite element cell division rate (blue) shifted forward in time by the time delay (τ_D = 12 minutes) and the linear transformation of the elongation rate as per equation 2 (red).

The time-shifted but direct proportionality relationship between the cell division and filamentation rates suggest that the filamentous phenotype adopted by efflux ON cells was due to cell division arrest, whereby rod-shaped cells ceased to divide into separate daughter cells but instead continued to grow in volume and length. For more information regarding the approach used to develop figure 35, please see chapter 7.

Cell filamentation behaviour has been observed in other bacterial species in response to a variety of stressful environments, including nutrient deficiency [210], extensive DNA damage through the SOS response pathway [211], host innate immune responses [212], and antibiotic treatment [213-215]. In addition, the filamentation response was not permanent, because periodically, the filamentation rate was reversed

during periods when the cells gradually reverted back towards a normal rod-shaped phenotype (Figure 35 and 36). The transitions between the alternating periods of increasing and decreasing filamentation rates in the efflux ON populations were notably abrupt and switch-like (Figure 35C).

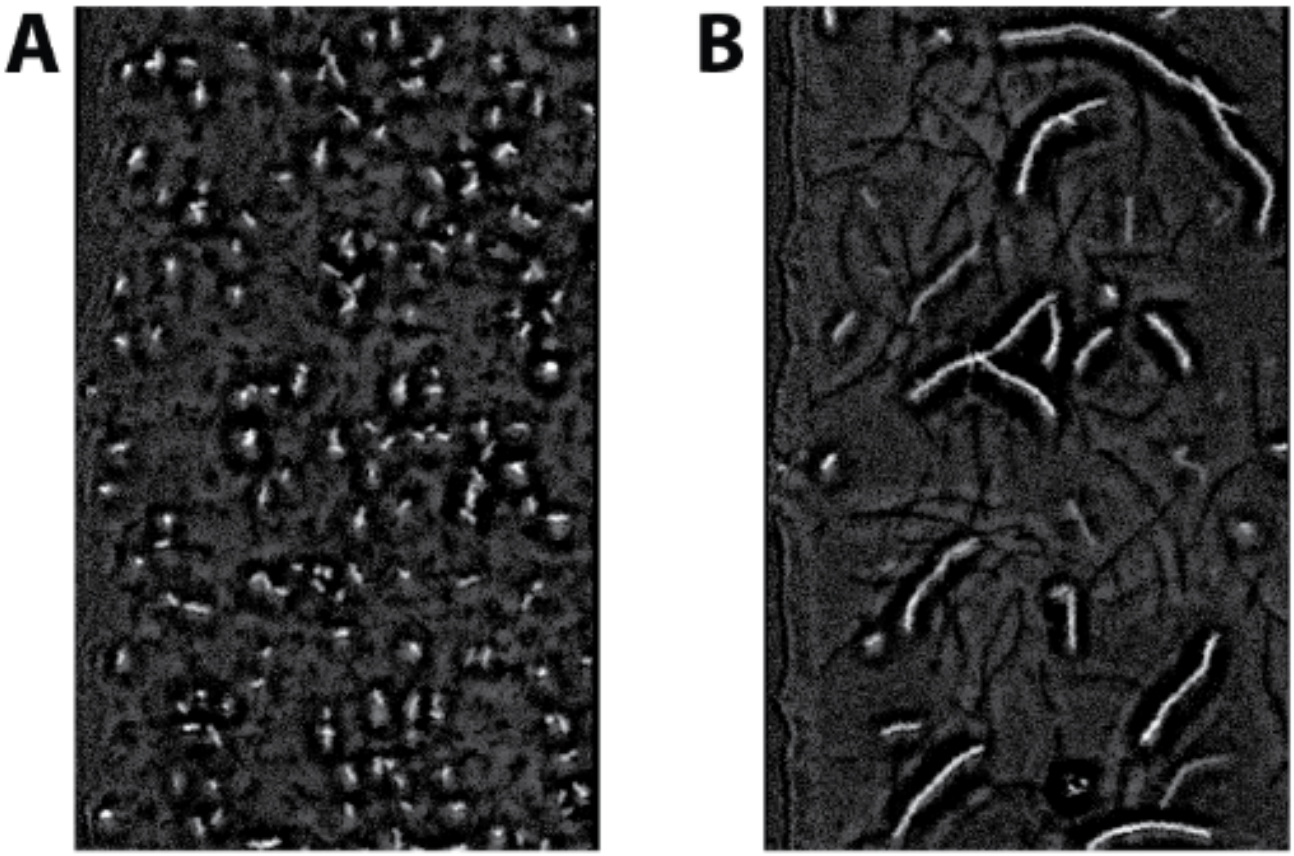

Figure 36| Rv1258 expression engendered two alternating, distinct morphological phenotypes in E. coli cells. The first phenotype comprised of normal-sized, rod-shaped, actively dividing cells depicted in panel (A). The second was characterized by arrested cell division and filamentous cells depicted in panel (B). The cells shown here were grown in a microchemostat with a dilution rate of 0.32 $hour^{-1}$ at 37ºC in LB medium and induced with 3.2 mg/L arabinose.

Consistent observations were made in conventional liquid batch cultures (Figure 37). Following the lag and exponential growth phases, the non-effluxing cultures entered stationary phase after ~8 hours of culturing with a cell density of ~1.6 (OD_{600}). The typical non-effluxing cell length decreased from ~10µm during lag phase to ~3µm during stationary phase. By contrast, efflux ON cultures

prematurely entered stationary phase after only 4 hours of culture with a lower cell density of ~0.8 (OD_{600}). The typical efflux ON cell length increased from ~10µm during lag phase to ~16µm during stationary phase. In the absence of continuous dilution, these stationary phase characteristics persisted throughout the remainder of the culturing process, in contrast to the microchemostat cultures that underwent oscillatory behaviour.

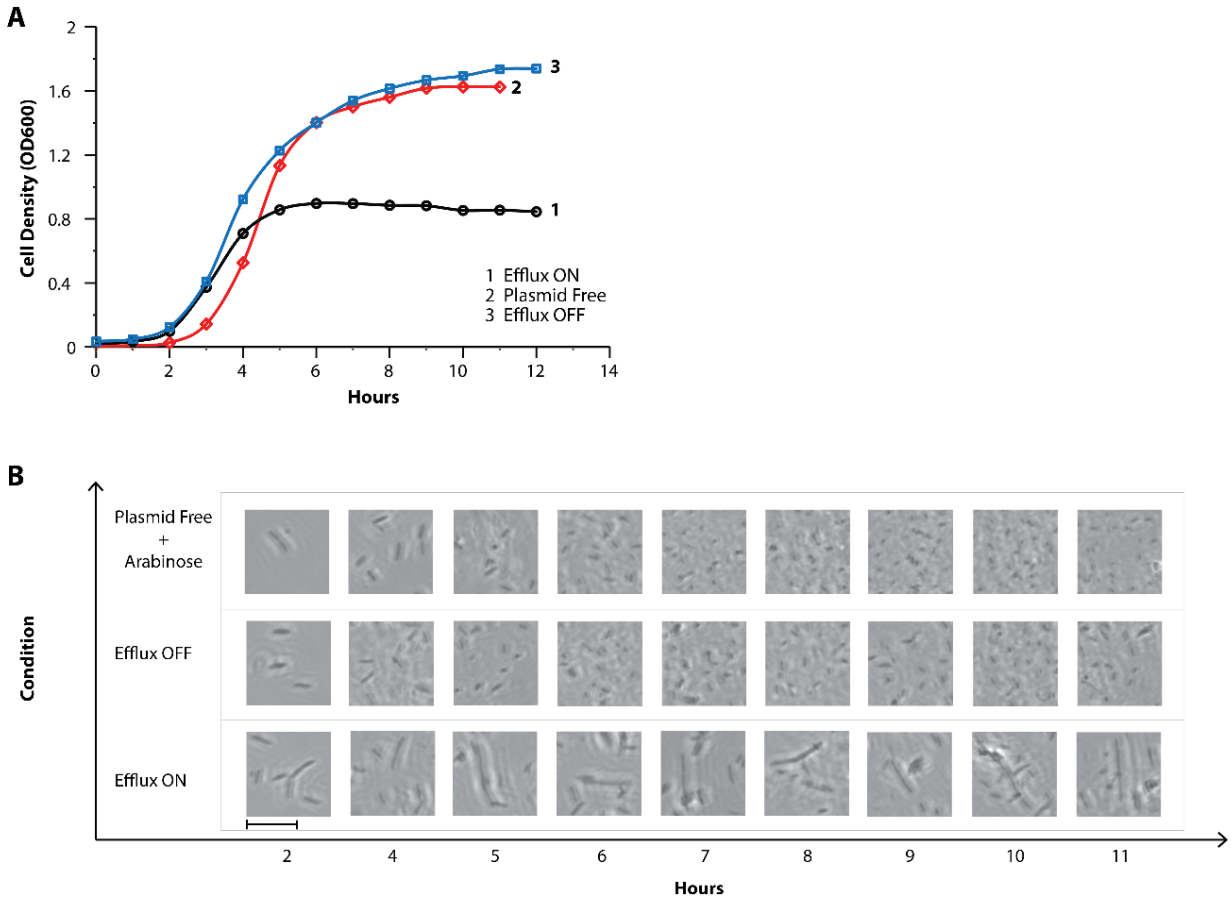

Figure 37| (A) Growth of *E. coli* cells in conventional liquid tissue culture flask batch cultures with the efflux pump ON (black circles), OFF (blue squares) or absent (red diamonds). Following lag and exponential growth phases, the non-effluxing cultures entered stationary phase after ~8 hours of culturing with a cell density of ~1.6 (OD_{600}). By contrast, efflux ON cultures prematurely entered stationary phase after only 4 hours of culture with a lower cell density of ~0.8 (OD_{600}). (B) Micrographs of the cells corresponding to the graphs in A at different time points. The typical non-effluxing cell length decreased from ~10µm during lag phase to ~3µm during stationary phase. The typical efflux ON cell length increased from ~10µm during lag phase to ~16µm during stationary phase. (Scale bar, 25 µm). Cells were inoculated into 10ml of LB broth and cultivated at 37°C with shaking at 280 rpm. Efflux ON and Plasmid Free populations were induced with 3.2 mg/L arabinose.

Results for Plasmid Free with and without arabinose did not differ. Optical density experiments were repeated twice. Each data point represents an average of three separately read optical densities

8.3 Efflux Activity—A Plausible cause of Oscillations in Cell Density and Length

8.3.1 The Removal of Oscillations through Efflux Inhibition

To ascertain that the damped oscillations in cell density and length in the efflux ON microchemostat cultures were due to expression of the Rv1258 gene, efflux pump inhibitors were used.

Addition of efflux inhibitors CCCP (carbonyl cyanide *m*-chlorophenyl hydrazone) and PAβN (phenylalanine-arginine beta-naphthylamide) to efflux-ON cultures suppressed the oscillatory dynamics, suggesting that the efflux-ON oscillatory behaviour may be due to efflux activity (Figure 38A and B). However, the steady state cell density in the efflux inhibited cultures was dramatically reduced (~0.3 cells/pL) relative to equivalent cultures without the inhibitors (~0.7 cells/pL). This reduced cell density can be attributed to the toxicity of the efflux inhibitors, which have been shown to permeabilize the outer membrane of gram negative bacteria, thereby reducing the cell viability[219,220]. It is possible that this low cell density may lead to a reduced total concentration of the efflux product, ultimately precluding oscillatory behaviour.

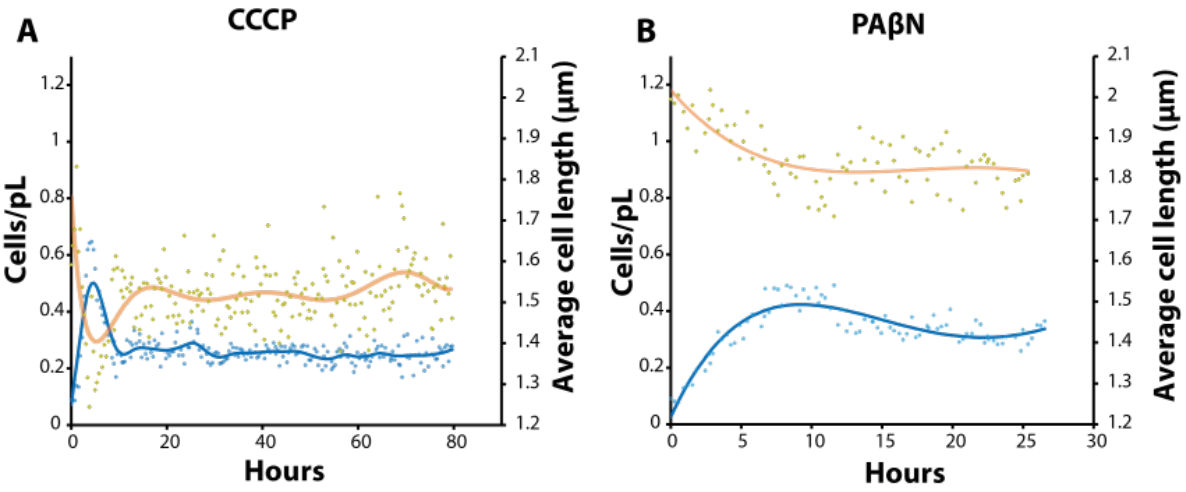

Figure 38| The effect of efflux pump inhibitors on *E. coli* growth dynamics. Bacterial cell density (blue curve; primary axis) and morphology (orange curve; secondary axis) as a function of time in microchemostat cultures to illustrate that the oscillatory behaviour in efflux-ON cells is due to

expression of the Rv1258 gene. (A and B) Efflux-ON cells cultured with efflux pump inhibitors CCCP (A) or PaβN (B) do not elicit oscillations. Cultures were induced with 3.2 mg/L arabinose. Cells were grown at 37°C in LB medium, at a dilution rate of D= 0.32 $hour^{-1}$. All experiments were repeated twice.

8.3.2 Removal of Oscillations through Gene Substitution

To ascertain that the damped oscillations in the efflux ON cultures were due to expression of the Rv1258 gene, we also utilized a control plasmid in which the green fluorescent protein (GFP) gene was substituted for the Rv1258 efflux pump gene (Figure 27B) [221]. As shown in Figure 39A, cells in reactor 1 carrying the GFP plasmid that were induced with arabinose (GFP ON) grew without oscillation in cell density to a steady-state of ~1 cell/pL. Unlike the cell density achieved by the cultures grown with efflux pump inhibitors (~0.3 cells/pL), the cell density achieved by the GFP expressing population (~1 cell/pL) was high enough to elicit oscillatory behaviour in the efflux-ON cultures. The uninduced GFP culture (GFP OFF) in reactor 2 also grew without oscillation in cell density to a steady state of ~2 cells/pL, which was double that of the GFP ON cultures. Corresponding cell lengths presented with no oscillations with GFP ON populations reaching 1.5 μm compared to 2 μm for the GFP OFF populations (Figure 39B).

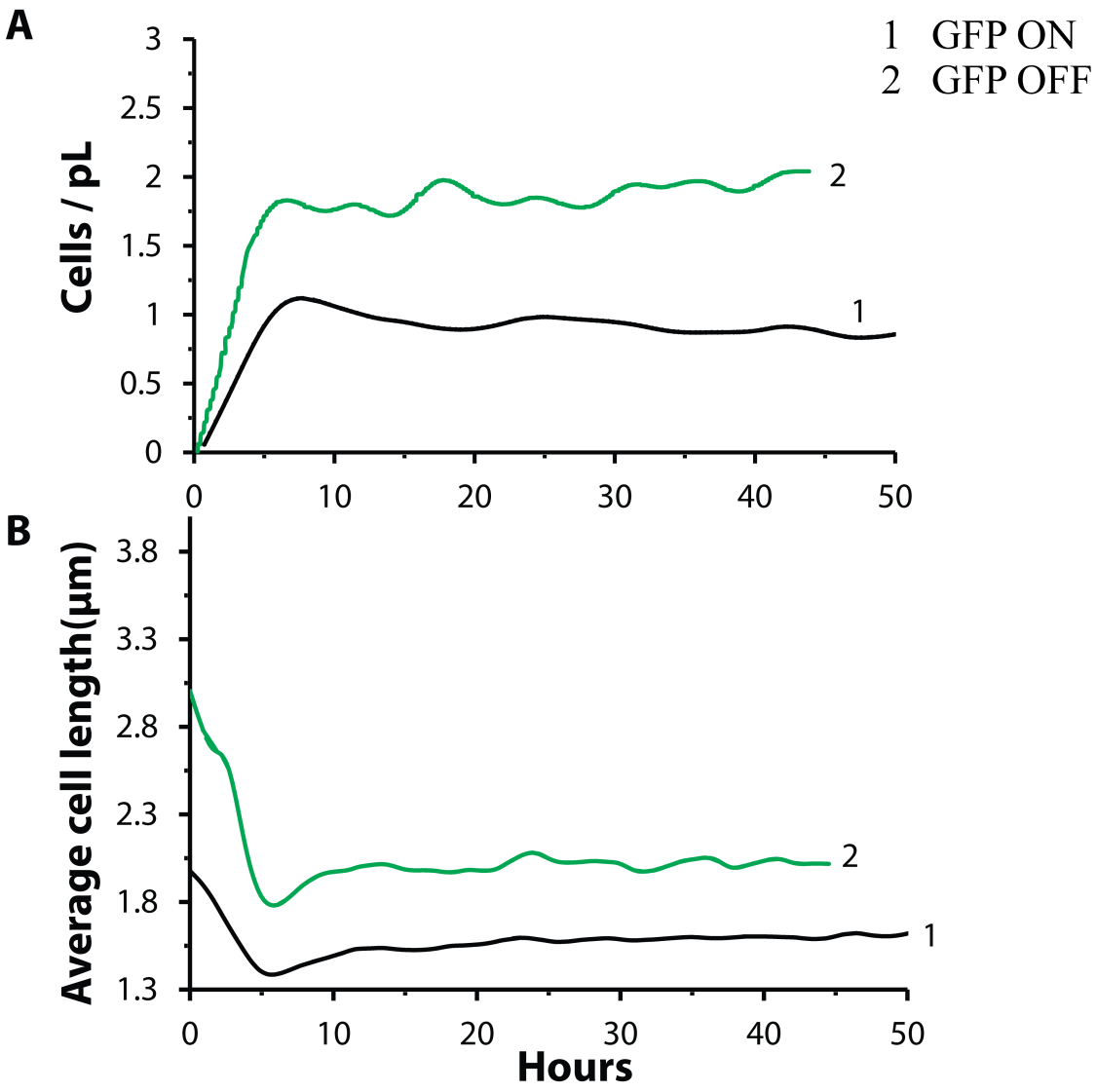

Figure 39| (A) Typical microchemostat growth curves of E. coli cells with GFP ON (reactor 1), or GFP OFF (reactor 2) (B) Graphs of the average specific cell length corresponding to each of the cell populations depicted in (A) measured at each time point. All graphs are smoothed spline interpolations of raw data shown in appendix C. Cells were grown at 37°C in LB medium at a dilution rate of 0.32 $hour^{-1}$ and induced with 3.2 mg/L arabinose. All experiments were repeated four times.

Induction with arabinose led to a ~25% reduction in the steady state cell density of GFP cells but increased the fraction of GFP fluorescent cells from ~8% in the GFP OFF population to ~67% in the GFP ON population (Figure 40). The reduced density of the GFP ON population relative to the GFP OFF culture demonstrates the fitness cost associated with expression of plasmid encoded genes. However, the variations in steady-state cell density of GFP ON cells were negligible compared to the overall population oscillations observed in the efflux ON cultures (Figure 33). Thus, the oscillations observed in the efflux ON cultures could neither be accounted for by arabinose induction nor the plasmid backbone but were attributable to Rv1258 gene expression.

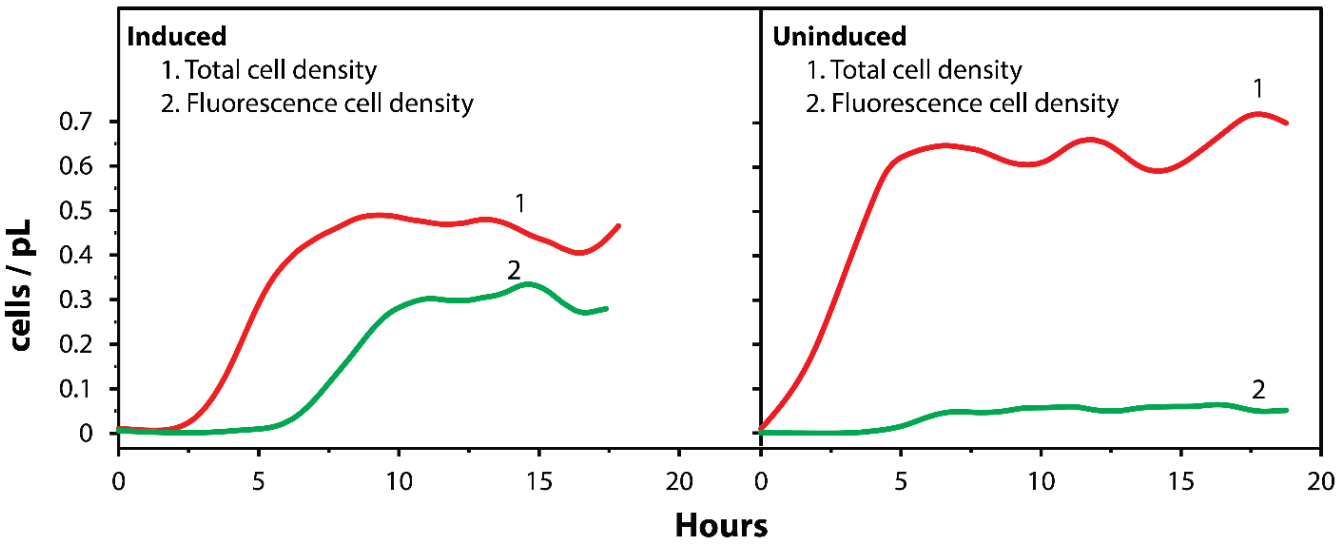

Figure 40| Microchemostat growth curves of *E. coli* cells carrying the GFP plasmid construct schematized in Figure 27B with an arabinose inducible promoter driving GFP gene expression. Cells were grown with arabinose (induced, Left) or without (uninduced, Right). The red growth curves represent the overall cell density and the green curves represent the density of the fluorescent cells. Cells were grown with a dilution rate of 0.32 $hour^{-1}$ at 37°C in LB medium and induced with 3.2 mg/L arabinose.

8.4 Oscillatory Dynamics Induced through an Extruded Natural Efflux Product

To conceptualize the mechanisms involved in bacterial efflux, we developed a hypothesis that states that "oscillatory dynamics in the efflux ON populations are due to an extruded product that acts on the population as a whole to induce cell filamentation and suppress growth."

Population-wide synchronized control of gene expression is necessary for such switch-like transitions; from which we can infer that the cyclic cell filamentation pattern was a response to fluctuations in a population-wide factor, such as the extracellular concentration of a stress factor. We have previously

shown that the observed filamentation pattern was caused by Rv1258 gene expression, and therefore we attributed the filamentation process to the extracellular concentration of a bio-chemical signal (natural efflux product) extruded from within the cells by the Rv1258 efflux pump.

This inference was supported by cell culture experiments performed using conditioned medium (i.e., medium containing the suspected growth-inhibiting factors extruded by the Rv1258 efflux pump). We observed a 20% reduction in the growth of GFP cells cultured in conditioned medium containing the growth inhibiting factors (obtained from a previous culture of efflux ON cells), relative to GFP cells cultured in medium conditioned with cells expressing the GFP gene (Figure 41).

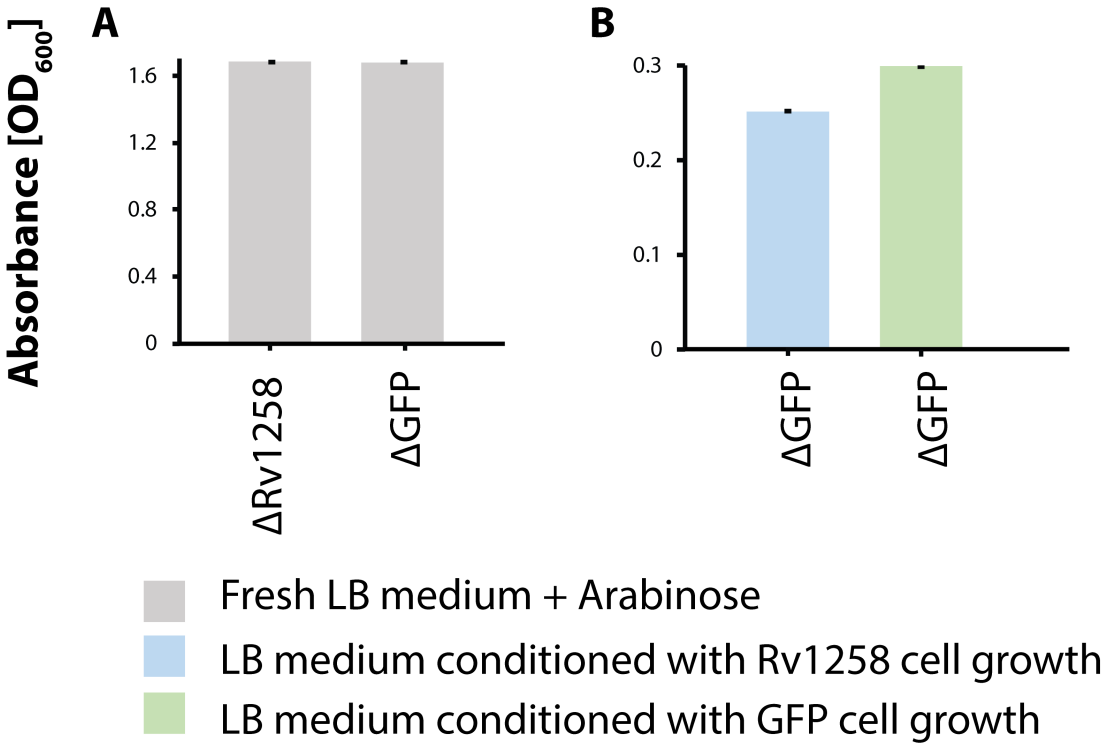

Figure 41| The effect of an extruded natural efflux product on the growth of cells expressing GFP. (A) Growth of *E. coli* cells expressing the Rv1258 and GFP plasmid-encoded genes in liquid media. Stationary phase OD600 readings are presented. For each condition, 10 ml of fresh LB medium containing arabinose was inoculated with cells containing the Rv1258 or GFP plasmid and incubated with shaking at 37ºC for 24 hours. (B) Growth of *E. coli* cells carrying the GFP plasmid in conditioned medium. Medium was conditioned with *E. coli* cells expressing the Rv1258 (blue bar) or the GFP plasmid (green bar). 10 ml of medium conditioned with *E. coli* cells expressing the Rv1258 or GFP plasmid-encoded genes was inoculated with cells containing the GFP plasmid and incubated with shaking at 37ºC for 24 hours. There was a 20% reduction in growth of GFP cells supported by the medium conditioned with cells expressing the Rv1258 gene. All experiments were repeated twice.

8.4.1 A Qualitative Model of Efflux Gene Expression

An extension of this inference is that the natural product extruded by the Rv1258 efflux pump suppresses its own production—a necessary condition for the observed oscillatory behaviour. Together, our results show that the Rv1258 efflux pump extrudes a natural product, synthesized intracellularly that is evidently non-disruptive to cell growth and morphology in the intracellular environment—a necessary requirement for the observed switch-like transitions. However, once extruded from the cell, the natural efflux product can accumulate in the extracellular environment and at sufficiently high concentrations, effect cell-division arrest, resulting in cell filamentation and a decreased production of the natural efflux product. Eventually, when the production rate of the natural efflux product falls below the dilution rate, the natural efflux product gets diluted out of the microchemostat culture, which reverses the filamentation process, and the population recovers and enters the next cycle (Figure 42).

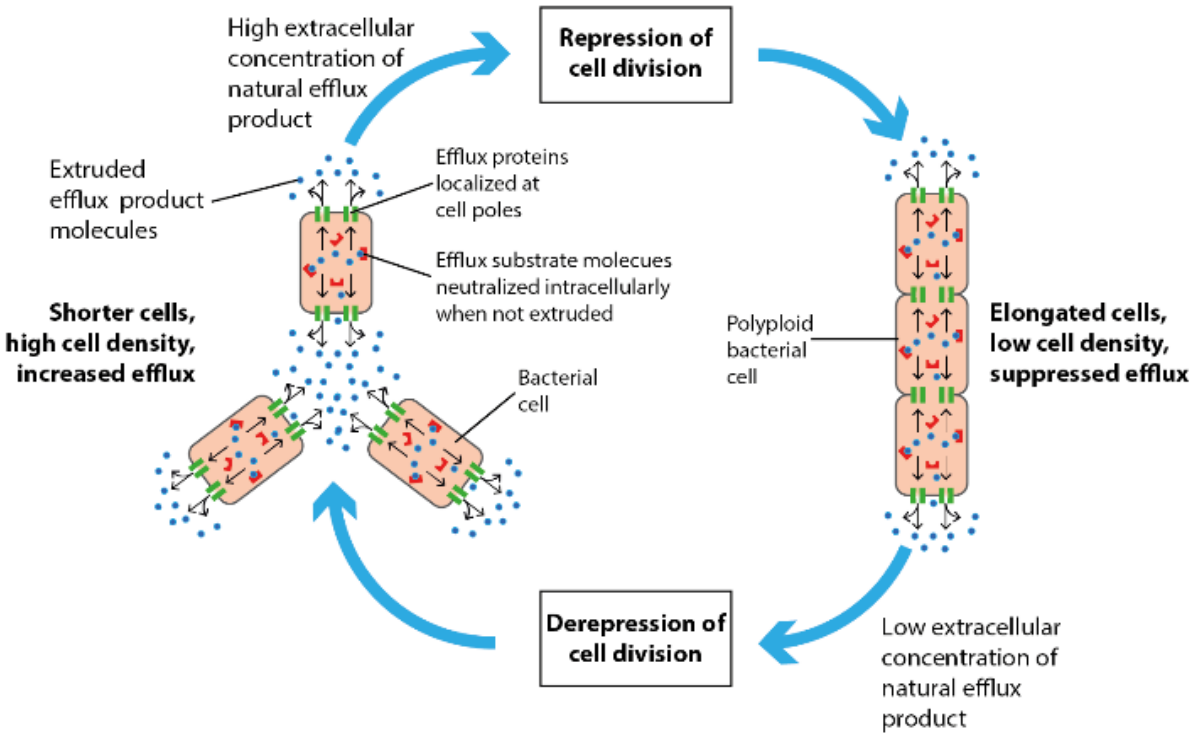

Figure 42| Schematized view of a model relating the rates of cell division and elongation during expression of the Rv1258 efflux pump. The efflux pump extrudes a natural substrate, synthesized intracellularly that is non-disruptive to cell growth and morphology in the intracellular environment where it is well regulated. However, once extruded by the efflux pump, this substrate can accumulate in the extracellular environment and at sufficiently high concentrations inhibit cell division, resulting

in cell elongation. The model also postulates that the Rv1258 efflux proteins are substantially located at the cell poles, such that elongated polyploid cells are less efficient efflux extruders because they have a smaller pole surface area ratio relative to normal size cells generated during active cell division. This phenomenon has also been observed in *Caulobacter crescentus* in a study conducted by Kirkpatrick and Viollier. Cell elongation results in a decrease in the extrusion of the natural efflux substrate, which is gradually diluted out by chemostat operation. A low extracellular concentration desuppresses cell division, which switches off the cell elongation process. Active cell division resumes, which in turn increases efflux of the natural substrate and ushers in the next cycle.

8.4.2 A Quantitative Model of Efflux Gene Expression

To further understand the dynamics of the *E. coli* expression system, we developed a simplified quantitative model that captures the essential features of the system.

In conventional liquid batch cultures, wild type, efflux-OFF and efflux-ON cultures initially grew at similar exponential growth rates of 1.03 hr^{-1}, 1.06 hr^{-1} and 1.04 hr^{-1} respectively (Figure 37A). However, although the wild type and efflux-OFF cultures entered stationary phase after ~6 hours at an optical density of ~1.6, the efflux-ON cultures prematurely entered a permanent stationary phase after ~4 hours at an optical density of ~0.8. As discussed previously, one plausible scenario for such an outcome is that the efflux-ON cultures were extruding a product that was harmless at low concentrations but became toxic above a threshold concentration and halted cell division abruptly. Similar observations were made for the microchemostat experiments. We formulated differential equations that capture the main aspects of this scenario and compared their numerical solutions to the patterns observed in the microchemostat cultures.

When the efflux pump is OFF, cell proliferation in the microchemostat cultures is modeled by the canonical chemostat equation 4 (chapter 4), where n, D and μ represent the number of cells, dilution rate and specific growth rate respectively.

In order to develop the model, we expressed the specific growth rate as $\mu = \mu_{max} \cdot H(N_{\square} - n)$, where μ_{max} is the maximum specific growth rate during the exponential phase. $H(N_{\square} - n)$ expressed as $\left(1 - 1/\left(1 + e^{2 \cdot c_n \cdot (N_\infty - n)}\right)\right)$ is a smooth approximation of the Heaviside step function modeling the change in the growth rate as the microchemostat culture transitions from exponential to stationary phase. c_n is the sharpness of this transition and N_∞ is the maximum number of cells the microchemostat reactor can sustain indefinitely in the absence of culture dilution. The growth rate is thus expressed as:

$$\frac{dn}{dt} = -n \cdot D + n \cdot \mu_{max} \cdot \left[1 - \left(\frac{1}{1+e^{2 \cdot c_n \cdot (N_{\square} - n)}}\right)\right] \quad [9]$$

When the efflux pump is turned ON, we express the specific growth rate as $\mu_p = \mu \cdot H(p_{\square} - p)$, where μ is the specific growth rate and p is the concentration of the efflux product. $H(p_{\infty} - p)$ expressed as $\left(1 - 1/\left(1 + e^{2 \cdot c_p \cdot (p_{\infty} - p)}\right)\right)$ is a smooth approximation of another Heaviside step function modeling the change in the growth rate as the efflux product transitions from a harmless level above the toxic threshold concentration. c_p is the sharpness of this transition and $p_{\square}$ is the threshold concentration above which the efflux product becomes toxic. The rate of production of p is expressed as a differential equation where k is the rate of extrusion of efflux products by each cell. Thus, the pump ON model consists of two coupled differential equations representing the rate of bacterial growth and extrusion of efflux products:

$$\frac{dn}{dt} = -n \cdot D + n \cdot \mu_{max} \cdot \left[1 - \left(\frac{1}{1+e^{2 \cdot c_n \cdot (N_{\square} - n)}}\right)\right] \cdot \left[1 - \left(\frac{1}{1+e^{2 \cdot c_p \cdot (p_{\square} - p)}}\right)\right] \quad [10]$$

$$\frac{dp}{dt} = -p \cdot D + n \cdot k \quad [11]$$

Numerical solutions to the model described in equations 9 to 11 were programmed into a spreadsheet using parameter values listed in Table 2, appendix D. The model predicted underdamped oscillations in the efflux-ON cell population density, which eventually reaches a steady-state (Figure 43).

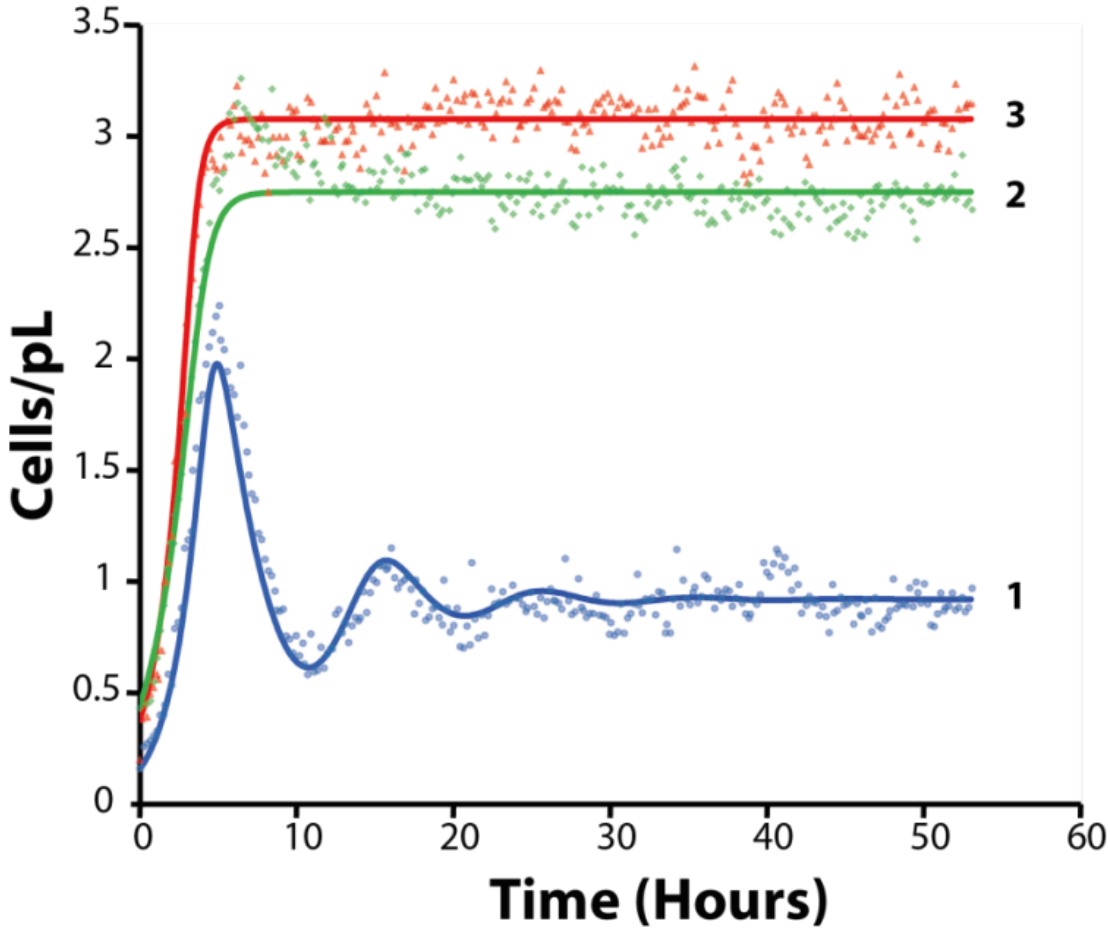

Figure 43| A model predicting underdamped oscillations in the efflux-ON cell population density. Model predictions (solid lines) have been plotted with typical data (data points). The model predicts damped oscillations in the efflux-ON cell density (1), which eventually reaches a steady-state. The behaviour of wild type (2) and efflux-OFF (3) cultures is consistent with typical microchemostat cell growth dynamics.

8.5 Efflux-Associated Drug Tolerance

8.5.1 Ethidium Bromide Tolerance

We next investigated the efflux phenotype due to Rv1258 expression at various concentrations of ethidium bromide (EtBr)—a known inhibitor for *E. coli* cell growth [216,217] that has previously been documented as a substrate of the Rv1258 pump [218]. As shown in the top row of Figure 44A, in the efflux OFF cultures, as the ethidium bromide concentration was increased from 0 to 0.25, 0.5 and 1µg/ml, the steady-state cell density decreased from ~2.6 to ~2.5, ~1.7, and <0.7 cells/pL respectively, illustrating the deleterious effect of EtBr in the absence of efflux. As described previously, in the absence of EtBr, the typical efflux ON culture displayed damped oscillations in the

cell density, attaining a steady-state density of ~0.7 cells/pL that was ~3× lower than the corresponding efflux OFF culture. However, in contrast to the efflux OFF trend, the efflux ON steady state density was maintained at ~0.7 cells/pL when the EtBr concentration increased to 0.25µg/ml EtBr, and even increased slightly to ~0.85 cells/pL at a higher EtBr concentration of 0.5µg/ml. Clearly, EtBr extrusion by the Rv1258 efflux pump enabled the efflux ON cells to maintain a high cell density—comparable to the density in the EtBr-free culture—at EtBr concentrations that affected growth in the equivalent efflux OFF cultures (0.25 and 0.5µg/ml). When the EtBr concentration was increased further to 1µg/ml, the Rv1258 efflux pump became overwhelmed and the efflux ON culture registered a major decrease in growth and steady-state density. The corresponding dynamics in cell length are shown in the bottom row of Figure 44A.

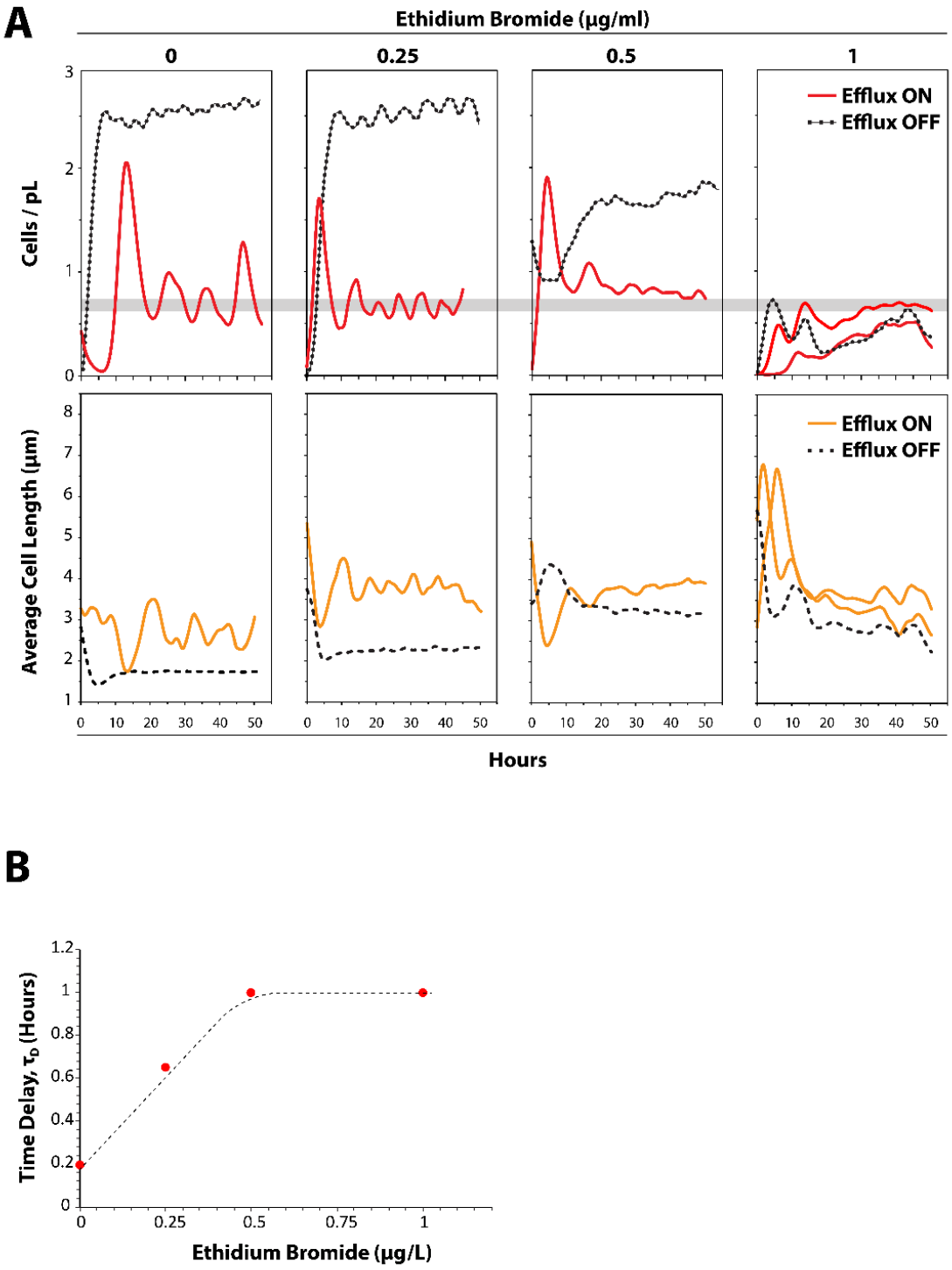

Figure 44| The effect of EtBr concentrations on population dynamics of *E.coli* cells (A) Top row graphs represent the effects of the ethidium bromide (EtBr) concentration on population dynamics of *E.coli* cells with efflux ON or OFF. In the efflux OFF cultures, the steady-state cell density decreased with increasing EtBr concentration. The efflux ON cultures maintained their steady state density as the concentration of EtBr was increased except for the highest EtBr concentration of 1µg/ml. Bottom

row graphs represent dynamics in cell length corresponding to the growth curves in the top rows. All graphs are smoothed spline interpolations of raw data shown in appendix C. Cells were grown at 37°C in LB medium at a dilution rate of 0.32 $hour^{-1}$ and induced with 3.2 mg/L arabinose. (B) Time delay (τ_D) between the growth and elongation oscillatory dynamics as a function of ethidium bromide concentration (EtBr). As the EtBr dose was increased from 0 to 0.25, 0.5 and 1µg/ml, the time-delay τ_D increased from 12 minutes, to 40 minutes, 1 hour and 1 hour, respectively. Each set of conditions were repeated twice.

At higher concentrations of EtBr (12.5 and 25µg/ml), microbial biofilms, which are not subject to wash-out through continuous bioreactor operation of the microchemostat, supplied most of the bulk culture cells in both the efflux OFF and ON cultures, leading to much higher cell densities than were achievable under more ideal chemostat conditions at lower EtBr concentrations (Figure 45). Exactly why biofilm formation was exacerbated at high concentrations of EtBr is unclear. However, as a result of elevated biofilm formation, we observed that at 12.5 µg/ml EtBr, the efflux ON and OFF microchemostat populations attained cell densities as high as ~2.5 cells/pL, which was at least 3× higher than the densities attained at 1ug/ml EtBr, in spite of the growth inhibitory effect of EtBr. At 25µg/ml of EtBr, the efflux ON cell density (~ 4 cells/pL) exceeded that of the efflux OFF culture (~3 cells/pL), further illustrating increased biofilm formation at higher concentrations of EtBr and the EtBr extrusion advantage conferred by the Rv1258 efflux pump to the efflux ON cells.

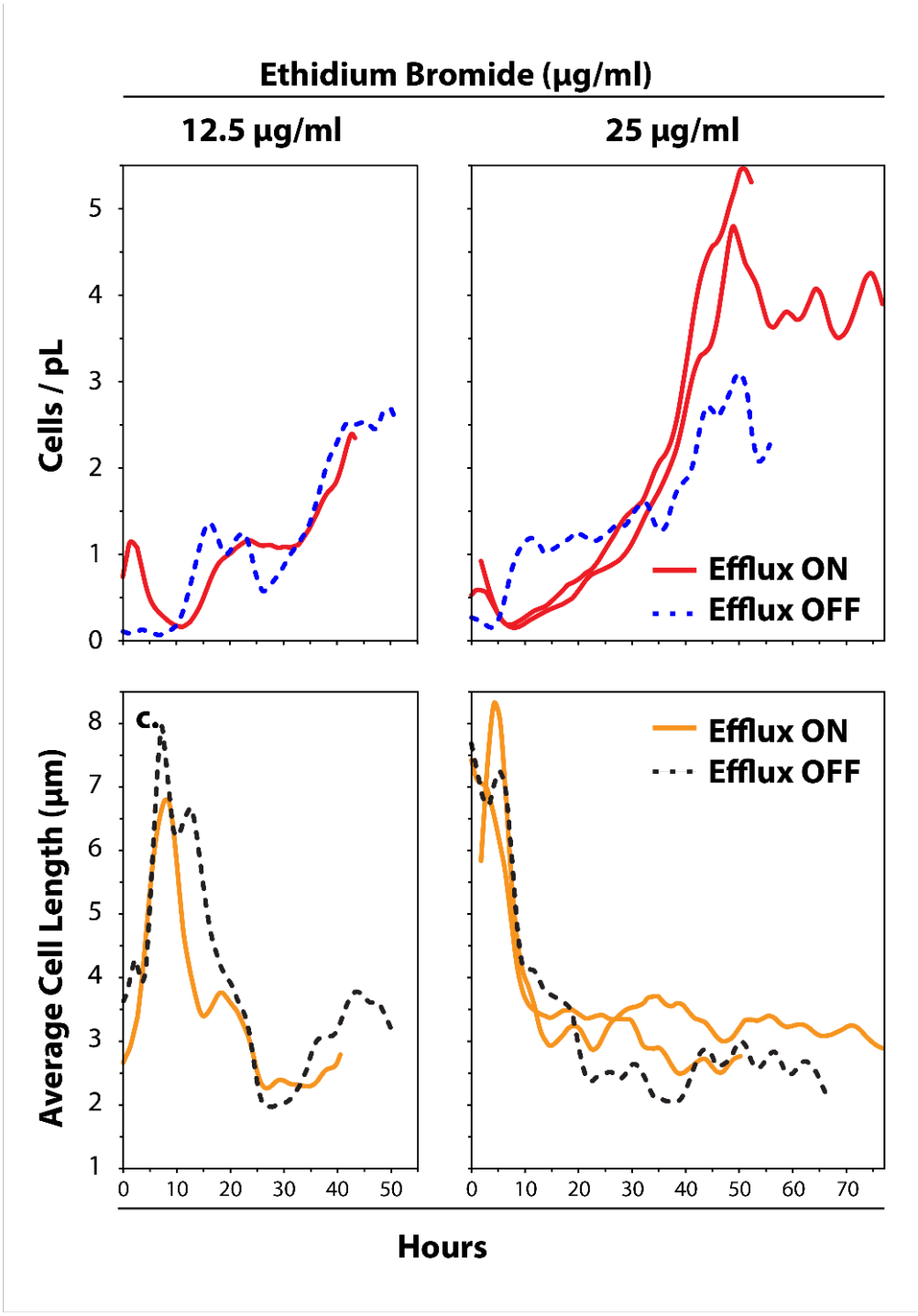

Figure 45| The effect of high concentrations of EtBr on *E.coli* population dynamics. Top and bottom row graphs represent the effects of high concentrations of ethidium bromide (EtBr) on population dynamics of *E.coli* cells with efflux ON or OFF. All graphs are smoothed spline interpolations of raw data shown in appendix C. Cells were grown at 37°C in LB medium at a dilution rate of 0.32 $hour^{-1}$ and induced with 3.2 mg/L arabinose. Each set of conditions were repeated twice.

The interference between the efflux extrusion of EtBr and the natural efflux product of the Rv1258 pump was also observable in the efflux ON cultures at the various concentrations of EtBr. As the EtBr dose was increased from 0 to 0.25, 0.5 and 1µg/ml, the frequency of the oscillations in the steady-state cell density and length increased while their amplitude decreased in tandem, and these oscillations essentially disappeared in the 0.5 and 1µg/mL EtBr concentration efflux ON graphs (Figure 44A). Furthermore, the time-delay τ_D between the cell density and cell length oscillations increased from 12 minutes, to 40 minutes, 1 hour and 1 hour, respectively (Figure 44B). The response dynamics slowed down as the EtBr concentrations was increased. We speculate that this behaviour was due to efflux substrate displacement whereby the EtBr molecules competed with the natural efflux product molecules for extrusion through the Rv1258 pump, which delayed accumulation of the natural efflux product in the extracellular environment and the onset of cell filamentation (Figure 46).

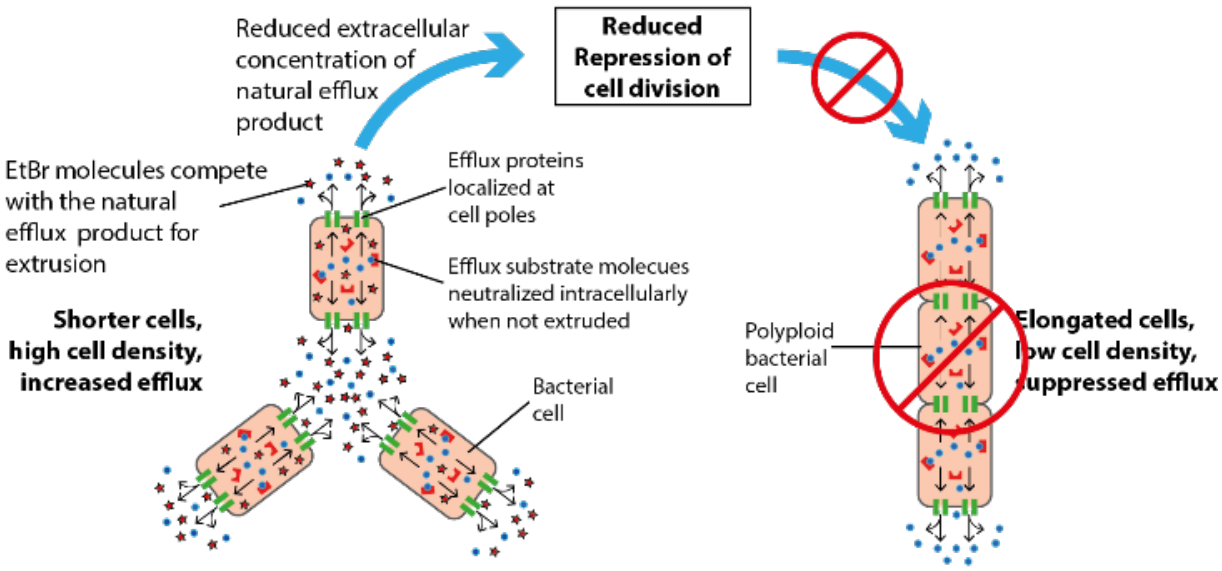

Figure 46| Schematized view of a model relating to the displacement of the natural efflux product by ethidium bromide. The efflux pump extrudes a natural substrate, synthesized intracellularly that is non-disruptive to cell growth and morphology in the intracellular environment where it is well regulated. However, once extruded by the efflux pump, this substrate can accumulate in the extracellular environment and at sufficiently high concentrations inhibit cell division, resulting in cell elongation. When ethidium bromide (EtBr) (which is also a substrate of the Rv1258 efflux pump) is added to the medium, it competes with the natural substrate for efflux extrusion. This minimizes the oscillatory dynamics in the cell density and increases the time delay between the cell density and cell elongation waves.

8.5.2 Streptomycin and Gentamicin Tolerance

We next investigated drug-tolerance under Rv1258 gene expression by introducing antibiotics including streptomycin and gentamicin to microchemostat cell populations that had reached a steady state density. In a representative set of experiments involving streptomycin (Figure 47A), the efflux pump was turned ON in culture 1; left OFF in culture 2; and absent (no plasmid) in culture 3. In the absence of streptomycin (time 0 to 40 hours), the non-effluxing cultures grew to a steady-state density of ~2 cells/pL, while the efflux ON cell density oscillated to a lower density of ~0.5 cells/pL. When medium containing streptomycin (0.78 μg/ml) was introduced at 40 hours, the non-effluxing cultures decayed exponentially and were washed out by 90 hours. By contrast, upon introduction of streptomycin, the cell density in the efflux ON culture 1 initially dropped to ~0.1 cells/pL but recovered at 60 hours to the pre-streptomycin steady state of ~0.5 cells/pL that was maintained during the remainder of the experiment, which lasted to 130 hours.

Similar dynamics were apparent when gentamicin (1.56 μg/ml) was introduced to different cell populations under otherwise similar conditions (Figure 47B). Prior to introducing gentamicin, the efflux OFF and plasmid-free populations attained steady-state cell densities of ~3 cells/pL, and the efflux ON culture ~0.5cells/pL. Upon introduction of gentamicin, the non-effluxing cells washed out of the microchemostat reactors while the efflux ON culture dropped to a cell density of ~0.1cells/pL and did not wash out of the reactor. The differences observed following streptomycin and gentomicin addition were consistent with previous experiments. These data suggest that streptomycin is a better substrate for the Rv1258 efflux pump compared to gentamicin. Altogether, these results illustrate that expression of the Rv1258 efflux pump increased tolerance to streptomycin and gentamicin.

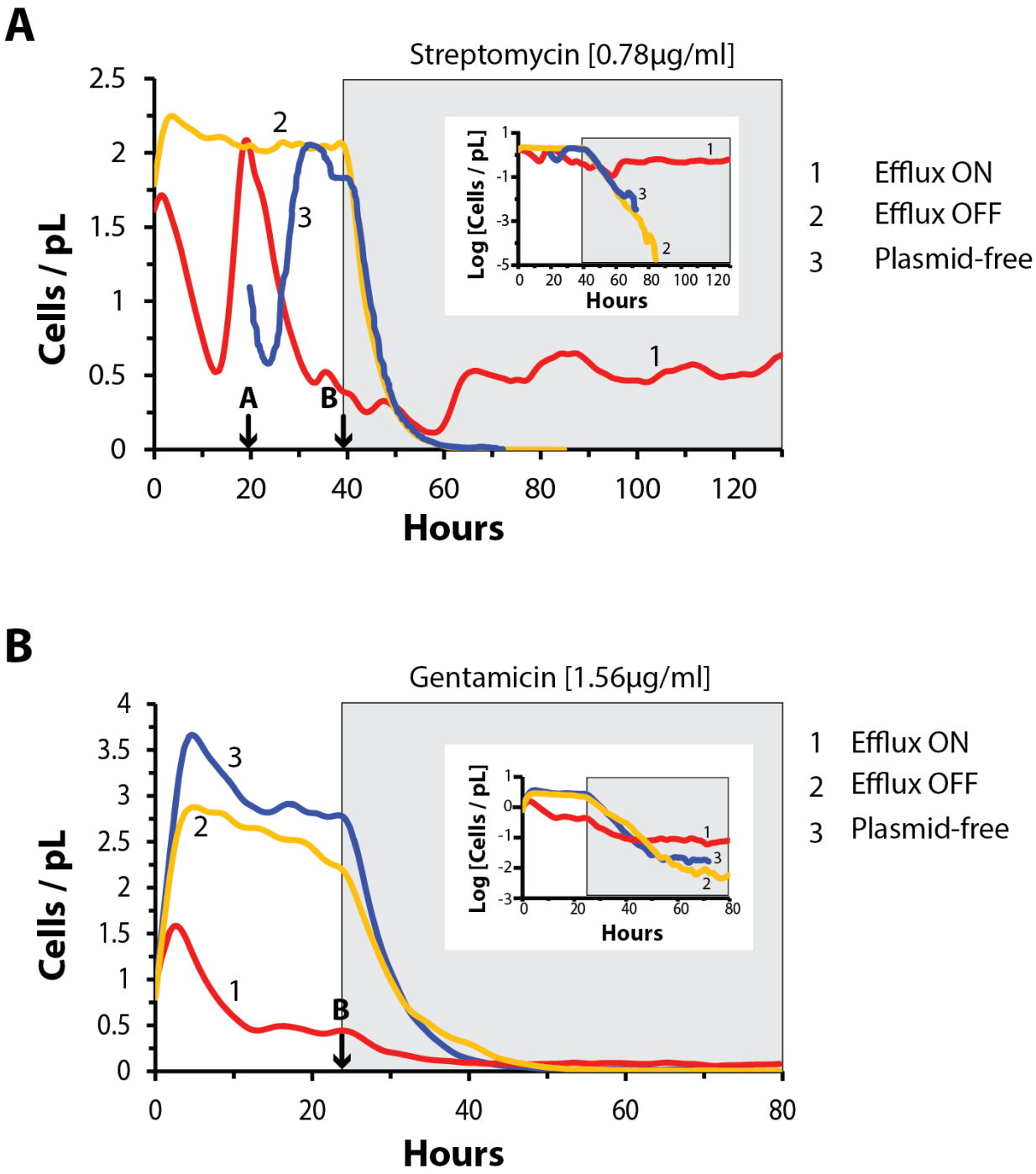

Figure 47| Efflux pump activation induces tolerance to streptomycin and gentamicin. (A) Growth of *E. coli* cells in the presence of streptomycin (0.78µg/ml) including a log scale in the inset. Initially, the efflux pump was turned ON in culture 1 and left OFF in culture 2. Culture 3, which was plasmid-free and inoculated at time 20 hours (point A) was cultivated on a separate chip in a different experiment under the same conditions. At 40 hours (point B), medium containing streptomycin was introduced to all cultures. The cell density in the non-effluxing cultures 2 and 3 decayed and washed out, whereas that of the effluxing culture 1 attained a non-trivial steady-state of 0.5 cells/pL. (B)

Growth of *E. coli* cells in the presence of gentamicin (1.56µg/ml) including a log scale in the inset. Initially, the efflux pump was turned ON in culture 1, left OFF in culture 2, and absent in culture 3. At 24 hours (point B), medium containing gentamicin was introduced to all cultures. Whereas the non-effluxing cultures washed out, the efflux ON culture attained a lower steady-state density of 0.1 cells/pL. All graphs are smoothed spline interpolations of raw data shown in appendix C. All cells were grown at 37°C in LB medium at a dilution rate of 0.16 $hour^{-1}$ and induced with 3.2 mg/L arabinose. All streptomycin experiments were repeated five times. Efflux ON and Plasmid-Free gentamicin experiments were repeated three times. Efflux OFF gentamicin experiments were repeated twice.

8.6 Loss of Efflux Gene Function

Throughout the project, we observed some interesting growth dynamics when cultures were grown in the microchemostat. Occasionally, some efflux-ON cultures escaped heterologous efflux pump regulation (Figure 48). In this case, the cells adopted a phenotype equivalent to cells that are not expressing the circuit (efflux OFF), with the cell density rapidly increasing whilst the cell size decreased. Conversely, growth in some Rv1258-bearing but uninduced cultures (efflux OFF) was halted briefly resulting in a dramatic decrease in cell density (Figure 49). This scenario resulted in the cells adopting an efflux ON phenotype, with the cell number decreasing whilst the length increased. A possible cause of this behaviour may be due to basal level expression of the Rv1258 gene in uninduced cultures which led to a slow but gradual increase in the efflux products reaching their toxic threshold concentration. These cell cultures recovered after a brief period once the efflux products were diluted out.

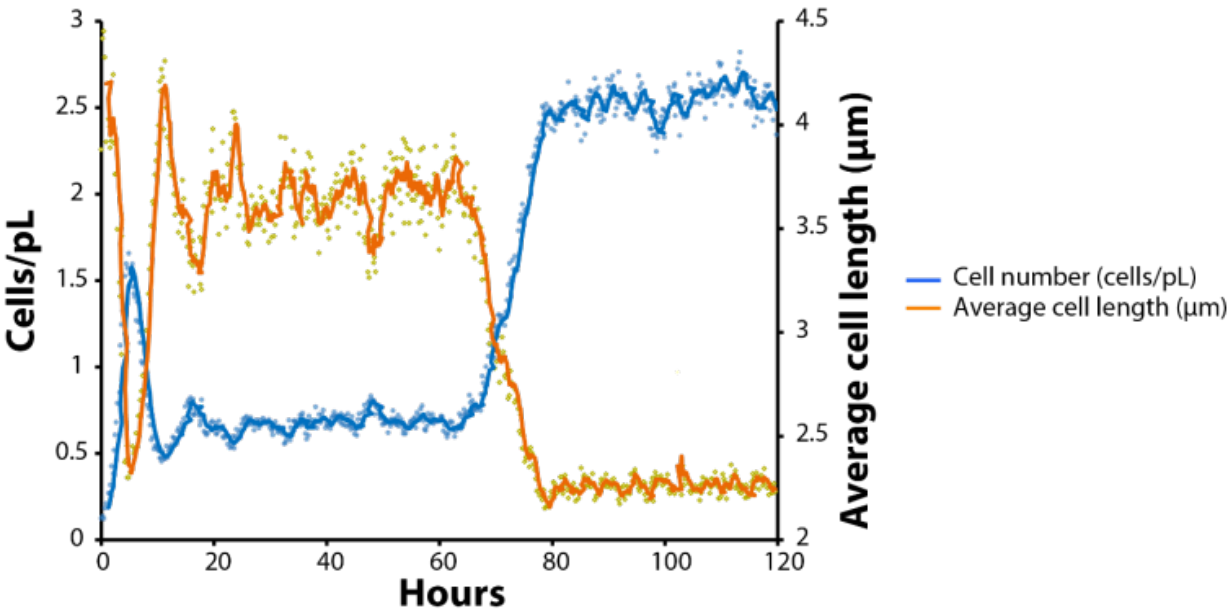

Figure 48| Interesting growth dynamics whereby Efflux-ON populations escaped heterologous efflux pump regulation. Microchemostat growth curves illustrating the cell density (blue curve; primary axis) and morphology (orange curve; secondary axis) of cells with the Rv1258 efflux pump turned ON. Although the culture is induced during the entire experiment, the cells escape regulation of the Rv1258 circuit at ~60 hrs. Cells were grown at 37°C in LB medium at a dilution rate of 0.32 $hour^{-1}$ and induced with 3.2 mg/L arabinose.

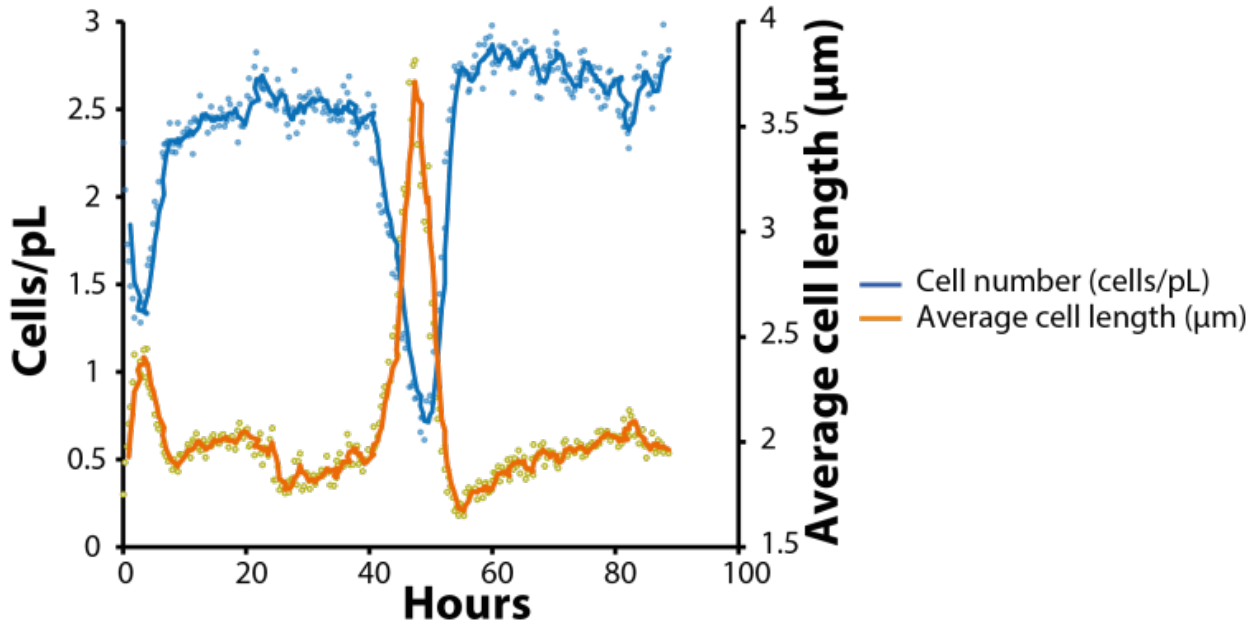

Figure 49| Basal level expression of Rv1258 in efflux OFF cultures. Microchemostat growth curves illustrating the cell density (blue curve; primary axis) and morphology (orange curve; secondary axis) of cells with the Rv1258 efflux pump OFF. Although the culture is uninduced during the entire experiment, the cell density on occasion plummets possibly due to basal level expression of the Rv1258 gene. Cells were grown at 37°C in LB medium, at a dilution rate of 0.32 $hour^{-1}$.

8.7 Mycobacterium Smegmatis Culture in the Microchemostat

Prior to the use of the *E.coli* expression system, we experimented with the use of the microchemostat to continuously culture *Mycobacterium smegmatis* as a model for future culture of *M. tuberculosis* using the microchemostat.

This organism is used as a laboratory model for the study of *M. tuberculosis*, and like tuberculosis, readily forms biofilms. As described previously, biofilm formation can interfere with microchemostat operation if uncontrolled. Conventionally, a lyses buffer (BPER) is used to slow down biofilm growth and prevent clogging of channels. This approach works well for organisms such as *E.coli* that grow in biofilms and as planktonic cells; however, *M. smegmatis* predominantly grows in biofilms, with its unique cell wall posing a major obstacle to lysis and subsequent removal from chamber walls. If left uncontrolled *M. Smegmatis* is able to form biofilms that can completely fill the reactor, thereby blocking channels (Figure 50A) and interfering with pump function (Figure 50B).

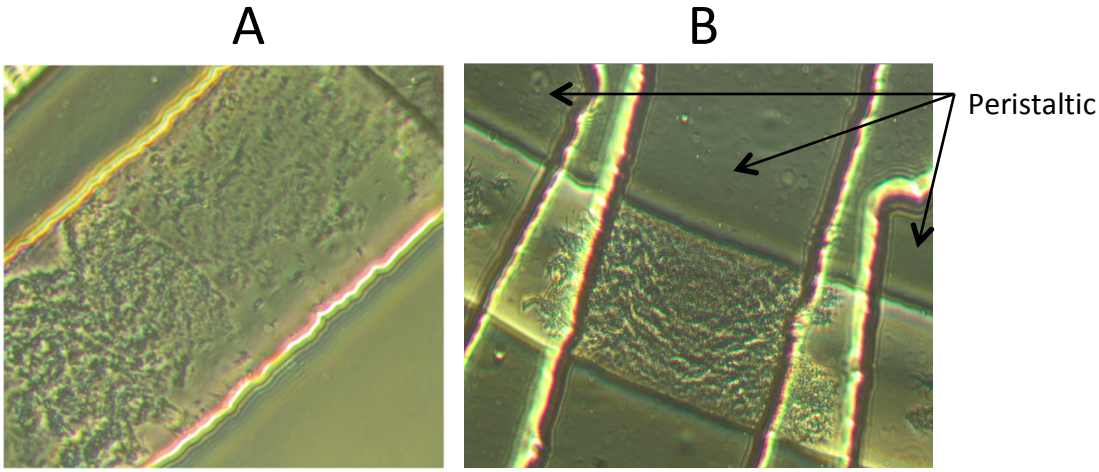

Figure 50| Optical micrographs showing *M. smegmatis* biofilms blocking the microchemostat growth chamber (A), and preventing peristaltic mixing (B).

Despite these challenges, we were able optimize the lysis time and slow down biofilm growth to allow for the continuous culture of *M. smegmatis* over ~10 days reaching a steady state cell density of ~0.1 pixels (Figure 51). This culture grew as a mixed population containing both small biofilms and planktonic cells (Figure 52). However, these biofilms were not allowed to grow to such an extent that they blocked channels or interfered with the functioning of the peristaltic pump.

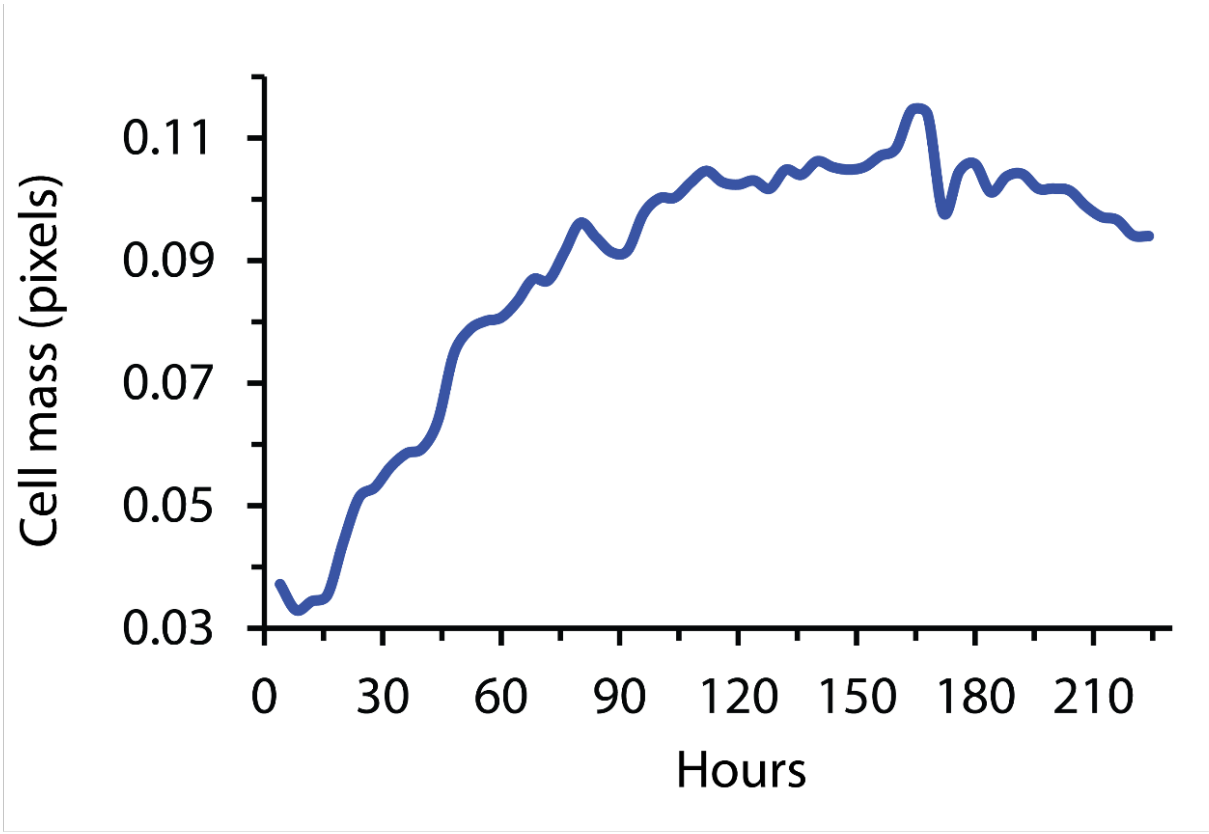

Figure 51| A microchemostat growth curve of M. smegmatis growing in a mixed population of biofilms and planktonic cells. The experiment was run for a period of ~10 days, reaching a steady state cell density of ~0.1pixels. Cells were grown at 37°C in 7H9 medium at a dilution rate of 0.036 $hour^{-1}$. This low dilution rate was necessary to account for the slow growth of *M. smegmatis*.

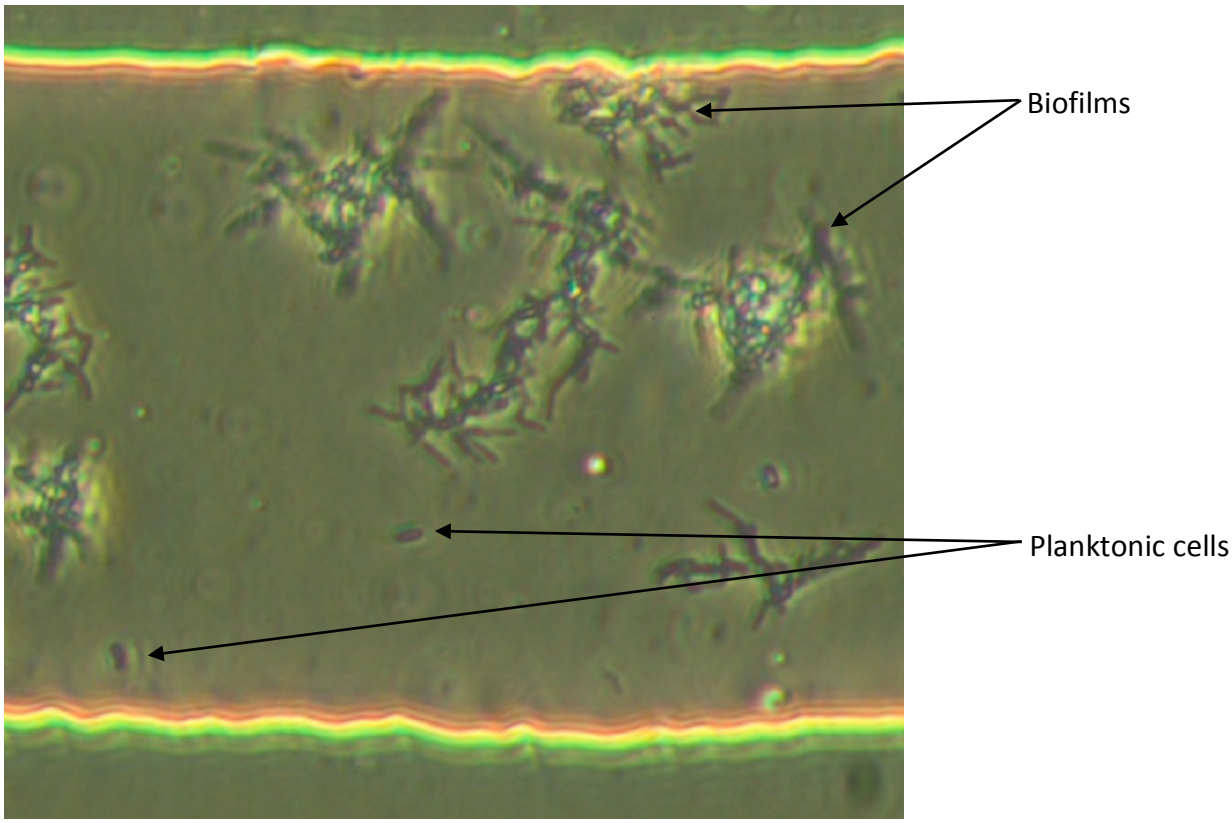

Figure 52| An optical micrograph of a mixed population of *M. smegmatis* cells containing both small biofilms and planktonic cells.

M. smegmatis cell density was determined by enumerating the number of pixels occupied by the cells at different time points within the growth chamber. This process was performed using algorithms written in Matlab. Individual cells were not counted as described previously for the *E.coli* constructs due to the presence of smegmatis biofilms that can impede the ability to achieve an accurate cell count.

Despite successfully culturing *M. smegmatis* in the microchemostat system, the presence of difficult-to-remove biofilms presented too many confounding factors. For this reason, we utilized the *E. coli* constructs created by Dr. Alissa Myrick for the study of *M. tuberculosis* efflux pumps. We believe the study of mycobacteria by culture is more suited to the Microdialyser system described previously (chapter 3). Unlike the microchemostat, the microdialyser system does not rely on continuous mixing for its operation. As a result, biofilm growth does not pose a major obstacle to the functioning of the device. The microchemostat is more suited to the study of fast growing organisms such as *E.coli* that can be lysed in order to keep the growth chambers free of biofilms.

CHAPTER 9

9. Discussion

The tap-like efflux pump gene designated Rv1258, which encodes a multidrug efflux pump in *M. tuberculosis* was isolated and expressed from a plasmid in transporter-deficient *E. coli* under control of an arabinose-inducible promoter (Figure 27A). Efflux gene expression dynamics were measured by monitoring the *E. coli* cells using a microchemostat—a miniaturized 10 nl bioreactor that enables automated culturing of small populations (10^2–10^4) of bacteria for hundreds of hours. By continually substituting a fraction of a bacterial culture with sterile nutrients, the microchemostat creates a near-constant environment that is ideal for long-term controlled studies of microbes and microbial communities. The *E. coli* expression system and the microchemostat have allowed us to fully interrogate a mycobacterial efflux pump (Rv1258) previously shown to be involved in the development of drug resistance to *M. tuberculosis*[87,93,112,113].

9.1 Oscillations through Efflux Gene Expression

Using these systems, we have been able to observe oscillations in the cell density of efflux ON populations. Efflux inhibitors CCCP and PaβN were able to completely remove these oscillatory dynamics, suggesting that this behaviour is due to efflux activity (Figure 38A and B). These results were confirmed using a control plasmid in which the green fluorescent protein (GFP) gene was substituted for the Rv1258 efflux pump gene (Figure 27B). GFP cells induced with arabinose grew without oscillation in cell density, thereby confirming the efflux inhibitor results. Thus, the oscillations observed in the efflux ON cultures could neither be accounted for by arabinose induction nor the plasmid backbone but were attributable to Rv1258 gene expression. Experimentation with other efflux constructs did not yield oscillations, suggesting that these characteristics are unique to Rv1258.

9.2 Oscillations Due to an Extruded Natural Efflux Product

Our data suggest that these oscillations occur due to the extrusion of a yet unidentified natural efflux product, which suppresses its own production and causes cell-division arrest and filamentation at sufficiently high extracellular concentrations.

Although the natural efflux product has not been identified, a number of studies have shown that bacterial efflux pumps can extrude products that may act extracellularly to suppress growth. For example, *Bacillus subtilis* is able to extrude spermidine, a polyamine that has been shown to be vital for cell survival. Bile salts have also been shown to be extruded by *E.coli* and are able to regulate growth through altering the extracullular pH[85,86].

During conventional cell culture experiments performed using tissue culture flasks, nutrients and growth factors were not replenished during the period of incubation. As a result, constitutive Rv1258 expression and subsequent extrusion of the natural efflux product led to suppressed growth and a filamentous phenotype, conditions that persisted indefinitely (Figure 37).

In the microchemostat where the cell culture was periodically substituted with fresh sterile medium, constitutive expression of the Rv1258 efflux gene and extrusion of the natural efflux product engendered alternating phases of two distinct phenotypes, which we refer to here as active and dormant efflux (Figure 42). These alternating phases appeared as oscillations in the growth curve and were only observable through the use of the microchemostat, illustrating the potential benefits this device offers for the study of cell biology.

The active efflux phenotype was characterized by normal-sized, actively dividing cells that were actively extruding a natural efflux product (Figure 36A). A decrease in the intracellular concentration of antibiotics extruded by the pump during this phase impairs their accessibility to the drug target and can facilitate progressive acquisition of chromosomal mutations that confer higher levels of resistance to the respective antibiotics[79].

Once extruded from the cell, the natural efflux product can accumulate in the extracellular environment and at sufficiently high concentrations induce a dormant phenotype on the bacteria. The dormant efflux phase was characterized by suppressed efflux product extrusion and the formation of filamentous cells with arrested cell division (Figure 36B). These filamentous cells gradually revert back towards a more normal cell shape, cell division rate and efflux product extrusion rate, thereby ushering in the next cycle (Figure 36A). Although drug molecule extrusion by the efflux pump may be suppressed during this phase, the filamentous shape represents a survival strategy known to protect bacteria from antibiotic medicines and allows bacteria to survive engulfment by phagocytic cells [206]. In addition, because most bactericidal antibiotics rely on bacteria to be actively dividing to achieve rapid killing, a dormant, filamentous phenotype engendered by efflux activity can in theory confer broader phenotypic resistance to drugs that the efflux pumps may not directly extrude. This dormant phenotype represents a novel method of resistance induced through efflux activation that, to the best of our knowledge, has not been described previously.

9.3 Efflux-Associated Drug Tolerance

Many drugs currently used for the treatment of drug susceptible and drug resistant TB target actively growing mycobacteria. For example, Isoniazid, one of the most effective and commonly used anti-TB drugs, has a high level of early bactericidal activity but only limited sterilizing activity[39]. As a result, there is limited activity against non-replicating bacteria[43]. Ethambutol, another first-line TB drug, has also been shown to be effective against actively growing bacilli through targeting cell wall biosynthesis[53]. In particular, it inhibits the synthesis of arabinogalactan[55]. This dormant phenotype engendered by Rv1258 efflux activation would therefore pose a significant challenge to the activity of these drugs that mainly target actively growing mycobacteria.

Two of the antibiotics tested in this study, streptomycin and gentamycin, are aminoglycosides that bind to the 30S subunit of the bacterial ribosome, thereby interrupting protein synthesis[222,223]. As a result, they both rely on active bacterial growth in order to remain effective. Active extrusion of these drugs, as well as the ability of the bacterial population to enter a dormant state may explain the significant bacterial tolerance observed in efflux ON populations in the presence of these drugs (Figure 47).

9.4 The Role of the Microchemostat

Although the microchemostat is not necessarily essential for the study of efflux pumps, its ability to allow for long-term growth of bacteria with single cell resolved measurements proved crucial to the characterization of Rv1258. This fully automated system enabled us to obtain cell density and morphology information every few minutes in real time, thereby allowing us to observe oscillatory dynamics induced through efflux activation that would not have been possible with conventional batch cultures (Figure 33). The scalability of microfluidic technologies provides the opportunity for high throughput screening of these transporters. In this particular study the microchemostat allowed us to conduct 14 independent experiments in parallel (Figure 25). However, this device can be scaled up to allow even 100 independent reactors on a single device.

9.5 Future Studies

Using the microchemostat, we have demonstrated that the RV1258 efflux pump has two distinct methods of resistance that may be clinically relevant. The active efflux phase is characterized by the extrusion of a natural efflux product that ushers in the dormant efflux phase. In order to better understand the mechanisms behind these two methods of resistance, it would be of interest to purify

the natural efflux product. This may yield useful information for the development of drugs in the future.

We have demonstrated, using Rv1258 as a test-case, that expression of *M. tuberculosis* efflux pumps in transporter-deficient *E. coli* cells combined with high resolution measurement of cellular properties using the microchemostat platform, can address the challenge of functional redundancy and enable researchers to more cleanly pinpoint compound substrates extrudable by the pump. In addition to this, we intend to use this approach to screen the performance of other discrete transporter proteins against a wider range of compounds and efflux pump inhibitors. This will be performed with the ultimate goal of reconstructing the functional interplay between the various transporters comprising the *M. tuberculosis* efflux system, their potential contribution to multidrug resistance and role in the basic biology of the species. Detailed knowledge of the molecular basis of *M. tuberculosis* efflux pumps is required for the development of new antibiotics that are not extruded or of inhibitors that block efflux pumps and allow traditional antibiotics to remain effective.

THESIS APPENDICES

Appendix A: Microfabrication Protocols for the Microchemostat

Mold Fabrication:

Push up Control Molds (Negative Photoresist)

Spin SU8 2015:	1500rpm x 1 min, Acceleration = 270rpm
	Film thickness = 25 microns
Pre-exposure Bake:	Contact bake on hotplate
	3 min x 65°C / 5 min x 95°C
Expose wafer:	2 - 5 seconds at 7 Mw/ cm^2 using a mask-aligner
Post-exposure Bake:	5 min x 65°C / 15 min x 95°C
Develop:	Develop using 100% Shipley SU8 Nanodeveloper for 1-2 minutes. Rinse with fresh developer and dry with house air.

Push Down Control Molds (Negative Photoresist)

Spin SU8 2015:	1500rpm x 1 min, Acceleration = 270rpm
	Film thickness = 24 microns
Pre-exposure Bake:	Contact bake on hotplate
	3 min x 65°C / 5 min x 95°C
Expose wafer:	2 – 5 seconds at 7 Mw/ cm^2 using a mask aligner
Post-exposure Bake:	5 min x 65°C / 15 min x 95°C
Develop:	Develop using 100% Shipley SU8 Nanodeveloper for 1-2 minutes. Rinse with fresh developer and dry with house air.

Flow Hybrid Mold

Step 1 (Negative Photoresist):

Spin SU8 2005:	4000 rpm x 1 min, Acceleration = 270rpm/sec
	Film thickness = ~3 - 4 microns
Pre-Exposure Bake:	Contact bake hotplate
	1 min x 65 C / 2min x 95 C
Expose wafer:	1 - 5 seconds at 7 Mw/ cm^2 using a mask aligner
Develop:	Develop using 100% Shipley SU8 Nanodeveloper for 1-2 minutes. Rinse with fresh developer and dry with house air.
Hard bake:	200°C for 1 -2 hours

Step 2 (Negative Photoresist). On the same mold,

Spin SU8 2010:	3000rpm x 1 min, Acceleration =130rpm/sec
	Film thickness = 10 microns
Pre-exposure Bake:	Contact bake hotplate
	1 min x 65°C / 2 min x 95°C
Expose wafer:	5 seconds at 7 Mw/ cm^2using a mask aligner
Post-exposure Bake:	1 min x 65°C / 3 min x 95°C
Develop:	Develop using 100% Shipley SU8 Nanodeveloper for 1-2 minutes. Rinse with fresh developer and dry with house air.
Hard bake:	200°C for 1 -2 hours

Step 3 (Positive Photoresist). On the same mold,

Priming:	HDMS vapor 2 min in plastic container
Spin ma-p1275 positive tone resist:	1200 rpm x 1 min, Acceleration = 133rpm/sec ramp up Film thickness = 10 microns
Soft bake:	Contact bake hotplate
	90 sec x 95°C
Expose wafer:	15 seconds at 7Mw / cm^2using a mask aligner
Develop:	Develop using 100% ma-D 531 developer. Rinse with deionized water and then dry under house dry air.
Reflow:	contact hotplate
	65°C x 3 min / 115°C x 15 min
Cooling:	Allow cooling to room temperature

Fabrication of the Microchemostat using Microfluidic Soft Lithography:

Priming:	All molds are primed by placing them in a plastic container (STP) with TMCS vapor for 3 min

Push Down Control Layer

Spin control layer	Combine 5:1 GE 615 TRV (35 g A: 7 g B)
	Mix in hybrid mixer (5 min mix / 5 min degas)
Molding:	Dispense 33 g onto push down control layer mold (placed in a 80mm petri dish lined with Aluminum foil)
Degas flow layer:	Performed by placing mold in a bell jar and creating a vacuum for ~15 minutes

Cure layer:	Binder® oven 80°C x 40 min

Push Up Control Layer

Spin control layer	Combine 20:1 GE 615 RTV (20 g A: 1 g B)
	Mix in hybrid mixer (5 min mix / 5 min degas)
Molding:	Dispense 5ml onto push up control layer mold
Spin:	1800 rpm x 60 sec, Acceleration = 500rpm/sec ramp
Cure layer:	Binder® oven 80°C x 40 min

Flow Layer

Spin flow layer	Combine 20:1 GE 615 RTV (20 g A: 1 g B)
	Mix in hybrid mixer (5 min mix / 5 min degas)
Molding:	Dispense 5ml onto flow layer mold
Spin:	2300 rpm x 60 sec, Acceleration = 500rpm/sec ramp
Cure layer:	Binder® oven 80°C x 40 min

Bonding

Push down peeling:	Push down layer is peeled from the mold
Cutting:	Next, cut the layer into shape using a blade
Hole punching:	All input and output ports are punched on the push down layer
Push down/Flow bonding:	Align push down control layer to flow layer using the Olympus SZX16 microscope.
	Bake in convection oven at 80°C x 40 min to bond layers

Cutting:	Cut around periphery of thick layer avoiding damage to the mold
Peel:	Peel bonded layers from the flow mold
	Punch all input and output ports
Bonding to push up layer:	Align bonded layer to the push up control layer using the Olympus SZX16 microscope.
	Bake in convection oven at 80°C x 40 min to bond layers
Cutting:	Once bonded, cut around periphery of thick layer avoiding damage to the mold
Peel:	Peel bonded layers from the flow mold
	Punch all input and output ports

Blank Layer

Spin blank layer:	Combine 30:1 GE 615 RTV (30 g A: 1 g B) Mix in hybrid mixer (5 min mix / 5 min degas)
Molding:	Dispense 5ml onto a clean glass substrate (slide or coverslip)
Spin:	1800 rpm x 60 sec, Acceleration = 500rpm/sec ramp
Cure layer:	Binder® oven 80°C x 40 min
Blank/combined layer bonding:	Place push up/flow/push down hybrid on blank layer. Inspect with the Olympus SZX16 microscope to ensure no air bubbles are present and no valves have collapsed.
Final bake:	Binder® oven 80°C x 8 hours

Appendix B: Matlab Data Processing Code

Matlab Algorithm for Detecting Cells in Phase Contrast Images

```
%%Authors: Jared_Mackenzie and Frederick_Balagaddé
%%K-Rith Bioengineering

%Select directory to process
format long;
Data_Start = 150;
data_pts = 'F:\Shots\DIL_800_23Jul2014_02_48PM\R2C5\DataSet150';
data_filename = 'F:\Shots\DIL_800_23Jul2014_02_48PM\R2C5\Data_150.xls';
data_filename_length = 'F:\Shots\DIL_800_23Jul2014_02_48PM\R2C5\Data_length_150.xls';
data_filename_area = 'F:\Shots\DIL_800_23Jul2014_02_48PM\R2C5\Data_area_150.xls';
Pictroot = 'Pict_F3_';
imageInfor2 = dir(data_pts );
imDate=imageInfor2.date;

%Create excel file for data
fid = fopen(data_filename, 'w');
fid2 = fopen(data_filename_length, 'w');
fid3 = fopen(data_filename_area, 'w');

for cint = 1:100
   cint2 = cint-1;
   stryng = num2str(cint2);
   fprintf(fid, stryng);
   fprintf(fid, ' \t');
end

for cint = 1:100
   cint2 = cint-1;
   stryng = num2str(cint2);
   fprintf(fid2, stryng);
   fprintf(fid2, ' \t');
end

for cint = 1:100
   cint2 = cint-1;
   stryng = num2str(cint2);
   fprintf(fid3, stryng);
   fprintf(fid3, ' \t');
end

fprintf(fid, '\n Count \t Time numeric \t Time (Hrs) \t Description \t Cells 1 \t Cells 2 \t Cells 3 \t Cells
4 \t Cells 5 \t Cells 6\t Cells 7 \t Cells 8 \t Cells Ave \t\t\t');
fprintf(fid2, '\n Count \t Length 1 \t Length 2 \t Length 3 \t Length 4 \t Length 5 \t Length 6\t Length 7
\t Length 8 \t Length \t\t\t');
fprintf(fid3, '\n Count \t Area 1 \t Area 2 \t Area 3 \t Area 4 \t Area 5 \t Area 6\t Area 7 \t Area 8 \t
Area \t\t\t');

for cint = 1:8
   stryng = strcat('Cells',num2str(cint));
   fprintf(fid, stryng);
   fprintf(fid, ' \t');
```

```
end

fprintf(fid, ' \t');
for cint = 1:8
   stryng = strcat('Length ',num2str(cint));
   fprintf(fid, stryng);
   fprintf(fid, ' \t');
end

fprintf(fid, ' \t');
fprintf(fid, 'Ave Length \t');

fprintf(fid, ' \t');
fprintf(fid, ' \t');
for cint = 1:8
   stryng = strcat('Area ',num2str(cint));
   fprintf(fid, stryng);
   fprintf(fid, ' \t');
end

fprintf(fid, ' \t');
fprintf(fid, 'Ave Area \t\t\t');

for cint = 1:8
   stryng = strcat('Sort Len  ',num2str(cint));
   fprintf(fid, stryng);
   fprintf(fid, ' \t');
end

fprintf(fid, ' \t');

fprintf(fid, 'SortLen Ave \t\t\t');


for cint = 1:8
   stryng = strcat('Sort Area  ',num2str(cint));
   fprintf(fid, stryng);
   fprintf(fid, ' \t');
end

fprintf(fid, ' \t');
fprintf(fid, 'SortArea Ave \t\t\n');
fprintf(fid2, ' \n');
fprintf(fid3, ' \n');



filename   =   strcat(data_pts,'\',Pictroot,'1.png');

%Select region of interest
I = imread(filename);
Active = I;
GreenPlane = I;
Image20 = imadjust(GreenPlane);
figure, imshow(Image20);
```

```
positionB0 = uint16(roipoly( Image20));

close all;


fprintf(fid, '%g \t', Data_Start+1);
fprintf(fid2, '%g \t', Data_Start+1);
fprintf(fid3, '%g \t', Data_Start+1);
%this_time = (new_time(k) - (min(time_dirs)))*1000000;

fprintf(fid, ' \t \t \t');
Sum_H = 0;
SUM_temp = 0;
SUM_OB =0;

%%%%%%%%%%%%%%%%%%%%%
for j = 2 : 9

     filename = strcat(data_pts,'\',Pictroot,num2str(j),'.png');
    I = imread(filename);
    %XX = rgb2gray(I);
    XX = I;
    %impix(j) = sum(sum(I2.*positionBG0));

    impix(j-1) =  sum(sum(XX.*uint16(positionB0)));
end

for j2 = 1:8
    im_div_min(j2) = round(2*impix(j2)/min(impix))/2;
end

impixmod = mode(im_div_min);
im_div_mod = impix/impixmod;
immultfact2 = im_div_min / impixmod;

for j = 2 : 9

    filename = strcat(data_pts,'\',Pictroot,num2str(j),'.png');
    I = imread(filename);
    %XX = rgb2gray(I);
    XX = I;
    A(:,:,j-1) =  imdivide(XX.*uint16(positionB0), immultfact2(j-1));

end

%%%%%%%%%%%%%%%%%%%%%


for jk = 1:4
    B(:,:,jk) = imlincomb(0.5,A(:,:,jk), 0.5, A(:,:,jk+4));
end

for jh = 1:2
    C(:,:,jh) = imlincomb(0.5,B(:,:,jh), 0.5, B(:,:,jh+2));
```

```
end

D = imlincomb(0.5,C(:,:,1), 0.5, C(:,:,2));
%adjust the image to allow for the detection of all cells
for ji = 1:8
   E = imsubtract(D, A(:,:,ji));

   %%%Changes
   F(:,:,ji) = immultiply(E,15); %15  %%%Changes
   H = filter2(fspecial('average', 6),F(:,:,ji))/65535; %6
   J = imadjust(H, [0.15 1], [0 1]);  %0.15 (0.1 on the 10_04_2014, 0.1 is too sensitive when few or no
cells present)
   K=graythresh(J);
   L(:,:,ji) = im2bw(J,K);
   [labelled,nn2(ji)] = bwlabel(L(:,:,ji),8); %8

   bw = bwareaopen(L(:,:,ji), 10);
   cc = bwconncomp(bw, 8);
   number_ob_per_pic(ji) = cc.NumObjects;

   fprintf(fid, '%g \t', cc.NumObjects);

   SUM_OB = SUM_OB + number_ob_per_pic(ji);
   SUM_temp = SUM_temp + mean2(L);

   %*%*%*%*%*%*%*%*%*%*%*%*%*%*%*%*%*%*%*%*%*%*%*%*%*%*%*%*%*%*%*%*%*%*%*%*%*%*%*%*%*%*%*%*%*%*%*%*%*%*
   numbobs = cc.NumObjects;
   STATS = regionprops(bw, 'MajorAxisLength');
   ave_length = 0;
   for obc=1:numbobs
      ave_length = ave_length + STATS(obc).MajorAxisLength;
      fprintf(fid2, '%g \t', STATS(obc).MajorAxisLength);
   end
   avelen(ji) = ave_length/numbobs;


   STATS2 = regionprops(bw, 'Area');
   ave_area = 0;
   for obc2=1:numbobs
      ave_area = ave_area + STATS2(obc2).Area;
      fprintf(fid3, '%g \t', STATS2(obc2).Area);
   end
   aveare(ji) = ave_area/numbobs;
   %Save processed images
   %*%*%*%*%*%*%*%*%*%*%*%*%*%*%*%*%*%*%*%*%*%*%*%*%*%*%*%*%*%*%*%*%*%*%*%*%*%*%*%*%*%*%*%*%*%*%*%*%*%*
   imwrite(A(:,:,ji), strcat(data_pts,'\or_Pict',num2str(ji),'.png'));
   imwrite(F(:,:,ji), strcat(data_pts,'\pre_processed_Pict',num2str(ji),'.png'));
imwrite(L(:,:,ji), strcat(data_pts,'\processed_Pict',num2str(ji),'.png'));
end
imwrite(A(:,:,8), strcat(data_pts,'\or_Pict',num2str(8),'.png'));
imwrite(F(:,:,8), strcat(data_pts,'\pre_processed_Pict',num2str(8),'.png'));
imwrite(bw, strcat(data_pts,'\processed_Pict',num2str(8),'.png'));

%Display processed images
figure, imshow(A(:,:,8));
```

```
figure, imshow(F(:,:,8));
figure, imshow(L(:,:,8));

%Average the number of cells
average_number_ob =  SUM_OB/8;
myAve = SUM_OB/8;
%Write to the excel file created previously
fprintf(fid, '%g \t', myAve);
fprintf(fid, '%g \t', 0); fprintf(fid, '%g \t', 0);

sort_obs = sort(number_ob_per_pic);

for myiny = 1:7
   fprintf(fid, '%g \t', sort_obs(myiny));
end

fprintf(fid, '%g \t', sort_obs(8));

%*%*%*%*%*%*%*%*%*%*%*%*%*%*%*%*%*%*%*%*%*%*%*%*%*%*%*%*%*%*%*%*%*%*%*%*%*%*%*%*
fprintf(fid, ' \t');

for tis2 = 1:8
   fprintf(fid, '%g \t', avelen(tis2));
end

fprintf(fid, ' \t');
fprintf(fid, '%g \t ', mean(avelen));
fprintf(fid, ' \t');

%%%%%%%%%%%%%%%%%%%%
fprintf(fid, ' \t');

for tis3 = 1:8
   fprintf(fid, '%g \t', aveare(tis3));
end

fprintf(fid, ' \t');
fprintf(fid, '%g \t ', mean(aveare));


%%%%%%%%%%%%%%%%
fprintf(fid, ' \t \t');
sort_lens = sort(avelen);

for myiny = 1:8
   fprintf(fid, '%g \t', sort_lens(myiny));
end

fprintf(fid, '\t');
fprintf(fid, '%g \t\t', mean(sort_lens(2:5)));


fprintf(fid, '\t');
sort_aveare = sort(aveare);
```

```
for myiny = 1:8
   fprintf(fid, '%g \t', sort_aveare(myiny));
end
fprintf(fid, '\t');
fprintf(fid, '%g \t\t', mean(sort_aveare(2:5)));


%%%%%%%%%%%%%%
fprintf(fid, ' \n');
fprintf(fid2, ' \n');
fprintf(fid3, ' \n');

%*%*%*%*%*%*%*%*%*%*%*%*%*%*%*%*%*%*%*%*%*%*%*%*%*%*%*%*%*%*%*%*%*%*%*%*%*%*
fclose(fid);
fclose(fid2);
fclose(fid3);
```

Matlab Algorithm for Detecting Fluorescent Cells

```
%%Authors: Jared_Mackenzie and Frederick_Balagaddé
%%K-Rith Bioengineering

%Select directory to process
format long;
Pictroot = 'Pict_F2_';
Data_Start = 30;
data_pts = 'F:\Shots\DIL_800_11Nov2015_03_19PM\R1C6\DataSet30';
data_filename = 'F:\Shots\DIL_800_11Nov2015_03_19PM\R1C6\DataSet20.xls';
data_filename_area = 'F:\Shots\DIL_800_11Nov2015_03_19PM\R1C6\Data_f_ area_20.xls';
data_filename_Brightness = 'F:\Shots\DIL_800_11Nov2015_03_19PM\R1C6\Data_f_bright_20.xls';
%Specify max and min brightness, as well as bin size
EdMax = 30000;
edMin = 5000;
BinSize = 5000;

imageInfor2 = dir(data_pts );
imDate=imageInfor2.date;

%Create excel file for data
fid = fopen(data_filename, 'w');
fid2 = fopen(data_filename_area, 'w');
fid3 = fopen(data_filename_Brightness, 'w');

for cint = 1:125
   cint2 = cint-1;
   stryng = num2str(cint2);
   fprintf(fid, stryng);
   fprintf(fid, ' \t');
end

for cint = 1:125
   cint2 = cint-1;
   stryng = num2str(cint2);
   fprintf(fid2, stryng);
   fprintf(fid2, ' \t');
end

for cint = 1:125
   cint2 = cint-1;
   stryng = num2str(cint2);
   fprintf(fid3, stryng);
   fprintf(fid3, ' \t');
end
fprintf(fid, '\n Count \t Time numeric \t Time (Hrs) \t Description \t Cells 1 \t Cells 2 \t Cells 3 \t Cells
4 \t \t Cells Ave \t\t\t');
fprintf(fid2, '\n Count \t area \t area \t area \t area 1 \t area 2 \t area 3 \t area 4 \t \t area Ave \t\t\t');
fprintf(fid3, '\n Count \t brightness \t brightness \t brightness \t brightness 1 \t brightness 2 \t
brightness 3 \t brightness 4 \t \t brightness \t\t\t');

for cint = 1:4
   stryng = strcat('SortCells',num2str(cint));
   fprintf(fid, stryng);
```

```
    fprintf(fid, ' \t');
end

fprintf(fid, ' \t');
for cint = 1:4
    stryng = strcat('Length ',num2str(cint));
    fprintf(fid, stryng);
    fprintf(fid, ' \t');
end

fprintf(fid, ' \t');
fprintf(fid, 'Ave Length \t');

fprintf(fid, ' \t');
fprintf(fid, ' \t');
for cint = 1:4
    stryng = strcat('Area ',num2str(cint));
    fprintf(fid, stryng);
    fprintf(fid, ' \t');
end

fprintf(fid, ' \t');
fprintf(fid, 'Ave Area \t\t\t');

for cint = 1:4
    stryng = strcat('Sort Len  ',num2str(cint));
    fprintf(fid, stryng);
    fprintf(fid, ' \t');
end

fprintf(fid, ' \t');

fprintf(fid, 'SortLen Ave \t\t\t');

for cint = 1:4
    stryng = strcat('Sort Area  ',num2str(cint));
    fprintf(fid, stryng);
    fprintf(fid, ' \t');
end

fprintf(fid, ' \t');
fprintf(fid, 'SortArea Ave \t\t');

fprintf(fid, ' \t');
fprintf(fid, 'MaxBrightBin \t');
fprintf(fid, 'MaxBBCt \t\t');

nBins = (EdMax - edMin)/BinSize;

for nb = 1:nBins
    fprintf(fid, strcat('b',num2str(nb),'cells \t'));
end
fprintf(fid, ' \t \t');
for nb = 1:nBins
    fprintf(fid, strcat('Bin',num2str(nb),'rnge \t'));
```

```
end
fprintf(fid, '\t\t');
fprintf(fid, '# fluorescent cells');
fprintf(fid, '\t\t');
fprintf(fid, 'Fn');
fprintf(fid, '\t');
fprintf(fid, 'mean_Fn');
fprintf(fid, '\t');
fprintf(fid, 'sum_original_brightness');
fprintf(fid, '\t');
fprintf(fid, 'sum_size_normalized_brightness');
fprintf(fid, '\t');
fprintf(fid, 'mean_size');
fprintf(fid, '\t');
fprintf(fid, 'mean_original_brightness');
fprintf(fid, '\t');
fprintf(fid, 'mean_size_normalized_brightness');
fprintf(fid, ' \t\t');


for cint = 1:4
    stryng = strcat('Inter-Brghtness ',num2str(cint));
    fprintf(fid, stryng);
    fprintf(fid, ' \t');
end

fprintf(fid, ' \n');
fprintf(fid2, ' \n');
fprintf(fid3, ' \n');


%%%%%%%%%%%%%%%%%%%%%%%%%%%%
%Select region of interest
%original code to replace when inserting into labview
 filename    =   strcat(data_pts,'\',Pictroot,'1.lvm');
I = dlmread(filename, '\t');
I2 = uint16(I);
I3 = immultiply(I2, 25);
 Image20 = imadjust(I3);
figure, imshow(Image20);
positionB0 = uint16(roipoly( Image20));

close all;
fprintf(fid, '%g \t', Data_Start+1);
fprintf(fid, ' \t \t \t');
fprintf(fid2, '%g \t', Data_Start+1);
fprintf(fid3, '%g \t', Data_Start+1);

Sum_H = 0;
SUM_temp = 0;
SUM_OB =0;

for j = 1 : 4
    filename = strcat(data_pts,'\',Pictroot,num2str(j),'.lvm');
    I = dlmread(filename);
```

```
    I2 = uint16(I);
    I3 = immultiply(I2, 25); %25
    A(:,:,j) =  I3.*uint16(positionB0);
end
for jk = 1:2
    B(:,:,jk) = imlincomb(0.5,A(:,:,jk), 0.5, A(:,:,jk+2));
end
D = imlincomb(0.5,B(:,:,1), 0.5, B(:,:,2));
obinum = 0;
areaBrightAve_bright(1,3) = 0;

%adjust the image to allow for the detection of all fluorescent cells
for ji = 1:4
    E = imsubtract(A(:,:,ji), D);
    %%%Changes
    F(:,:,ji) = immultiply(E,15); %15  %%%Changes
    ft2 = imadjust(F(:,:,ji));
    H = filter2(fspecial('average', 4),ft2)/65535; %4
    J = imadjust(H, [0.4 1], [0 1]);  %0.5 (0.1 on the 10_04_2014, 0.1 is too sensitive when few or no
cells present)
    K=graythresh(J);
    L(:,:,ji) = im2bw(J,K);
    [labelled,nn2(ji)] = bwlabel(L(:,:,ji),8); %8
    bw = bwareaopen(L(:,:,ji), 10); %10
    cc = bwconncomp(bw, 8);

    imwrite(A(:,:,ji), strcat(data_pts,'\or_Pict',num2str(ji),'.png'));
    imwrite(F(:,:,ji), strcat(data_pts,'\pre_processed_Pict',num2str(ji),'.png'));
    %imwrite(grain3, strcat(data_pts,'\fin_Pict',num2str(ji),'.png'));
    imwrite(bw, strcat(data_pts,'\processed_Pict',num2str(ji),'.png'));


    number_ob_per_pic(ji) = cc.NumObjects; %number of cells
    fprintf(fid, '%g \t', cc.NumObjects);
    SUM_OB = SUM_OB + number_ob_per_pic(ji);
    SUM_temp = SUM_temp + mean2(L);
    %*%*%*%*%*%*%*%*%*%*%*%*%*%*%*%*%*%*%*%*%*%*%*%*%*%*%*%*%*%*%*%*%*%*%*%*%*%*%*%*%*%*%*%*
    numbobs = cc.NumObjects;
    STATS = regionprops(bw, 'MajorAxisLength');
    ave_length = 0;
    for obc=1:numbobs
        ave_length = ave_length + STATS(obc).MajorAxisLength;
    end
    avelen(ji) = ave_length/numbobs;
    STATS2 = regionprops(bw, 'Area');
    ave_area = 0;
    for obc2=1:numbobs
        ave_area = ave_area + STATS2(obc2).Area;
    end
    aveare(ji) = ave_area/numbobs;
    %*%*%*%*%*%*%*%*%*%*%*%*%*%*%*%*%*%*%*%*%*%*%*%*%*%*%*%*%*%*%*%*%*%*%*%*%*%*%*%*%*%*%*%*
    %Determines the number of fluorescent cells
    for obnum = 1:numbobs
        obinum = obinum+1;
        grain = false(size(bw));
```

```
        grain(cc.PixelIdxList{obnum}) = true;

        grain2 = uint16(grain);
        grain3 = A(:,:,ji).*grain2;
        %determines the brightness of each individual cell
        areaBrightAve_bright(obinum,1) = sum(sum(grain)); %number of pixels
        areaBrightAve_bright(obinum,2) = sum(sum(grain3)); %original brightness
        areaBrightAve_bright(obinum,3) = sum(sum(grain3))/sum(sum(grain)); %average brightness =
original brightness / number of pixels

        fprintf(fid2, '%g \t', areaBrightAve_bright(obinum,1));
        fprintf(fid3, '%g \t', areaBrightAve_bright(obinum,2));

        Fn = ((obinum*9)/8);


%
%               fprintf(fid, num2str(obinum)); fprintf(fid, '\t');
%               fprintf(fid, '%g \t', areaBrightAve_bright(obinum,1));
%               fprintf(fid, '%g \t', areaBrightAve_bright(obinum,2));
%               fprintf(fid, '%g \n', areaBrightAve_bright(obinum,3));
    end
end
grain = false(size(bw));
grain2 = uint16(grain);
grain3 = A(:,:,ji).*grain2;
%Determines the average number of fluorescent cells
Fn = ((obinum*9)/8);
mean_Fn = mean(Fn(:,1));
sum_original_brightness = sum(areaBrightAve_bright(:,2));
sum_size_normalized_brightness = sum(areaBrightAve_bright(:,3));

mean_size = mean(areaBrightAve_bright(:,1));
mean_original_brightness = mean(areaBrightAve_bright(:,2));
mean_size_normalized_brightness = mean(areaBrightAve_bright(:,3));
  %Display processed images
figure, imshow(A(:,:,4)); % L(:,:,ji); bw;  A(:,:,1);
figure, imshow(F(:,:,4));
figure, imshow(L(:,:,4));
figure, imshow(bw);
figure, imshow(bw);

imwrite(A(:,:,4), strcat(data_pts,'\or_Pict',num2str(4),'.png'));
imwrite(F(:,:,4), strcat(data_pts,'\pre_processed_Pict',num2str(4),'.png'));
imwrite(grain3, strcat(data_pts,'\fin_Pict',num2str(4),'.png'));
imwrite(bw, strcat(data_pts,'\processed_Pict',num2str(4),'.png'));
%Write to created excel file
myAve = SUM_OB/4;
fprintf(fid, '\t');
fprintf(fid, '%g \t', myAve);
fprintf(fid, '%g \t', 0); fprintf(fid, '%g \t', 0);
sort_obs = sort(number_ob_per_pic);
for myiny = 1:4
    fprintf(fid, '%g \t', sort_obs(myiny));
end
```

```
%*%*%*%*%*%*%*%*%*%*%*%*%*%*%*%*%*%*%*%*%*%*%*%*%*%*%*%*
fprintf(fid, ' \t');
for tis2 = 1:4
    fprintf(fid, '%g \t', avelen(tis2));
end

fprintf(fid, ' \t');
fprintf(fid, '%g \t ', mean(avelen));
fprintf(fid, ' \t');
%%%%%%%%%%%%%%%%%%%%%%%%%%
fprintf(fid, ' \t');

for tis3 = 1:4
    fprintf(fid, '%g \t', aveare(tis3));
end

fprintf(fid, ' \t');
fprintf(fid, '%g \t ', mean(aveare));
%%%%%%%%%%%%%%%%%%%
fprintf(fid, ' \t \t');
sort_lens = sort(avelen);

for myiny = 1:4
    fprintf(fid, '%g \t', sort_lens(myiny));
end
fprintf(fid, '\t');
fprintf(fid, '%g \t\t', mean(sort_lens(1:4)));
fprintf(fid, '\t');
sort_aveare = sort(aveare);
for myiny = 1:4
    fprintf(fid, '%g \t', sort_aveare(myiny));
end
fprintf(fid, '\t');
fprintf(fid, '%g \t\t', mean(sort_aveare(1:4)));
fprintf(fid, ' \t');
edges1 = [edMin:BinSize:EdMax];
h = hist(areaBrightAve_bright(:,3), edges1);
[MyMax,peakBin] = max(h);
hVals = h;
bar(h);
xlabel('Fluorescence'); % x-axis label
ylabel('#Cells/bin'); % y-axis label
saveas(gcf,strcat(data_pts,'\histogram.png')) ;

fprintf(fid, '%g \t', peakBin);
fprintf(fid, '%g \t\t', MyMax);
fprintf(fid, '%g \t', hVals);
fprintf(fid, ' \t\t');
fprintf(fid, '%g \t', edges1);
% fprintf(fid, '%g\t\t', obinum);
fprintf(fid, '%g \t\t',obinum);
fprintf(fid, '%g \t',Fn);
fprintf(fid, '%g \t',mean_Fn);
fprintf(fid, '%g \t',sum_original_brightness);
fprintf(fid, '%g \t',sum_size_normalized_brightness);
```

```
fprintf(fid, '%g \t',mean_size);
fprintf(fid, '%g \t',mean_original_brightness);
fprintf(fid, '%g \t',mean_size_normalized_brightness);

%%%%%%%%%%%%%%%

sumbright = 0;
fprintf(fid, ' \t');
for myiny = 1:4
    fprintf(fid, '%g \t', sum(sum(F(:,:,myiny))));

    sumbright = sumbright + sum(sum(F(:,:,myiny)));
end

 sumbright =  sumbright/4;

 fprintf(fid, '%g \t\t', sumbright);


fprintf(fid, ' \n');
fprintf(fid2, ' \n');
fprintf(fid3, ' \n');



% fprintf(fid, '\n\n');
% fprintf(fid, '\n');
% fprintf(fid, 'c count'); fprintf(fid, '\t\t');
% fprintf(fid, 'size'); fprintf(fid, '\t');
% fprintf(fid, 'original brightness'); fprintf(fid, '\t');
% fprintf(fid, 'size normalized brightness'); fprintf(fid, '\t');

% %
% for ccount = 1:obinum
%     fprintf(fid, '\n');
%     fprintf(fid, '%g \t\t', ccount);
%     fprintf(fid, '%g \t',areaBrightAve_bright(ccount,1));
%     fprintf(fid, '%g \t',areaBrightAve_bright(ccount,2));
%     fprintf(fid, '%g \t',areaBrightAve_bright(ccount,3));
%
% end

fclose(fid);
fclose(fid2);
fclose(fid3);
```

Appendix C: Raw Data of *E. coli* Cells Cultured in the Microchemostat

These results show the cell density on the primary axis (red curve with black dots) and average specific cell length on the secondary axis (orange curve with gray dots) as a function of time. Cells were grown at 37°C in LB medium under conditions indicated on the right of each graph.

Raw Data for Figures 32, 33 and 39

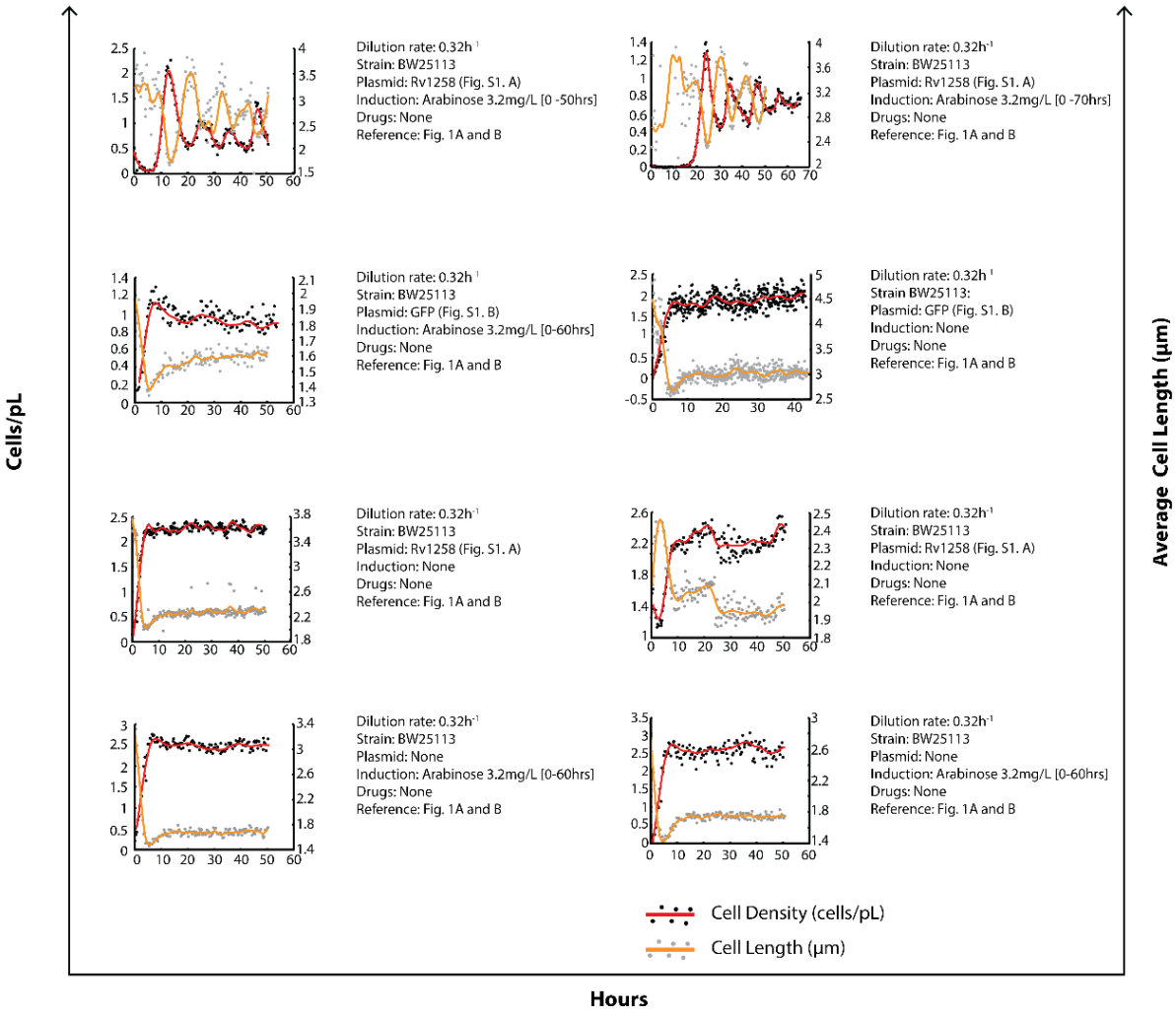

Raw Data for Figure 44

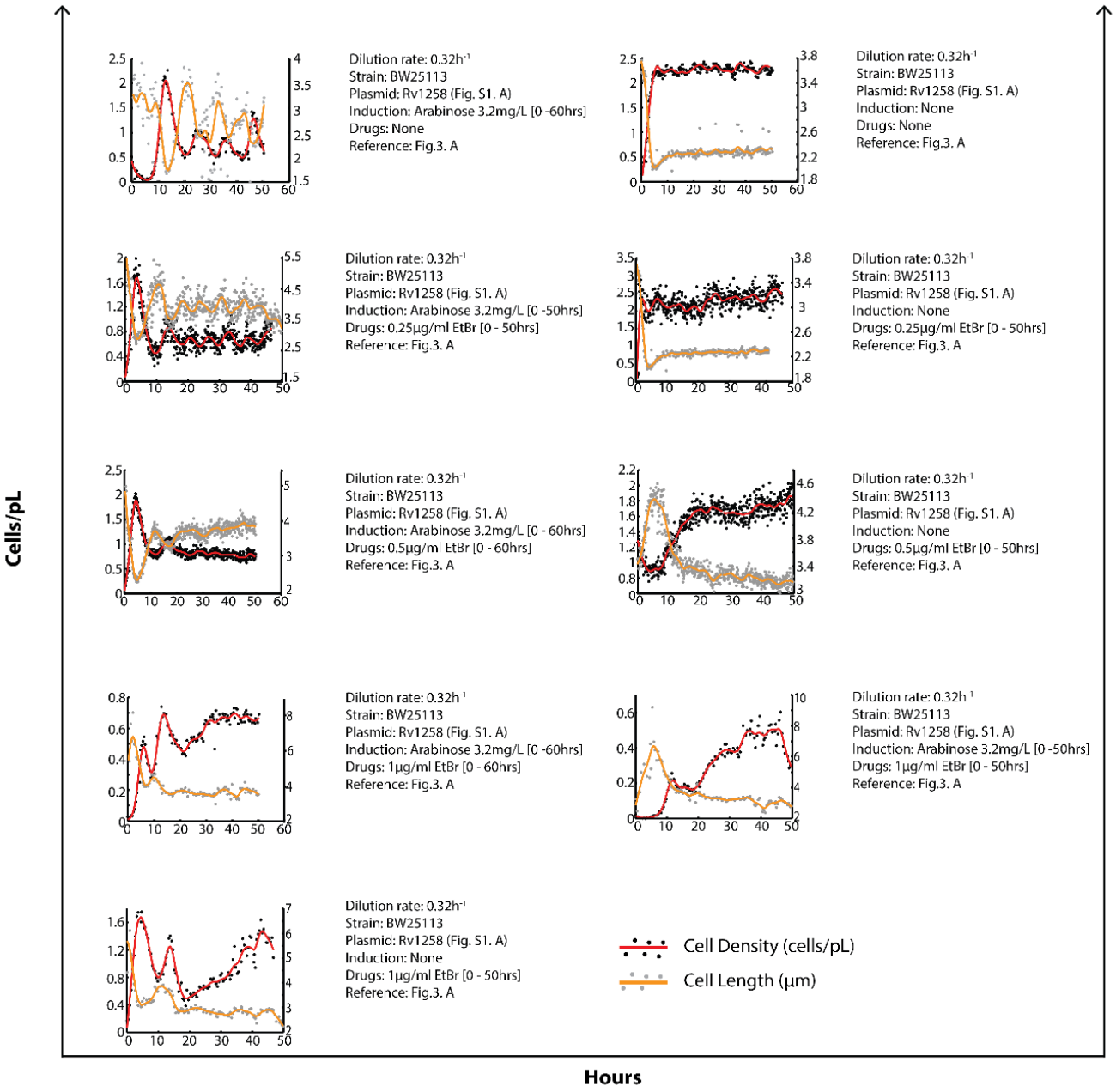

Raw Data for Figure 45

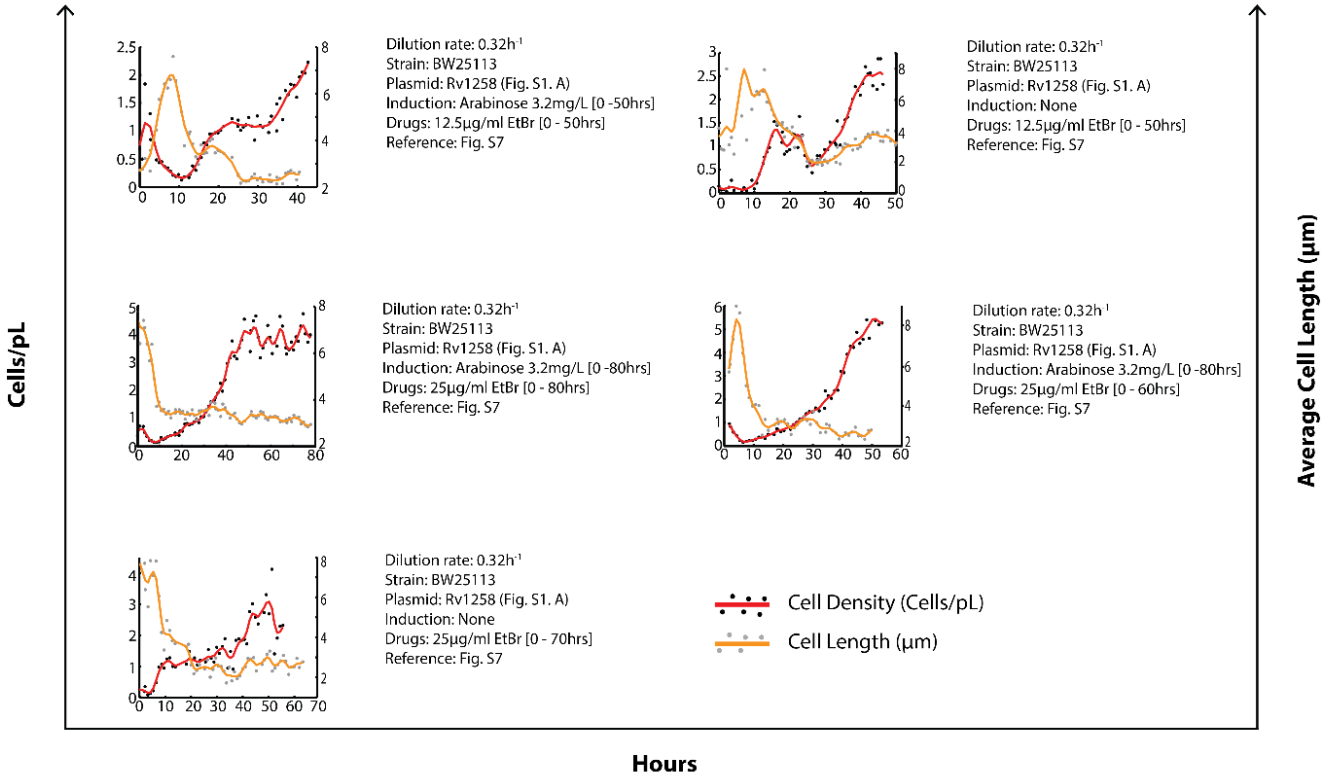

Raw Data for Figure 47

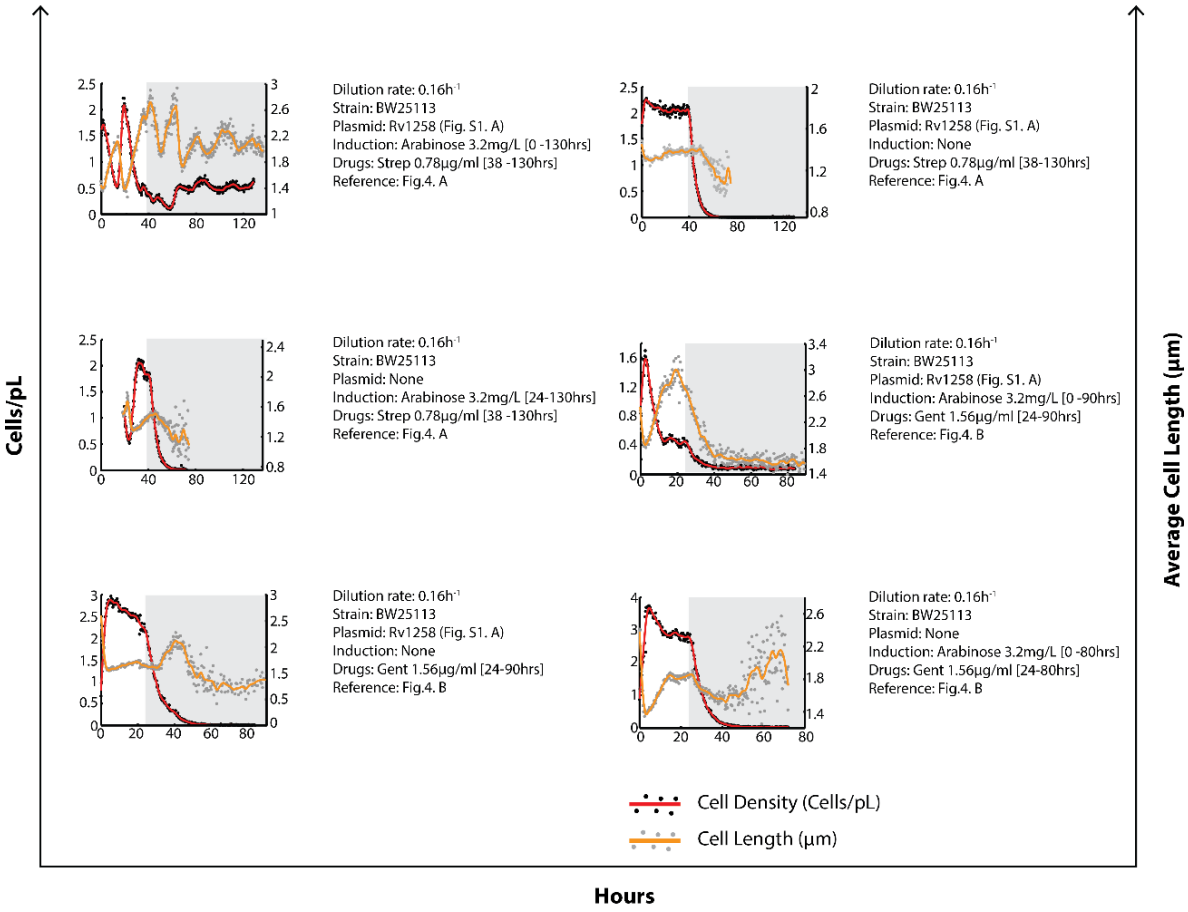

Appendix D: Transgenic Efflux Pump Model Parameter Values

Dilution rate ***D*:** The dilution rate D (hr^{-1}) was calculated analytically using the expression $D = -\ln[1 - F]/T$ where F is the fraction of microchemostat culture replaced with fresh medium during each dilution event and T is the time interval between consecutive dilution events: for example, D = 0.2 hr^{-1} for 25% discrete dilution (F = 1/4) every hour (T = 1 hour).

Maximum growth rate $\boldsymbol{\mu_{max}}$: The specific growth rate is determined from the exponential growth constant μ of the microchemostat cultures using the expression $\mu_{max} = \mu + D$.

Efflux pump-OFF parameters $\boldsymbol{c_n}$, $\boldsymbol{n_\infty}$: Efflux pump-OFF parameters including c_n and n_∞ were determined by adjusting trial initial values of these parameters until the simulated growth curves matched the pump-OFF growth curves obtained from actual microchemostat data.

Efflux pump-ON parameters $\boldsymbol{k}$, $\boldsymbol{c_p}$, $\boldsymbol{p_\infty}$: Efflux pump-ON parameters including k, c_n and n_∞, were determined by adjusting trial initial values of these parameters until the simulated growth curves matched the pump-ON growth curves obtained from actual microchemostat data.

Table 2| Numerical values of the key parameters in Equations 9-11

#	**Parameter**	**Description**	**Value**
1	D	Microchemostat dilution rate	$0.32\ hr^{-1}$
2	μ_{max}	Maximum specific growth rate of pump-OFF cultures	$1.03\ hr^{-1}$
3	c_n	Heaviside function parameter representing the sharpness of the transition in cell density from exponential to stationary phase.	$0.008\ cells^{-1}$
4	n_∞	Heaviside function parameter representing the maximum number of cells the microchemostat reactor can sustain indefinitely in the absence of culture dilution.	$2.81\ cells/pl$
5	k	Rate of extrusion of transgenic efflux products by each cell	$0.14\ \frac{[mass\ units]}{ml \cdot cell \cdot sec}$
6	c_p	Heaviside function parameter representing the sharpness of the transition in efflux product concentration from harmless to a toxic level.	$0.05\ \frac{ml}{[mass\ units]}$
7	p_∞	Heaviside function parameter representing the threshold concentration above which the efflux product becomes toxic.	$55\ \frac{[mass\ units]}{ml}$

REFERENCES

1 Morens, D. M., Folkers, G. K. & Fauci, A. S. Emerging infections: a perpetual challenge. *The Lancet Infectious Diseases* **8**, 710-719, doi:10.1016/s1473-3099(08)70256-1 (2008).

2 WHO. Global AIDS Update 2016. (World Health Organization, Geneva, Switzerland, 2016).

3 Bryant, C. D. *Handbook of Death and Dying*. (2003).

4 Weiss, R. A. How does HIV cause AIDS? *Science* **260**, 1273-1279, doi:10.1126/science.8493571 (1993).

5 Moore, R., D & Chaisson, R. E. Natural history of HIV infection in the_era of combination antiretroviral therapy. *AIDS* **13**, 1933-1942 (1999).

6 Toruner, M. *et al.* Risk Factors for Opportunistic Infections in Patients With Inflammatory Bowel Disease. *Gastroenterology* **134**, 929-936, doi:10.1053/j.gastro.2008.01.012 (2008).

7 Fattorini, L., Piccaro, G., Mustazzolu, A. & Giannoni, F. Targeting Dormant Bacilli to Fight Tuberculosis. *Mediterranean Journal of Hematology and Infectious Diseases* **5**, e2013072, doi:10.4084/MJHID.2013.072 (2013).

8 Torrey, H. L., Keren, I., Via, L. E., Lee, J. S. & Lewis, K. High Persister Mutants in Mycobacterium tuberculosis. *PloS one* **11**, e0155127, doi:10.1371/journal.pone.0155127 (2016).

9 Granich, R. *et al.* Prevention of Tuberculosis in People Living with HIV. *Clinical Infectious Diseases* **50** (2010).

10 Martinson, N. A., Hoffmann, C. J. & Chaisson, R. E. Epidemiology of Tuberculosis and HIV: Recent Advances in Understanding and Responses. *Proceedings of the American Thoracic Society* **8**, 288-293, doi:10.1513/pats.201010-064WR (2011).

11 Havlir, D. V., Haileyesus, G., Ian, S. & Nunn, P. Opportunities and Challenges for HIV Care in Overlapping HIV and TB Epidemics. *Journal of the American Medical Association* **300**, 423-430 (2008).

12 WHO. (tbalert, 2016).

13 Daniel, T. M. The history of tuberculosis. *Respiratory Medicine* **100**, 1862-1870, doi:10.1016/j.rmed.2006.08.006 (2006).

14 Hayman, J. Mycobacterium Ulcerans: An Infection From Jurassix Time? *The Lancet* **324**, 1015-1016, doi:10.1016/S0140-6736(1984)91110-3.

15 Gutierrez, M. C. *et al.* Ancient Origin and Gene Mosaicism of the Progenitor of Mycobacterium tuberculosis. *PLoS Pathogens* **1**, e5, doi:10.1371/journal.ppat.0010005 (2005).

16 Bates, J. H. & Stead, W. W. The history of tuberculosis as a global epidemic. *Medical Clinics of North America* **77**, 1205-1217 (1993).

17 Cole, S. T. *et al.* Deciphering the biology of Mycobacterium tuberculosis from the complete genome sequence. *Nature* **393**, 537-534 (1998).

18 Organization, W. H. Global Tuberculosis Report. *Geneva, Switzerland: World Health Organization* (2014).

19 Kasprowicz, V. O., Achkar, J. M. & Wilson, D. The Tuberculosis and HIV Epidemic in South Africa and the KwaZulu-Natal Research Institute for Tuberculosis and HIV. *Journal of Infectious Diseases* **204**, S1099-S1101, doi:10.1093/infdis/jir414 (2011).

20 Zumla, A., George, A., Sharma, V., Herbert, N. & Baroness Masham of, I. WHO's 2013 global report on tuberculosis: successes, threats, and opportunities. *The Lancet* **382**, 1765-1767, doi:10.1016/S0140-6736(2013)62078-4.

21 National Tuberculosis management guidlines. *Department of Health South Africa.* 1-117 (2009).

22 Abdool Karim, S. S., Churchyard, G. J., Abdool Karim, Q. & Lawn, S. D. HIV infection and tuberculosis in South Africa: an urgent need to escalate the public health response. *Lancet* **374**, 921-933, doi:10.1016/S0140-6736(09)60916-8 (2009).

23 Churchyard GJ *et al.* Tuberculosis control in South Africa: successes, challenges and recommendations. *South African Medical Journal* **104**, 244-248 (2014).

24 CDC. The Difference between Latent TB Infection and Active TB disease. 1-2 (2008).

25 Lin, P. L. & Flynn, J. L. Understanding Latent tuberculosis: A moving target. *Journal of Immunology* **185**, 15-22, doi:10.4049/jimmunol.0903856 (2010).

26 Nachega, J. B. & Chaisson, R. E. Tuberculosis Drug Resistance: A Global Threat. *Clinical Infectious Diseases* **36**, 24-30 (2003).

27 Wells, W. A. Curing TB with sunlight. *The Journal of Cell Biology* **172**, 958-958, doi:10.1083/jcb.1727rr2 (2006).

28 Madansein, R. *et al.* Surgical Treatment of Complications of Pulmonary Tuberculosis, including Drug-Resistant Tuberculosis. *International Journal of Infectious Diseases* **32**, 61-67, doi:10.1016/j.ijid.2015.01.019 (2015).

29 Brownrigg, G. M. Thoracoplasty for Tuberculosis. *Canadian Medical Association Journal* **61**, 601-602 (1949).

30 Jassal, M. & Bishai, W. R. Extensively drug-resistant tuberculosis. *Lancet* **9**, 19-30 (2009).

31 Davies, P. D. The role of DOTS in tuberculosis treatment and control. *American Journal of Respiritory Medicine* **2**, 203-209 (2003).

32 Perron, G. G., Kryazhimskiy, S., Rice, D. P. & Buckling, A. Multidrug Therapy and Evolution of Antibiotic Resistance: When Order Matters. *Applied and Environmental Microbiology* **78**, 6137-6142 (2012).

33 Chait, R., Craney, A. & Kishony, R. Antibiotic interactions that select against resistance. *Nature* **446**, 668-671, doi:http://www.nature.com/nature/journal/v446/n7136/suppinfo/nature05685_S1.html (2007).

34 Kim, S., Lieberman, T. D. & Kishony, R. Alternating antibiotic treatments constrain evolutionary paths to multidrug resistance. *Proceedings of the National Academy of Sciences* **111**, 14494-14499, doi:10.1073/pnas.1409800111 (2014).

35 CDC. TB Elimination: Treatment of Drug susceptible TB disease in Persons Not Infected with HIV. (2012).

36 Mahajan, R. Bedaquiline: First FDA-approved tuberculosis drug in 40 years. *International Journal of Applied & Basic Medical Research* **3**, 1-2, doi:doi:10.4103/2229-516x.112228 (2013).

37 Deoghare, S. Bedaquiline: A new drug approved for treatment of multidrug-resistant tuberculosis. *Indian Journal of Pharmacology* **45**, 536-537, doi:10.4103/0253-7613.117765 (2013).

38 Chhabra, N., Aseri, M. L., Dixit, R. & Gaur, S. Pharmacotherapy for multidrug resistant tuberculosis. *Journal of Pharmacology & Pharmacotherapeutics* **3**, 98-104, doi:10.4103/0976-500X.95502 (2012).

39 Herbert, D. *et al.* Bactericidal action of ofloxacin, sulbactam-ampicillin, rifampin, and isoniazid on logarithmic-and stationary-phase cultures of Mycobacterium tuberculosis. *Antimicrobial Agents and Chemotherapy* **40**, 2296-2299 (1996).

40 Ojha, A. K. *et al.* Growth of Mycobacterium tuberculosis biofilms containing free mycolic acids and harbouring drug-tolerant bacteria. *Molecular Microbiology* **69**, 164-174, doi:10.1111/j.1365-2958.2008.06274.x (2008).

41 Jindani, A., Doré, C. J. & Mitchison, D. A. Bactericidal and Sterilizing Activities of Antituberculosis Drugs during the First 14 Days. *American Journal of Respiratory and Critical Care Medicine* **167**, 1348-1354, doi:10.1164/rccm.200210-1125OC (2003).

42 Sirgel, F. A. *et al.* The Early Bactericidal Activities of Rifampin and Rifapentine in Pulmonary Tuberculosis. *American Journal of Respiratory and Critical Care Medicine* **172**, 128-135, doi:10.1164/rccm.200411-1557OC (2005).

43 Zhang, Y., Yew, W. W. & Barer, M. R. Targeting Persisters for Tuberculosis Control. *Antimicrobial agents and chemotherapy* **56**, 2223–2230 (2012).

44 Machado, D. *et al.* Contribution of efflux to the emergence of isoniazid and multidrug resistance in Mycobacterium tuberculosis. *PloS One* **7**, e34538, doi:10.1371/journal.pone.0034538 (2012).

45 Zhang, Y., Heym, B., Allen, B., Young, D. & Cole, S. The catalase-peroxidase gene and isoniazid resistance of Mycobacterium tuberculosis. *Nature* **358**, 591-593 (1992).

46 Huyen, M. N. T. *et al.* Epidemiology of Isoniazid Resistance Mutations and Their Effect on Tuberculosis Treatment Outcomes. *Antimicrobial Agents and Chemotherapy* **57**, 3620-3627 (2013).

47 van Ingen, J. *et al.* Why Do We Use 600 mg of Rifampicin in Tuberculosis Treatment? *Clinical Infectious Diseases : An Official Publication of the Infectious Diseases Society of America* **52**, e194-199, doi:10.1093/cid/cir184 (2011).

48 Ramswamy, S. & Musser, J. M. Molecular genetic Basis of Antimicrobial agent resistance in *Mycobacterium tuberculosis*: 1998 Update. *Tubercle and Lung Disease* **79**, 3–29 (1998).

49 Mitchison, D. A. Basic Mechanisms of Chemotherapy. *Chest* **76**, 771-780, doi:http://dx.doi.org/10.1378/chest.76.6.771 (1979).

50 Denkinger, C. M., Pai, M. & Dowdy, D. W. Do We Need to Detect Isoniazid Resistance in Addition to Rifampicin Resistance in Diagnostic Tests for Tuberculosis? *PloS one* **9**, e84197, doi:10.1371/journal.pone.0084197 (2014).

51 Shi, W. *et al.* Pyrazinamide inhibits trans-translation in Mycobacterium tuberculosis: a potential mechanism for shortening the duration of tuberculosis chemotherapy. *Science* **333**, 1630-1632, doi:10.1126/science.1208813 (2011).

52 Zhang, Y., Wade, M. M., Scorpio, A., Zhang , H. & Sun, Z. Mode of action of pyrazinamide: disruption of Mycobacterium tuberculosis membrane transport and energetics by pyrazinoic acid. *Journal of Antimicrobial Chemotherapy* **52**, 790-795 (2003).

53 Almeida Da Silva, P. E. & Palomino, J. C. Molecular basis and mechanisms of drug resistance in Mycobacterium tuberculosis: classical and new drugs. *The Journal of Antimicrobial Chemotherapy* **66**, 1417-1430, doi:10.1093/jac/dkr173 (2011).

54 Zhang, Y. & Mitchison, D. The curious characteristics of pyrazinamide: a review. *International Journal of Tuberculosis and Lung Disease* **7**, 6-21 (2003).

55 Takayama, K., Armstrong, E. L., Kunugi, K. A. & Kilburn, J. O. Inhibition by Ethambutol of Mycolic Acid Transfer into the Cell Wall of Mycobacterium smegmatis. *Antimicrobial Agents and Chemotherapy* **16**, 240-242 (1979).

56 Telenti, A. *et al.* The emb operon, a gene cluster of Mycobacterium tuberculosis involved in resistance to ethambutol. *Nature Medicine* **3**, 567-570 (1997).

57 NIAID. *First line TB drugs*, <http://www.tbonline.info/galleries/image/11/> (2016).

58 Pyle, M. M. Relative numbers of resistant tubercle bacilli in sputa of patients before and during treatment with streptomycin. *Proceedings of the Staff Meetings. Mayo Clinic* **22**, 465-473 (1947).

59 Briggs, M. A., Emerson, C., Modi, S., Taylor, N. K. & Date, A. Use of isoniazid preventive therapy for tuberculosis prophylaxis among people living with HIV/AIDS: a review of the literature. *Journal of Acquired Immune Deficiency Syndromes (1999)* **68 Suppl 3**, S297-305, doi:10.1097/qai.0000000000000497 (2015).

60 International Union Against Tuberculosis Committee on Prophylaxis. Efficacy of various durations of isoniazid preventive therapy for tuberculosis: five years of follow-up in the IUAT trial. International Union Against Tuberculosis Committee on Prophylaxis. *Bulletin of the World Health Organization* **60**, 555-564 (1982).

61 Cohn, D. L., Bustreo, F. & Raviglione, M. C. Drug-Resistant Tuberculosis: Review of the Worldwide Situation and the WHO/IUATLD Global Surveillance Project. *Clinical Infectious Diseases* **24**, 121-130 (1997).

62 WHO. World Health Organization Global Tuberculosis report 2015. (*World Health Organization*, Geneva, Switzerland, 2015).

63 Jiaquan, X. U., Murphy, S. L., Kochanek, K. D. & Bastian, B. A. Deaths: Final Data for 2013. *National Vital Statistics Reports. U.S. Department of Health and Human Services. Centers for Disease Control and Prevention* **64**, 1-12 (2016).

64 Fonseca, J. D., Knight, G. M. & McHugh, T. D. The complex evolution of antibiotic resistance in Mycobacterium tuberculosis. *International Journal of Infectious Diseases : IJID : Official Publication of the International Society for Infectious Diseases* **32**, 94-100, doi:10.1016/j.ijid.2015.01.014 (2015).

65 Organization, W. H. World Health Organisation Treatment of tuberculosis: guidelines- 4th ed. *WHO, Geneva* (2009).

66 Fonseca, J., Knight, G. & McHugh, T. The complex evolution of antibiotic resistance in Mycobacterium tuberculosis. *International Journal of Infectious Diseases* **32**, 94-100 (2015).

67 Gandhi, N. R. *et al.* Extensively drug-resistant tuberculosis as a cause of death in patients co-infected with tuberculosis and HIV in a rural area of South Africa. *The Lancet* **368**, 1575-1580, doi:10.1016/S0140-6736(06)69573-1 (2006).

68 Gandhi, N. R. *et al.* Extensively drug-resistant tuberculosis as a cause of death in patients co-infected with tuberculosis and HIV in a rural area of South Africa. *The Lancet* **368**, 1575-1580, doi:10.1016/s0140-6736(06)69573-1 (2006).

69 Hughes, J. & Osman, M. Diagnosis and management of Drug-Resistant Tuberculosis in South African Adults. Vol. 104 (2014).

70 Migliori, G. B., De Iaco, G., Besozzi, G., Centis, R. & Cirillo, D. M. First tuberculosis cases in Italy resistant to all tested drugs. *Eurosurveillance* **12**, 1 (2007).

71 Velayati, A. A., Farnia, P. & Masjedi, M. R. The totally drug resistant tuberculosis (TDR-TB). *International Journal of Clinical and Experimental Medicine* **6**, 307-309 (2013).

72 Almeida, D. *et al.* Mutations in pepQ Confer Low-Level Resistance to Bedaquiline and Clofazimine in Mycobacterium tuberculosis. *Antimicrobial Agents and Chemotherapy* **60**, 4590-4599 (2016).

73 Balganesh, M. *et al.* Efflux pumps of Mycobacterium tuberculosis play a significant role in antituberculosis activity of potential drug candidates. *Antimicrobial Agents and Chemotherapy* **56**, 2643-2651, doi:10.1128/AAC.06003-11 (2012).

74 McMurray, D. N. *Medical Microbiology. 4th edition.*, (1996).

75 Barrios, M. A. *et al.* Comparison of 3 agar media in Fung double tubes and Petri plates to detect and enumerate Clostridium spp. in broiler chicken intestines. *Poultry Science* **92**, 1498-1504, doi:10.3382/ps.2012-02677 (2013).

76 Law, S.-T. & Lee, M. K. A middle-aged lady with a pyogenic liver abscess caused by Clostridium perfringens. *World Journal of Hepatology* **4**, 252-255, doi:10.4254/wjh.v4.i8.252 (2012).

77 Harshey, R. M. & Ramakrishnan, T. Rate of Ribonucleic Acid Chain Growth in Mycobacterium tuberculosis H37Rv. *Journal of Bacteriology* **129**, 616-622 (1977).

78 Verma, A., Sampla, A. K. & Tyagi, J. S. Mycobacterium tuberculosis rrn Promoters: Differential Usage and Growth Rate-Dependent Control. *Journal of Bacteriology* **181**, 4326-4333 (1999).

79 Li, X. Z., Zhang, L. & Nikaido, H. Efflux pump-mediated intrinsic drug resistance in Mycobacterium smegmatis. *Antimicrobial Agents and Chemotherapy* **48**, 2415-2423, doi:doi:10.1128/aac.48.7.2415-2423.2004 (2004).

80 Brennan, P. J. Structure, function, and biogenesis of the cell wall of Mycobacterium tuberculosis. *Tuberculosis (Edinburgh, Scotland)* **83**, 91-97 (2003).

81 Alderwick, L. J., Birch, H. L., Mishra, A. K., Eggeling, L. & Besra, G. S. Structure, function and biosynthesis of the Mycobacterium tuberculosis cell wall: arabinogalactan and lipoarabinomannan assembly with a view to discovering new drug targets. *Biochemical Society Transactions* **35**, 1325-1328, doi:10.1042/bst0351325 (2007).

82 Park, S.-H. & Bendelac, A. CD1-restricted T-cell responses and microbial infection. *Nature* **406**, 788-792 (2000).

83 Webber, M. A. & Piddock, L. J. V. The importance of efflux pumps in bacterial antibiotic resistance. *Journal of Antimicrobial Chemotherapy* **51**, 9-11, doi:10.1093/jac/dkg050 (2003).

84 Piddock, L. J. Multidrug-resistance efflux pumps — not just for resistance. *Nature Reviews Microbiology* **4**, 629-636 (2006).

85 Woolridge, D. P. *et al.* Efflux of the natural polyamine spermidine facilitated by the Bacillus subtilis multidrug transporter Blt. *The Journal of biological chemistry* **272**, 8864-8866 (1997).

86 Rosenberg, E. Y., Bertenthal, D., Nilles, M. L., Bertrand, K. P. & Nikaido, H. Bile salts and fatty acids induce the expression of Escherichia coli AcrAB multidrug efflux pump through their interaction with Rob regulatory protein. *Molecular Microbiology* **48**, 1609-1619 (2003).

87 Ramon-Garcia, S., Martin, C., Ainsa, J. A. & De Rossi, E. Characterization of tetracycline resistance mediated by the efflux pump Tap from Mycobacterium fortuitum. *The Journal of Antimicrobial Chemotherapy* **57**, 252-259, doi:10.1093/jac/dki436 (2006).

88 Kourtesi, C. *et al.* Microbial Efflux Systems and Inhibitors: Approaches to Drug Discovery and the Challenge of Clinical Implementation. *Open Microbiology Journal* **7**, 34-52 (2013).

89 Szumowski, J. D., Adams, K. N., Edelstein, P. H. & Ramakrishnan, L. Antimicrobial efflux pumps and Mycobacterium tuberculosis drug tolerance: evolutionary considerations. *Current Topics in Microbiology and Immunology* **374**, 81-108, doi:10.1007/82_2012_300 (2013).

90 Ball, P. R., Shales, S. W. & Chopra, I. Plasmid-mediated tetracycline resistance in Escherichia coli involves increased efflux of the antibiotic. *Biochemical and Biophysical Research Communications* **93**, 74-81 (1980).

91 McMurry, L., Petrucci, R. E. & Levy, S. B. Active efflux of tetracycline encoded by four genetically different tetracycline resistance determinants in Escherichia coli. *Proceedings of the National Academy of Sciences of the United States of America* **77**, 3974-3977 (1980).

92 Kumar, A. & Schweizer, H. P. Bacterial resistance to antibiotics: active efflux and reduced uptake. *Advanced Drug Delivery Reviews* **57**, 1486-1513, doi:10.1016/j.addr.2005.04.004 (2005).

93 Da Silva, P. E., Von Groll, A., Martin, A. & Palomino, J. C. Efflux as a mechanism for drug resistance in Mycobacterium tuberculosis. *FEMS Immunology and Medical Microbiology* **63**, 1-9, doi:10.1111/j.1574-695X.2011.00831.x (2011).

94 Pao, S. S., Paulsen, I. T. & Saier, M. H. Major Facilitator Superfamily. *Microbiology and Molecular Biology Reviews* **62**, 1-34 (1998).

95 Borges-Walmsley, M. I., McKeegan, K. S. & Walmsley, A. R. Structure and function of efflux pumps that confer resistance to drugs. *Biochemical Journal* **376**, 313-338 (2003).

96 Dean, M., Hamon, Y. & Chimini, G. The human ATP-binding cassette (ABC) transporter superfamily. *Journal of Lipid Research* **42**, 1007-1017 (2001).

97 Sun, J., Deng, Z. & Yan, A. Bacterial multidrug efflux pumps: mechanisms, physiology and pharmacological exploitations. *Biochemical and Biophysical Research Communications* **453**, 254-267, doi:10.1016/j.bbrc.2014.05.090 (2014).

98 Magnet, S., Courvalin, P. & Lambert, T. Resistance-Nodulation-Cell Division-Type Efflux Pump Involved in Aminoglycoside Resistance in Acinetobacter baumannii Strain BM4454. *Antimicrobial Agents and Chemotherapy* **45**, 3375-3380, doi:10.1128/AAC.45.12.3375-3380.2001 (2001).

99 Tal, N. & Schuldiner, S. A coordinated network of transporters with overlapping specificities provides a robust survival strategy. *Proceedings of the National Academy of Sciences of the United States of America* **106**, 9051-9056, doi:10.1073/pnas.0902400106 (2009).

100 Bay, D. C., Rommens, K. L. & Turner, R. J. Small multidrug resistance proteins: a multidrug transporter family that continues to grow. *Biochimica et Biophysica Acta* **1778**, 1814-1838, doi:10.1016/j.bbamem.2007.08.015 (2008).

101 Kuroda, T. & Tsuchiya, T. Multidrug efflux transporters in the MATE family. *Biochimica et Biophysica Acta* **1794**, 763-768, doi:10.1016/j.bbapap.2008.11.012 (2009).

102 Youm, J. & Saier, M. H., Jr. Comparative analyses of transport proteins encoded within the genomes of Mycobacterium tuberculosis and Mycobacterium leprae. *Biochimica et Biophysica Acta* **1818**, 776-797, doi:10.1016/j.bbamem.2011.11.015 (2012).

103 Sarathy, J. P., Dartois, V. & Lee, E. J. The role of transport mechanisms in mycobacterium tuberculosis drug resistance and tolerance. *Pharmaceuticals* **5**, 1210-1235, doi:10.3390/ph5111210 (2012).

104 De Rossi, E., Ainsa, J. A. & Riccardi, G. Role of mycobacterial efflux transporters in drug resistance: an unresolved question. *FEMS Microbiology Reviews* **30**, doi:doi:10.1111/j.1574-6976.2005.00002.x (2006).

105 Lee, R. E. *et al.* Spectinamides: a new class of semisynthetic antituberculosis agents that overcome native drug efflux. *Nature Medicine* **20**, 152-158 (2014).

106 Louw, G. E. *et al.* Rifampicin reduces susceptibility to ofloxacin in rifampicin-resistant Mycobacterium tuberculosis through efflux. *American Journal of Respiratory and Critical Care Medicine* **184**, 269 - 276, doi:doi:10.1164/rccm.201011-1924OC (2011).

107 Domenech, P., Reed, M. B. & Barry, C. E., 3rd. Contribution of the Mycobacterium tuberculosis MmpL protein family to virulence and drug resistance. *Infection and Immunity* **73**, 3492-3501, doi:10.1128/IAI.73.6.3492-3501.2005 (2005).

108 Li, X., Barre, N. & Poole, K. Influence of the MexA-MexB-OprM multidrug efflux system on expression of the MexC-MexD-OprJ and MexE-MexF-OprN multidrug efflux systems in Pseudomonas aeruginosa. *Journal of Antimicrobial Chemotherapy* **46**, 885-893 (2000).

109 Liu, J., Takiff, H. E. & Nikaido, H. Active efflux of fluoroquinolones in Mycobacterium smegmatis mediated by LfrA, a multidrug efflux pump. *Journal of Bacteriology* **178**, 3791-3795 (1996).

110 Viveiros, M. *et al.* Isoniazid-induced transient high-level resistance in Mycobacterium tuberculosis. *Antimicrobial Agents and Chemotherapy* **46**, 2804-2810 (2002).

111 Hartkoorn, R. C., Uplekar, S. & Cole, S. T. Cross-resistance between clofazimine and bedaquiline through upregulation of MmpL5 in Mycobacterium tuberculosis. *Antimicrobial Agents and Chemotherapy* **58**, 2979-2981, doi:10.1128/aac.00037-14 (2014).

112 De Rossi, E. *et al.* Molecular cloning and functional analysis of a novel tetracycline resistance determinant, tet(V), from Mycobacterium smegmatis. *Antimicrobial Agents and Chemotherapy* **42**, 1931-1937 (1998).

113 Ainsa, J. A. *et al.* Molecular Cloning and Characterization of Tap, a Putative Multidrug Efflux Pump Present in Mycobacterium fortuitum and Mycobacterium tuberculosis. *Journal of Bacteriology* **180**, 5836–5843 (1998).

114 Burian, J. *et al.* The mycobacterial antibiotic resistance determinant WhiB7 acts as a transcriptional activator by binding the primary sigma factor SigA (RpoV). *Nucleic Acids Research* **41**, 10062-10076, doi:10.1093/nar/gkt751 (2013).

115 Geiman, D. E., Raghunand, T. R., Agarwal, N. & Bishai, W. R. Differential gene expression in response to exposure to antimycobacterial agents and other stress conditions among seven Mycobacterium tuberculosis whiB-like genes. *Antimicrobial Agents and Chemotherapy* **50**, 2836-2841, doi:10.1128/aac.00295-06 (2006).

116 Morris, R. P. *et al.* Ancestral antibiotic resistance in Mycobacterium tuberculosis. *Proceedings of the National Academy of Sciences of the United States of America* **102**, 12200-12205, doi:10.1073/pnas.0505446102 (2005).

117 Jiang, X. *et al.* Assessment of efflux pump gene expression in a clinical isolate Mycobacterium tuberculosis by real-time reverse transcription PCR. *Microbial Drug Resistance* **14**, 7-11, doi:10.1089/mdr.2008.0772 (2008).

118 Schnappinger, D. *et al.* Transcriptional Adaptation of Mycobacterium tuberculosis within Macrophages: Insights into the Phagosomal Environment. *The Journal of Experimental Medicine* **198**, 693-704, doi:10.1084/jem.20030846 (2003).

119 Adams, K. N. *et al.* Drug tolerance in replicating mycobacteria mediated by a macrophage-induced efflux mechanism. *Cell* **145**, 39-53, doi:10.1016/j.cell.2011.02.022 (2011).

120 Ramakrishnan, L., Federspiel, N. A. & Falkow, S. Granuloma-specific expression of Mycobacterium virulence proteins from the glycine-rich PE-PGRS family. *Science* **288**, 1436-1439 (2000).

121 Matthys, F., Van der Stuyft, P. & Van Deun, A. Universal tuberculosis control targets: not so smart. *International Journal of Tuberculosis Lung Disease* **13**, 923-924 (2009).

122 Ahmad, S., Mokaddas, E., Al-Mutairi, N., Eldeen, H. S. & Mohammadi, S. Discordance across Phenotypic and Molecular Methods for Drug Susceptibility Testing of Drug-Resistant <italic>Mycobacterium tuberculosis</italic> Isolates in a Low TB Incidence Country. *PloS one* **11**, e0153563, doi:10.1371/journal.pone.0153563 (2016).

123 Louie, M. & Cockerill, F. R., 3rd. Susceptibility testing. Phenotypic and genotypic tests for bacteria and mycobacteria. *Infectious Disease Clinics of North America* **15**, 1205-1226 (2001).

124 Gazi, M. A., Islam, M. R., Kibria, M. G. & Mahmud, Z. General and advanced diagnostic tools to detect Mycobacterium tuberculosis and their drug susceptibility: a review. *European journal of Clinical Microbiology & Infectious Diseases : Official Publication of the European Society of Clinical Microbiology* **34**, 851-861, doi:10.1007/s10096-014-2306-5 (2015).

125 Singhal, R. & Myneedu, V. P. Microscopy as a diagnostic tool in pulmonary tuberculosis. *International Journal of Mycobacteriology* **4**, 1-6, doi:10.1016/j.ijmyco.2014.12.006 (2015).

126 Prasad, C. S. B. R., Narasimha, A. & Harendra Kumar, M. Negative staining of mycobacteria - A clue to the diagnosis in cytological aspirates: Two case reports. *Annals of Tropical Medicine and Public Health* **4**, 110-112, doi:10.4103/1755-6783.85763 (2011).

127 Ryan, G. J. *et al.* Multiple *M. tuberculosis* Phenotypes in Mouse and Guinea Pig Lung Tissue Revealed by a Dual-Staining Approach. *PloS one* **5**, e11108, doi:10.1371/journal.pone.0011108 (2010).

128 Padmapriyadarsini, C., Narendran, G. & Swaminathan, S. Diagnosis & treatment of tuberculosis in HIV co-infected patients. *The Indian Journal of Medical Research* **134**, 850-865, doi:10.4103/0971-5916.92630 (2011).

129 Canetti, G. *et al.* Mycobacteria: laboratory methods for testing drug sensitivity and resistance. *Bulletin of the World Health Organization* **29**, 565-578 (1963).

130 Kim, S. J. Drug-susceptibility testing in tuberculosis: methods and reliability of results. *European Respiratory Journal* **25**, 564-569, doi:10.1183/09031936.05.00111304 (2005).

131 Central TB Division. Revised National TB Control Programme Training Manual for Mycobacterium tuberculosis Culture & Drug susceptibility testing. *Ministry of Health and Family Welfare, Nirman Bhawan*, 1-66 (2009).

132 Madkour, M. M. *Tuberculosis*. (Springer, 2004).

133 Tortoli, E. *et al.* Use of BACTEC MGIT 960 for Recovery of Mycobacteria from Clinical Specimens: Multicenter Study. *Journal of Clinical Microbiology* **37**, 3578-3582 (1999).

134 Tortoli, E., Benedetti, M., Fontanelli, A. & Simonetti, M. T. Evaluation of Automated BACTEC MGIT 960 System for Testing Susceptibility of Mycobacterium tuberculosis to Four Major Antituberculous Drugs: Comparison with the Radiometric BACTEC 460TB Method and the Agar Plate Method of Proportion. *Journal of Clinical Microbiology* **40**, 607-610, doi:10.1128/JCM.40.2.607-610.2002 (2002).

135 Williams-Bouyer, N., Yorke, R., Lee, H. I. & Woods, G. L. Comparison of the BACTEC MGIT 960 and ESP Culture System II for Growth and Detection of Mycobacteria. *Journal of Clinical Microbiology* **38**, 4167-4170 (2000).

136 Brown, A. C. *et al.* Rapid Whole-Genome Sequencing of Mycobacterium tuberculosis Isolates Directly from Clinical Samples. *Journal of Clinical Microbiology* **53**, 2230-2237, doi:10.1128/JCM.00486-15 (2015).

137 Chen, L., Zhang, D. T., Zhang, J., Su, Y. A. & Zhang, H. Whole-Genome Sequences of Two Clinical Isolates of Extensively Drug-Resistant Mycobacterium tuberculosis from Zunyi, China. *Genome Announcements* **2**, doi:10.1128/genomeA.00910-14 (2014).

138 Koser, C. U. *et al.* Whole-genome sequencing for rapid susceptibility testing of M. tuberculosis. *The New England Journal of Medicine* **369**, 290-292, doi:10.1056/NEJMc1215305 (2013).

139 Luetkemeyer, A. F. *et al.* Evaluation of two line probe assays for rapid detection of Mycobacterium tuberculosis, tuberculosis (TB) drug resistance, and non-TB Mycobacteria in HIV-infected individuals with suspected TB. *Journal of Clinical Microbiology* **52**, 1052-1059, doi:10.1128/jcm.02639-13 (2014).

140 Rufai, S. B. *et al.* Comparison of Xpert MTB/RIF with Line Probe Assay for Detection of Rifampin-Monoresistant Mycobacterium tuberculosis. *Journal of Clinical Microbiology* **52**, 1846-1852, doi:10.1128/JCM.03005-13 (2014).

141 Rossau, R. *et al.* Evaluation of the INNO-LiPA Rif. TB assay, a reverse hybridization assay for the simultaneous detection of Mycobacterium tuberculosis complex and its resistance to rifampin. *Antimicrobial Agents and Chemotherapy* **41**, 2093-2098 (1997).

142 Skenders, G. K., Holtz, T. H., Riekstina, V. & Leimane, V. Implementation of the INNO-LiPA Rif. TB(R) line-probe assay in rapid detection of multidrug-resistant tuberculosis in Latvia. *International Journal of Tuberculosis and Lung Disease* **15**, 1546-1552, i, doi:10.5588/ijtld.11.0067 (2011).

143 Cavusoglu, C., Turhan, A., Akinci, P. & Soyler, I. Evaluation of the Genotype MTBDR Assay for Rapid Detection of Rifampin and Isoniazid Resistance in Mycobacterium tuberculosis Isolates. *Journal of Clinical Microbiology* **44**, 2338-2342, doi:10.1128/JCM.00425-06 (2006).

144 Brossier, F., Veziris, N., Jarlier, V. & Sougakoff, W. Performance of MTBDR plus for detecting high/low levels of Mycobacterium tuberculosis resistance to isoniazid. *The International Journal of Tuberculosis and Lung Disease* **13**, 260-265 (2009).

145 Piatek, A. S. *et al.* GeneXpert for TB diagnosis: planned and purposeful implementation. *Global Health, Science and Practice* **1**, 18-23, doi:10.9745/ghsp-d-12-00004 (2013).

146 Nhu, N. T. Q. *et al.* Evaluation of GeneXpert MTB/RIF for Diagnosis of Tuberculous Meningitis. *Journal of Clinical Microbiology* **52**, 226-233, doi:10.1128/JCM.01834-13 (2014).

147 Zeka, A. N., Tasbakan, S. & Cavusoglu, C. Evaluation of the GeneXpert MTB/RIF assay for rapid diagnosis of tuberculosis and detection of rifampin resistance in pulmonary and extrapulmonary specimens. *Journal of Clinical Microbiology* **49**, 4138-4141, doi:10.1128/jcm.05434-11 (2011).

148 Kalokhe, A. S. *et al.* Multidrug-resistant tuberculosis drug susceptibility and molecular diagnostic testing: a review of the literature. *The American Journal of the Medical Sciences* **345**, 143-148, doi:10.1097/MAJ.0b013e31825d32c6 (2013).

149 Cepheid. *GeneXpert® IV*, <http://www.cepheid.com/us/cepheid-solutions/systems/genexpert-systems/genexpert-iv> (2016).

150 Luthuli, B. B., Purdy, G. E. & Balagaddé, F. K. Confinement-Induced Drug-Tolerance in Mycobacteria Mediated by an Efflux Mechanism. *PloS one* **10**, e0136231, doi:10.1371/journal.pone.0136231 (2015).

151 Whitesides, G. M. The origins and the future of microfluidics. *Nature* **442**, 368-373, doi:10.1038/nature05058 (2006).

152 Halldorsson, S., Lucumi, E., Gomez-Sjoberg, R. & Fleming, R. M. Advantages and challenges of microfluidic cell culture in polydimethylsiloxane devices. *Biosensors & Bioelectronics* **63**, 218-231, doi:10.1016/j.bios.2014.07.029 (2015).

153 Hansen, C. Microfluidics in structural biology: smaller, faster… better. *Current Opinion in Structural Biology* **13**, 538-544, doi:10.1016/j.sbi.2003.09.010 (2003).

154 Thorsen, T., Maerkl, S. J. & Quake, S. R. Microfluidic Large-Scale integration. *Science* **298**, 580-584 (2002).

155 Li, X., Ballerini, D. R. & Shen, W. A perspective on paper-based microfluidics: Current status and future trends. *Biomicrofluidics* **6**, 011301, doi:doi:http://dx.doi.org/10.1063/1.3687398 (2012).

156 Hansen, C. L., Skordalakes, E., Berger, J. M. & Quake, S. R. A robust and scalable microfluidic metering method that allows protein crystal growth by free interface diffusion. *Proceedings of the National Academy of Sciences of the United States of America* **99**, 16531-16536, doi:10.1073/pnas.262485199 (2002).

157 Mark, D., Haeberle, S., Roth, G., von Stetten, F. & Zengerle, R. Microfluidic lab-on-a-chip platforms: requirements, characteristics and applications. *Chemical Society Reviews* **39**, 1153-1182, doi:10.1039/b820557b (2010).

158 Macosko, Evan Z. *et al.* Highly Parallel Genome-wide Expression Profiling of Individual Cells Using Nanoliter Droplets. *Cell* **161**, 1202-1214, doi:10.1016/j.cell.2015.05.002 (2015).

159 Strohmeier, O. *et al.* Centrifugal microfluidic platforms: advanced unit operations and applications. *Chemical Society Reviews* **44**, 6187-6229, doi:10.1039/c4cs00371c (2015).

160 Baumann, B. QIAGEN Lake Constance: a "disk player" for rapid diagnoses. *QIAGEN Lake Constance GmbH*, 1-5 (2013).

161 Xia, Y., Si, J. & Li, Z. Fabrication techniques for microfluidic paper-based analytical devices and their applications for biological testing: A review. *Biosensors & Bioelectronics* **77**, 774-789, doi:10.1016/j.bios.2015.10.032 (2016).

162 Whitesides, G. *Microfluidic Device*, <http://wyss.harvard.edu/viewmedia/100/microfluidic-device;jsessionid=024A3D63FA759840267C33E21B72D6F4.wyss2> (2016).

163 Herold, K. E. & Rasooly, A. *Lab on a Chip Technology: Fabrication and Microfluidics*. (Caister Academic Press, 2009).

164 Iliescu, C., Taylor, H., Avram, M., Miao, J. & Franssila, S. A practical guide for the fabrication of microfluidic devices using glass and silicon. *Biomicrofluidics* **6**, 016505-016505-016516, doi:10.1063/1.3689939 (2012).

165 Unger, M. A., Chou, H. P., Thorsen, T., Scherer, A. & Quake, S. R. Monolithic microfabricated valves and pumps by multilayer soft lithography. *Science* **288**, 113-116 (2000).

166 Sugiura, S., Edahiro, J., Kikuchi, K., Sumaru, K. & Kanamori, T. Pressure-driven perfusion culture microchamber array for a parallel drug cytotoxicity assay. *Biotechnology and Bioengineering* **100**, 1156-1165, doi:10.1002/bit.21836 (2008).

167 Balagadde, F. K., You, L., Hansen, C. L., Arnold, F. H. & Quake, S. R. Long-term monitoring of bacteria undergoing programmed population control in a microchemostat. *Science* **309**, 137-140, doi:10.1126/science.1109173 (2005).

168 Novick, A. & Szilard, L. Description of the chemostat. *Science* **112**, 715-716 (1950).

169 Rotman, B. A Simplified Device for Continuous Growth of Microorganisms. *Journal of Bacteriology* **70**, 485-486 (1955).

170 Herbert, D., Elsworth, R. & Telling, R. C. The Continuous Culture of Bacteria; a Theoretical and Experimental Study. *Microbiology* **14**, 601-622, doi:doi:10.1099/00221287-14-3-601 (1956).

171 Monod, J. Technique, Theory and Applications of Continuous Culture. *Annales de I'Institut Pasteur* **79**, 390-410 (1950).

172 de Crecy, E. *et al.* Development of a novel continuous culture device for experimental evolution of bacterial populations. *Applied Microbiology and Biotechnology* **77**, 489-496, doi:10.1007/s00253-007-1168-5 (2007).

173 Chou, C. S. & Friedman, A. *Introduction to Mathematical Biology: Modeling, Analysis, and Simulation*. (2010).

174 Qu, M. & Bhattacharya, S. K. Toxicity and biodegradation of formaldehyde in anaerobic methanogenic culture. *Biotechnology and Bioengineering* **55**, 727-736, doi:10.1002/(SICI)1097-0290(19970905)55:5<727::AID-BIT3>3.0.CO;2-D

10.1002/(sici)1097-0290(19970905)55:5<727::aid-bit3>3.0.co;2-d (1997).

175 Brown, E. & Allen-Vercoe, E. Analysis of the fungal, archaeal and bacteriophage diversity in the human distal gut. *Studies by Undergraduate Researchers at Guelph* **4**, 75-82 (2011).

176 Slavkin, H. C. Biofilms, microbial ecology and Antoni van Leeuwenhoek. *Journal of the American Dental Association (1939)* **128**, 492-495 (1997).

177 Donlan, R. M. & Costerton, J. W. Biofilms: survival mechanisms of clinically relevant microorganisms. *Clinical Microbiology Reviews* **15**, 167-193 (2002).

178 Costerton, J. W., Lewandowski, Z., Caldwell, D. E., Korber, D. R. & Lappin-Scott, H. M. Microbial Biofilms. *Annual Reviews Microbiology* **49**, 711-745 (1995).

179 Hancock, R. E. W. A brief on bacterial biofilms. *Nature Genetics* **29**, 360-360 (2001).

180 Desai, M. M., Fisher, D. S. & Murray, A. W. The speed of evolution and maintenance of variation in asexual populations. *Current biology : CB* **17**, 385-394, doi:10.1016/j.cub.2007.01.072 (2007).

181 Jiang, X. *et al.* Impacts of mutation effects and population size on mutation rate in asexual populations: a simulation study. *BMC evolutionary biology* **10**, 298, doi:10.1186/1471-2148-10-298 (2010).

182 Andre, J. B. & Godelle, B. The evolution of mutation rate in finite asexual populations. *Genetics* **172**, 611-626, doi:10.1534/genetics.105.046680 (2006).

183 Zhang, Y. & Telenti, A. *Genetics of drug resistance in Mycobacterium tuberculosis*. (*Molecular genetics of mycobacteria*. ASM Press, Washington, DC, 2000).

184 Wade, M. M. & Zhang, Y. Mechanisms of drug resistance in Mycobacterium tuberculosis. *Frontiers in Bioscience : A Journal and Virtual Library* **9**, 975 - 994 (2004).

185 De Rossi, E. *et al.* The Multidrug Transporters Belonging to Major Facilitator Superfamily (MFS) in Mycobacterium tuberculosis. *Molecular Medicine* **8**, 714-724 (2002).

186 Li, G. *et al.* Efflux Pump Gene Expression in Multidrug-Resistant Mycobacterium tuberculosis Clinical Isolates. *PloS one* **10**, e0119013, doi:10.1371/journal.pone.0119013 (2015).

187 Gumbo, T. *et al.* Isoniazid's bactericidal activity ceases because of the emergence of resistance, not depletion of Mycobacterium tuberculosis in the log phase of growth. *The Journal of Infectious Diseases* **195**, 194-201, doi:10.1086/510247 (2007).

188 Li, X.-Z., Barré, N. & Poole, K. Influence of the MexA-MexB-OprM multidrug efflux system on expression of the MexC-MexD-OprJ and MexE-MexF-OprN multidrug efflux systems in Pseudomonas aeruginosa. *Journal of Antimicrobial Chemotherapy* **46**, 885-893 (2000).

189 Pasca, M. R., Guglierame, P., De Rossi, E., Zara, F. & Riccardi, G. mmpL7 gene of Mycobacterium tuberculosis is responsible for isoniazid efflux in Mycobacterium smegmatis. *Antimicrobial Agents and Chemotherapy* **49**, 4775-4777, doi:10.1128/aac.49.11.4775-4777.2005 (2005).

190 Tal, N. & Schuldiner, S. A coordinated network of transporters with overlapping specificities provides a robust survival strategy. *Proceedings of the National Academy of Sciences* **106**, 9051-9056 (2009).

191 Organization, W. H. *Global tuberculosis Report 2015*. (World Health Organization, 2015).

192 Lee, R. E. *et al.* Spectinamides: a new class of semisynthetic antituberculosis agents that overcome native drug efflux. *Nature Medicine* **20**, 152-158 (2014).

193 Louw, G. E. *et al.* Rifampicin reduces susceptibility to ofloxacin in rifampicin-resistant Mycobacterium tuberculosis through efflux. *American Journal of Respiratory and Critical Care Medicine* **184**, 269-276 (2011).

194 Schmalstieg, A. M. *et al.* The antibiotic resistance arrow of time: efflux pump induction is a general first step in the evolution of mycobacterial drug resistance. *Antimicrobial Agents and Chemotherapy* **56**, 4806-4815, doi:10.1128/aac.05546-11 (2012).

195 Rodrigues, L., Machado, D., Couto, I., Amaral, L. & Viveiros, M. Contribution of efflux activity to isoniazid resistance in the Mycobacterium tuberculosis complex. *Infection, Genetics and Evolution : Journal of Molecular Epidemiology and Evolutionary Genetics in Infectious Diseases* **12**, 695-700, doi:10.1016/j.meegid.2011.08.009 (2012).

196 Poole, K. Efflux pumps as antimicrobial resistance mechanisms. *Annals of Medicine* **39**, 162-176 (2007).

197 Balagadde, F. K. *et al.* A synthetic Escherichia coli predator-prey ecosystem. *Molecular Systems Biology* **4**, doi::10.1038/msb.2008.24 (2008).

198 Balagadde, F. K., You, L. C., Hansen, C. L., Arnold, F. H. & Quake, S. R. Long-term monitoring of bacteria undergoing programmed population control in a microchemostat. *Science* **309**, 137-140, doi:10.1126/science.1109173 (2005).

199 Jeyaseelan, L. *et al.* Tuberculosis of the Cuboid: A Case Report and Review of the Literature. *The Journal of Foot and Ankle Surgery* **54**, 713-716 (2015).

200 Sarathy, J. P., Dartois, V. & Lee, E. J. D. The role of transport mechanisms in Mycobacterium tuberculosis drug resistance and tolerance. *Pharmaceuticals* **5**, 1210-1235 (2012).

201 De Rossi, E., Ainsa, J. A. & Riccardi, G. Role of mycobacterial efflux transporters in drug resistance: an unresolved question. *FEMS Microbiology Reviews* **30**, 36-52, doi:10.1111/j.1574-6976.2005.00002.x (2006).

202 Aínsa, J. A. *et al.* Molecular cloning and characterization of Tap, a putative multidrug efflux pump present in Mycobacterium fortuitum and Mycobacterium tuberculosis. *Journal of Bacteriology* **180**, 5836-5843 (1998).

203 Ramón-García, S., Martín, C., Aínsa, J. A. & De Rossi, E. Characterization of tetracycline resistance mediated by the efflux pump Tap from Mycobacterium fortuitum. *Journal of Antimicrobial Chemotherapy* **57**, 252-259 (2006).

204 De Rossi, E. *et al.* The multidrug transporters belonging to major facilitator superfamily in Mycobacterium tuberculosis. *Molecular Medicine (Cambridge, Mass.)* **8**, 714 - 724 (2002).

205 Justice, S. S., Hunstad, D. A., Cegelski, L. & Hultgren, S. J. Morphological plasticity as a bacterial survival strategy. *Nature Reviews Microbiology* **6**, 162-168 (2008).

206 Bos, J. *et al.* Emergence of antibiotic resistance from multinucleated bacterial filaments. *Proceedings of the National Academy of Sciences* **112**, 178-183 (2015).

207 Zhang, Q. *et al.* Acceleration of Emergence of Bacterial Antibiotic Resistance in Connected Microenvironments. *Science* **333**, 1764-1767, doi:10.1126/science.1208747 (2011).

208 Herbert, D. *et al.* Bactericidal action of ofloxacin, sulbactam-ampicillin, rifampin, and isoniazid on logarithmic-and stationary-phase cultures of Mycobacterium tuberculosis. *Antimicrobial Agents and Chemotherapy* **40**, 2296-2299 (1996).

209 Justice, S. S., Hunstad, D. A., Cegelski, L. & Hultgren, S. J. Morphological plasticity as a bacterial survival strategy. *Nature Reviews Microbiology* **6**, 162-168 (2008).

210 Pine, L. & Boone, C. J. Comparative cell wall analyses of morphological forms within the genus Actinomyces. *Journal of Bacteriology* **94**, 875-883 (1967).

211 Bos, J., Yakhnina, A. A. & Gitai, Z. BapE DNA endonuclease induces an apoptotic-like response to DNA damage in Caulobacter. *Proceedings of the National Academy of Sciences* **109**, 18096-18101 (2012).

212 Justice, S. S., Hunstad, D. A., Seed, P. C. & Hultgren, S. J. Filamentation by Escherichia coli subverts innate defenses during urinary tract infection. *Proceedings of the National Academy of Sciences* **103**, 19884-19889 (2006).

213 ROLINSON, G. N. Effect of β-lactam antibiotics on bacterial cell growth rate. *Microbiology (Reading, England)* **120**, 317-323 (1980).

214 Ryan, D. & Monsey, D. Bacterial filamentation and in vivo efficacy: a comparison of several cephalosporins. *Journal of Antimicrobial Chemotherapy* **7**, 57-63 (1981).

215 Miller, C. *et al.* SOS response induction by ß-lactams and bacterial defense against antibiotic lethality. *Science (New York, N.Y.)* **305**, 1629-1631 (2004).

216 Tomchick, R. & Mandel, H. Biochemical effects of ethidium bromide in micro-organisms. *Microbiology (Reading, England)* **36**, 225-236 (1964).

217 Tønnesen, T. & Friesen, J. The effects of daunomycin and ethidium bromide on Escherichia coli. *Molecular and General Genetics MGG* **124**, 177-186 (1973).

218 Coelho, T. *et al.* Enhancement of antibiotic activity by efflux inhibitors against multidrug resistant Mycobacterium tuberculosis clinical isolates from Brazil. *Frontiers in Microbiology* **6**, 330 (2015).

219 Lamers, R. P., Cavallari, J. F. & Burrows, L. L. The efflux inhibitor phenylalanine-arginine beta-naphthylamide (PAbetaN) permeabilizes the outer membrane of gram-negative bacteria. *PloS One* **8**, e60666, doi:10.1371/journal.pone.0060666 (2013).

220 Mahamoud, A., Chevalier, J., Alibert-Franco, S., Kern, W. V. & Pages, J. M. Antibiotic efflux pumps in Gram-negative bacteria: the inhibitor response strategy. *The Journal of Antimicrobial Chemotherapy* **59**, 1223-1229, doi:10.1093/jac/dkl493 (2007).

221 Yang, D. C. *et al.* An ATP-binding cassette transporter-like complex governs cell-wall hydrolysis at the bacterial cytokinetic ring. *Proceedings of the National Academy of Sciences* **108**, 1052-1060 (2011).

222 Sharma, D., Cukras, A. R., Rogers, E. J., Southworth, D. R. & Green, R. Mutational analysis of S12 protein and implications for the accuracy of decoding by the ribosome. *Journal of Molecular Biology* **374**, 1065-1076, doi:10.1016/j.jmb.2007.10.003 (2007).

223 Tangy, F., Moukkadem, M., Vindimian, E., Capmau, M. & Le Goffic, F. Mechanism of action of gentamicin components. Characteristics of their binding to Eschevichiu coli ribosomes. *European Journal of Biochemistry.* **147**, 381-386 (1985).